VOLUME 87 NO. HY5
SEPTEMBER 1961
PART 1

JOURNAL of the

Hydraulics Division

PROCEEDINGS OF THE

AMERICAN SOCIETY OF CIVIL ENGINEERS

BASIC REQUIREMENTS FOR MANUSCRIPTS

Original papers and discussions of current papers should be submitted to the Manager of Technical Publications, ASCE. Authors should indicate the technical division to which the paper is referred. The final date on which a discussion should reach the Society is given as a footnote with each paper. Those who are planning to submit material will expedite the review and publication procedures by complying with the following basic requirements:

1. Titles must have a length not exceeding 50 characters and spaces.

2. A summary of approximately 50 words must accompany the paper, a 300-word synopsis must precede it, and a set of conclusions must end it.

3. The manuscript (an original ribbon copy and two duplicate copies) should be double-spaced on one side of 8½-inch by 11-inch paper. Three copies of all illustrations, tables, etc., must be included.

4. The author's full name, Society membership grade, and footnote reference stating present employment must appear on the first page of the paper.

5. Mathematics are recomposed from the copy that is submitted. Because of this, it is necessary that letters be drawn carefully, and that special symbols be properly identified. The letter symbols used should be defined where they first appear, in the illustrations or in the text, and arranged alphabetically in an Appendix.

6. Tables should be typed (an original ribbon copy and two duplicate copies) on one side of 8½-inch by 11-inch paper. Specific illustrations and explanation must be made in the text for each table.

7. Illustrations must be drawn in black ink on one side of 8½-inch by 11-inch paper. Because illustrations will be reproduced with a width of between 3-inches and 4½-inches, the lettering must be large enough to be legible at this width. Photographs should be submitted as glossy prints. Explanations and descriptions must be made within the text for each illustration.

8. The desirable average length of a paper is about 12,000 words and the absolute maximum is 18,000 words. As an approximation, each full page of typed text, table, or illustration is the equivalent of 300 words.

9. Technical papers intended for publication must be written in the third person.

10. The author should distinguish between a list of "Reading References" and a "Bibliography," which would encompass the subject of his paper.

This Journal is published bi-monthly by the American Society of Civil Engineers. Publication office is at 2500 South State Street, Ann Arbor, Michigan. Editorial and General Offices are at United Engineering Center, 345 East 47th Street, New York 17, N. Y. $4.00 of a member's dues are applied as a subscription to this Journal. Second-class postage paid at Ann Arbor, Michigan.

The index for 1960 was published as ASCE Publication 1961-15 (list price $2.00); indexes for previous years are also available.

Vol. 87, No. HY 5

Journal of the
HYDRAULICS DIVISION
Proceedings of the American Society of Civil Engineers

CONTENTS

September, 1961

Papers

(over)

Note.—Part 2 of this Journal is the 1961-33 Newsletter of the Hydraulics Division.

The three preceding issues of this Journal are dated March 1961, May 1961, and July 1961.

DISCUSSION

Journal of the
HYDRAULICS DIVISION
Proceedings of the American Society of Civil Engineers

HYDRAULIC DESIGN OF HOLLOW-JET VALVE STILLING BASINS

By G. L. Beichley,[1] M. ASCE and A. J. Peterka,[2] F. ASCE

SYNOPSIS

Hydraulic model and prototype tests made to generalize and prove the hydraulic design of a new type of stilling basin which utilizes the hollow-jet lve for discharge control are described. Dimensionless curves are derived om model data and are used to define the important dimensions of the basin the usual combinations of valve size, operating head, and discharge. Sam- e problems are presented to illustrate the use of the design curves and the neral hydraulic design procedures. Prototype tests on the Boysen and Fal- n Dam stilling basins are described and analyzed to help establish the reli- ility of the recommended basins. Basin dimensions obtained from individual odel tests on six stilling basins are shown to compare favorably with the di- ensions obtained from the dimensionless curves and methods given in this per.

INTRODUCTION

The hollow-jet valve stilling basin described in this paper is of a new type is used to dissipate hydraulic energy at the downstream end of an outlet rks control structure. To reduce cost and save space, the stilling basin is ally constructed within or adjacent to the powerhouse structure as shown Figs. 1 and 2. The hollow-jet valve, Fig. 3, controls and regulates the flow.

Note.—Discussion open until February 1, 1962. To extend the closing date one month, ritten request must be filed with the Executive Secretary, ASCE. This paper is part ne copyrighted Journal of the Hydraulics Division, Proceedings of the American So- y of Civil Engineers, Vol. 87, No. HY 5, September, 1961.

[1] Hydraulic Engineer, Bureau of Reclamation, Denver, Colorado.
[2] Hydraulic Engineer, Bureau of Reclamation, Denver, Colorado.

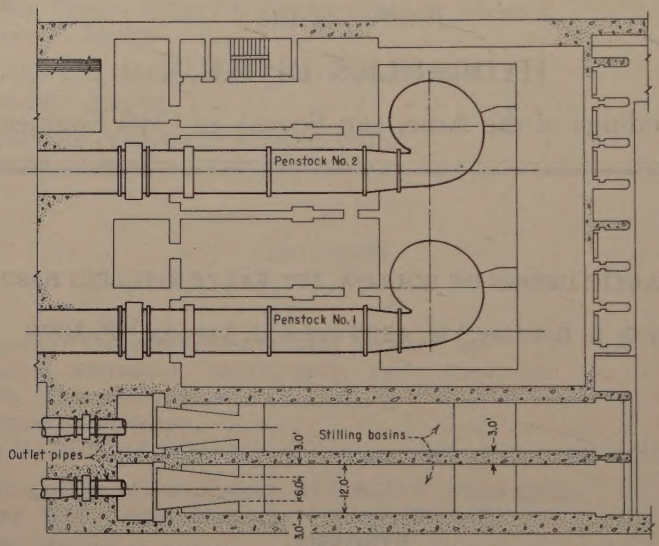

(a) HORIZONTAL SECTION THROTUGH POWERHOUSE

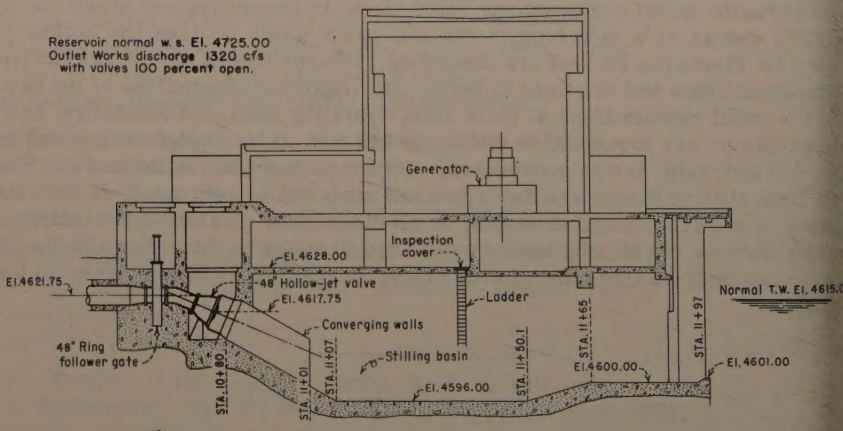

(b) POWERHOUSE SECTION-THROUGH OUTLET STILLING BASIN

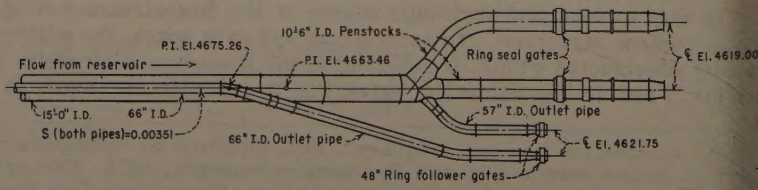

(c) PIPE LAYOUT-PLAN

FIG. 1.—BOYSEN DAM OUTLET WORKS STILLING BASIN AND POWER PLANT

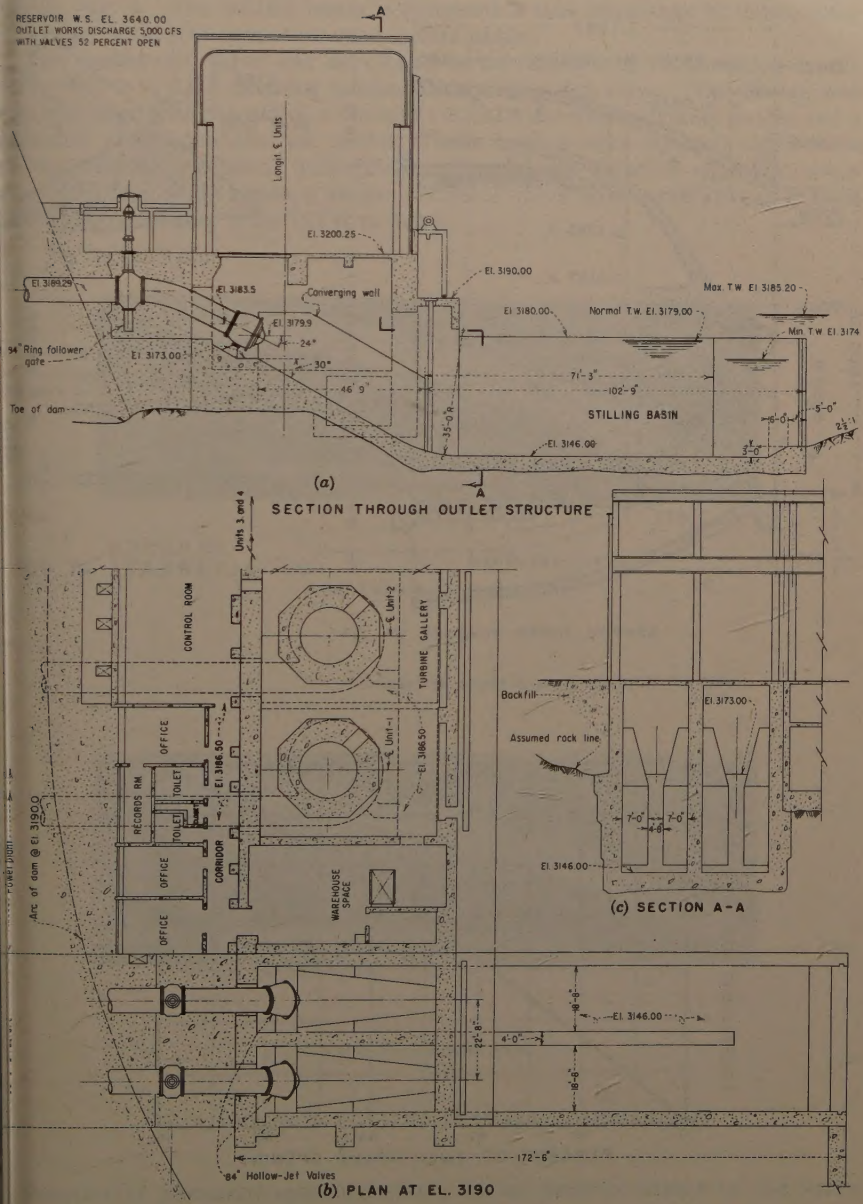

FIG. 2.—YELLOWTAIL DAM PROPOSED OUTLET WORKS STILLING BASIN AND POWERPLANT

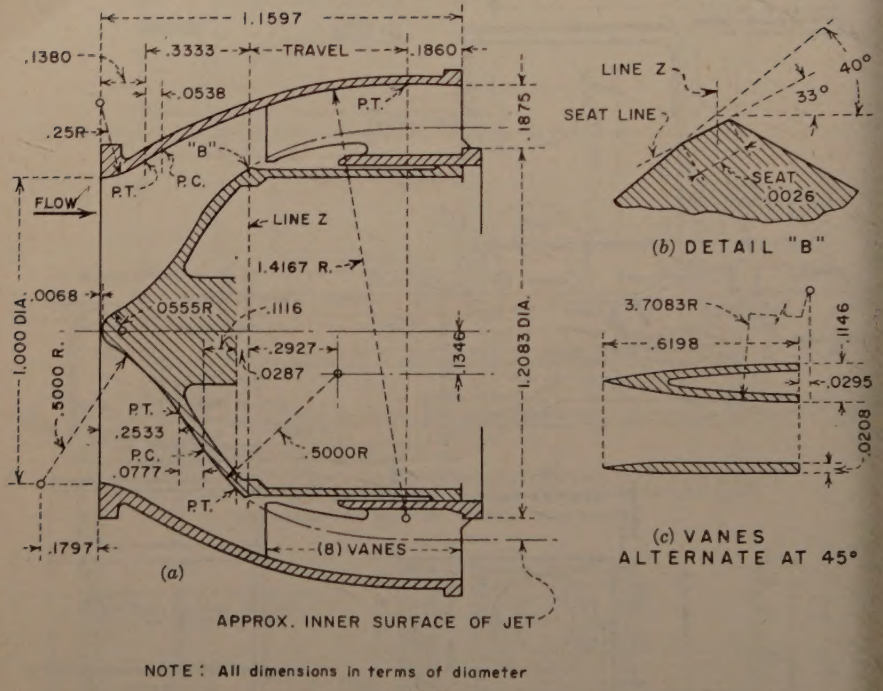

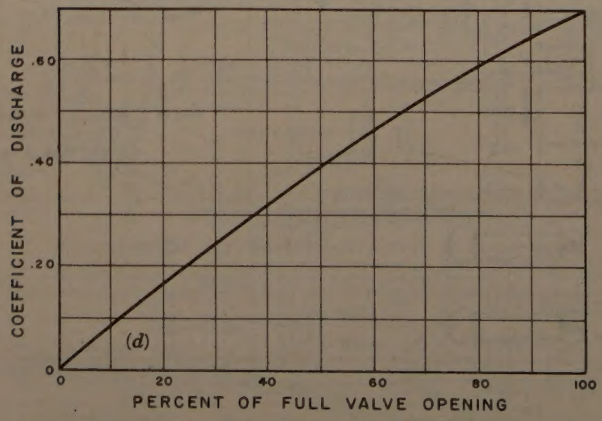

FIG. 3.—HOLLOW-JET VALVE DIMENSIONS AND DISCHARGE COEFFICIENTS

Regardless of the valve opening or head, the outflow has the same pattern, an annular or hollow jet of water of practically uniform diameter throughout its length, Fig. 4. The stilling basin is designed to take advantage of the hollow-jet shape; solid jets cannot be used in this basin.

The hollow-jet valve was developed by the Bureau of Reclamation in the early 1940's to fill a need for a dependable regulating valve. The design was accomplished with the aid of a complete 6-in.-diameter hydraulic model and a sectional 12-in.-diameter air model. These models were tested in the Bureau of Reclamation Hydraulic Laboratory. To evaluate the valve characteristics at greater than scale heads, a 24-in.-diameter valve was tested at Hoover Dam under heads ranging from 197 ft to 349 ft.

(*a*) Valve fully open

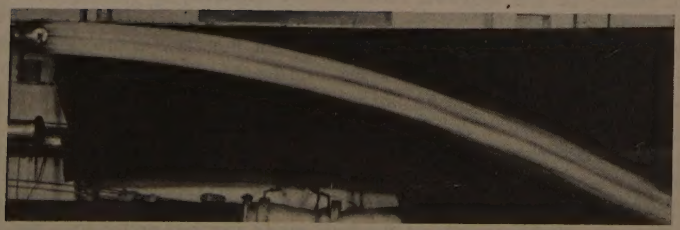

(*b*) Valve 50 percent open

FIG. 4.—SIX-INCH HOLLOW-JET VALVE DISCHARGING

Piezometer pressure measurements, thrust determinations on the valve needle, and rates of discharge were studied in both field and laboratory tests. It was found that the hydraulic characteristics of the larger valves could be predicted from the performance of the smaller model valves. From these tests and investigations of prototype valves up to 96 in. in diameter, the valve has been proved to be a satisfactory control device.

Cavitation damage, found on a few of the many prototype valves in use, was minor in nature and was caused by local irregularities in the body casting and by misalinement of the valve with the pipe. These difficulties have been eliminated by careful foundry and installation practices. On one installation, damage that occurred on the cast iron valve support vanes may have been caused by abrasive sediment in the water. The design itself is cavitation free.

Because a large valve operating at high heads can discharge flows having an energy content of up to 150,000 hp, a stilling basin is usually required downstream from the valve. In early designs, the valve was discharged horizontally onto a trajectory curved floor which was sufficiently long to provide a uniformly distributed jet entering the hydraulic jump stilling pool. This resulted in an extremely long structure, twice or more the length of the basin recommended herein. When two valves were used side by side, a long, costly dividing wall was also required. Hydraulic model tests showed that the basin length could be reduced more than 50% by turning the hollow-jet valves downward and using a different energy dissipating principle in the stilling basin. The first stilling basin of this type was developed for use at Boysen Dam, a relatively low-head structure. Basins for larger discharges and higher heads were later developed from individual hydraulic models of the outlet works at Falcon, Yellowtail, Trinity, and Navajo Dams. It became apparent at this time that generalized design curves could be determined to cover a wide range of operating heads and discharges. Therefore, a testing program was initiated to provide the necessary data. A brief description of the individual model tests made to develop the basin type is given in the following section. Table 1 gives a summary of basin dimensions, valve sizes, test heads, and discharges for these structures.

DEVELOPMENT OF BASIN FEATURES

Boysen Dam.—In the Boysen Dam model studies, a series of basic tests was made to determine the optimum angle of entry of a hollow-jet into the tail water. For flat angles of entry, the jet did not penetrate the pool but skipped along the tail water surface. For steep angles, the jet penetrated the pool but rose almost vertically to form an objectionable boil on the water surface. When the valves were depressed 24° from the horizontal, Fig. 1, and a 30° sloping floor was placed downstream from the valve to protect the underside of the jet from turbulent eddies, optimum performance resulted. The submerged path of the valve jet was then sufficiently long that only a minimum boil rose to the surface. The size and intensity of the boil were further reduced when converging walls were placed on the 30° sloping floor to protect the sides of the jet until it was fully submerged. The converging walls have another function, however; they compress the hollow-jet between them to give the resulting thin jet greater ability to penetrate the tail water pool. Sudden expansion of the jet as it leaves the converging walls plus the creation of fine grain turbulence in the basin account for most of the energy losses in the flow. Thorough breaking-up of the valve jet within the basin and good velocity distribution over the entire flow cross section account for the low velocities leaving the basin. Fig. 5 shows the performance of a hollow-jet basin both with and without the converging walls.

Pressures on the inside face and downstream end of the converging walls were measured to determine whether low pressures which might induce cavitation were present. The lowest pressure, measured on the end of the wall,

vas 3 ft of water above atmospheric; therefore, cavitation should not occur. Pressures measured on the sloping floor, and under and near the impinging et, were all above atmospheric. Maximum pressures did not exceed one-ourth of the total head at the valve.

TABLE 1.—COMPARISON OF BASIN DIMENSIONS[a, b, c]

Basin Dimensions (1)	Boysen (2)	Falcon, U. S. (3)	Falcon, Mexico (4)	Yellowtail (5)	Trinity (6)	Navajo (7)
Valve diameter, in ft	4	6	7.5	7	7	6
Head at valve, in ft	86	81.5	81.9	380	315	217
Design Q, in cfs	660	1,460	2,285	2,500	3,835	2,340
Coefficient C	0.70	0.70	0.70	0.41	0.70	0.70
Percentage valve open	100	100	100	52	100	100
Depth D, in ft	16.2 19	21.0 22.5	24.7 25.2	31.5 32.6	38.5 38	30.0 35[e]
Depth D_S, in ft	13.6 14	17.4 17.5	20.2 19.5	25.9 25.6	31.5 31.8	24.6 24
Length L, in ft	60.4 58	74.4 73.9	86.2 94	104 102.8	129 123	103 110[e]
Width W, in ft	10.2 12	14.7 16.2	18 16.2	19.2 18.7	19.6 18.9	16.2 18.0[e]
End sill height	3 4	3 3	3.1 3	3.9 3	4.8 5	. . .[e] . . .[e]
End sill slope	3.3:1[d]	2:1	2:1	2:1	2:1	. . .[e]
Converg wall height	3.0 d	4.5 d	3.9 d	3.1 d	3.5 d	3.4 d
Converg wall gap	0.50 W	0.52 W	0.65 W	0.25 W	0.25 W	0.23 W
Center wall length	1.5 L[d]	0.5 L	0.4 L	0.7 L	0.3 L	0.5 L
Channel slope	. . .[d]	4:1	4:1	2.5:1	2:1	6:1[e]

[a] Upper values in each box were calculated from Figs. 11 through 15; lower values each box were developed from individual model studies.
[b] Valve tilt 24°; inclined floor 30° in all cases.
[c] See Figs. 1, 2, 6, 7, 8, 9, and 11.
[d] Special case, for structural reasons.
[e] Special case, for diversion flow requirements (dentated sill used and basin size increased).

Scour downstream from the end sill was mild and prototype wave heights re only 0.5 ft in the river channel. A vertical traverse taken near the end l showed surface velocities to be about 5 fps, decreasing uniformly to about ps near the floor.

Falcon Dam.—In the Falcon Dam tests, two separate basins were developed, one for the United States outlet works and one for the Mexican outlet works, Figs. 6 and 7. In these tests, the basic concepts of the Boysen design were proved to be satisfactory for greater discharges. In addition, it was confirmed

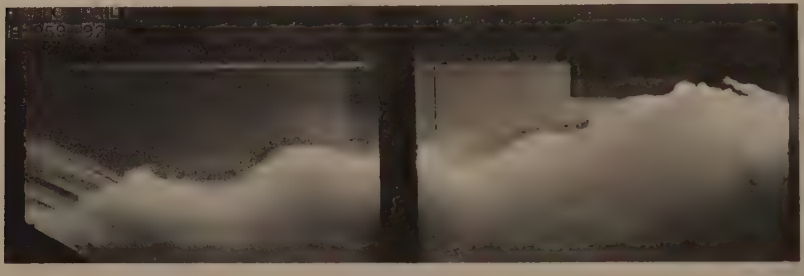

(*a*) Stilling action without converging walls

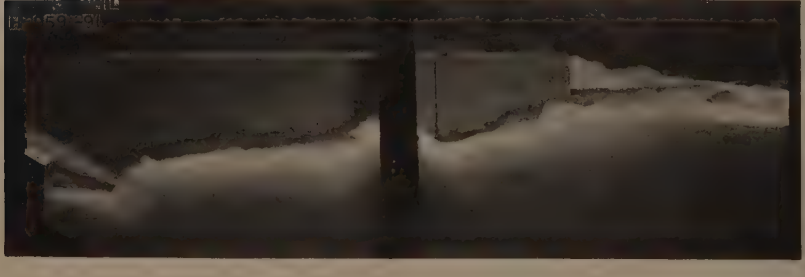

(*b*) Stilling action with short converging walls

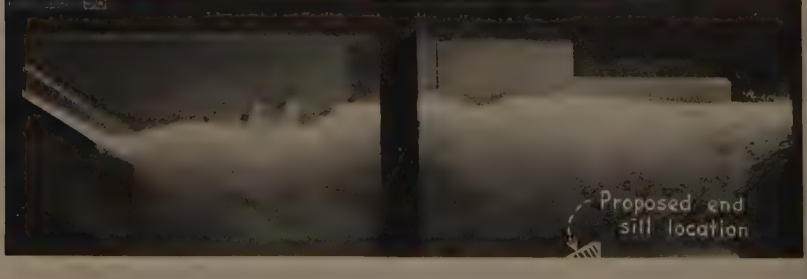

(*c*) Stilling action with recommended converging walls

FIG. 5.—HOLLOW-JET VALVE STILLING BASIN WITH AND WITHOUT CONVERGING WALLS

that dentils on the end sill were not necessary and that the center dividing wall need not extend the full length of the basin. A low 2:1 sloping end sill was sufficient to provide minimum scour and wave heights. Maximum pressures on

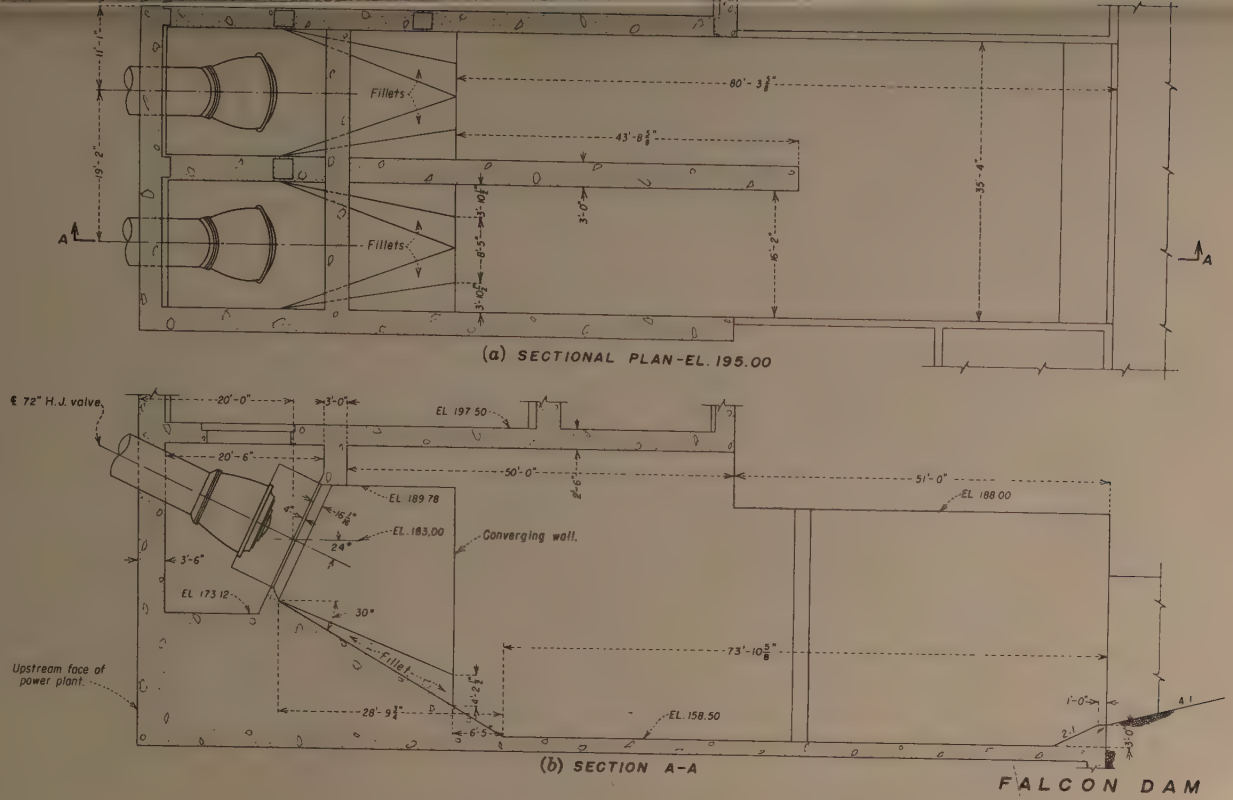

FIG. 6.—UNITED STATES OUTLET WORKS

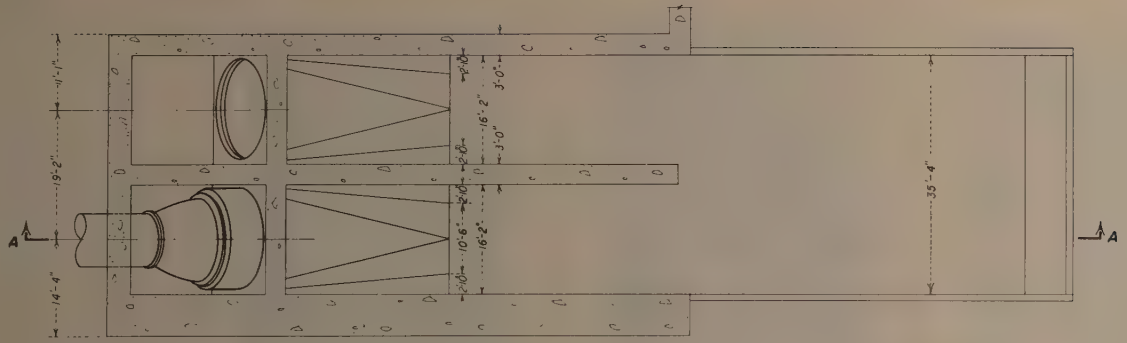

(a) SECTIONAL PLAN—EL. 195.00

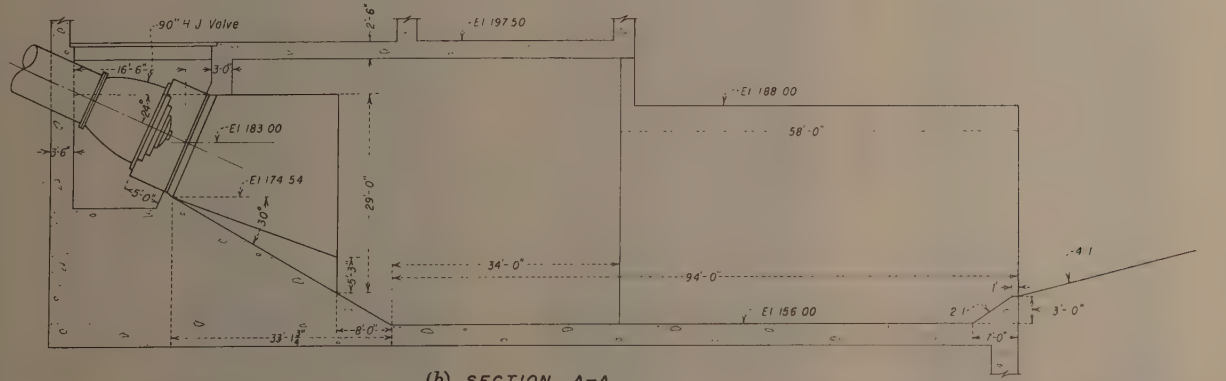

(b) SECTION A–A

FALCON DAM

FIG. 7.—MEXICAN OUTLET WORKS

the floor beneath the impinging jet were found to be about one-third of the total head at the valve, somewhat greater than found in the Boysen tests, but still not excessive.

Yellowtail Dam.—In the Yellowtail Dam model studies, the head and discharge were both considerably higher than in the Boysen and Falcon tests. Because of the high velocity flow from the valves, it was found necessary to extend the converging walls to the downstream end of the sloping floor, Fig. 2, and to reduce the wall gap to about one-quarter of the basin width. These refinements improved the stilling action within the basin, Fig. 5 (c), and made it possible to further reduce the basin length. Scour was not excessive, and the water surface in the downstream channel was relatively smooth. Pressures on the converging walls and other critical areas in the basin were found to be above atmospheric.

Trinity Dam.—The Trinity Dam outlet works utilized a head almost 4 times greater and a discharge 5 times greater than at Boysen Dam. In the development tests, it was found that the performance of this type of basin would be satisfactory for extremely high heads and discharges. Although several variations in the basin arrangement were investigated, no new features were incorporated in the design. Fig. 8 shows the developed design.

Navajo Dam.—The experimental work on the Navajo outlet works was complicated by the fact that the hollow-jet valve basin, Fig. 9, had to first serve as a temporary diversion works stilling basin. Since the diversion works basin was larger than required for the outlet works basin, it was possible to insert the proper appurtenances in the temporary basin to convert it to a permanent outlet works basin. The development tests indicated that a larger than necessary basin does not in itself guarantee satisfactory performance of the hollow-jet valve basin. Best outlet works performance was obtained when the temporary basin was reduced in size to conform to the optimum size required for the permanent structure. Since the Navajo Dam outlet works model was available both during and after the generalization tests, the model was used both to aid in obtaining the generalized data and to prove that the design curves obtained were correct.

GENERALIZATION STUDY

Because development work on individual basins had reached a point where the general arrangement of the basin features was consistent, and because the basin had been proved satisfactory for a wide range of operating conditions, a testing program was inaugurated to provide data for use in generalizing the basin design. The purpose of these tests was to provide basin dimensions and hydraulic design procedures for any usual combinations of valve size, discharge, and operating head. The main purpose of this paper is to describe these tests, to explain the dimensionless curves which are derived from the test data, and to show, by means of sample problems, the procedures which may be used to hydraulically design a hollow-jet valve stilling basin. Prototype tests on the Boysen and Falcon basins are included to demonstrate that hollow-jet valve basins, that fit the dimensionless curves derived in the general study, will perform as well in the field as predicted from the model tests.

Test Equipment.—The outlet works stilling basin model shown in Fig. 10 was used for the generalization tests. The glass-walled testing flume contained two stilling basins separated by a dividing wall. The right-hand basin

FIG. 8.—TRINITY DAM OUTLET WORKS

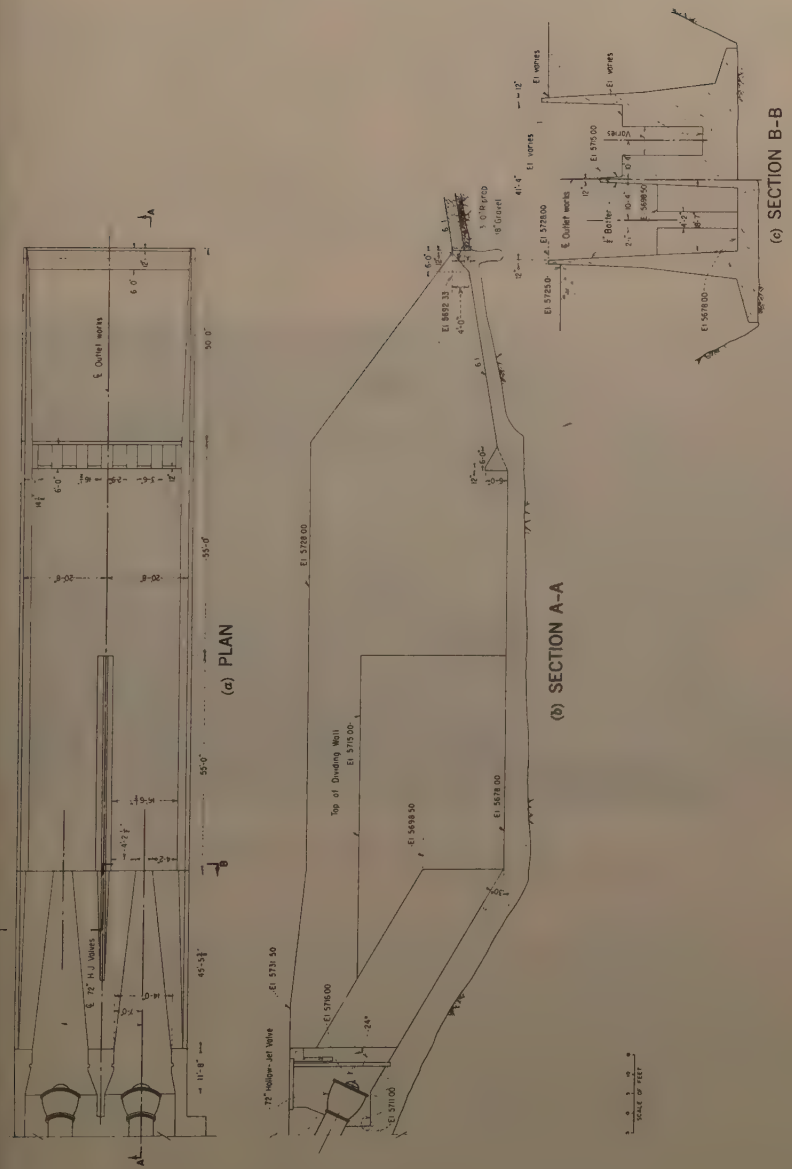

FIG. 9.—NAVAJO DAM OUTLET WORKS STILLING BASIN

having the glass panel as one wall was operated singly to determine the basin length, width, and depth requiremetns; both basins were used to study the performance with and without flow in an adjacent basin.

The glass panel permitted observation of the stilling action and the flow currents within and downstream from the basin. The length, width, and depth of the basin were varied by inserting false walls or by moving the basin within the test box. The tail box contained an erodible sand bed to represent the discharge channel bed.

The test valves were exact models of a prototype valve in that the flow surfaces were exactly reproduced, and could be opened and closed to any partial opening. The models were 3-in. valves machined from bronze castings.

The pressure head at each model valve was measured using a piezometer located in the 3-in. supply pipe 1 diameter upstream from the valve flange.

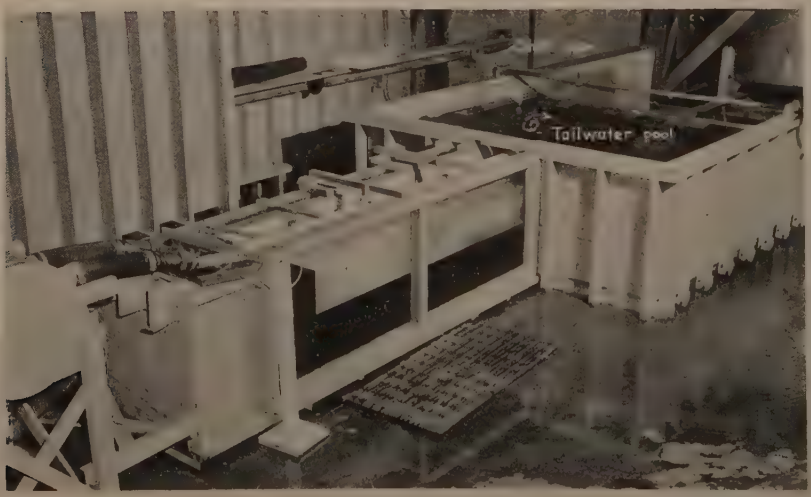

FIG. 10.—HOLLOW-JET VALVE STILLING BASIN MODEL USED FOR GENERALIZATION TESTS

Discharges were measured using calibrated venturi meters permanently installed in the laboratory. The tail water elevation in the discharge channel was controlled with a hinged tailgate in the tail box. Tail water elevations were determined visually from a staff gage on the tail box wall located approximately 62 valve diameters downstream from the valves.

Preliminary Procedures.—The investigation was begun by tabulating the important dimensions of the Boysen, Falcon, Yellowtail, and Trinity outlet works basins and expressing them in dimensionless form, as shown in Table 1. Based on these dimensions, a model was constructed as shown in Fig. 11, using the 3-in. valve dimension to establish the absolute model size. More weight was given to the Yellowtail and Trinity basins because they were developed for higher heads and contained refinements in the converging wall design which improved the basin performance at high heads. Also, the latter basins had

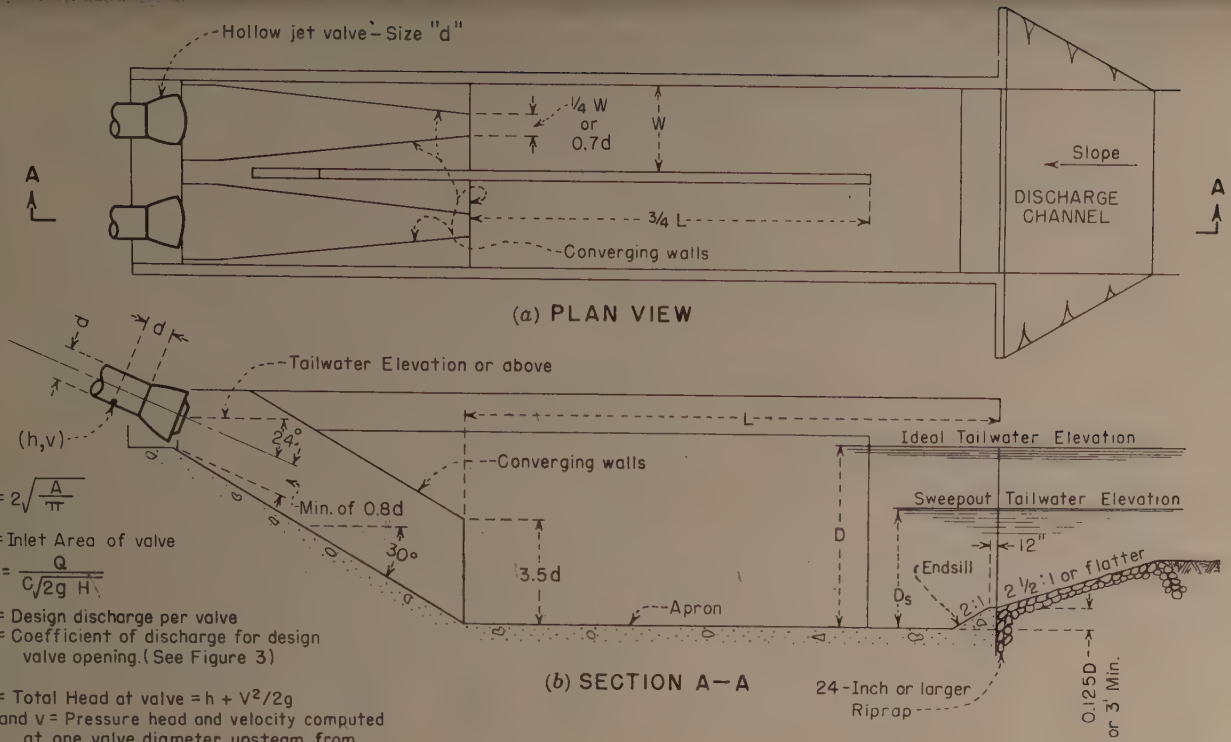

FIG. 11.—GENERALIZED DESIGN

been model tested over a greater operating range than were the earlier low-head basins.

To provide practical dishcarge limits for the tests, the 3-in. model was assumed to represent an 84-in. prototype valve, making the model scale 1:28. Discharges of 2,000 sec-ft to 4,000 sec-ft with one valve open 100% were considered to be the usual design discharges for a valve of this size. To produce these discharges, heads of 100 ft to 345 ft of water at the valve would be required.

Initial tests were made with the stilling basin apron longer than necessary and with no end sill in place. For a given discharge, the ideal depth of tail water was determined from visual inspection of the stilling action as it occurred over a range of tail water elevations. For each ideal tail water determination, the minimum length of concrete apron was estimated after an inspection of the flow currents in the model had indicated where an end sill should be placed in the prototype. Confirming tests were then conducted successively on a representative group of basins having the apron lengths previously determined and having an end sill at the end of the apron. Adjustments were then made as necessary to the preliminary values to obtain final ideal tail water depths and apron lengths. In the latter tests, the height of the valve above the maximum tail water elevation was adjusted to simulate a typical prototype installation. Similar tests were then made with the valve open 75% and 50%. Finally, a series of tests was made to determine the ideal width of stilling basin and the range of widths over which satisfactory performance could be expected.

Preliminary Tests.—In a typical test, the desired discharge was set by means of the laboratory venturi meters and passed through the hollow-jet valve or valves opened 100%. The tail water elevation was adjusted to provide the best energy dissipating action in the basin. The optimum value, tail water depth D in Fig. 11, was judged by the appearance and quality of the stilling action in the basin and on the smoothness of the tail water surface.

For discharges of 2,000 sec-ft to 4,000 sec-ft, it was found that the tail water could be raised or lowered about 3 ft (0.1 ft in model) from the ideal tail water elevation without adversely affecting the basin performance. Increasing the tail water depth beyond this margin reduced the efficiency of the stilling action and allowed the jet to flow along the bottom of the basin for a greater distance before being dissipated. This also produced surges in the basin and increased the wave heights in the discharge channel. Decreasing the tail water depth below the 3-ft margin moved the stilling action downstream in the basin and uncovered the valve jets at the end of the converging walls. This increased the flow velocity entering the discharge channel and increased the tendency to produce bed scour. Uncovering of the stilling action also produced objectionable splashing at the upstream end of the basin. If the tail water depth was decreased further, the flow swept through the basin with no stilling action having occurred. The latter tail water depth was measured and recorded as the sweep-out depth D_S. These tests were made with the dividing wall extended to the end of the basin, since this provided the least factor of safety against jump sweep out. With a shorter dividing wall, sweep out occurs at a tail water elevation slightly less than D_S.

With the ideal tail water depth set for a desired flow, the action in the basin was examined to determine the ideal length, L, of the basin apron, Fig. 11. The apron length was taken to the point where the bottom flow currents began to rise from the basin floor of their own accord, without assistance from an end sill, Fig. 5 (c). The water surface directly above and downstream from

this point was fairly smooth, indicating that the stilling action had been completed and that the paved apron and training walls need not extend farther. In the preceding individual model studies, it had been found that when the basin was appreciably longer than ideal, the ground roller at the end sill carried bed material from the discharge channel over the end sill and into the basin. If this action occurred in a prototype structure the deposited material would swirl around in the downstream end of the basin and cause abrasive damage to the concrete apron and end sill. It had also been found that scour tendencies in the discharge channel were materially increased if the basin was appreciably shorter than ideal. Therefore, the point at which the currents turned upward from the apron, plus the additional length required for an end sill, was determined to be the optimum length of apron. At this point, the scouring velocities were a minimum and any scouring tendencies would be reduced by the sloping end sill to be added later.

Practical difficulties were experienced in determining the exact length of apron required, however. Surges in the currents flowing along the basin floor caused the point of upturn to move upstream and downstream a distance of 1/4 to 1/2 D in a period of 15 sec to 20 sec in the model. An average apron length was therefore selected in the preliminary tests. For this reason, too, the end sill would help to neutralize the scouring tendencies which increased as the bottom currents surged downstream.

The depth D, sweep-out depth D_s, and length L were then determined for the range of discharges possible with the hollow-jet valve open 75%, and finally 50%, using the testing methods described in the preceding paragraphs. Partial openings were investigated because the valve size is often determined for the minimum operating head and maximum design discharge. When the same quantity is discharged at higher heads, the valve opening must be reduced. It may be necessary, therefore, to design the basin for maximum discharge with the valves opened less than 100%. When the relation between head and velocity in the valve is changed materially, the minimum required basin dimensions will be affected. The data for the partially opened valves are also useful in indicating the basin size requirements for discharges greater or less than the design flow conditions.

Final Tests and Procedures.—The final tests were made to correct or verify the dimensions obtained in the preliminary tests and to investigate the effect of varying the basin width. Scour tendencies were also observed to help evaluate the basin performance. D, D_s, and L for the three valve openings are functions of the energy in the flow at the valve. The energy may be represented by the total head, H, at the valve, Fig. 11. Therefore, to provide dimensionless data which may be used to design a basin for any size hollow-jet valve, D, D_s, and L values from the preliminary tests were divided by the valve diameter d, and each variable was plotted against H/d. The resulting curves, similar to those in Figs. 12, 13, and 14, were used to obtain dimensions for a group of model basins which were tested with the end sill at the end of the apron and with the valves placed to give the proper vertical distance between the valve and the tail water. For each model basin, a 3:1 upward sloping erodible bed, composed of fine sand, was installed downstream from the end sill. The bed was kept sufficiently low that it did not interfere with tail water manipulation, even when the tail water was lowered for the sweep-out tests. Test procedure was essentially as described for the preliminary tests.

Basin Depth and Length.—The preliminary depth curves for both ideal tail water depth and sweep-out tail water depth needed but little adjustment. The preliminary basin lengths were found to be too long for the high heads and too

short for the lower heads, although both adjustments were relatively minor The adjusted and final curves are shown in Figs. 12, 13, and 14.

It was observed that a longer apron than indicated by Fig. 14 was necessary when the tail water depth exceeded the tail water depth limit in Fig. 12. As the stilling action became drowned, the action in the basin changed from fine-grain turbulence to larger and slower moving vertical eddies. The bottom flow currents were not dissipated as thoroughly or as quickly and were visible on the apron for a greater distance, thereby increasing the necessary length of basin. The action is similar to that observed in hydraulic jumps which are drowned by excessive tail water depths. A moderate amount of drowning is tolerable, but it is important that the ideal tail water depth be maintained within stated limits if the best performance is desired. The tail water depth limits, 0.1 ft above and below the ideal depth, expressed in dimensionless form is 0.4 d. If this limit is exceeded, a model study is recommended.

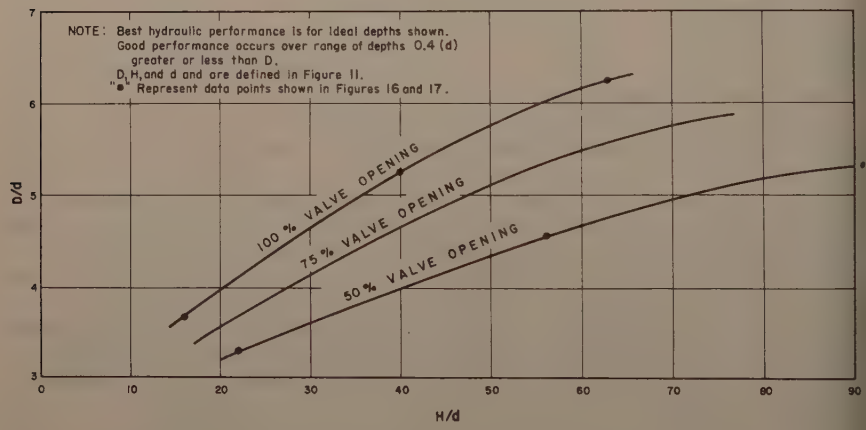

FIG. 12.—IDEAL TAIL WATER DEPTH

Basin Width.—To determine the effect of basin width, tests on several basins were made in which only the basin width was varied. It was found that the width could be increased to 3.0 times the valve diameter before the action became unstable. The width could be decreased to 2.5 times the valve diameter before the stilling action extended beyond the ideal length of basin. However the H/d ratio and the valve opening were found to affect the required basin width as shown for 100%, 75%, and 50% valve openings in Fig. 15.

Basin width is not a critical dimension but certain precautions should be taken when selecting a minimum value. If the tail water is never to be lower than ideal, as shown by the curves in Fig. 12, the basin width may be reduced to 2.5 d. If the tail water elevation is to be below ideal, however, the curve values for width in Fig. 15 should be used. In other words, the lower limits for both tail water and basin width should not be used in the same structure. The combined minimums tend to reduce the safety factor against jump sweep-out and poor overall performance results. The basin width should not be increased above 3.0 d to substitute for some of the required length or depth o

the basin. If unusual combinations of width, depth, and length are needed to fit a particular space requirement, a model study is recommended.

Basin Performance.—The six model basins shown operating in Figs. 16 and 17 illustrate the performance to be expected from the recommended structures. The operating conditions in Figs. 16 and 17 correspond to points shown in Figs. 12, 14, and 15. Fig. 16 shows the operation for 100% valve opening; Fig. 17 shows the operation for 50% opening. The photographs may be used to determine the model appearance of the prototype basin and may help to provide a visual appraisal of the prototype structure. Wave heights, boil heights, or other visible dimensions may be scaled from the photographs (using the scale shown in the photographs) and converted to prototype dimensions by multiplying the scaled distances by the model scale. To determine the model scale, the prototype valve diameter in inches should be divided by 3 (the model valve diameter). To determine which of the six photographs represents the prototype in question, the H/d ratio should be used to select the photograph which most nearly represents the design problem. It is permissible to interpolate between photographs when necessary.

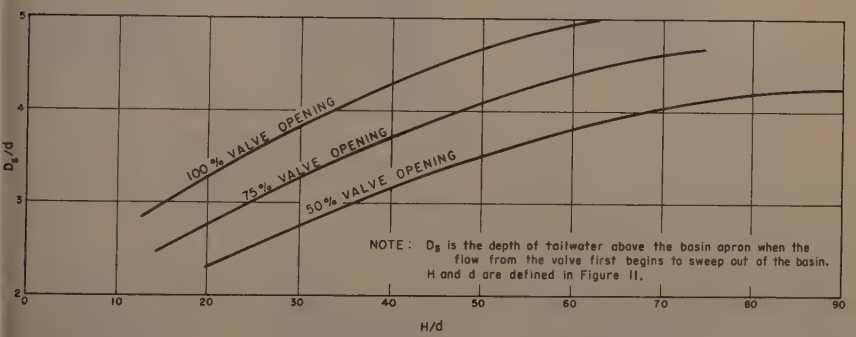

FIG. 13.—TAIL WATER SWEEPOUT DEPTH

Center Dividing Wall.—Prototype stilling basins usually have two valves placed a minimum distance apart, and alined to discharge parallel jets. It is necessary, without exception, to provide dividing walls between the valves for satisfactory hydraulic performance. When both valves are discharging without a dividing wall, the flow in the double basin sways from side to side to produce longitudinal surges in the tail water pool. This action occurs because the surging downstream from each valve does not have a fixed period, and the resulting harmonic motion at times becomes intense. When only one valve is discharging, conditions are worse. The depressed water surface downstream from the operating valve induces flow from the higher water level on the nonoperating side. Violent eddies carry bed material from the discharge channel into the basin and swirl it around. This action in the prototype would damage the basin as well as the discharge channel. In addition, the stilling action on the operating side is impaired.

To provide acceptable operation with one valve operating, the dividing wall should extend to three-fourths of the basin length or more. However, if the two adjacent valves discharge equal quantities of flow at all times, the length

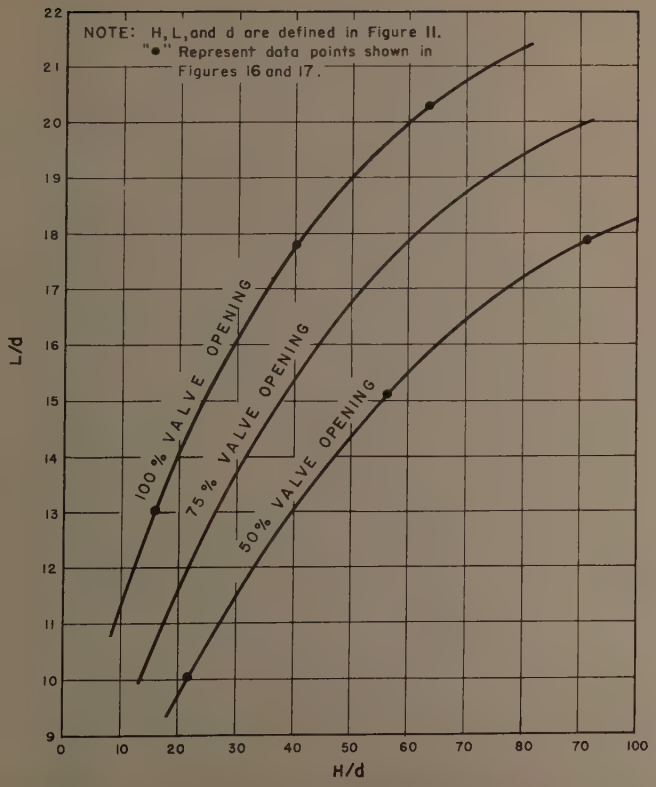

FIG. 14.—STILLING BASIN LENGTH

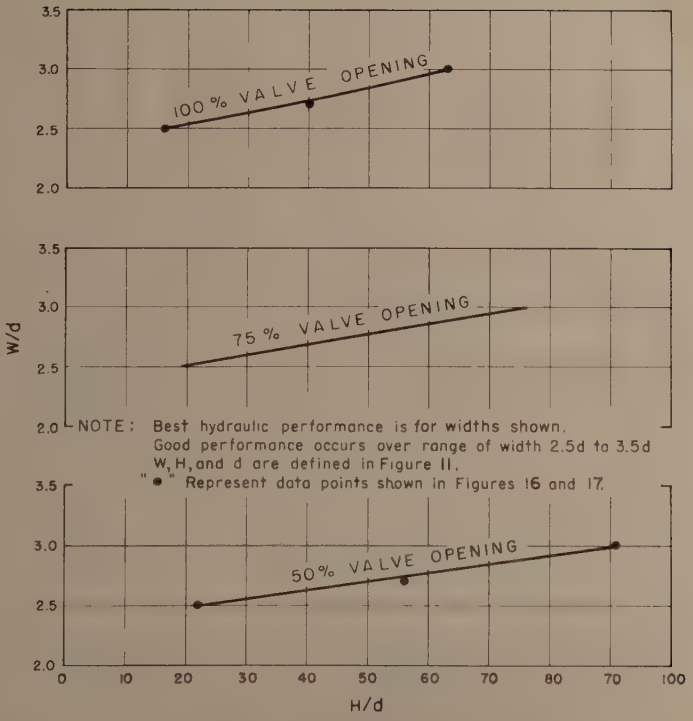

FIG. 15.—BASIN WIDTH PER VALVE

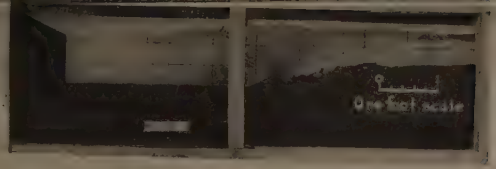

(a) H/d=16, D/d=3.7, L/d=12.9, W/d=2.5

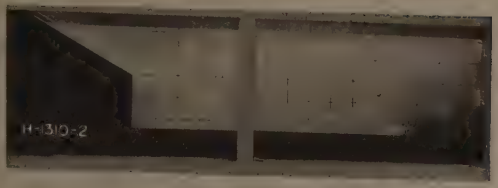

(b) H/d=40, D/d=5.2, L/d=17.8, W/d=2.7

(c) H/d=63, D/d=6.2, L/d=20.3, W/d=3.0

FIG. 16.—HOLLOW-JET VALVE STILLING BASIN PERFORMANCE, VALVE 100% OPEN

(a) H/d=22, D/d=3.3, L/d=10.0, W/d=2.5

(b) H/d=56, D/d=4.5, L/d=15.0, W/d=2.7

(c) H/d=91, D/d=5.3, L/d=17.8, W/d=3.0

FIG. 17.—HOLLOW-JET VALVE STILLING BASIN PERFORMANCE VALVE 50% OPEN

of the center dividing wall may be reduced to one-half of the basin length. The margin against sweep out is increased, but the stability of the flow pattern is decreased as the dividing wall is shortened. In some installations, a full-length wall may be desirable to help support the upper levels of a powerplant, Fig. 1. If other arrangements of the center wall are required a model study is recommended.

Valve Placement.—A hollow-jet valve should not operate submerged because of the possibility of cavitation occurring within the valve. However, the valve may be set with the valve top at maximum tail water elevation, and the valve will not be underwater at maximum discharge. The valve jet sweeps the tail water away from the downstream face of the valve sufficiently to allow usual ventilation of the valve. However, as a general rule, it is recommended that the valve be placed with its center (downstream end) no lower than tail water elevation.

Riprap Size.—A prototype basin is usually designed for maximum discharge, but will often be used for lesser flows at partial and full valve openings. For these lesser discharges, the basin will be larger than necessary, and in most respects, the hydraulic performance will be improved. However, at less than design discharge, particularly those close to the design discharge, the ground roller will tend to carry some bed material upstream and over the end sill into the basin. The intensity of this action is relatively mild over most of the discharge range, and movement of material may be prevented by placing riprap downstream from the end sill. Riprap, having 50% or more of the individual stones 24 in. to 30 in. or larger in diameter, should provide a stable channel downstream from the end sill. The riprap should extend a distance D, or more, from the end sill. If the channel is excavated and slopes upward to the natural river channel, the riprap should extend from the end sill to the top of the slope, or more. The riprap should not be terminated on the slope.

The justification for choosing riprap as described is as follows: Because of the fixed relationships between depth and width of basin, the average velocity leaving the basin will seldom exceed 5 fps, regardless of structure size. Surface velocities will therefore seldom exceed 7 fps to 8 fps and bottom velocities 3 fps to 4 fps. To protect against these velocities, stones 10 in. to 12 in. in diameter would be ample. However, the critical velocity for riprap stability is the upstream velocity of the ground roller which has a curved path and tends to lift the stones out of place. Model tests showed that graded riprap up to 24 in. to 30 in. in diameter was sufficient to provide bed stability.

APPLICATION OF RESULTS

Problems.—Design a stilling basin for (a) 1 hollow-jet valve discharging 1,300 cfs, and (b) a double basin for 2 valves discharging 650 cfs each. In both problems, the reservoir is 108 ft above maximum tail water elevation.

One-valve Stilling Basin Design.—The valve size should be determined from the equation:

$$Q = C\,A\,\sqrt{2\,g\,H} \quad \ldots\ldots\ldots\ldots\ldots\ldots \quad (1$$

in which Q is the design discharge, C is the coefficient of discharge, A is the inlet area to the valve, g is the acceleration of gravity, and H is the usable or total head at the valve with the valve center placed at maximum tail water elevation. In this example, the usable head at the valve is estimated to be 80% of the total head of 108 ft, or 86 ft.

From Fig. 3, for 100% valve opening:

$$C = 0.7$$

Then, from Eq. 1

$$A = 25 \text{ sq ft}$$

nd

$$d = 5.67 \text{ ft}$$

n which d is the inlet diameter of the valve and also the nominal valve size. ince nominal valve sizes are usually graduated in 6-in. increments,

$$d = 6 \text{ ft}$$

ould be selected. Because the selected valve is larger than required, it would ot be necessary to open the valve fully to pass the design flow at the maximum ead.

Having determined the valve size and therefore the diameter of the supply onduit, the probable head losses in the system from reservoir to valve may e computed. In this example, the computed losses are assumed to be 20 ft, hich leaves 88 ft of head at the valve. Using Eq. 1, C is computed to be 0.61; om Fig. 3, the valve opening necessary to pass the design discharge at the esign head is 83%.

he basin depth, length, and width may be determined from Figs. 12, 13, 14, nd 15 using the head ratio

$$\frac{H}{d} = \frac{88}{6} = 14.67$$

or 83% valve opening, Fig. 12 shows the depth ratio

$$\frac{D}{d} = 3.4$$

ne depth of the basin is

$$D = 20.4 \text{ ft}$$

erefore, the apron is placed 20.4 ft below the maximum tail water elevation.

or 83% valve opening, Fig. 14 shows the length ratio

$$\frac{L}{d} = 11.2$$

e length of the basin is

$$L = 67 \text{ ft}$$

r 83% valve opening, Fig. 15 shows the width ratio

$$\frac{W}{d} = 2.5$$

e width of the basin is

$$W = 15 \text{ ft}$$

e dimensions of other components of the basin may be determined from . 11.

The tail water depth at which the flow will sweep from the basin may be determined from Fig. 13. For 83% valve opening, the depth sweep-out ratio

$$\frac{D_s}{d} = 2.7$$

The sweep-out depth is

$$D_s = 16.2 \text{ ft}$$

Since 20.4 ft of depth is provided, the basin has a safety factor against sweep-out of 4.2 ft of tail water depth. In most installations this is sufficient, but if a greater margin of safety is desired, the apron elevation may be lowered

$$0.4 \text{ (d)} = 2.4 \text{ ft}$$

If greater economy and less margin of safety are desired, the basin floor may be placed 2.4 ft higher to provide only 18 ft of depth

If the tail water depth from Fig. 12 is adopted, the water surface profile will be similar to that shown in Fig. 16 (a), since the H/ d value of 16 in Fig. 16 (a) is comparable to 14.67 in this example. If tail water depth 2 ft greater or less than the ideal is adopted for the prototype, the water surface profile will be moved up or down accordingly. Water surfaces may be estimated by multiplying the variations shown in Fig. 16 (a) by the quotient obtained by dividing the prototype valve diameter of 72 in. by the mdoel valve diameter of 3 in. Wave heights in the downstream channel will be considerably less as indicated in other photographs showing downstream conditions.

Two-valve Stilling Basin Design.—If two valves are to be used to discharge the design flow of 1,300 sec-ft, a double basin with a dividing wall is required. The discharge per valve is 650 cfs, and at 100% valve opening the valve coefficient is 0.7, Fig. 3. The head on the valve is estimated to be 86 ft as in the first example. From Eq. 1, the inlet area of the valve is found to be 12.48 sq ft. A 48-in. valve provides practically the exact area required.

For this example, it is assumed that the computations to determine head losses have been made and that the estimated head of 86 ft at the valves is correct. Therefore, 100% valve opening will be necessary to pass the design flow.

Using the methods given in detail in the first example:

$$\frac{H}{d} = 21.5$$

$$\frac{D}{d} = 4.06, \text{ from Fig. 12}$$

and

$$D = 16.2 \text{ ft}$$

$$\frac{D_s}{d} = 3.3, \text{ from Fig. 13}$$

then

$$D_s = 13.2 \text{ ft}$$

The tail water depth for sweep out is therefore 3.0 ft below the ideal tail water depth. If more or less insurance against the possibility of sweep out is desired, the apron may be set lower or higher by the amount

$$0.4\ (d) = 1.6 \text{ ft}$$

To aid in determining the apron elevation, the effect of spillway, turbine, or other discharges on the tail water range may need to be considered.

$$\frac{L}{d} = 14.4, \text{ from Fig. 14}$$

then

$$L = 58 \text{ ft}$$

$$\frac{W}{d} = 2.6, \text{ from Fig. 15}$$

hen

$$W = 10.4 \text{ ft}$$

Since two valves are to be used, the total width of the basin will be 2(W) plus he thickness of the center dividing wall. The length of the center dividing wall should be three-fourths of the apron length or 43.5 ft long, Fig. 11. If it is ertain that both valves will always discharge equally, the wall need be only ne-half the apron length or 29 ft long. The hydraulic design of the basin may e completed using Fig. 11.

If the tail water depth determined from Fig. 12 is adopted, the water surace profile for determining wall heights may be estimated by interpolating beween Fig. 16 (a) and (b). Water surface variations may be predicted by multiplying values scaled from the photographs by the ratio 48/3.

PROTOTYPE PERFORMANCE

The Boysen Dam and Falcon Dam outlet works stilling basins, Figs. 1, 6, nd 7, fit the design curves derived from the generalized study quite well, and ave been field tested and found to perform in an excellent manner. Table 1 hows the important dimensions of these basins and indicates that the values omputed from the design curves of this paper are in good agreement with ose obtained from the individual model tests.

Boysen Dam.—The outlet works basin at Boysen Dam is designed for 1,320 s from two 48-in. hollow-jet valves 100% open at reservoir elevation 4725.00. esign tail water elevation at the basin is 4616.00. The model performance of is basin is shown in Figs. 18 and 19.

The prototype tests, Figs. 20, 21, and 22, were conducted with the reserir at elevation 4723.5 and with the powerplant both operating and shut down. ne spillway was not operating. The outlet works discharge was measured a temporary gaging station located about 1/2 mile downstream from the m using a current meter to determine the discharge. Tail water elevations ere read on the gage located in the powerhouse.

The prototype performed as well as predicted by the model and was condered satisfactory in all respects. However, the field structure entrained ore air within the flow than did the model. This caused the prototype flow to pear more bulky, and "white water" extended farther into the downstream annel than was indicated in the model. A comparison of the model and prorype photographs, Figs. 19 and 22, illustrates this difference. Greater air

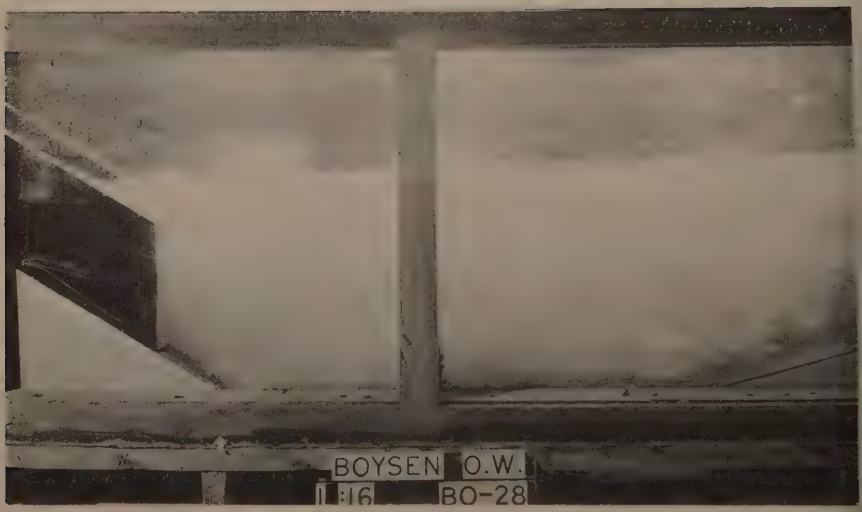

FIG. 18.—BOYSEN DAM, LEFT VALVE OF OUTLET WORKS BASIN, DISCHARGING 660 CFS 1:16 SCALE MODEL

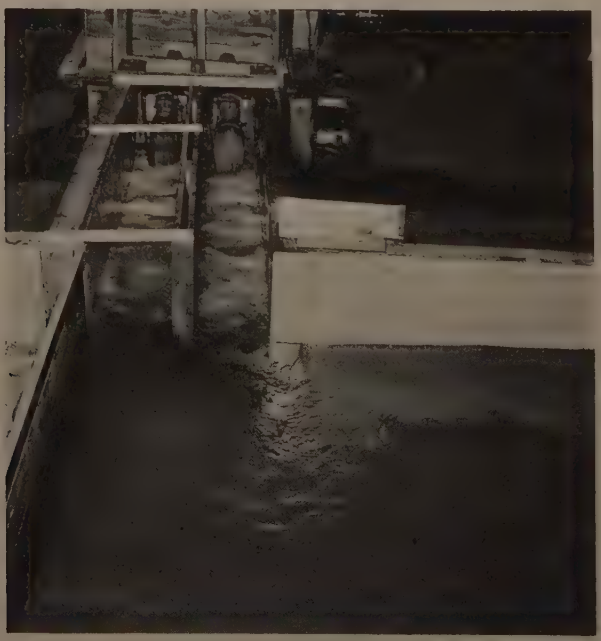

FIG. 19.—BOYSEN DAM, OUTLET WORKS DISCHARGING 1320 CFS 1:16 SCALE MODEL

Both valves fully open. Reservoir elevation 4723.5. Dashed lines show the outline of converging walls located beneath spray. Compare with Figure 18

FIG. 20.— BOYSEN DAM, LEFT VALVE OF OUTLET WORKS BASIN DISCHARGING 732 CFS LOOKING UPSTREAM

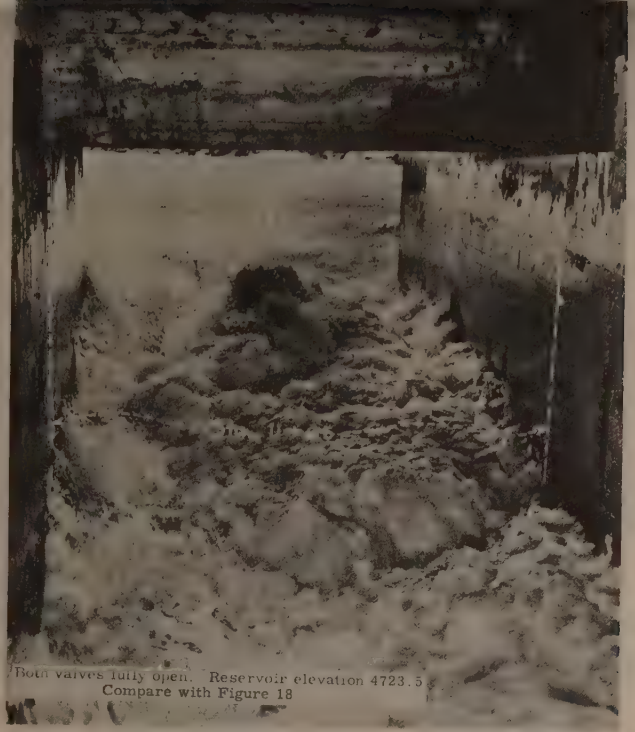

Both valves fully open. Reservoir elevation 4723.5 Compare with Figure 18

FIG. 21.—BOYSEN DAM, LEFT VALVE OF OUTLET WORKS BASIN DISCHARGING 732 CFS LOOKING DOWN-STREAM

Both valves fully open and both turbines operating at normal load. Reservoir elevation 4723.5. Tailwater elevation 4617. Compare with Figure 19.

FIG. 22.—BOYSEN DAM OUTLET WORKS DISCHARGING 1344 CFS

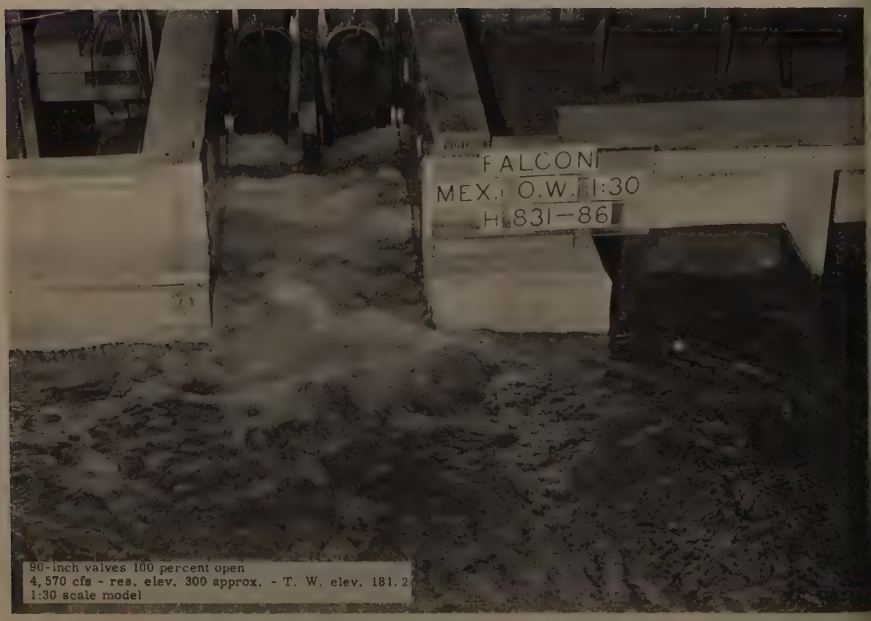

90-inch valves 100 percent open
4,570 cfs - res. elev. 300 approx. - T. W. elev. 181.2
1:30 scale model

FIG. 23.—MEXICAN OUTLET WORKS - FALCON DAM

entrainment in the prototype is usually found when making model prototype comparisons, particularly when the difference between model and prototype velocities is appreciable. In other respects, however, the prototype basin was as good or better than predicted from the model tests.

For the initial prototype test, only the left outlet valve was operated; the powerhouse was not operating. At the gaging station, the discharge was measured to be 732 cfs after the tail water stabilized at elevation 4614.5. (This is a greater discharge than can be accounted for by calculations. It is presumed that valve overtravel caused the valve opening to exceed 100% even though the indicator showed 100% open.) It was possible to descend the steel ladder, Fig. 1, to closely observe and photograph the flow in the stilling basin, Figs. 20 and 21. The basin was remarkably free of surges and spray; the energy dissipating action was excellent. There was no noticeable vibration at the valves or in the basin. The flow leaving the structure caused only slightly more disturbance in the tailrace than the flow from the draft tubes when the turbines were operating at normal load.

Operation of the prototype provided an opportunity to check the air requirements of the structure, which could not be done on the model. With the inspection cover removed, Fig. 1, the basin was open to the rooms above. Air movements through the inspection opening and in the powerplant structure were negligible, which indicated that ample air could circulate from the partially open end of the stilling basin, Fig. 21.

When both valves were discharging fully open, the tail water stabilized at elevation 4615. A discharge measurement at the gaging station disclosed that both valves were discharging 1,344 cfs. Since the left valve had been found to discharge 732 cfs, the right valve was discharging 612 cfs.

The reason for the difference in discharge is that the 57-inch-inside-diameter outlet pipe to the left valve is short and is connected to the 15-foot-diameter header which supplies water to the turbines, Fig. 1. The right valve is supplied by a separate 66-inch-diameter pipe extending to the reservoir. Therefore, greater hydraulic head losses occur in the right valve supply line, which accounts for the lesser discharge through the right valve. Although it was apparent by visual observation that the left valve was discharging more than the right valve, Fig. 22, no adverse effect on the performance of the outlet works stilling basin or on flow conditions in the powerhouse tailrace could be found.

The outlet works basin performance was also observed with the turbines operating and the tail water at about elevation 4617. No adverse effects of the outlet works discharge on powerplant performance could be detected. Flow conditions in the tailrace area were entirely satisfactory, Fig. 22. Since the tests were made at normal reservoir level and maximum discharge, the stilling basin was subjected to a severe test.

Falcon Dam.—The outlet works basin on the Mexico side at Falcon Dam is designed to accommodate 4,570 cfs from two 90-in. valves or 2,400 cfs from one valve, with the valves 100% open and the reservoir at elevation 300. The tail water elevation is 181.2 when the powerplant is discharging 5,400 cfs in conjunction with both valves. The model performance of this basin is shown in Figs. 23 and 24.

The outlet works basin on the United States side at Falcon Dam is designed to discharge 2,920 cfs from two 72-in. valves, or 1,600 cfs from one valve, with the valves 100% open and the reservoir at elevation 310. Tail water is at

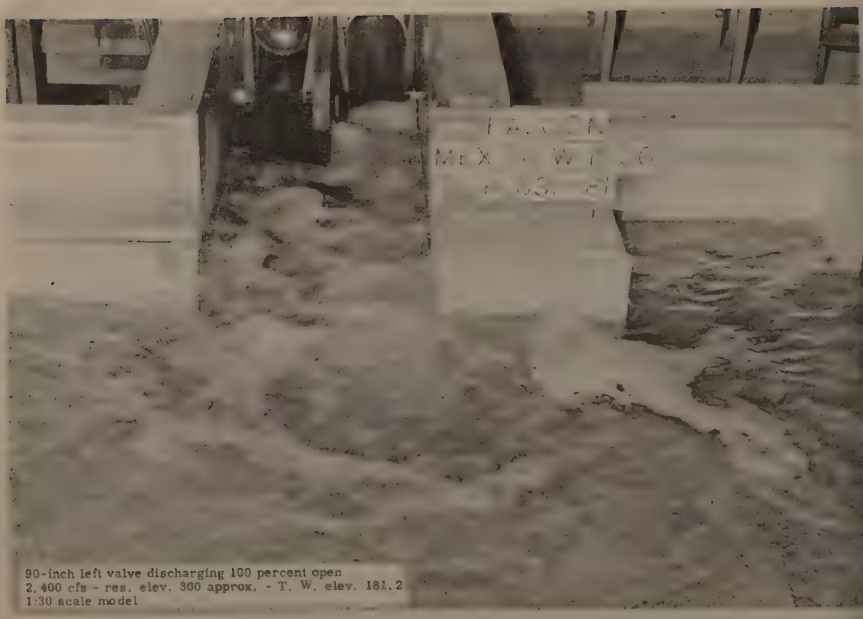

FIG. 24.—MEXICAN OUTLET WORKS - FALCON DAM

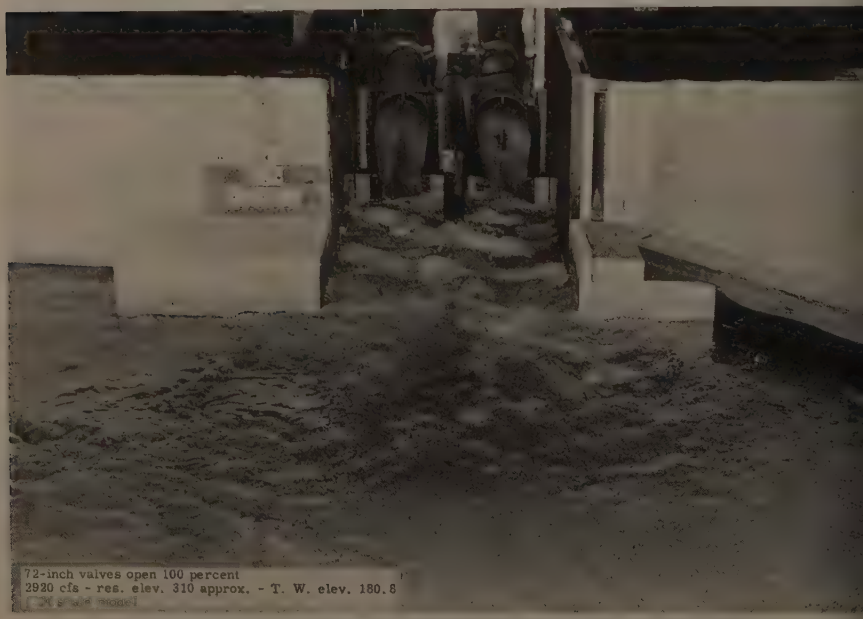

FIG. 25.—UNITED STATES OUTLET WORKS - FALCON DAM

FIG. 26.—UNITED STATES OUTLET WORKS - FALCON DAM

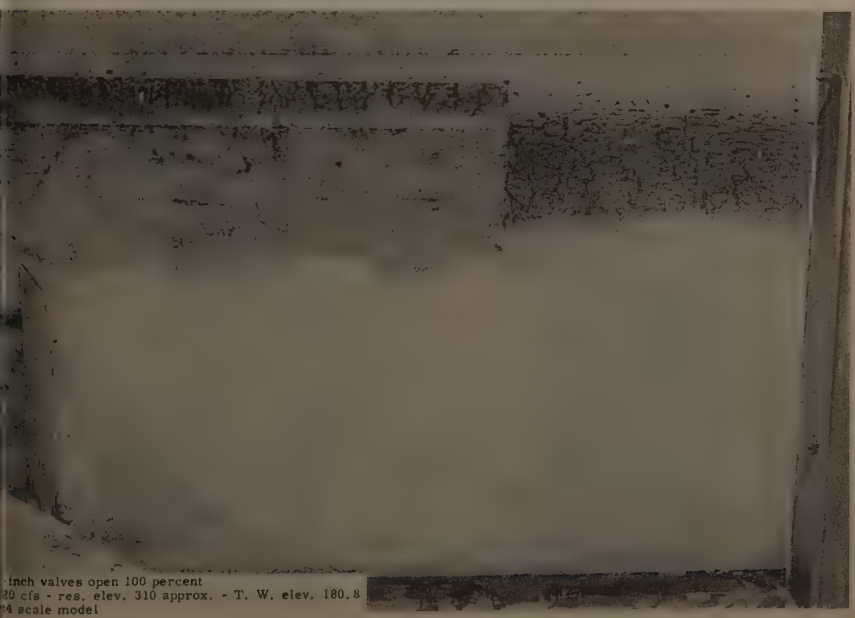

FIG. 27.—UNITED STATES OUTLET WORKS - FALCON DAM

90-inch left valve discharging - 100 percent open
2,300 cfs approx. - res. elev. 301.83. - T. W. elev. 183.0
Compare with Figure 24

FIG. 28.—MEXICAN OUTLET WORKS - FALCON DAM

72-inch left valve discharging 100 percent open
1,750 cfs approx. - res. elev. 301.83 - T. W. elev. 182.7
Compare with Figures 26 & 27

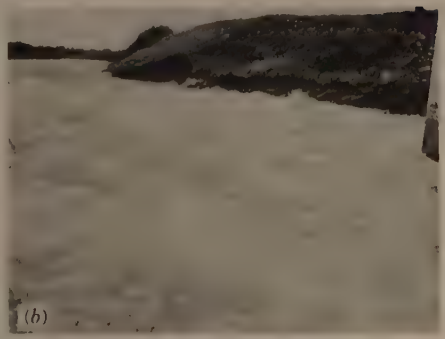

FIG. 29.—UNITED STATES OUTLET WORKS - FALCON DAM

90-inch outlet works valves open 100 percent discharging
4,500 cfs approx. - T. W. elev. 183.6.
Turbine gates 72 percent open - 100 percent load.

72-inch outlet works valves open 100 percent discharging
3,000 cfs approx. - T. W. elev. 184.1.
Turbine gates 72 percent open - 100 percent load.

FIG. 30.—FALCON DAM MEXICAN & UNITED STATES POWER-PLANTS & OUTLET WORKS DISCHARGING AT RESERVOIR ELEVATION 301.83.

elevation 180.8 when two valves are operating and 180.5 when one valve is operating. The model performance of this basin is shown in Figs. 25, 26, and 27.

The prototype tests at Falcon, Figs. 28, 29, and 30, were conducted at near maximum conditions; the reservoir was at elevation 301.83, and the valves were 100% open. In each outlet works, the valves were operated together and individually. Single-valve operation represents an emergency condition and subjects the stilling basin to the severest test, Figs. 28 and 29. All turbines at both powerplants were operating at 72% gate and 100% load during all tests. The prototype valve discharges were determined from discharge curves based on model test data.

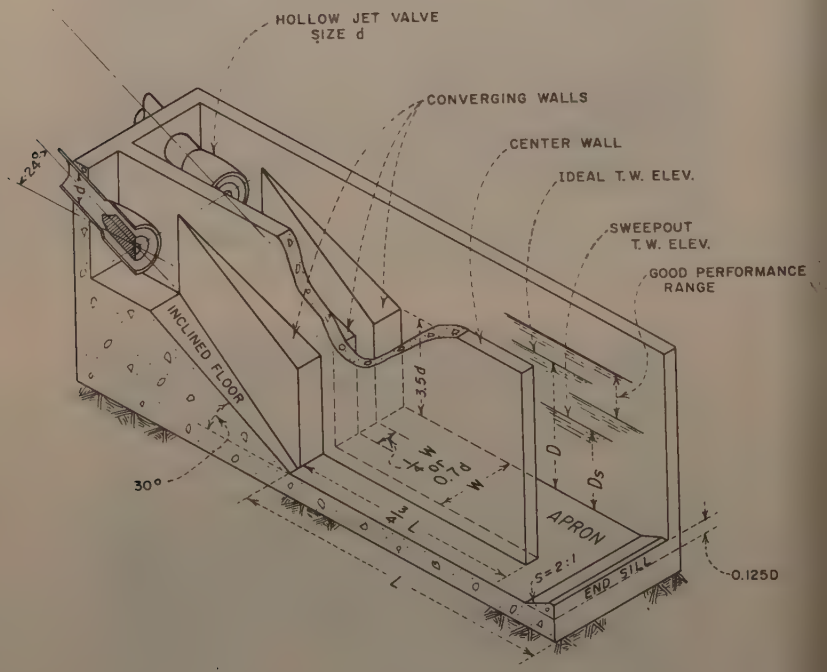

FIG. 31.—DEVELOPED BASIN

Here, too, more white water was evident in the prototype than in the model. The greater amount of air entrainment in the prototype, evident in the photographs, caused bulking of the flow at the end of the stilling basin and a higher water surface than was observed in the model. However, the prototype tail water is 3 ft to 4 ft higher than shown in the model photograph, and this probably helps to produce a higher water surface boil at the downstream end of the ba-

sin by reducing the efficiency of the stilling action. In other respects, the prototype basin performed as predicted by the model.

CONCLUSIONS

The schematic drawing, Fig. 31, shows the developed basin and the relationships between important dimensions.

A brief description of the seven steps required to design a stilling basin is given below:

1. Using the design discharge Q, the total head at the valve H, and the hollow-jet valve discharge coefficient C from Fig. 3, solve the equation $Q = C A \sqrt{2 g H}$ for the valve inlet area A and compute the corresponding diameter d which is also the nominal valve size.

2. Use H/d in Fig. 12 to find D/d and thus D, the ideal depth of tail water in the basin. Determine the elevation of the basin floor, tail water elevation minus D. It is permissible to increase or decrease D by as much as 0.4 (d).

3. Use H/d in Fig. 14 to find L/d and thus L, the length of the horizontal apron.

4. Use H/d in Fig. 15 to find W/d and thus W, the width of the basin for one valve.

5. Use H/d in Fig. 13 to find D_s/d and thus D_s, the tail water depth at which the action is swept out of the basin. D minus D_s gives the margin of safety against sweep out.

6. Complete the hydraulic design of the basin from the relationships given in Fig. 11.

7. Use the H/d ratio to select the proper photograph in Figs. 16 and 17 to see the model and help visualize the prototype performance of the design. The water surface profile may be scaled from the photograph using the scale on the photograph. To convert to prototype dimensions, multiply the scaled values by the ratio d (in.)/3.

Stilling basin dimensions calculated as indicated above are in close agreement with the dimensions obtained from individual model tests of the basins for Boysen, Falcon, Yellowtail, Trinity, and Navajo Dams, Table 1. Since the Boysen and Falcon basins performed satisfactorily during prototype tests, it is believed that satisfactory future projects may be hydraulically designed from the material presented herein.

ACKNOWLEDGMENTS

Data and material used in this paper were obtained through cooperation of individuals too numerous to acknowledge singly, yet their wholehearted interest aided materially in providing a complete analysis of the problem. Their assistance is gratefully acknowledged.

The hollow-jet valve stilling basin was developed in the Hydraulic Laboratory, Division of Engineering Laboratories, through close coordination with the Mechanical Branch and the Dams Branch of the Divsioni of Design, all of the Bureau of Reclamation, Assistant Commissioner and Chief Engineer's Office, Denver, Colorado.

The prototype tests at Boysen Dam were made with the cooperation of the Bureau's Region 6 office in Billings, Montana, and the Yellowstone-Bighorn Projects Office, Cody, Wyoming. Bureau personnel at Boysen Dam operated the hydraulic structures and assisted in obtaining data. United States Geological Survey personnel at Riverton, Wyoming, made the river gagings, and State of Wyoming personnel made downstream river adjustments to permit above-normal discharges.

The prototype tests at Falcon Dam, which included tests on both the United States and Mexico outlet works and powerplants, were conducted by personnel at Falcon Dam through arrangements with the International Boundary and Water Commission, El Paso, Texas.

Journal of the
HYDRAULICS DIVISION
Proceedings of the American Society of Civil Engineers

PREDICTION OF CAVITATION DAMAGE

By N. S. Govinda Rao,[1] F. ASCE, and A. Thiruvengadam[2]

SYNOPSIS

A non-dimensional number called cavitation damage number has been proposed, based on the concept of dynamic indentations produced by short range shock-waves due to the collapse of the cavitation bubbles. This number gives the ratio of the energy absorbed by the material in deformation to the energy of the collapse of the bubble. The cavitation damage number has been correlated with the number of cavities collapsing in a given period. The present concept adopted explains most of the experimental observations made by various research workers in this field. (A few of them being the threshold velocity for the inception of damage, incubation period, effect of time, effect of corrosion, and so on.) Experiments show that it is possible to predict the eroded length, breadth, and area if the geometry of the cavitating body and the value of the cavitation parameter are known. These results indicate the possibilities of predicting possible cavitation damage and thus aid in the proper choice of the material for fabricating any hydraulic machine or a structure.

INTRODUCTION

Although Osbourne Reynolds began experiments on cavitation as early as 94, the method of prediction of cavitation damage has still not been ration-

Note.—Discussion open until February 1, 1962. To extend the closing date one month, written request must be filed with the Executive Secretary, ASCE. This paper is part the copyrighted Journal of the Hydraulics Division, Proceedings of the American Society of Civil Engineers, Vol. 87, No. HY 5, September, 1961.

[1] Prof. of Civ. and Hydr. Engrg., Indian Inst. of Science, Bangalore 12, India.
[2] Senior Research Fellow, Civ. and Hydr. Engrg. Sect., Indian Inst. of Science, Bangalore 12, India.

alized. Because of the serious interest created by the severe destruction of ships' propellers, work was first initiated by the propeller sub-committee in 1915, and their report was published in 1919.[3] In spite of an impressive accumulation of theoretical and experimental results since then, the problems of predicting the inception of damage, the cumulative damage and the expected life of a material in a given flow system have not been solved. The work reported in this paper is a start in providing data on which the future progress in this field of study may be made.

Types of Cavitation.—Though there are various classifications available in literature, cavitation in hydraulic flow can be grouped broadly into two types: (1) cavitation that has its inception in the boundary layer (2) cavitation that has its inception in the free turbulent shear layer. For example the boundary layer cavitation takes place over a cylindrical body with hemispherical nose [Fig. 1 (a)], and the free turbulent shear layer cavitation takes place in the wake of a circular cylinder [Fig. 1 (b)]. The results presented pertain to the second group; namely, the cavitation occurring in the wake of an obstruction or a discontinuity called "cavitating body" [Fig. 1 (b)].

Existing Theories of Damage.—The various theories of damage previously propounded are given in Table 1 in chronological order. These theories can be classified into four main groups: (a) Mechanical action theory, (b) Electrochemical corrosion theory, (c) Thermodynamic melting theory, and (d) Instantaneous chemical reaction theory.

Mechanical Action Theory.—Workers espousing the mechanical action theory differed in the actual mechanism or process by which the material is removed. Parsons and Cook,[4] Fottinger, Ackeret[5,6] and deHaller[7,8] came to the conclusion that the water hammer pressures were the main reason for the damage. This concept is practically the origin of all the other theories. Boetcher[9] introduced the idea of surface fatigue and found that the pieces were removed from surface by fatigue cracks. This idea was followed by the individual dent formation concept. These dents were photographed as early as 1935 by J. C. Hunsaker.[10] Poulter[11] imagined that liquid particles penetrated through the crevices in the material and shattered the material due to high pressures of collapse of the bubbles.

Electro-Chemical Corrosion Theory.—The electro-chemical corrosion theory has gained support because of the observed decrease in damage due to cathodic protection reported by Petracchi,[12] Nechleba[13] and Wheeler. But the idea of corrosion fatigue explains all these observations.

Thermodynamic Action Theory.—The thermodynamic action theory was suggested by Wislicenus.[14] But there is no experimental evidence that the adia-

---

[3] "Investigations into the Causes of Corrosion or Erosion of Propellers," by C. A Parsons and S. S. Cook, Engineering, Vol. 107, 1919, p. 515.

[4] Item 1 Table 1.

[5] Items 3,4 Table 1.

[6] Items 3,4 Table 1.

[7] Items 4,6 Table 1.

[8] Items 4,6 Table 1.

[9] Item 5 Table 1.

[10] "Progress Report on Cavitation Research at M.I.T.," by J. C. Hunsaker, Transactions, ASME, 1935, p. 423.

[11] Item 11 Table 1.

[12] Item 13,14 Table 1.

[13] Items 13,14 Table 1.

[14] Item 12 Table 1.

TABLE 1.—THEORIES OF DAMAGE

Year	Author	Details of the Mechanism Proposed
(1919)	Parsons and Cook	Conducted nose cone experiment demonstrating water hammer pressures. First to propose the mechanical action theory
(1917)	Rayleigh	Calculation of the energy of collapse of the bubble Showed the possibility of high intensity pressures
(1926)	Ackeret, J.	First to suggest the effect of flow velocity on the intensity of erosion. Based on this fact he discarded the corrosion theory and accepted the mechanism of cavity collapse as the case cause of damage
(1932)	Ackeret, J.	
(1933)	de Haller	He concluded that in several tests the pressures developed by the collapse of voids, both calculated and observed, are of too small an order of adequately to account for cavitation damage
(1935)	Boetcher, H. M.	'Surface fatigue' or 'cavitation fatigue'. First to find a correlation between damage and hardness. He recommends high corrosion fatigue strength as remedy
(1936)	Ackeret and de Haller	They used a percussion wave to produce superficial damage on various metals and demonstration of mechanical damage
(1937)	Vater, M.	Suggested 'Periodic strains'
(1938)	Mueller, H.	First to suggest the concept of threshold velocity for each material below which no damage can be caused to occur. Compares threshold velocity to fatigue limit. Suggested that the mechanical action depends on the corrosive influence of the testing liquid
(1941)	Beeching	Metal surface is disrupted by local stresses resulting from the collapse of vapour pockets. Accepts an influence of corrosion similar to its influence on fatigue limit
(1948)	Knapp, R. T. and Hollander	Studied the life history of the bubble and found agreement with Rayleigh's calculations
(1947)	Poulter	Suggested liquid penetration through crevices and pushing the material out by the liquid momentarily under high pressure
(1947)	Wislicenus	Increase in temperature due to adiabatic compression of the bubble and local melting of the material. No experimental proof
(1949)	Petracchi	Influence of cathodic protection. Electric currents due to local mechanical stresses
(1955)	Nechleba, M.	Generation of corrosive currents to a thermocouple action resulting from local heating of the metal by the temperature rise of the collapsing cavity. Supports Poulter's view
(1955)	Plesset and Ellis	First to prove plastic deformation by X-ray diffraction patterns
(1955)	Knapp, R. T.	Suggested that at the instant of collapse, minute regions of high intensity 'water hammer' pressures are produced. The stored energy radiates from the collapse centre as a spherical shock wave whose intensity decreases rapidly as its radius increases.
(1955)	Guth, W.	First to photograph the shock wave radiated from the bubble by means of Schlieren's Photographic Method
(1955)	Irving Taylor	Conjectures about instantaneous chemical action from nascent radicals. No experiments

batic compression of the bubble can produce that order of temperatures so as to melt the materials. Materials such as stone, concrete, and brick get damaged at much lower velocities, in which case the temperature produced would be very low when compared with the temperature required to melt these materials.

The instantaneous chemical reaction theory proposed by Irving Taylor[15] has no experimental evidence.

Theory Adopted.—Theory adopted in the present investigations is based on the mechanical action theory. During the positive pressure phase of the life cycle of the cavitation bubble, it collapses due to the condensation of vapor inside the bubble as a result of the increase in pressure of the surrounding liquid that then flows radially inwards. Near the center, the motion is arrested violently, and the kinetic energy of the violent hydrodynamic mass is largely

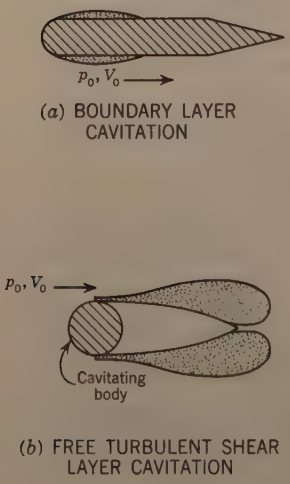

FIG. 1

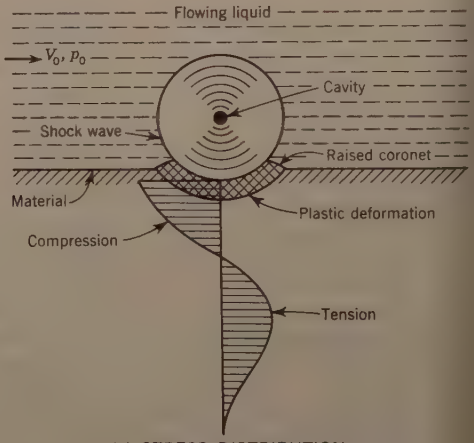

FIG. 2.—DEFINITION SKETCH FOR THE SHOCK WAVE AND DEFORMATION

converted into an intense but short range shock wave. It is this high pressure shock wave that is mostly responsible for the deformation of the material. The dents so formed were photographed by R. T. Knapp[16] by using soft annealed aluminum. W. Güth photographed the shock waves by using the Schlieren method.[17] The writers have produced similar dents in several materials like brass, copper, stainless steel, and aluminum.

If a bubble produces a shock wave whose intensity is more than the dynamic yield strength of the material, then the material is plastically deformed. It is

[15] Item 18 Table 1.

[16] "Recent Investigations of Cavitation and Cavitation Damage," by R. T. Knapp, Transactions, ASME, Vol. 77, 1955, p. 1050.

[17] "The Formation of Pressure Waves by Cavitation," by W. Guth, Proceedings, Symposium on Cavitation in Hydrodynamics, N.P.L. London, Appendix 1, 1955.

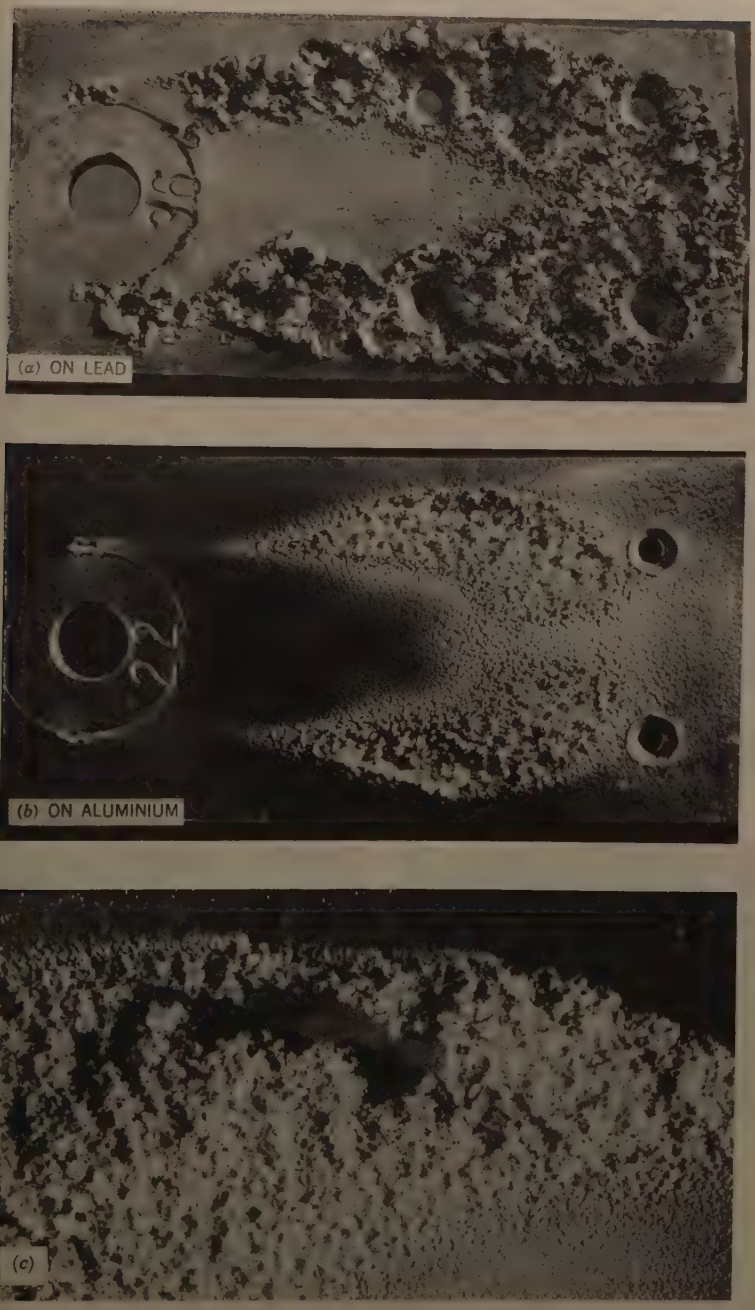

FIG. 3.—DAMAGE BEHIND CIRCULAR CYLINDER

displaced sideways towards the free surface, undergoing relatively severe distortion to produce the raised coronet, characteristic of indentation (Fig. 2).

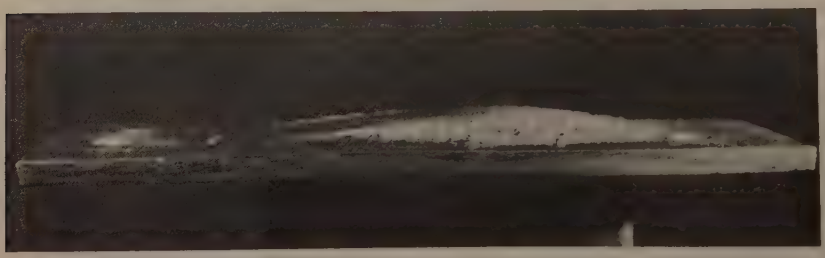

FIG. 4.—BULGING OF THE PLATE SIMILAR TO A SHOT-PEENED PLATE

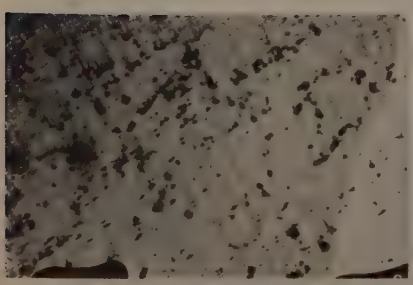

(*a*) UNDAMAGED SURFACE

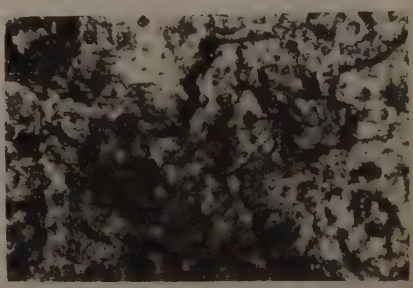

(*b*) DEVELOPMENT OF DAMAGE

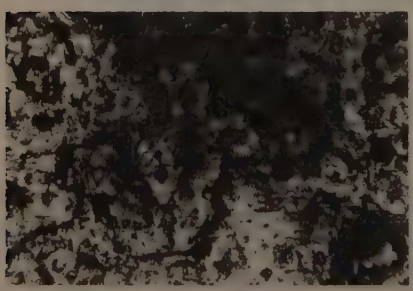

(*c*) FLOW OF METAL

(*d*) FORMATION OF DEEP CRATERS

FIG. 5.—MICROPHOTOGRAPH OF ALUMINUM SURFACE

When innumerable bubbles are collapsing, deep pits are formed and the surface becomes spongy [Figs. 3 (a), 3 (b) and 3 (c)]. The test piece bulges out as in the case of shot-peening (Fig. 4).

By micro-examination it is possible to detect the distorted metal and fatigue cracks. Figs. 5 (a), 5 (b), 5 (c) and 5 (d) show the plan view of the test piece as shown in a metallurgist microscope magnified eighty-four times. Fig. 5 (a)

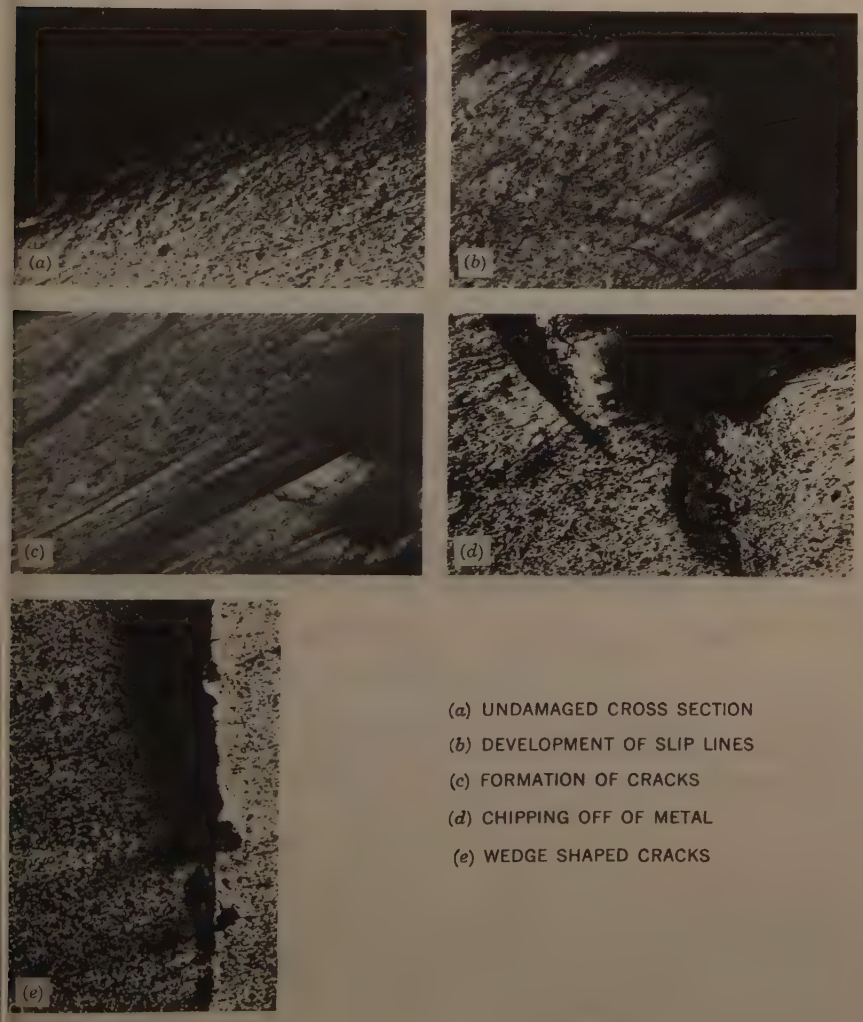

FIG. 6.—CROSS SECTION OF DAMAGED PLATE

hows the undamaged surface, and Figs. 5 (b), 5 (c) and 5 (d) show how the lastic deformation develops into big craters. Because the shock pressures re repeated, the failure will have to be cumulative as in the case of progres- ive fatigue failure. Figs. 6 (a), 6 (b), 6 (c), 6 (d) and 6 (e) show the cross-

section of the aluminum test piece (at 84 times magnification) at various stages of the deformation. Figs. 6 (b) and 6 (c) show how cracks are formed due to repeated impacts. Figs. 6 (d) and 6 (e) show how material gets chipped off from the surface finally. Fig. 7 shows the spherical dents produced by the shock waves going through towards the backside of the plate. The photo has been taken from the backside of the test piece.

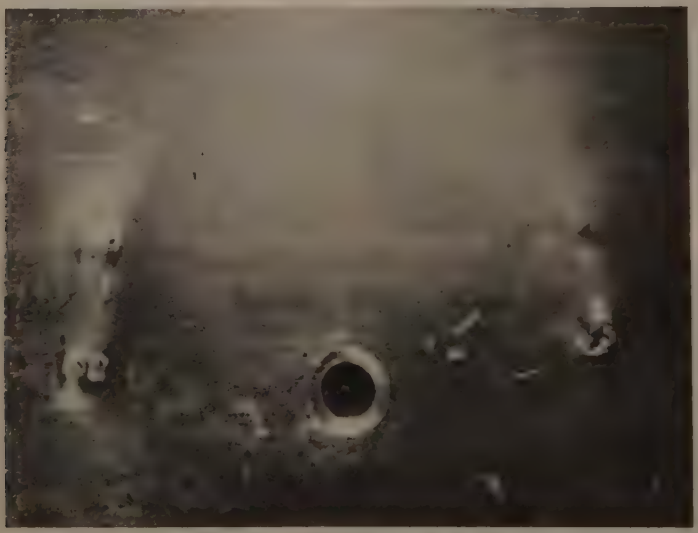

FIG. 7.—BACKSIDE OF PLATE SHOWING SPHERICAL DENTS THROUGH AFTER 14 HR

Notation.—The letter symbols adopted for use in this paper are defined where they first appear, in the illustrations or in the text, and are arranged alphabetically, for convenience of reference, in the Appendix.

CAVITATION DAMAGE NUMBER

If one imagines the shock waves as solid balls dynamically impinging over the solid surface, just as in the case of the dynamic hardness tests, the volume deformed is proportional to the energy creating the indentation. The energy creating the indentation is proportional to the energy of collapse of the bubble. Hence the volume deformed, the dynamic yield stress of the material, and the energy of collapse are related by

$$Y \, \Delta v \propto E_c \quad \ldots\ldots\ldots\ldots\ldots\ldots (1)$$

in which Y is the dynamic yield stress of the material, Δv denotes the volume deformed per collapse of the bubble and E_c refers to the energy of collapse of each bubble.

Now the energy of collapse of the bubble E_c is given by

$$E_c \propto p_o \, R_o^3 \quad \ldots\ldots\ldots\ldots\ldots\ldots (2)$$

in which p_o is the static pressure of the liquid surrounding the bubble at the moment the bubble begins collapsing and R_o is the maximum possible radius of the bubble at the beginning of the collapse. The value of R_o can be estimated from the equation

$$p_{min} + \frac{2\sigma}{R_o} = p_v \quad \ldots\ldots\ldots\ldots\ldots\ldots \quad (3)$$

in which p_{min} is the minimum pressure the liquid can withstand (that is, the tensile strength of the liquid), σ is the surface tension of the liquid and p_v is the vapor pressure of the liquid.

Hence,

$$R_o = \frac{2\sigma}{p_v - p_{min}} \quad \ldots\ldots\ldots\ldots\ldots\ldots \quad (4)$$

Therefore, the value of R_o depends only on the physical properties of the liquid such as the tensile strength, vapor pressure, and surface tension. In this case p_{min} will be a function of the gas content of the liquid and p_v will have to be corrected for the partial pressures of gases in the liquid.

Now it is necessary to estimate the number of bubbles per cavity. Each bubble would occupy an area equal to πR_o^2. If the area of the cavity is A_c then the number of bubbles n per cavity is given by

$$n = \frac{A_c}{\pi R_o^2} \quad \ldots\ldots\ldots\ldots\ldots\ldots (5)$$

The volume deformed per bubble is Δv, which from Eqs. 1 and 2, is

$$\Delta v = \frac{E_c}{Y} \propto \frac{p_o R_o^3}{Y} \quad \ldots\ldots\ldots\ldots\ldots\ldots (6)$$

Therefore, the total volume v deformed per cavity is

$$v = n\,\Delta v \propto \frac{A_c}{\pi R_o^2} \frac{p_o R_o^3}{Y} = \text{constant}\, \frac{A_c\, p_o\, R_o}{Y} \quad \ldots\ldots\ldots (7)$$

Hence,

$$\frac{v\,Y}{A_c\, p_o\, R_o} = \text{constant} \quad \ldots\ldots\ldots\ldots\ldots\ldots (8)$$

But v/A_c is the average depth of erosion if the area of erosion A_e is taken equal to the area of the cavity A_c (Fig. 18); that is

$$\frac{v}{A_e} = i \quad \ldots\ldots\ldots\ldots\ldots\ldots (9)$$

That is, v is the volume deformed per cavity, A_e is the area of erosion (which is equal to the area of the cavity), and i is the average depth of erosion. The value i is a measure of the intensity of erosion.

Eq. 8 yields the ratio of the energy absorbed by the material to the energy of collapse of the bubble for one cycle. If there are N cycles, the cumulative energy absorbed by the material will be equal to $Y \sum_0^N i$. The total energy of

collapse will be proportional to $N\ p_o\ R_o$. Hence, the ratio of the energy absorbed by the material for the deformation to the total energy expended by the cavities in doing work after N cycles is given by

$$\frac{Y \sum_{0}^{N} i}{N\ R_o\ p_o} = \text{constant} \quad \ldots\ldots\ldots\ldots\ldots\ldots (10)$$

Eq. 10 gives a non-dimensional number known as the "cavitation damage number."

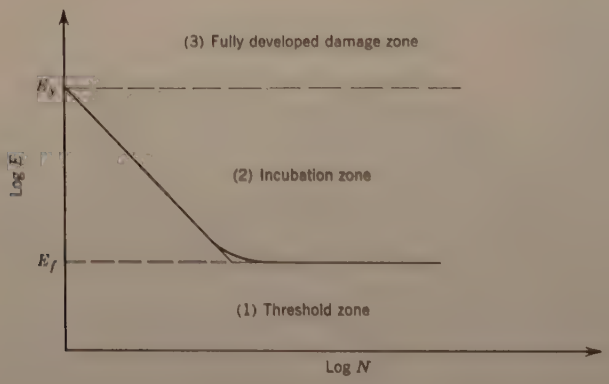

FIG. 8.—E-N DIAGRAM

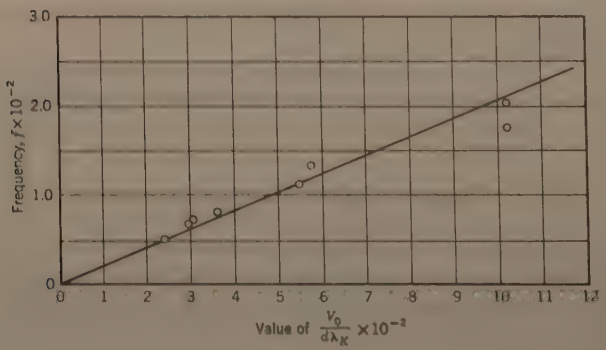

FIG. 9.—FREQUENCY AS A FUNCTION OF $\frac{V_o}{d\lambda_K}$

The exact relationship between the cumulative absorption of energy by the material and the number of cycles of dynamic indentation is an unsolved problem in plasticity. If the mechanism of repeated dynamic indentation is as-

sumed to be similar to the Charpy's impact fatigue,[18] then the E - N diagram in which E is the energy of indentation and N is the number of indentations, (Fig. 8) can be divided into three zones.

Zone 1.—When the energy of indentation E is below the fatigue limit of indentation (E_f) which will produce no plastic deformation for infinite number of cycles, then there is no damage at all. This is called the threshold zone $E < E_f$.

Zone 2.—When the energy of indentation is above the fatigue limit (E_f) but below the yield limit (E_Y) (the yield limit being the minimum energy of indentation for which the plastic deformation takes place at the first cycle itself), then the damage will start after a given number of cycles depending on the energy level of the indentation. This zone is called the incubation zone. The number of cycles required for incubation is denoted as N_i. The N_i and E are related by[19]

$$(N_i)^m E = \text{constant} \quad \ldots\ldots\ldots\ldots\ldots\ldots (11)$$

in which m is a constant depending on the material.

Zone 3.—When the energy of indentation is more than the yield energy, then the damage starts from the first cycle. This is called the fully developed damage zone. In the present paper only the third zone will be analyzed in detail.

NUMBER OF CAVITIES

Now the number of cycles through which the indentation has undergone is equal to the number of cavities produced by the flow. In 1935, Hunsaker[10] found that the Strouhal number was a constant if the length of the cavity is taken as the linear dimension.

$$\frac{f\,l}{V_o} = \text{constant} \quad \ldots\ldots\ldots\ldots\ldots\ldots (12)$$

in which f is the frequency of shedding of the cavities, l is the length of the cavity, and V_o is the velocity of flow. In 1955, K. K. Shalnav[20] reported that for a given length of the cavity the frequency was directly proportional to the velocity. The writers, using Knapp's data[21] found that Hunsaker's finding was true even for axis-symmetric cavities. Hence, it is assumed that this relationship is true irrespective of the geometry, and only the constant of proportionality will change with geometry.

---

18 Fatigue of Metals, by H. F. Moore and J. B. Kommers, McGraw-Hill Book Co., Inc., New York, 1st edition, 1927, p. 171.

19 "A Generalisation of Cumulative Damage," by R. M. Mains, Transactions, ASME, Journal of Basic Engineering, Vol. 82, 1960, p. 435.

20 "Experimental Study of the Intensity of Erosion Due to Cavitation," by K. K. Shalnav, Proceedings, Symposium on Cavitation in Hydrodynamics, N.P.L. London, 1955, p. 22-1.

21 "Further Studies of the Mechanics and Damage Potential of Fixed Type of Cavities," by R. T. Knapp, Symposium on Cavitation in Hydrodynamics, N.P.L. London, 1955, p. 19-1.

Eq. 12 can be written as

$$\frac{f\,d}{V_o}\frac{l}{d} = \text{constant} \quad \ldots\ldots\ldots\ldots\ldots\ldots (13)$$

in which d is the characteristic linear dimension of the body as used in the Strouhal number and l/d is the relative length of the cavity, λ_K.

Hence,

$$f \propto \frac{V_o}{d\,\lambda_K} \quad \ldots\ldots\ldots\ldots\ldots\ldots (14)$$

This relationship is shown in Fig. 9 plotted from Knapp's data.[21]

Now the number of cycles of indentation will be equal to the number of cavities that have passed in a given time t. Hence.

$$N = f\,t \propto \frac{V_o t}{d\,\lambda_K} \quad \ldots\ldots\ldots\ldots\ldots\ldots (15)$$

Experimental investigations were conducted to determine the relationship between the cavitation damage number C_D and the number of cycles of indentation N.

EXPERIMENTAL SET-UP AND PROCEDURE

For these studies, two set-ups were used. One was the rotating disc apparatus first used by R. E. H. Rasmussen[22] and developed by the United States Navy.[23] The second one was a two-dimensional open circuit water tunnel.

Rotating Disc Apparatus.—The rotating disc apparatus consisted of a circular chamber in which a circular metallic disc was rotated at controlled speeds by means of a variable speed motor (Fig. 10). The test liquid was circulated through the chamber by means of a pump. The pressure and the quantity of the liquid in circulation could be controlled by means of two valves one upstream and one downstream of the chamber. By controlling the quantity of the liquid in circulation, the temperature of the liquid could be controlled. The rotation of the liquid within the chamber along with the rotating disc was reduced by providing baffle plates on both sides of the rotating disc. A total clearance of 5/8 in. was allowed for the disc to rotate between the baffles. The disc was made from two 1/16 in. metal plates fixed to each other. Several holes of various diameters were made through the disc and the test specimens were fixed behind the circular and rectangular holes of various sizes.

Two-dimensional Open Circuit Water Tunnel.—The two-dimensional open circuit water tunnel consisted of a 100 hp turbine pump, pressure regulating

22 "Some Experiments on Cavitation Erosion in Water Mixed with Air," by R. E. H. Rasmussen, Symposium on Cavitation in Hydrodynamics, N.P.L. London, 1955, p. 20-1.

23 "Study of Corrosion and Cavitation Erosion Damage," by J. Z. Lichtman, D. H. Kallas, C. K. Chattan, and E. P. Coehran, Transactions, ASME, Vol. 80, 1958, p. 1325.

FIG. 10.—LAYOUT OF ROTATING DISC APPARATUS

manifold, bypass needle valve, contraction cone, test section, and diffuser. The test section was 4 in. by 3/4 in. by 13 in. The maximum velocity attainable at the test section was 100 fps with a static pressure of 200 ft. Fig. 14 shows the layout. A circular cylinder was fixed in the test section and the damage shown

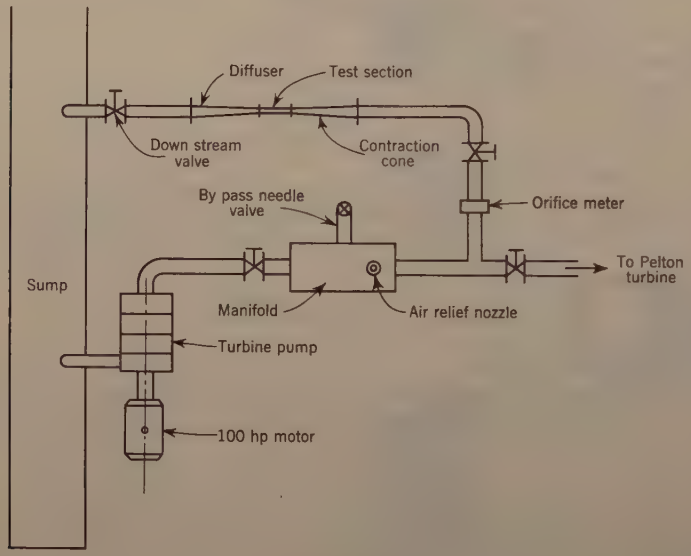

FIG. 11.—LAYOUT OF TWO-DIMENSION WATER-TUNNEL

in Figs. 3 (a), 3 (b), was reproduced in the wake of the cylinder. Further details regarding this tunnel are available.[24]

EXPERIMENTAL RESULTS AND ANALYSIS

Prediction of Damaged Area.—Firstly it is necessary to predict the length, the breadth, and the area of damage so that that particular area can be protected by a stronger material. Further the area of damage is required to compute the total volume loss from the cavitation damage number. Therefore, experiments were conducted with a circular cylinder as the cavitating body that produced cavitation when it was kept in a stream of flow. These experiments were conducted in the two-dimensional open-circuit water-tunnel described previously. The geometry of the flow behind the circular cylinder can be considered as being of three regions at high Reynolds numbers. In a thin layer around the body the first region will be the boundary layer flow; outside this layer at the front and sides of the body the flow is irrotational; behind the body

24 "Cavitation and Cavitation Damage," by A. Thiruvengadam, thesis presented to the Indian Inst. of Science, in Bangalore, India, in 1959, in partial fulfillment of the requirements for the degree of Master of Science.

there will be the third region of free turbulent shear flow or wake flow. The wake region consists of two zones divided by the free streamlines (Figs. 12 and 13). The first zone is a region of high shear due to velocity gradient, and it is

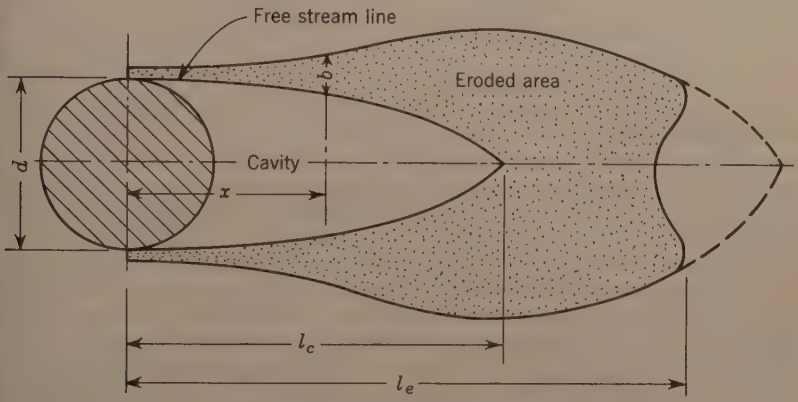

FIG. 12.—CAVITY FLOW (DEFINITION SKETCH)

FIG. 13.—DAMAGE IN THE SHEAR LAYER

extremely turbulent. The second zone is a region of comparatively low disturbance. The shear layers springing from both the sides of the cylinder

merge with each other after some diameters from the cylinder. The velocity distribution becomes uniform again at an infinite (large) distance from the body. In the case of high velocity flow of a liquid, the second zone becomes gaseous filled with the vapor of the liquid. The inner boundary of the shear layer becomes the free-streamline of the classical theory (the condition of free-streamline being that the velocity and, hence, pressure should be constant along the streamline).

By the method of conformal transformation coupled with the free-streamline theory, Riabouchinsky, Birkhoff[25] and various other workers have tried to evaluate the boundary of the wake cavity. Such a procedure deals only with an ideal liquid. They cannot be applied to a real liquid that is in a highly turbulent two phase flow. The classical theories deal merely with the overall forces or changes in pressure rather than the local details of the flow pattern. In fact, the real conditions of flow are quite contradictory to the free-streamline theory at the junction of the boundary of the wake and the irrotational flow covering it. Because of the high shear along the unguided surfaces of discontinuity at the boundary, the wake, which is a large cavity itself becomes the seat of intense turbulence that diffuses laterally as it is carried downstream (especially at flows of high Reynolds numbers). This can be seen through a stroboscope. The cavitation damage takes place only at the boundary of the cavity. Each vortex in the shear layer is entrained with a cloud of vapor bubbles, and the diffusion of these bubble-filled vortices into the main flow causes the collapse of these bubbles. Fig. 13 is in support of this view. There is no damage within the free-streamlines, as there is no violent collapse of the bubbles, because of the constancy of pressure within the free-streamlines (dotted lines in Fig. 13). Fig. 12 is an actual plot of this shear layer in relation to the circular cylinder (full scale). Fig. 14 shows the variation of the width of erosion with the longitudinal distance. From this it can be concluded that the width of erosion follows the pattern of vortex diffusion in the turbulent shear layer.

Experiments were conducted to study the manner in which the eroded dimensions vary with cavitation parameter. The rotating disc apparatus (Fig. 10) was used for this purpose. The velocity, pressure and size of the hole were varied independently in the rotating disc apparatus. Figs. 15 (a), 16 (a) and 17 (a) show how the relative length of erosion, relative breadth of erosion, and the area of erosion vary with the cavitation parameter for circular holes of 1.27 cm, 0.95 cm, and 0.635 cm. Figs. 15 (b), 16 (b) and 17 (b) show the same relationship for square holes of 1.27 cm, 0.95 cm, and 0.625 cm. These results indicate that the eroded area and the relative length of the cavity depend only on the cavitation parameter and the geometry of the flow system. This result will be useful in predicting the eroded area of prototypes from model studies.

The area of erosion is a function of time because of the cumulative nature of the damage. The area increases with time until it becomes equal to the area of the cavity itself. This relationship is plotted in Fig. 18 for two values of K. Throughout this analysis only the final area has been taken as the area of erosion.

---

25 Wakes, Jets and Cavities, by G. Birkoff and E. H. Zarantonello, Academic Press, New York, 1957.

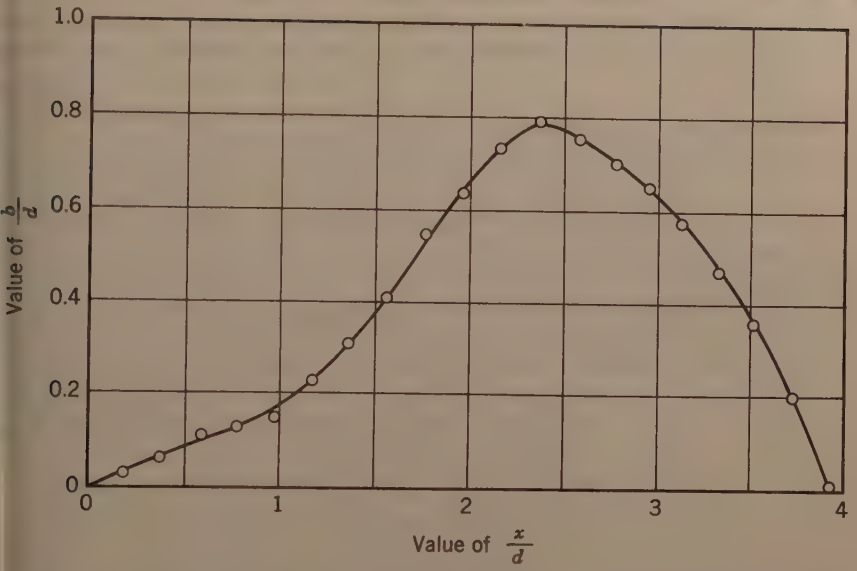

FIG. 14.—VARIATION OF WIDTH OF DAMAGED AREA WITH LONGITUDINAL DISTANCE

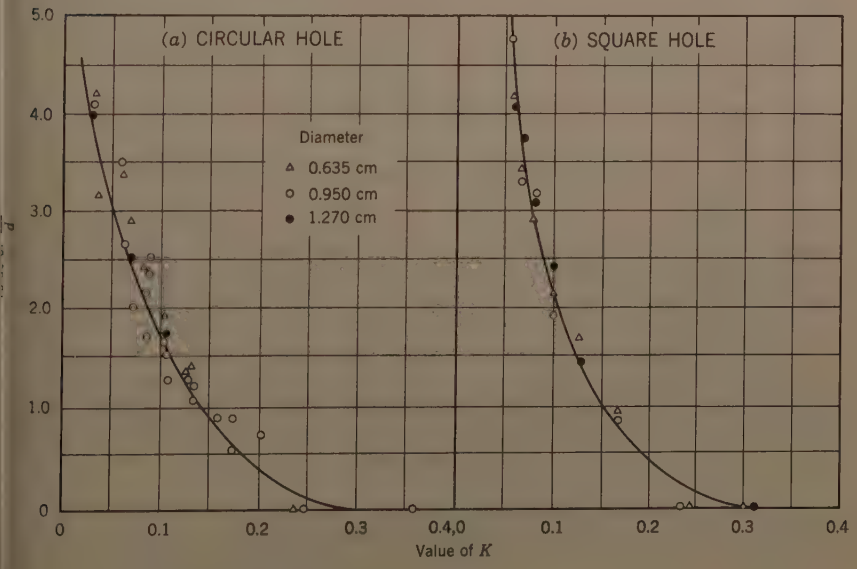

FIG. 15.—RELATIVE LENGTH VERSUS CAVITATION PARAMETER, K

Prediction of Cavitation Damage.—Experiments were conducted to determine the relationship bewteen the cavitation damage number C_D and the number of cycles of stress application. The cumulative increase in the average

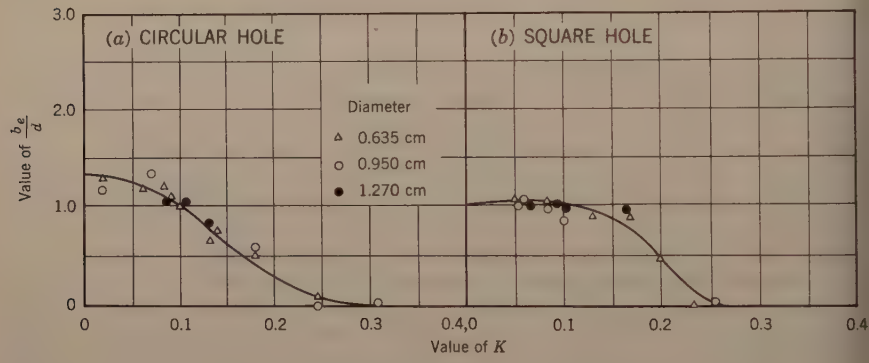

FIG. 16.—RELATIVE BREADTH VERSUS K

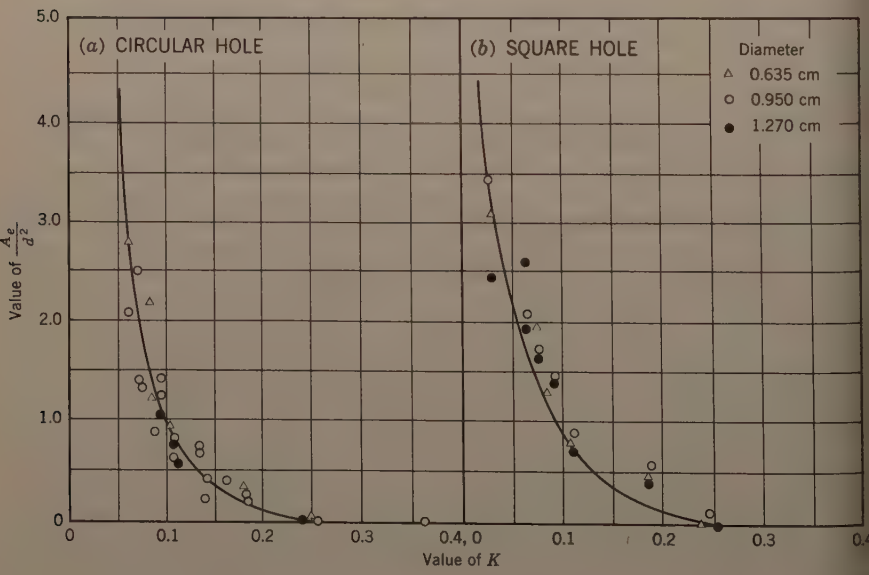

FIG. 17.—RELATIVE AREA VERSUS K

depth of erosion $\sum i$ was computed by finding out the weight loss and dividin it by the area of the cavity and the density of the material,

$$\sum i = \frac{\sum \Delta w}{\rho_m A_e} \quad \ldots\ldots\ldots\ldots\ldots\ldots \quad (16)$$

which $\sum \Delta w$ is the weight loss, ρ_m denotes the density of the material, and e refers to the final area of erosion. The number of stress applications was ken to be equal to the number of cavities given by Eq. 15. The pressure at hich the bubbles start collapsing was assumed to be proportional to the free ream pressure p_o. The maximum radius R_o of the bubbles was assumed to e constant for a given temperature. The value of C_D was calculated, based on ese assumptions. As the material used was 99% pure aluminum, the value of e yield stress as given by the manufacturer was taken to be equal to 786 kg r sq cm. The pressure was varied from 0.351 kg per sq cm to 1.05 kg per cm, and the velocity was varied from 34.6 m per sec to 46.6 m per sec. ie experiments were stopped after 2 min, 5 min, 10 min, 20 min, and 30 min

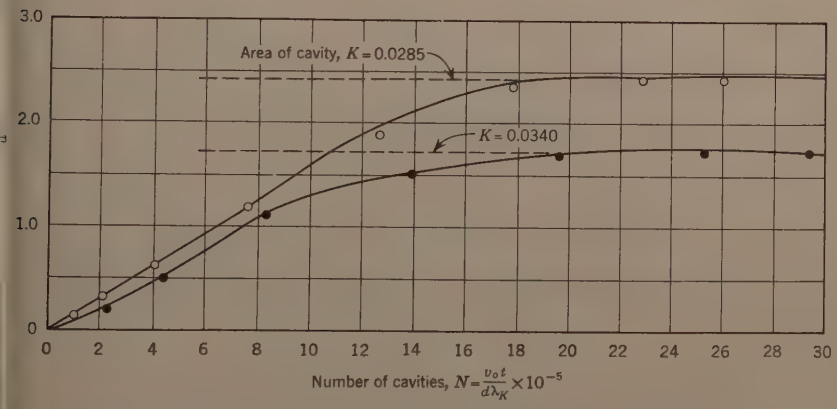

FIG. 18.—EFFECT OF TIME ON THE AREA OF DAMAGE

ervals. For each pressure and velocity, the total duration of tests varied m 2 hr to 3 hr. Fig. 19 (a) shows the relation between C_D and N for square es. The variables were V_o, p_o, λ_K, t and d. There seems to be an excellent relation between C_D and N. Fig. 19 (b) shows C_D as a function N for cir- ar holes. Fig. 19 (c) shows the results for a circular cylinder kept in the -dimensional open circuit water tunnel. In this case time was the only iable. These experimental results support the theory of the shock wave in- tation and the concept of the cavitation damage number. In addition to this, correlation is useful for the prediction of the cumulative damage caused cavitation.

The phenomenon of cavitation damage involves three major groups of var- es: (1) the properties of the material; (2) the properties of the liquid; and the characteristics of the flow.

Experiments were conducted in the two-dimensional open circuit tunnel to estigate the effect of the mechanical properties of the material. Five sheets ommercially pure (99%) aluminum with different mechanical properties

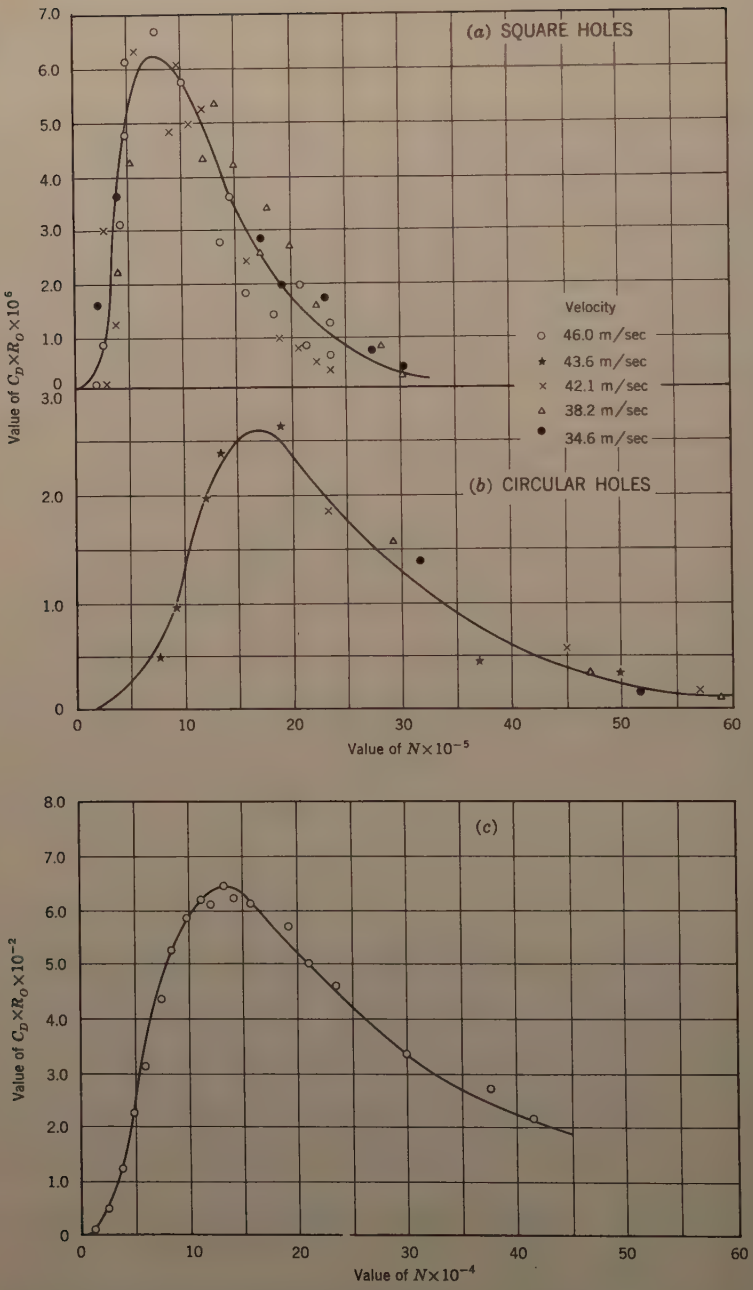

FIG. 19.—CAVITATION DAMAGE NUMBER AS A FUNCTION OF NUMBER OF CAVITIES

vere procured from the Indian Aluminum Company and tested. The results re shown in Figs. 20 (a), 20 (b), 20 (c) and 20 (d). It can be seen that $\sum i$ is nversely proportional to all the mechanical properties because each mechanical property is proportional to the other. The same chemical composition vas used to ensure that there was no corrosion otherwise. Another important oint is that none of the five sheets underwent any static corrosion in the months they were used for tests in the laboratory water.

In the case of brittle materials like concrete, brick, and stone the damage s again inversely proportional to the compressive strength of the material Fig. 20 (e)]. These facts indicate that in the absence of any external static

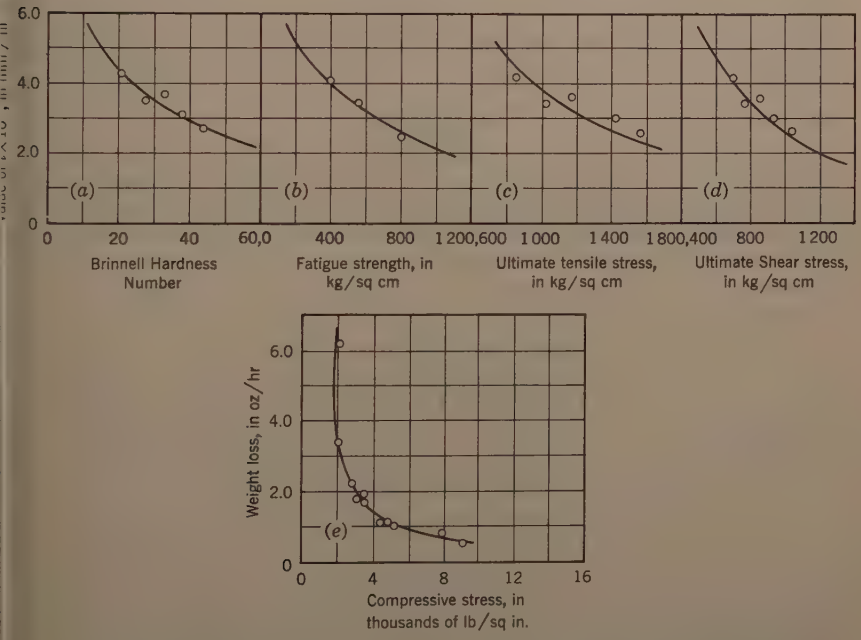

IG. 20.—EFFECT OF MECHANICAL PROPERTIES OF THE MATERIAL ON DAMAGE

orrosion by the liquid, the mechanical property may be used to represent the roperty of the material. This explains the inclusion of yield stress in the avitation damage number.

The properties of the liquid had not been varied in this investigation. The quid tested was laboratory water at 32°C. The temperature was that of the owing water. But the concept of cavitation damage number still takes into ccount the physical properties of the liquid such as surface tension, vapor ressure, and the tensile strength of the liquid that, again, depends on the gas ontent of the liquid. It is assumed that R_0 is constant as long as these properties are the same. The validity of this assumption is yet to be established.

It is now necessary to investigate the manner in which the characteristics the flow such as the geometry of the flow, pressure, velocity, and time af-

fect the phenomenon. For a given geometry, the number of cavities produced is a function of the velocity of flow, time, the characteristic linear dimension, and the relative length of the cavity. The relative length of the cavity again depends on the pressure and velocity of flow. Finally, the energy level of collapse depends on the pressure. Hence, all these parameters were varied in the experiments, and the correlation seems to be satisfactory in the fully developed damage zone (zone 3 of Fig. 8).

If such a correlation is established universally for different materials, for different liquids, and for different flow geometries then the extent of likely cumulative damage in any prototype can be confidently predicted. Just as a designer of a hydrodynamic system can get an idea of the drag forces if the coefficient of drag is known, or of the lift forces if the coefficient of lift is known, an idea of the cumulative intensity of damage is known by the value of the cavitation damage number. The following example will illustrate the method involved.

EXAMPLE

Determine the cumulative damage caused in 1 hr by a circular hole of 2.5 cm diameter rotating with a velocity of 45 m per sec and with a free stream pressure of 0.75 kg per sq cm. The material is aluminum with a yield stress of 786 kg per sq cm. The liquid is water at 32°C.

Solution.

Cavitation parameter:

$$K = \frac{p_o - p_v}{\frac{1}{2}\rho V_o^2} = 0.0692$$

From Fig. 15 (a)

$$\frac{l_e}{d} = \lambda_K = 2.7;$$

Thus

$$l = 2.7 \times 2.5 = 6.75 \text{ cm}$$

From Eq. 15

$$N = \frac{V_o t}{d \lambda_K} \quad \ldots\ldots\ldots\ldots\ldots\ldots (15)$$

or

$$\frac{(45)\ (3600)\ (100)}{(2.50)\ (2.7)} = 2.34 \times 10^6$$

From Fig. 19 (b), corresponding to this value of N,

$$C_D \times R_o \times 10^6 = 1.95$$

From

$$C_D = \frac{\sum i\ Y}{R_o\ p_o\ N} \quad \ldots\ldots\ldots\ldots\ldots\ldots (17)$$

$$C_D = \frac{1.95}{R_o \times 10^6}$$

Cumulative depth:

$$\sum i = \frac{1.95}{10^6} \times \frac{p_o\ N}{Y} = 0.435 \times 10^{-2}\ \text{cm}$$

Cumulative volume:

$$\sum v = \sum i \times A_e$$

From Fig. 16 (a)

$$\frac{A_e}{d^2} = 2.6$$

or

$$A_e = 16.25\ \text{sq cm}$$

and

$$\sum v = 0.435 \times 10^{-2} \times 16.25$$

$$= 7.06 \times 10^{-2}\ \text{cu cm}$$

Thus the cumulative weight loss equals $\left(\sum v\right)\ (\rho_m)$

$$= \left(7.06 \times 2.7 \times 10^{-2}\ \text{g}\right)\ (2.7\ \text{gm per cu cm})$$

in which ρ_m is the density of aluminum

$$= 191\ \text{mg}$$

This method would be very useful if standard charts could be prepared for the guidance of designers. The generalization of this method is possible when a better understanding can be had of the aspects presented in the following sections.

Concept of Inception of Damage and Incubation Period.—In Fig. 8, the E - N diagram was divided into three zones. The work analyzed here belongs to the third zone, namely the fully developed damage zone. For the first zone, the inception zone, it is noticed that there is a lower limit for the velocity of flow named as the threshold velocity below which the material will not be damaged at all. In any flow system the cavitation starts when the value of cavitation parameter K reaches a critical value K_i. Thus,

$$K_i = \frac{p_i - p_v}{\frac{1}{2}\ \rho\ V_o^2} \quad \ldots\ldots\ldots\ldots\ldots\ldots (18)$$

in which p_i is the free stream pressure at which the cavitation starts for a given velocity V_o. Therefore, for a given velocity V_o, the maximum possible pressure is p_i, above which there is no cavitation at all. Therefore, the maximum energy of collapse for that velocity is proportional to $p_i R_o^3$. This value of $p_i R_o^3$ should exceed the fatigue limit of the material in repeated dynamic indentation. But it is known that the impact fatigue and bending fatigue are directly related linearly.[18] Similarly, if it is assumed that the indentation fatigue (or surface fatigue) and the bending fatigue are directly related, then the bending fatigue limit S_f can be used for the correlation.

Then the stress produced by the shock wave will be proportional to the value p_i:

$$p_i \propto p_c > S_f \quad \ldots\ldots\ldots\ldots\ldots\ldots (19)$$

in which p_c is the stress induced by the shock waves. That is

$$p_i > B\ S_f \quad \ldots\ldots\ldots\ldots\ldots\ldots (20)$$

in which B is a constant
Substituting the value of p_i from Eq. 18

$$\left(\frac{1}{2}\rho\ V_o^2\ K_i + p_v\right) > B\ S_f \quad \ldots\ldots\ldots\ldots\ldots\ldots (21)$$

or

$$V_o^2 > \left[\frac{B\ S_f - p_v}{\frac{1}{2}\rho\ K_i}\right] \quad \ldots\ldots\ldots\ldots\ldots\ldots (22)$$

Thus,

$$V_o \text{ Threshold} = \sqrt{\frac{B\ S_f - p_v}{\frac{1}{2}\rho\ K_i}} \quad \ldots\ldots\ldots\ldots\ldots\ldots (23)$$

Thus, for any cavitating flow system, there is a threshold velocity given by Eq. 23 which is a function of the fatigue limit of the material, the cavitation inception parameter, the vapor pressure, and density of the fluid.

For zone 2, the incubation zone, certain number of cycles are required before the plastic yielding starts. This value of the number of cycles is given by Eq. 11. Investigations are in progress (as of 1960) to analyze these two zones.

Effect of Corrosive Environment.—It is well-known that a corrosive environment reduces the fatigue limit considerably. Hence, the threshold velocity is also lowered. This explains the observed increase in damage when corrosive liquids are used. This is the reason cathodic protection reduces cavitation damage. Experiments are being conducted to investigate the effect of corrosive liquids and cathodic protection on cavitation damage number.

CONCLUSIONS

1. For a given flow geometry, if the value of the cavitation parameter is given, then the length of erosion, breadth of erosion, and the area of erosion can be predicted by model analysis.

2. If the mechanism of damage is assumed as the dynamic indentation produced by the short range shock waves arising from the collapse of vapor bubbles, then a useful non-dimensional number known as cavitation damage number is obtained. This number is the ratio of the energy absorbed by the material in deformation to the energy of collapse of the bubbles.

3. It is assumed that the number of repetition of the dynamic indentations is equal to the number of cavities passed during a given interval, and the cavitation damage number has been correlated with the number of cavities.

4. The trend of the experimental correlation can be explained from the cumulative damage hypothesis used in connection with fatigue failures. The material deforms elastically as the number of cycles are increased to a defined number and, hence, it does not absorb any energy in the elastic recovery stage. However, when the plastic deformation begins the material absorbs more and more energy and eventually reaches a stage of viscous flow. At the same time, the attenuation of shock waves takes place because of the damping of the liquid covering the eroded pit. As the depth of erosion increases the damping also increases. Consequently the energy of collapse transmitted to the material for producing deformation decreases. This explains the decreasing trend of the curve.

APPENDIX.—NOTATION

The following symbols adopted for use in this paper, conform essentially with "American Standard Letter Symbols for Hydraulics" (ASA Z10.2-1942), prepared by a committee of the American Standards Association with Society representation, and approved by the Association in 1942:

e = area of erosion;

D = cavitation damage number;

l = characteristic linear dimension of the body as used in the Strouhal number;

E = energy of indentation;

E_c = energy of collapse f each bubble;

E_f = fatigue limit of indentation;

E_Y = yield limit;

f = frequency of shedding of the cavity;

h = average depth of erosion

K = cavitation parameter

L = length of cavity;

n = number of indentation;

p = pressure;

p_v = free stream pressure at which cavitation starts for a given velocity V_o;

p_o = static pressure of liquid surrounding the bubble at the moment the bubble begins collapsing;

p_{min} = minimum pressure liquid can withstand;

p_v = vapor pressure of liquid;

R_o = maximum possible radius of the bubble at the beginning of the collapse

S_f = bending fatigue limit;

t = time;

V_o = velocity of flow;

v = total volume deformed per cavity;

Δv = volume deformed per collapse of bubble;

$\sum \Delta w$ = weight loss;

Y = dynamic yield stress of material;

λ_K = relative length of the cavity, l/d;

ρ_m = density of material; and

σ = surface tension of liquid.

Journal of the
HYDRAULICS DIVISION
Proceedings of the American Society of Civil Engineers

VIBRATION OF GATES DURING OVERFLOW AND UNDERFLOW

By Eduard Naudascher,[1]

SYNOPSIS

Violent vibrations may occur at gates being subjected simultaneously to verflow and underflow. Model studies have been made to evaluate frequency nd magnitude of the exciting forces for different types of gates and aprons. esign criteria and the basic mechanism of excitation are presented.

INTRODUCTION

Gates in low dams or weirs operated under large depths of overflow in mbination with underflow may be subject to a violent vibration brought about a periodically changing flow pattern on the downstream side. Because of the re occurrence of such operating conditions, little attention was given to this use of gate vibration prior to 1948, and since then only a few observations

Note.—Discussion open until February 1, 1962. To extend the closing date one month, written request must be filed with the Executive Secretary, ASCE. This paper is part the copyrighted Journal of the Hydraulics Division, Proceedings of the American Society of Civil Engineers, Vol. 87, No. HY 5, September, 1961.

[1] Asst. Prof. and Research Engrg., Iowa Inst. of Hydr. Research, State Univ. of Iowa, wa City, Iowa; on leave from the Institut für Hydromechanik, Technische Hochschule, rlsruhe, Germany.

have been reported on.[2,3,4,5,6,7,8,9] In 1953 Petrikat[3] described model tests of a tainter gate in which the entire test apparatus was destroyed due to vibration. The gate, designed for a tropical river, was operated with simultaneous overflow and underflow during flood periods when the head greatly exceeded the gate height.

Vibrations of this kind may occur as well with gates consisting of two or more sections such as tainter, roller, or vertical lift gates—each having an attached flap—and any type of split-leaf spillway gates. With such gates the flood waters will at first be released by lowering the flap or the upper gate leaf. Later, in order not to raise the pool level unduly, both gate sections are lifted. During this course of operation, water is discharged above and below the gate and vibrations are usually inevitable. The same vibration phenomenon is also encountered during the handling of stop logs in running water.[7,8]

This paper is an abstract of an extensive model investigation conducted at the Hydromechanics Laboratory, Karlsruhe Institute of Technology, Germany. Its purpose is to make available the most important aspects of the problem as to criteria for preferable types of gates and aprons, magnitude and frequency of the exciting forces, and means of mitigating the vibration. Greater use has been made of dimensionless representation than in the original report, and emphasis is placed on the explanation of the exciting mechanism of the vibration. A complete description of the investigation is to be found in the writer's doctoral dissertation.[10]

SIMILARITY CONDITIONS

In general, the vibration of a gate with overflow and underflow has to be considered as a self-excited vibration with four coupling members (Fig. 1):

1. Upper jet (referred to also as nappe)
2. Lower jet
3. Space between jets
4. Elastic gate

---

2 "Recherches sur le fonctionnement simultane des barrages mobiles en deversoir et vannes de fond," by L. Escande, La Houille Blanche, Nr. special B, 1948, 728.

3 "Die schwingungsanfachenden Kraefte in Wehrbau," by K. Petrikat, Man-Forschungsheft, 4, 1953, p. 69.

4 "Schwingungsuntersuchungen an Stahlwasserbauten," by K. Petrikat, Der Stahlbau 24, 1955, p. 198, p. 202, p. 272.

5 "The Forces on a Horizontally Pivoted Butterfly Weir," by G. H. Lean, Proceedings, 6th General Meeting, Internatl. Assoc. of Hydr. Researchers, Vol. 3, The Hague 1955, C3.

6 "Downpull Forces on Verticle Lift Gates," Corps of Engrs., U. S. Army, Waterways Experiment Sta. Tech. Report No. 2-447, Vicksburg, 1956.

7 "Etude Experimentale de manoevre des batardeaux en eau vive," by L. Escande and L. Castex, Proceedings, 6th General Meeting, Internatl. Assoc. of Hydr. Researchers Vol. 4, The Hague, 1955, D16.

8 "Untersuchungen ueber das Einsetzen von Wehrdammbalken in der Stroemung," by H. Escher, Schweiz. Bauzeitung, 75, 1957, p. 429.

9 Unpublished reports of the Inst. f. Hydromechanik, by P. Boess, Stauanlagen und Wasserversorgung, Karlsruhe, 1956.

10 "Beitrag zur Untersuchung der schwingungserregenden Kaefte an gleichzeitig ueber - und unterstroemten Wehrverschluessen," by E. Naudascher, Techn. Mitt. Krupp Vol. 17, No. 5, 1959, p. 230.

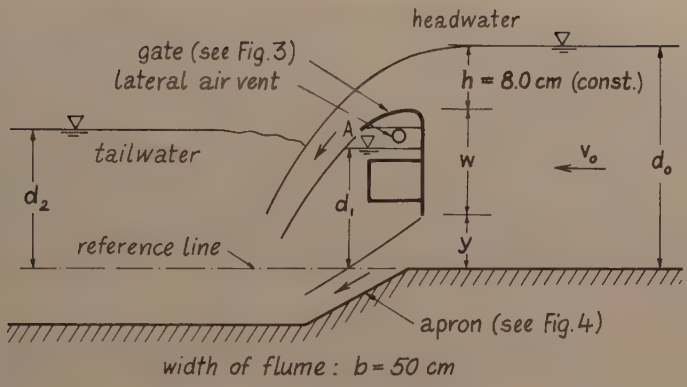

FIG. 1.—GATE WITH OVERFLOW AND UNDERFLOW. DEFINITION OF SYMBOLS

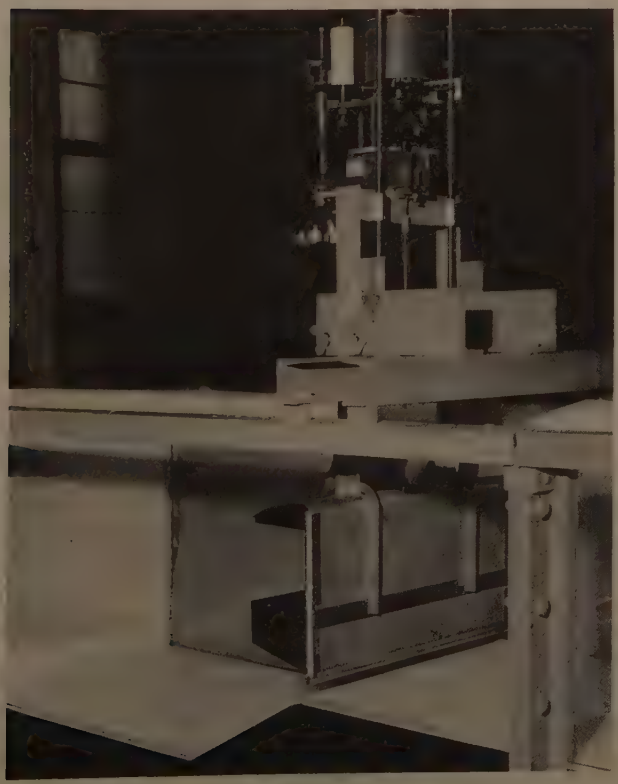

FIG. 2.—MODEL OF DOUBLE-LEAF GATE IN A 50-CM GLASS-WALLED FLUME WITH SOME OF THE MEASURING APPARATUS. OBLIQUE VIEW FROM UPSTREAM

As far as the flow is concerned, this vibration is governed mainly by the inertia and gravity forces of the moving liquid. The complexity of the problem is implied by a question as to how far the elasticity and damping characteristics of the gate are involved. The gate may vibrate in different ways, including those of flexure and torsion. In order to simulate the dynamic behavior of the gate as well as the dynamic behavior of the flow, at least two model laws have to be satisfied: that of Cauchy (for structural elasticity) and that of Froude. This is impracticable in most cases; moreover, it would restrict the applicability of the test results to a few specific cases. To overcome this difficulty, the model gate was made very stiff and retained by fixed, in contrast to elastic, supports.

Under these conditions, the Froude conversion laws can be applied, that is, for forces,

$$\frac{F_m}{F_p} = \lambda^3 \quad \ldots\ldots\ldots\ldots\ldots\ldots \quad (1)$$

for frequencies,

$$\frac{f_m}{f_p} = \lambda^{-1/2} \quad \ldots\ldots\ldots\ldots\ldots\ldots \quad (2)$$

in which λ is the ratio of the length in the model to that in the prototype. The last of the four coupling members has practically been eliminated by this simplification. Consequently, the vibration of the gate to be expected in the prototype as a first approximation can be computed as a forced vibration, when the excitation due to the unsteady flow system is known from model experiments.

In the case of one degree of freedom, for instance, that in the direction of the prototype gate suspension—the forced vibration of the gate is described by

$$m\frac{d^2x}{dt^2} + c\,x + \left[k_1\frac{dx}{dt} \pm k_2\left(\frac{dx}{dt}\right)^2 \pm K_3\right] = P_e \cos(\omega t) \quad \ldots \quad (3)$$

in which $m\frac{d^2x}{dt^2}$ = inertia force; $c\,x$ = elastic force; $k_1\frac{dx}{dt}$ = viscous damping force $\pm k_2\left(\frac{dx}{dt}\right)^2$ = turbulent damping force, $\pm K_3$ = Coulomb's friction force, $\pm$ = always opposing motion; $P_e \cos(\omega t)$ = exciting force in x-direction due to the flow; and x = deflection of the gate from equilibrium position; t = time; m = mass of the gate and added mass of the water; c = spring modulus in x-direction; k_1 and k_2 = damping coefficients; and ω = angular frequency of the excitation.

The error in this simplification will become smaller as the stiffness and the damping of the prototype gate become larger. The permissibility of the discussed simplification was checked by exploratory tests with a flexible suspended model gate which are to be described later. Final conclusions may only be obtained by prototype measurements.

MODEL OF A DOUBLE LEAF GATE

Experiments were conducted for two different arrangements. The first (Fig. 2) was based on the design of a double leaf gate in the River Ruhr at

Duisburg, Germany, because the opportunity of comparing model and prototype results existed. The lower leaf of this gate is of the girder-plate type, the underside of which was provided with 15 holes, 4 mm in diameter (model dimensions). About half of the clear width was represented in the model. Three types of lower leaf were tested in combination with five types of apron. Although performed on a double leaf gate, the model tests are also applicable to a gate with an attached flap in the lowered position. A pipe of 1.2-cm inner diameter served for aeration of the nappe.

Flow Regimes.—An important quantity defining the flow conditions near the gate is the elevation of the water surface beneath the gate crest. This "inner"

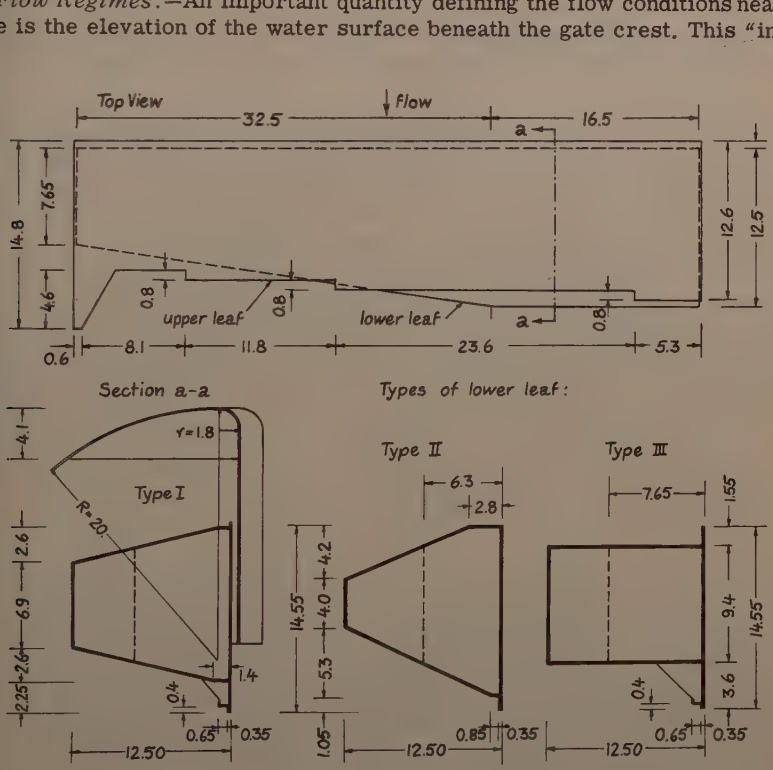

FIG. 3.—FIRST TEST ARRANGEMENT. MODEL OF GATE TYPES TESTED IN COMBINATION WITH APRON TYPE 1 (DIMENSIONS IN cm)

water level depends on the momentum of upper and lower jet, on the type of apron, and on the size of the lateral air vent aerating the nappe (Fig. 5). The elevation of the downstream edge of the crest (point A in Fig. 1) represents the upper limit for d_1. Because the edge is irregular (Fig. 3), this limit does not appear clearly defined in Fig. 5. The lower limit for d_1 is reached when the tailwater drops below a certain level leaving d_1—and, hence, the discharge unaffected by tailwater conditions. Analogous to the terminology for sluice gates, the corresponding discharge will be called "free" despite the fact that the lower jet may still be submerged. For d_2/d_0 approaching unity, the nappe that is usu-

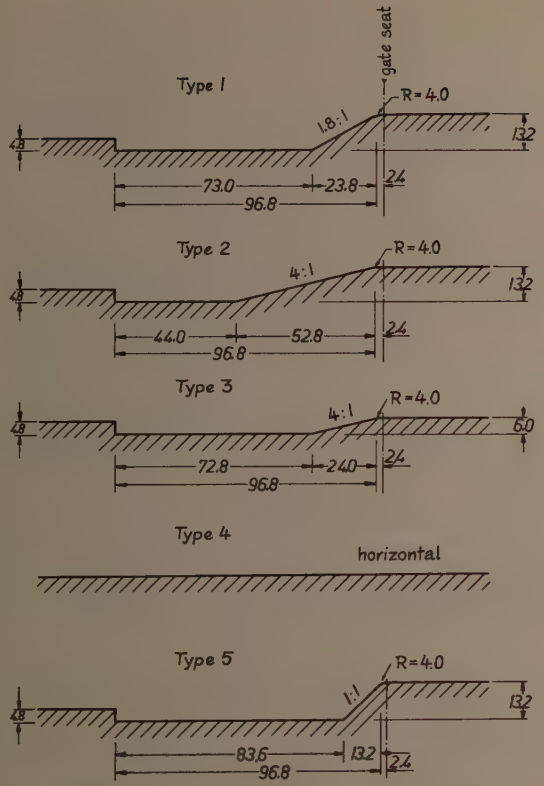

FIG. 4.—APRON TYPES TESTED IN COMBINATION WITH GATE TYPE I (DIMENSIONS IN cm)

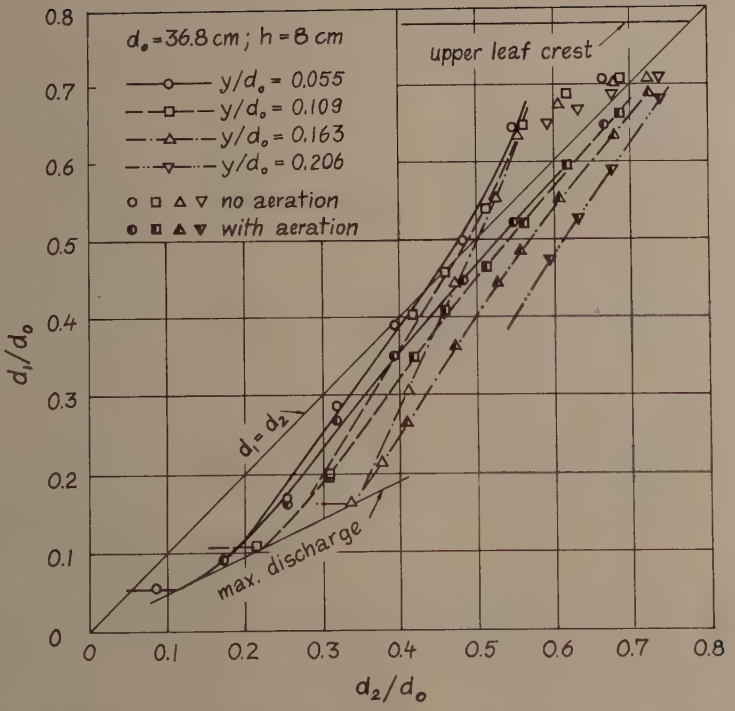

FIG. 5.—TAILWATER RELATIONSHIP FOR APRON TYPE 1

ally submerged under the surface roller (Fig. 10(a)) remains on the water surface.

These three flow regimes may thus be distinguished:

1. The flow with the nappe remaining on the water surface
2. The flow with submerged nappe
3. The flow with free discharge

Hydrodynamic Forces on the Lower Leaf.—The hydrodynamic forces acting vertically on the lower leaf have been determined by a beam balance (see Fig. 2) keeping the gate supported on a set of adjusting screws 0.1 mm aprat. Only when the force exceeded the weight set by the balance was the model shortly displaced from its supports. In this way the extremes of the hydrodynamic load that were reached or exceeded about once a second were measured. This concept was adopted in order to exclude peak values due to sporadic shock loads. A correction was made for the difference in buoyancy of the lower leaf. A typical plot of these downward or upward forces against the head differential between headwater and tailwater is represented in Fig. 6. The difference ΔF between upper and lower curves indicates the force fluctuation that is responsible for the gate vibration.

Excitation.—A measure of the magnitude of the excitation may be set forth in form of a coefficient, similar to the lift coefficient of airfoils, by dividing the amplitude of the fluctuating vertical force $\Delta F/2$ by the product of the horizontal projection of the lower leaf A and the dynamic pressure. Substituting $\gamma (d_0 - d_2)$ for the dynamic pressure, the excitation coefficient is defined as

$$c'_e = \frac{\Delta F}{2 \gamma A (d_0 - d_2)} \quad \ldots\ldots\ldots\ldots\ldots\ldots \quad (4)$$

It must be kept in mind that ΔF does not represent the peak-to-peak value but, rather, a double amplitude that is exceeded about once a second.

Excitation coefficients for the investigated types of lower leaf (Fig. 3) are shown in Fig. 7. In combination with apron type 1 (Fig. 4) the leaf type II was found to be most favorable. In combination with lower leaf type I, the excitation coefficient was a minimum for apron type 1 and a maximum for a horizontal floor or a downstream slope of 1:1 (Fig. 8). With increasing gate opening the excitation coefficient increases without noticeable change in frequency.

Influence of the Geometry of Gate and Apron.—The most violent pressure fluctuations are to be found in the vicinity of the juncture of upper and lower jets. The more the exposed areas of the gate are withdrawn from this zone, the less will be the transmission of pressure pulsation to the gate. To withdraw the gate structure from this zone, the floor downstream from the gate as well as the bottom of the gate have to be inclined as much as possible. A sloped floor with a depressed stilling basin was found to be most effective, because this permits a larger range of dispersion of the nappe (Fig. 9). This means an increase in damping for equal head differentials Δd.

There are limitations to this general rule. When the space between the gate bottom and the surface of the lower jet becomes very small, as shown in Fig. 9(c), the shedding of vortices from this surface and, hence, the excitation will

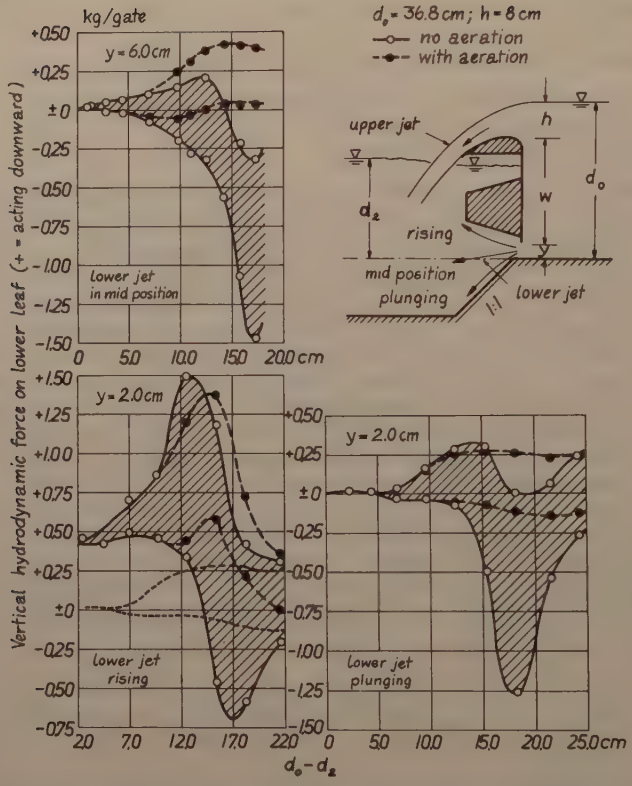

FIG. 6.—HYDRODYNAMIC FORCE ACTING VERTICALLY ON LOWER LEAF TYPE I FOR APRON TYPE 5. (HORIZONTAL PROJECTION OF LOWER LEAF A = 533.8 sq cm)

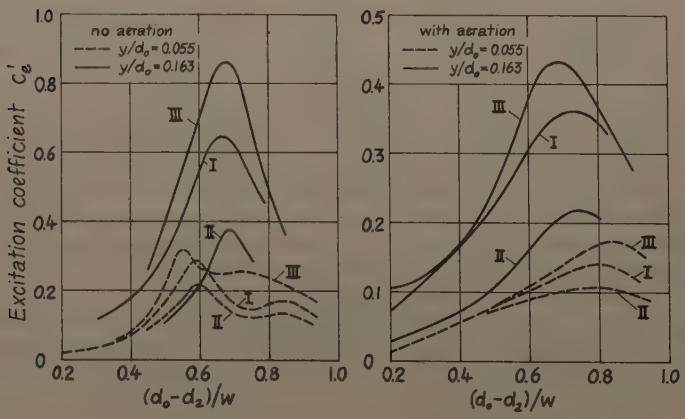

FIG. 7.—EXCITATION COEFFICIENT c_e' FOR GATE TYPES I - III

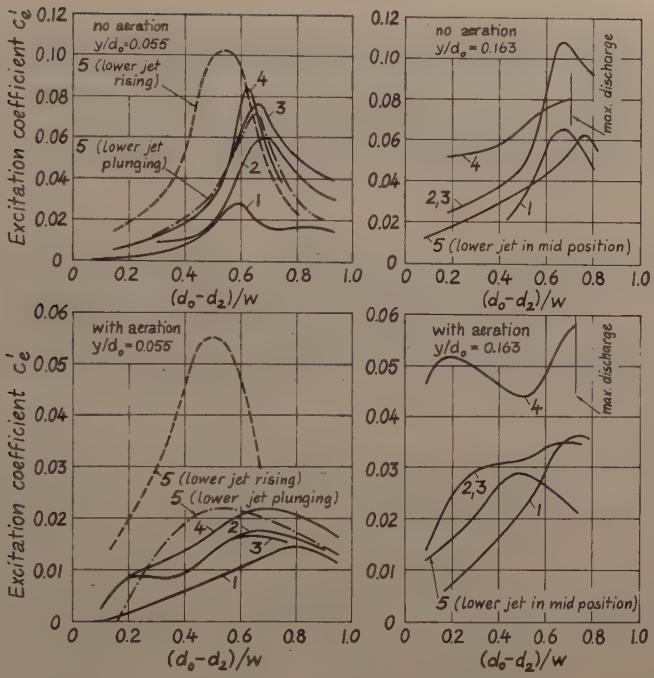

FIG. 8.—EXCITATION COEFFICIENT FOR GATE TYPE I IN COMBINATION WITH APRON TYPES 1 - 5 (FIG. 4). d_0 = 36.8 cm, h = 8 cm

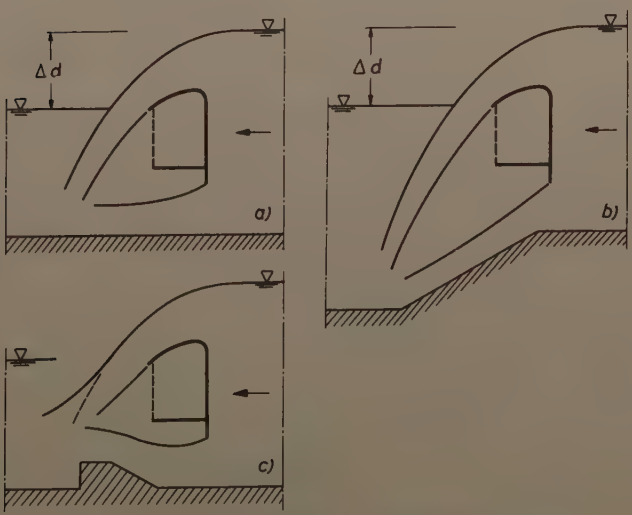

FIG. 9.—EFFECT OF THE DOWNSTREAM SLOPE

be disturbed. This phenomenon can be utilized to mitigate vibration.[11,12] The decreased excitation coefficients for the bottom plate type b, as compared with type a, are due to the same cause (Fig. 21). The other exception from the rule is an excessively steep floor that leads to a separation of the lower jet. For small gate openings, flows with rising and plunging jet are equally possible at the same headwater-tailwater conditions (Fig. 10). As long as no major disturbance by the surface roller occurs, the separated limiting streamlines of the lower jet tend to cling either to the floor or to the gate bottom, provided the gate is not of the open-truss type. Although the generation of vortices was prevented in the case of the rising jet, both unfavorable negative pressures along the gate bottom and shaking at high frequency were observed (Fig. 6). The rising jet was more likely to form at high tailwater levels, the plunging jet more at low. For rather large gate openings, the lower jet remained in mid position independent of the tailwater. The influence of the crest shape was investigated with the second test arrangement (Fig. 14).

Influence of the Aeration.—Without aeration of the nappe the tendency toward vibration was greater in every case investigated. As will be explained in the last section, this is due to increased pressure change beneath the nappe. It is interesting to note that there was a well-defined maximum of the exciting forces for nonaerated flow at a certain head differential that was independent of the gate opening. From Fig. 7 the head differential is found to be approximately $d_0 - d_2 = 16$ cm or the ratio $d_2/d_0 = 0.57$. According to Fig. 5 this ratio corresponds to the condition at which the inner water level reaches the downstream edge of the gate crest (point A in Fig. 1), that is, when the air space below the nappe just disappears. By means of a momentum consideration of the flow in the vicinity of the gate, it can be shown that the underpressure beneath the nappe becomes a maximum for this condition. Of course, the aeration had no effect within the range of small head differentials $d_0 - d_2$ when the lateral air vent was submerged.

Influence of the Elasticity.—As a supplement to the series of tests with the gate in fixed positions, measurements were conducted with an elastic gate suspension. By means of a spring suspension system the lower leaf was free to vibrate vertically. The upper leaf remained fixed. In the following only the most significant results are reported.

The frequency of the gate vibration is unaffected by the natural gate frequency within the accuracy of measurement, as verified by Fig. 11. By plotting the frequency against the difference $d_1 - y$, which for a constant d_0 is a measure of the velocity at the surface of the lower jet as well as of the mass of water included between the jets, a fairly good correlation was obtained. Further evidence that the frequency of the excitation depdns on these quantities will be given later, analytically. The scattering of the data in Fig. 11 can be explained by the random pulsation of the surface roller and by the fluctuating inner water surface. Both sources of disturbance grow with dropping tailwater level. When the inner water surface approaches the gate bottom, only non-periodic shock loads are induced by waves (Fig. 16(a) and Fig. 17(a)).

As shown in the last section, the gate vibration is self-controlled. An additional control may apparently be effected by the elasticity of the gate if

11 "Die schwingungsanfachenden Kraefte im Wehrbau," by K. Petrikat, Man-Forschungsheft, 4, 1953, p. 16.

12 "Beitrag zur Untersuchung der schwingungserregenden Kraefte an gleichzeitig ueber - und unterstroemten Wehrverschluessen," by E. Naudascher, Tech. Mitt. Krupp Vol. 17, No. 5, 1959, p. 270.

a) With overflow: h = 8.0 cm ; w = 24.8 cm ; y = 4.0 cm ; $d_o - d_z$ = 9.6 cm.

b) Without overflow: h = 0 ; w = 24.8 cm ; y = 4.0 cm ; $d_o - d_z$ = 16.0 cm.

FIG. 10.—VARIATION IN JET POSITION AT APRON TYPE 5 FOR OTHERWISE IDENTIAL CONDITIONS

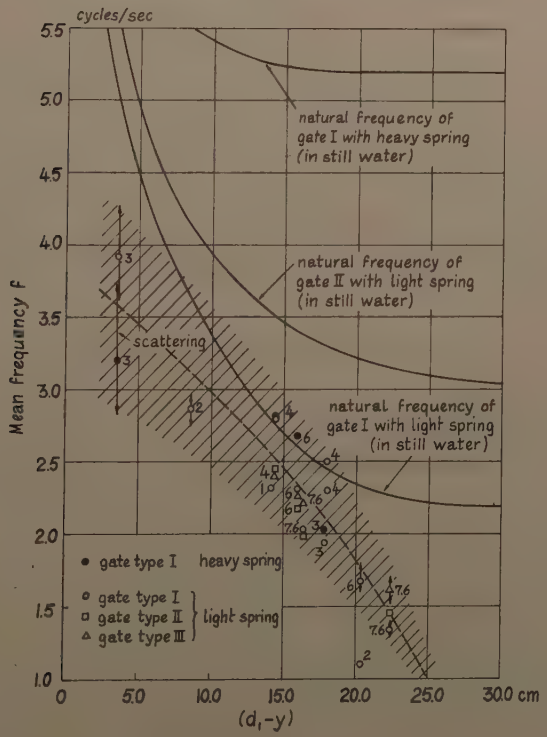

FIG. 11.—MEAN FREQUENCY OF GATE VIBRATION. APRON TYPE 1, d_0 = 36.8 cm, h = 8 cm. AERATED NAPPE. (NUMBERS INDICATE GATE OPENING IN cm)

that the gate lip will be periodically deflected. With the lower leaf flexibly suspended, it was possible to magnify the gate deflections appreciably by knocking lightly on the flume wall with the frequency of the alternately generated vortices (Fig. 12). The reason seems to be an augmentation of control rather than an extraneous excitation, because the external impulses had no component in the direction of freedom of motion of the gate. Of course, an amplification of a multiply coupled vibration like the one under consideration depends strongly on the tuning of the individual coupling members that might have been rather favorable in these tests. It is planned to check this phenomenon of extraneous control by field tests because of its possible importance. For instance, a similar effect may be induced by ship engines in navigable rivers.

Means of Mitigating Vibration.—Criteria for favorable types of gate and apron have been given. In case the remaining excitation would still affect the safety of the structure, additional means of mitigating vibration have to be considered.

The disturbance of the excitation by a sill downstream from the gate has already been mentioned in connection with Fig. 9. Extensive studies with the second test arrangement (Fig. 14) indicated that one or two horizontal plates, placed close to the juncture of upper and lower jet, have also a stabilizing effect on the flow.[10] Both devices are objectionable with respect to removal of gravel and debris. Therefore, it is more advisable to use two lateral ledges attached to the piers and to slope the floor downstream from the gate at 1 on 2 (but not steeper than 1 on 1.8). By deflecting the upper jet these ledges give rise to eddies along a vertical axis that disturb and break up the exciting vortices generated along a horizontal axis. Most effective was the arrangement depicted in Fig. 13, because it provided additional aeration. None of the flow spoilers attached to the crest, which were successfully used to cure fluctuating nappes, had any effect here.[10]

The excitation can be completely disturbed by introducing another jet into the wake either through a controlled opening in the skin plate or by deflecting parts of the upper jet back toward the gate. The realization of such a device is difficult, however.

MODEL OF AN IDEALIZED GATE

In the first test arrangement there were no means to separate irregularities in the fluctuating hydrodynamic force and shock loads from the main force oscillation. The precise relationship with time of the pressure and force fluctuation was studied with an arrangement of an idealized gate the base of which was simply represented by a bottom plate (Fig. 14).

Depending on the type of gate, four cases of loading may generally be distinguished (Fig. 15). They can be interpreted as different combinations of three zones in which the hydrodynamic forces are transmitted to the gate structure. The loading of an upper leaf or a flap, for instance, is signified by Fig. 15, III. The resultant exciting force can be found by superposition for any of these cases when the pressure amplitudes within the regions a, b, c and their temporal correlation is known. Hence, it was decided to record simultaneously the pressure fluctuation at a few representative points in these regions.

In addition, the torque exerted on the bottom plate was measured in order to obtain the resultant excitation on this plate directly. For this reason the plate was hinged at the upstream edge and connected to a strain-gage dynamo-

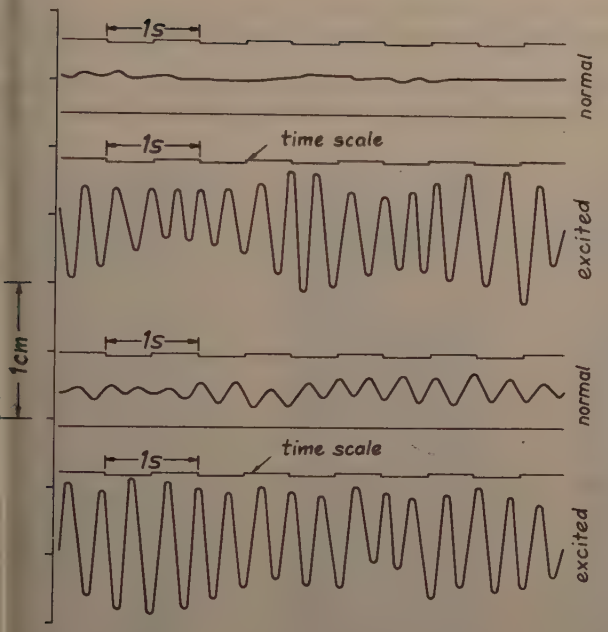

FIG. 12.—EFFECT OF EXTRANEOUS EXCITATION ON VERTICAL DEFLECTION OF LOWER LEAF TYPE I FOR APRON TYPE 1

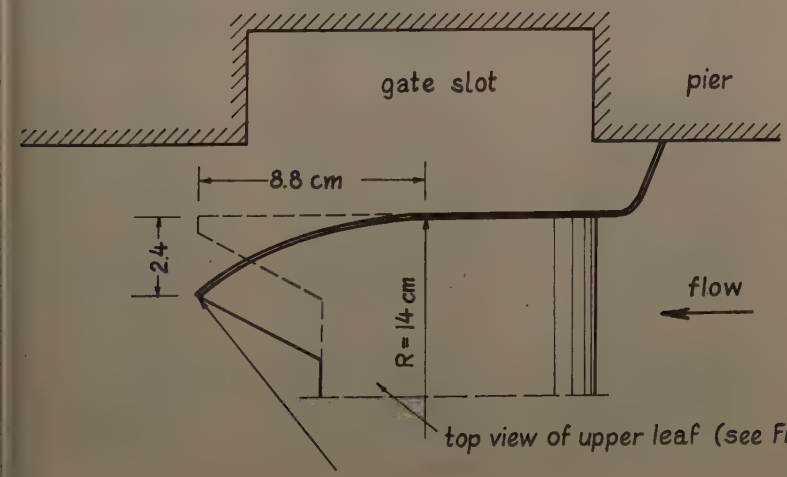

FIG. 13.—DEVICE TO MITIGATE VIBRATION: CURVED SIDE SHIELD ON UPPER LEAF

meter. The flow process was recorded on movie film and synchronized with the torque measurement (Fig. 16). Some of the essential findings are reported below.

Depending on the flow regime, rather different conditions for the vibration are encountered. The flow with the nappe remaining on the surface has much

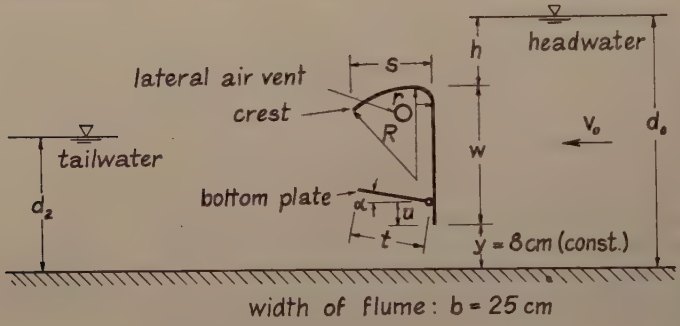

Crest shape

Type	A	B	C
s [cm]	13.5	13.0	0
r [cm]	2.0	2.0	sharp
R [cm]	20.0	∞	crested

Arrangement of bottom plate

Type	a	b	c
t [cm]	13.0	12.5	12.5
α	30°	0°	0°
u [cm]	2.5	3.0	1.0

FIG. 14.—SECOND TEST ARRANGEMENT. TYPES OF AN IDEALIZED GATE TESTED IN COMBINATION WITH HORIZONTAL FLOOR

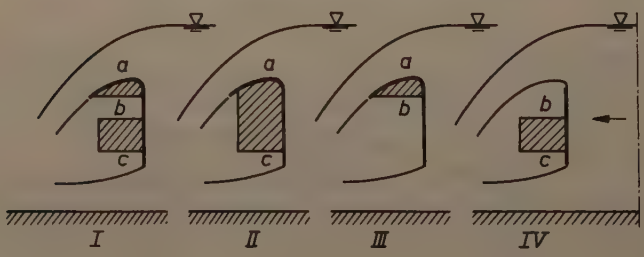

FIG. 15.—COMBINATIONS OF REGIONS A, B, C WHERE HYDRODYNAMIC FORCES ARE TRANSMITTED TO THE GATE (CASES OF LOADING)

similarity with a cylinder in a parallel flow producing a von Kármán vorte trail. The similarity deviates because a waved water surface exists and th approaching velocity is not an independent variable. For the free discharg gravity forces, which are negligible in the first-mentioned regime, have pre dominant significance. Furthermore, an air space beneath the nappe begins

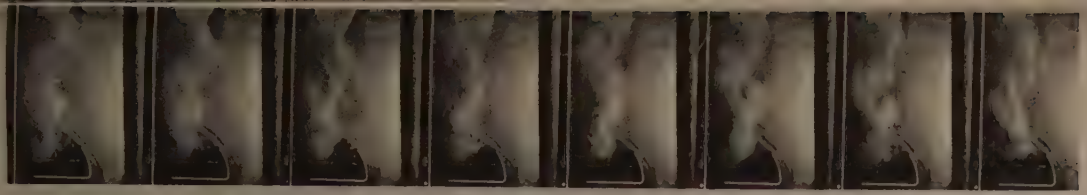

a) Type A,a (see Fig. 14), h = 5 cm; w = 25 cm; y = 8 cm; $d_o - d_2$ = 13.4 cm; with aeration. (see Fig. 17a)

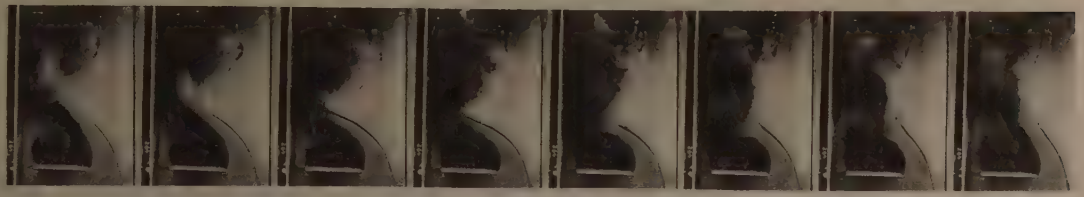

b) Vertical sharp edged plate, h = 15 cm; w = 25 cm; y = 8 cm; $d_o - d_2$ = 12.4 cm; no aeration.

c) Type A,a (see Fig. 14), h = 15 cm; w = 17.5 cm; y = 8 cm; $d_o - d_2$ = 1.6 cm; aeration has no influence.

FIG. 16.—PHOTOGRAPHS TAKEN CONSECUTIVELY AT RATE OF 14 FRAMES PER SEC

interact with the flow system as soon as a free water surface exists behind the gate. In the case of a submerged nappe the vibration is affected in addition by the turbulent motion of the surface roller (Fig. 16(b)). A further complication arises from a multitude of possible geometric boundary situations.

The steady state of gate vibration and, hence, a functional concept of the excitation is impeded mainly by three effects:

1. The air space beneath the nappe usually disturbs the vibration process by irregular motion of the inner water surface and by air bubbles carried along in slugs by the upper jet. For high depth of overflow, however, the excitation is large enough to control the surface fluctuations as well as the air entrainment (Fig. 23).
2. The motion of the surface roller, being in general nonperiodic, tends to put the vibration out of phase, particularly at high submergence of the nappe, at small depths of overflow, or for nonaerated flow. At extremely low submergence, on the other hand, the roller action can be controlled, and even a magnification of the excitation due to a kind of regenerative process was sometimes observed.
3. Structural parts of the gate extending into the wake were found to be specific sources of vibration disturbance whenever they were close to the nappe or the lower jet. As the nappe was brought in contact with the gate (for example, with crest type C), it fluctuated with increased frequency but diminished amplitude only below the line of contact. The ideal shape of a gate with both overflow and underflow would follow the shape of the wake (Fig. 22).

Some oscillograms obtained from torque measurements are presented in Fig. 17. Before evaluation all superimposed secondary effects, mostly caused by free vibrations of the measuring equipment, were eliminated graphically. The remaining irregularity in frequency and amplitude was taken into account by evaluating mean and maximum values. In all instances the largest amplitude coincided with the lowest frequency, presumably because the virtual mass of water increased with amplitude.

When the air space in the wake was held at atmospheric pressure by means of an air vent, a higher frequency and lower excitation always obtained (Fig. 19). A similar increase in frequency followed by a cessation of excitation was observed for decreasing h/w. Partially responsible for this is the mentioned disturbance by the air space beneath the nappe which grows as h/w becomes smaller. The critical values of h/w below which vibration could not be maintained are shown[2] in Fig 18. The effect of structural parts close to the surface of the lower jet is demonstrated in Fig. 20. The lower the bottom plate was placed, the higher were the measured frequencies. From Fig. 21 it becomes evident that the corresponding excitation was decreased. With the combination of crest type A and bottom plate type a, two modes of vibration seemed to be equally possible for small head differentials (Figs. 17(b), 19(a), and 21(a)).

Modified excitation coefficients were determined by

$$c_e = \frac{a\,\Delta p}{\gamma(d_0 - d_2)} \qquad (5)$$

in which $a_{\Delta p}$ is the amplitude of the mean pressure difference between the upper and lower sides of the bottom plate, as evaluated from torque measurements, or by

$$c_e'' = \frac{a_p}{\gamma(d_0 - d_2)} \quad \ldots\ldots\ldots\ldots\ldots\ldots \quad (6)$$

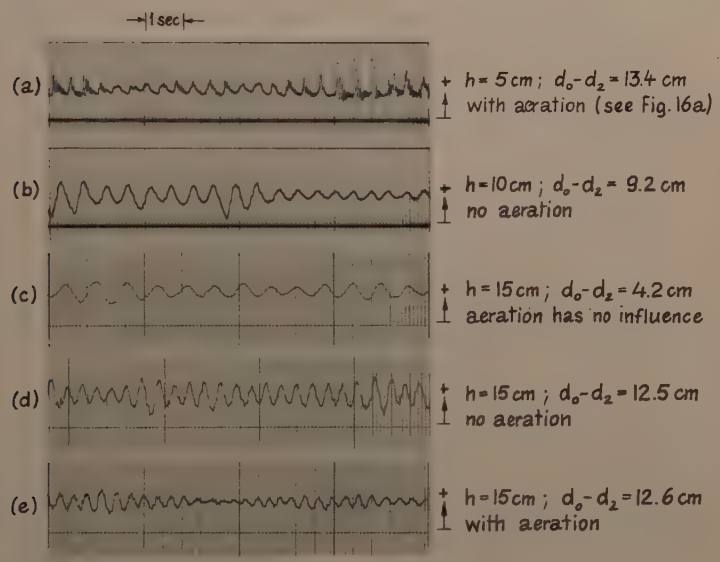

FIG. 17.—OSCILLOGRAMS FROM TORQUE MEASUREMENTS FOR TYPE A, a (FIG. 14). w = 25 cm, s = 8 cm, + = FORCE ACTING UPWARD

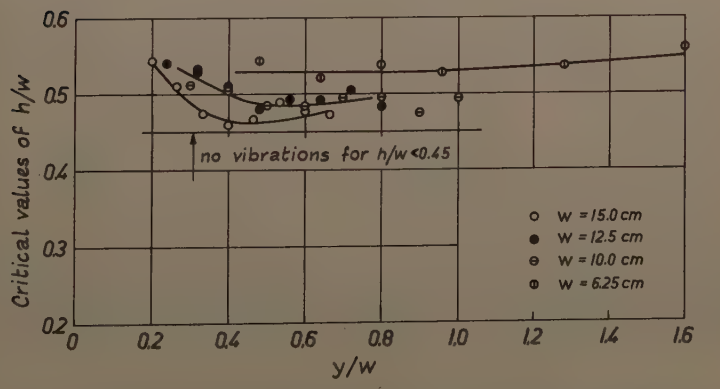

FIG. 18.—CRITICAL CONDITIONS FOR GATE VIBRATION AT NON-AERATED FREE DISCHARGE. GATE TYPE C WITHOUT BOTTOM PLATE

in which a_p is the amplitude of the pressure fluctuation at a specific point of the gate structure. The quantity $(d_0 - d_2)$ represents the differential between headwater and tailwater. In determining $a_{\Delta p}$ it was assumed that the pressure

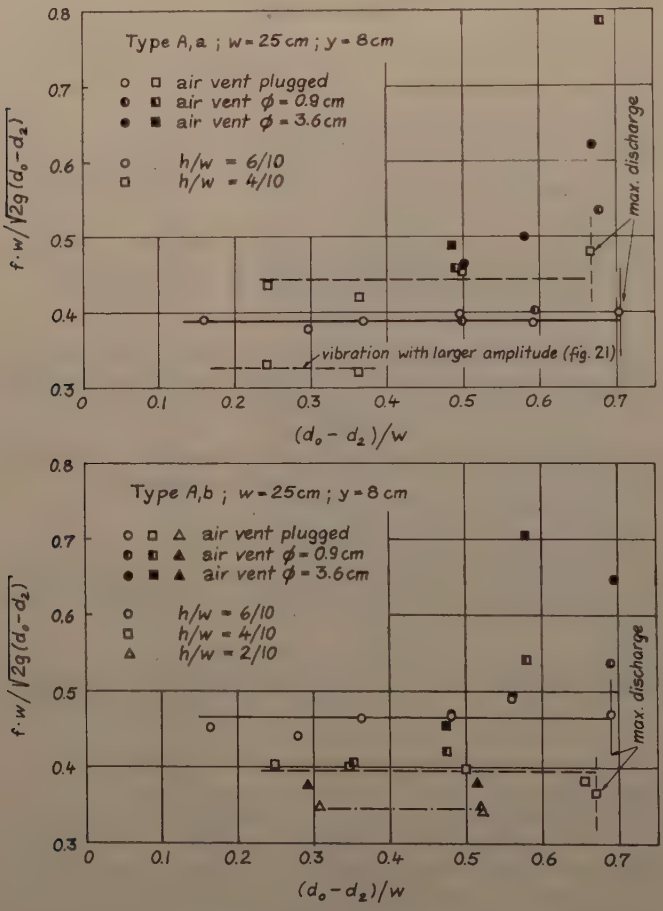

FIG. 19.—MEAN FREQUENCY f OBTAINED FROM TORQUE MEASUREMENTS

amplitudes are evenly distributed over the bottom plate. Actually the pressur amplitudes were larger toward the tip of the plate. The exact value of c_e coul be obtained by an integration of c''_e - values over the areas involved.

All measurements were performed for constant headwater and tailwater elevations. Comparative experiments with rising or falling tailwater resulted in similar vibration phenomena, mostly with magnified excitation.

ATTEMPT TO ANALYZE THE MECHANISM OF EXCITATION

In Fig. 23 an attempt has been made to sketch six consecutive flow patterns taking place during one cycle of the vibration process for the case without any

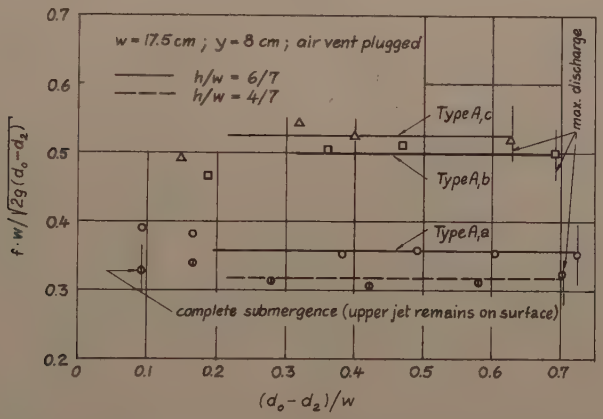

FIG. 20.—MEAN FREQUENCY f OBTAINED FROM PRESSURE MEASUREMENTS

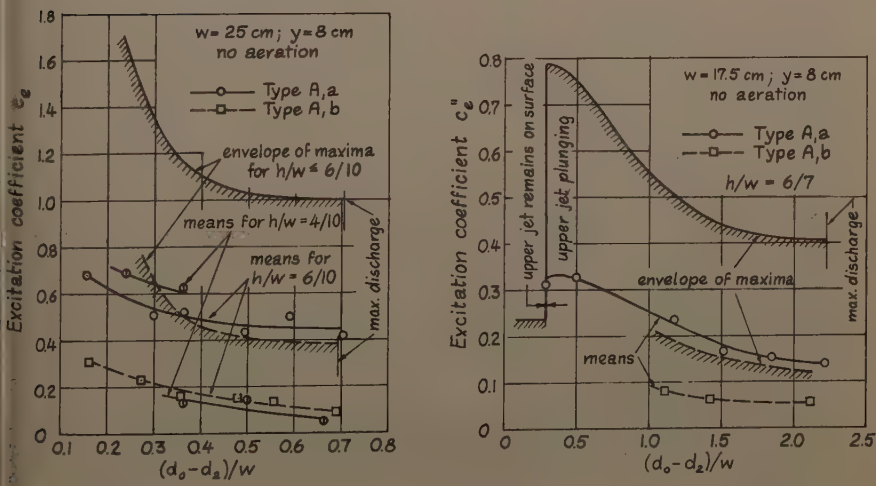

FIG. 21.—EXCITATION COEFFICIENT c_e FROM TORQUE MEASUREMENTS, AND c_e'' FROM PRESSURE MEASUREMENTS AT UNDERSIDE OF TIP OF BOTTOM PLATE

of the above-listed disturbing effects. (The air bubble shown in Fig. 23 is considered to be too small to disturb the excitation.)

It can be shown that for the free-surface potential flow around a vertical flat plate (Fig. 22) there exists an unstable state of equilibrium analogous to the one for a cylinder in parallel flow demonstrated by Foeppl.[13] There are two surfaces of discontinuity or mixing zones. The upper one may be approximated by a cycloid which essentially depends on the velocity v_u and the magnitude of the negative pressure behind the overflow edge. (M. C. Woronetz[14] gives an analysis of three characteristic nappe shapes. These shapes were also recognized in the case of combined overflow and underflow. For certain flow conditions they all occurred in periodic sequence.) The configuration of vortices contained within these surfaces is unstable. In a real fluid the vortices tend to grow until finally they are carried along with the flow. An infinitesimal disturbance is sufficient to initiate a periodic shedding of vortices.

Assume that the counterclockwise vortex is growing as shown on Fig. 23(a), Fig. 23(b) up to Fig. 23(c) where it occupies the entire wake. As a result, the velocity gradient and the vorticity in the lower boundary of the wake will increase to such an extent that this surface will gradually break up and form a clockwise vortex. To keep the total circulation constant, a counterclockwise circulation around the plate is induced at the some time. (In the model this circulation was demonstrated by means of dye injected on the upstream side of the gate.) Therefore, the clockwise vortex grows and increases the instability of the upper surface of discontinuity until, in Fig. 22 (f), this upper surface breaks up.

The simultaneous fluctuation of the nappe can be explained by the superposed circulation around the plate which, in Fig. 23(a), reduces the velocity v_u and augments v. Consequently, the trajectories of the nappe tend to move upstream toward the plate which is in accordance with equations derived elsewhere.[14] Simultaneously, the lower jet sucks up the remainder of the previously generated vortex due to its higher kinetic energy which, in addition to the velocity change, helps to bring the nappe closer to the plate on account of pressure reduction beneath the nappe. At the phases represented by Figs. 23(d), (e), and (f) the lower jet is decelerated so that more and more retarded and reversed fluid enters the wake and increases the pressure there. Together with the acceleration in the upper streamlines this causes the nappe to swing away from the plate.

The reason why the aeration of the nappe plays an important role in the vibration phenomenon is that the periodic pressure change described above does not develop to the same degree when the nappe is ventilated. Nevertheless, vibrations have been experienced with the ventilated nappe as well. Their violence depends to a large extent on the size of the air vent (concerning air demand see G. H. Hickox.[15] With the nappe submerged by the surface roller the phenomenon becomes more difficult to survey on account of the interaction of a third mixing zone (Fig. 16(b)). The excitation mechanism, however, remains essentially the same.

The force pulsation exerted on the bottom plate (Fig. 14) finds its explanation in the periodic supply and evacuation of separated fluid, taking place par-

---

13 Mathematische Stroemungslehre, by W. Mueller, Springer, Berlin, 1928, p. 108.

14 "Sur la forme de la nappe des deversoirs sans aerage," by M. C. Woronetz, C. R. hebd. Seances Academie Sci. 238, 1954, p. 1688.

15 "Aeration of Spillways," by G. H. Hickox, Transactions, ASCE, Vol. 109, 1944, p. 537.

ticularly between bottom plate and surface of the lower jet. Thereby a secondary flow is superposed on the flow that is represented in Fig. 23, producing a downward force on the plate in phases a and b and an upward force in phases d and e. The time intervals between the phases of Fig. 23 are not necessarily equal. The smaller the depth of overflow or the lower the tailwater, the shorter the time the nappe requires to swing away from the gate, because an air-

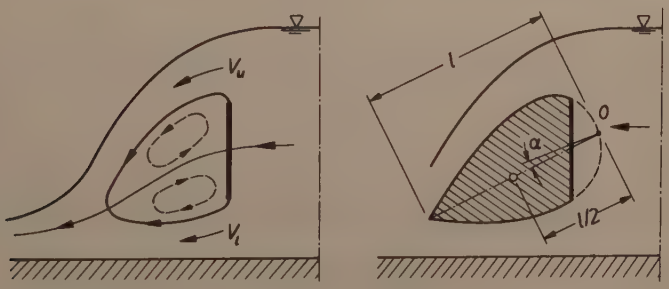

FIG. 22.—WAKE BEHIND A VERTICAL FLAT PLATE FOR FREE SURFACE FLOW

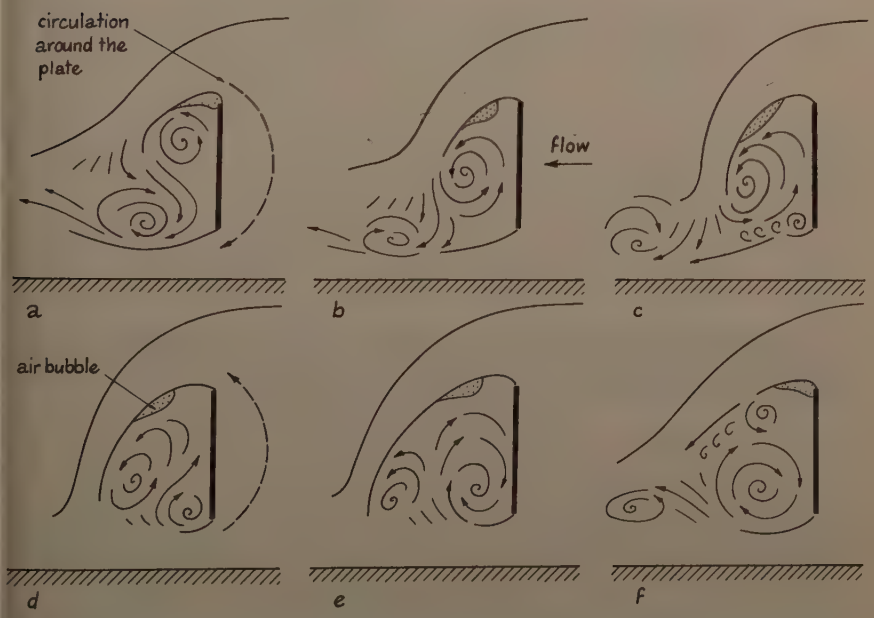

FIG. 23.—SCHEMATIC REPRESENTATION OF ONE CYCLE OF THE VIBRATION PHENOMENON. FREE DISCHARGE WITH THROTTLED AIR VENT

water mixture can enter the wake near the toe of the nappe (Fig. 16(b)). This is the reason that the rate of change in force is greater, sometimes even abrupt, in the upward direction (Fig. 17(b)). For a large depth of overflow and a small head differential, the excitation is nearly harmonic (Fig. 17(c)).

With this concept of the periodic flow conditions, and with reference to a hypothesis about the formation of the von Kármán vortex trail[16], an expression for the frequency of the excitation may be dervied. The basic idea is to consider the wake behind the obstacle as a cylindrical oscillator free to rotate with respect to an imaginary axis 0 (Fig. 22). The circulation around this oscillator, as indicated by dotted lines in Fig. 23, superposed on the main flow then produces a transverse force known as the Magnus effect. Due to the convex boundaries of the wake, an acceleration of the adjacent flow causes pressure drop and vice versa. Consequently, in the lowest position the wake is acted on by a lifting force (Fig. 25(c)) and in the highest position by a downward force (Fig. 23(f)). These forces may, hence, be defined as restoring or spring forces. Furthermore, there are self-controlled driving forces due to the breaking up of the surfaces of discontinuity that take place with a phase displacement of $\pi/2$ against the reversal of wake motion, as explained above. These two groups of forces combined with the inertia forces of the wake mass are in a state of equilibrium that can be expressed by the differential equation

$$m \frac{d^2x}{dt^2} - k \frac{dx}{dt} + c\,x = 0 \quad \ldots\ldots\ldots\ldots\ldots \quad (7)$$

assuming that

1. The "spring force" varies linearly with the wake "deflection" x.
2. The "driving force" is proportional to dx/dt.
3. The wake mass m remains constant during vibration.

When the driving force, in vibration theory known as the negative damping, is small with respect to the other forces and smaller than 20% of the critical damping,[17] then the frequency of the wake vibration may be approximated by the natural frequency of the undamped system

$$f = \frac{\sqrt{\frac{c}{m}}}{2\,\pi} \quad \ldots\ldots\ldots\ldots\ldots\ldots \quad (8)$$

Because the cross section of the wake is similar to that of an airfoil (Fig. 22(b)), an equation may be set up for the "spring force" per unit width in a manner analogous to that for the lift of an airfoil:[18]

$$c\,x = (2\,\pi\,\eta\,\alpha)\,\frac{1}{2}\rho v^2 \quad \ldots\ldots\ldots\ldots\ldots \quad (9)$$

The term within parenthesis represents a lift coefficient for small angular displacements $\alpha \leq \pi/30$, η is a form coefficient, and $\alpha = 0$ denotes the position of the profile axis at which cx = 0. The slight variation in direction of the approaching velocity v due to the angular displacements is neglected.

---

16 "Formation of Vortex Streets," by G. Birkhoff, Journal of Applied Physics, Vol. 24, 1953, p. 98.

17 Mechanical Vibrations, by J. P. Den Hartog, 4th edition, McGraw-Hill Book Co., Inc., New York, 1956, p. 50.

18 Technische Stroemungslehre, by B. Eck, 5th edition, Springer, Berlin, 1958, p. 308.

Suppose the mass m of the wake is concentrated at the center of the profile axis (Fig. 22); then

$$x = \frac{\alpha l}{2} \quad \ldots\ldots\ldots\ldots\ldots\ldots \quad (10)$$

The mass per unit width can be expressed by

$$\frac{m}{b} = \zeta w^2 \rho \quad \ldots\ldots\ldots\ldots\ldots\ldots \quad (11)$$

in which ζw^2 is the cross-sectional area of the mass in terms of the gate height w and ρ is the density of water. By substituting Eqs. 9, 10, and 11 in Eq. 8,

$$f = \sqrt{\frac{\eta}{2 \pi \zeta}} \left(\frac{v}{w}\right) \ldots\ldots\ldots\ldots\ldots\ldots \quad (12)$$

is obtained. (At the limit $d_2 \to d_0$ and $h = y \to \infty$ the square root of the last equation corresponds to the Strouhal number.[19]

The analysis, of course, is rather crude and incomplete. There is still no functional relationship between the coefficients η and ζ and the remaining variables of the problem. The mass coefficient ζ, for instance, should account for the added mass in the adjacent jets and the surface roller, and also indicate the influence of structural parts within the wake that prevent some of the water mass from oscillating. Nevertheless, it is remarkable that if one replace v by $\sqrt{2\, g(d_0 - d_2)}$ and plot the dimensionless quantity f w/v against the ratio $(d_0 - d_2)/w$ in Figs. 19 and 20, nearly straight lines parallel to the abscissa are obtained for various test series in the case of nonaerated flow.

CONCLUSIONS

1. In contrast to conditions of gates subject to either overflow or underflow, in which the occurrence of vibration is very limited, vibration under conditions of simultaneous overflow and underflow persists through almost any variation of flow conditions as long as the depth of overflow is greater than a critical value.

2. With decreasing tailwater depth, the exciting forces increase up to the stage at which a free water surface begins to develop beneath the nappe. The disturbance of the excitation thus caused will set in earlier and become more intensive with increased nappe aeration efficiency.

3. Means of mitigating the vibration that are not objectionable from a structural or functional viewpoint are found to have only limited effect. The excitation will be efficiently minimized only when favorable types of gate and apron are selected.

4. In general the structural elements of the gate, exposed to the pulsating forces, should be withdrawn as far as possible from the confluence of upper and lower jet. This is accomplished most effectively by a sloping downstream floor. The slope should not exceed 1 on 1.8, however, because a steeper slope will lead to separation and instability of the lower jet. On the other hand, there is a critical distance between gate bottom and lower jet. Reducing this distance

19 "Ueber eine besondere Art der Tonerregung," by V. Strouhal, Wiedemann Ann., , 1878, p. 216.

further will result in a sudden drop of excitation accompanied by an increase in frequency.

5. From comparative experiments on a fixed and a flexibly suspended model gate it has been found that the complex phenomenon of a self-excited and multiply coupled gate vibration can be approximated by a forced vibration, the excitation of which is to be determined from tests with the gate in fixed positions.

6. Exterme magnification of the gate deflections can be obtained by means of extraneous control. This is important with gates in navigable rivers, because pressure waves induced by ship engines may adversely affect the gate vibration.

7. The frequency of the excitation is defined satisfactorily by a coefficient similar to the Strouhal number.

Journal of the
HYDRAULICS DIVISION
Proceedings of the American Society of Civil Engineers

PRESSURES ON SPILLWAY FLIP BUCKETS

By Armando Balloffet,[1] F. ASCE

SYNOPSIS

Pressures on cylindrical flip buckets may be computed by assuming an irotational vortex flow. Correlation between maximum theoretical pressures us determined and maximum pressures observed in model studies is presented. This correlation shows that, despite the simplifications involved, the eory may provide a good estimate of the maximum pressure, both for chute d for tunnel spillway flip buckets.

INTRODUCTION

Flip buckets are often used when large amounts of energy must be disposed at the end of spillways. Flip buckets are not dissipating devices, for dispation usually requires the depth provided by a hydraulic jump, and it is safe state that no appreciable energy is taken from the flow by its deflection due the flip bucket. Erosion in the river bed will produce enough depth for dispation due to turbulence and air compression. A natural stilling pool thus rmed replaces the man-made dissipator, which would usually be very exnsive if the flow and the head are considerable.

In the design of a flip bucket, prime consideration is given to the force to ich the structure is subjected as a result of the dynamic effect of the curvi- ear flow over it.

Note.—Discussion open until February 1, 1962. To extend the closing date one month, written request must be filed with the Executive Secretary, ASCE. This paper is part the copyrighted Journal of the Hydraulics Division, Proceedings of the American Soety of Civil Engineers, Vol. 87, No. HY 5, September, 1961.

[1] Senior Design Engineer, Tippetts-Abbett-McCarthy-Stratton, Engineers and Architts, New York, N. Y.; Lecturer in Civil Engineering, Columbia University, New York, Y.

A first approach to the problem is to compute the overall dynamic effect, or total force caused by the jet deflection, which can be determined by applying the momentum equation. For this, the assumption is made that the true jet deflection is parallel to the slope of the bucket lip.

In addition, it is also necessary to determine the maximum pressure that the structure must support and the pressure diagram, the resultant of which must coincide with the dynamic force computed by momentum considerations.

It is true that every large spillway is a particular problem and that the designer, in many cases, should seek a laboratory endorsement for his layout. Although the laboratory should have a very early role in the design stage, the designer first should resort to previous experimental results on similar structures and to theoretical studies. His conclusions will then produce a layout suitable for experimental work. When the magnitude of the structure does not warrant a model investigation, the designer must analyze the forces involved without specific experimental confirmation.

This paper presents the results of studies made to compare the pressure on cylindrical flip buckets as computed by theoretical considerations with that measured in model investigations.

Notation.—The letter symbols adopted for use in this paper are defined where they first appear, in the illustrations or in the text, and are arranged alphabetically, for convenience of reference, in the Appendix.

THEORETICAL PRESSURE COMPUTATION

Previous studies on flip buckets were presented by D. B. Gumensky,[2] who assumed that the angular velocity of the water on the flip bucket would remain constant for the whole depth. J. H. Douma,[3] assumed that the velocity distribution on the bucket would be that of an irrotational vortex: $V = \frac{A}{r}$, in which A is a constant and r is the radius of any streamline. According to this flow pattern, all the streamlines are circular and concentric with the bucket. This assumption has also been adopted for the studies described herein.

Referring to Fig. 1, the upper streamline of such flow has a radius equal to R - d; the bucket radius is R, and the thickness of the vortex is d. The difference in piezometric heads between any two points (1 and 2), is located respectively on the upper streamline and on the bucket, is given by Bernoulli's equation applied to an irrotational flow:[4]

$$\Delta h = \frac{V_1^2 - V_2^2}{2g} \quad \ldots\ldots\ldots\ldots\ldots\ldots \quad (1)$$

in which V_1 and V_2 are the velocities at points 1 and 2 respectively. Thus:

$$\Delta h = \frac{V_1^2}{2g}\left(1 - \frac{V_2^2}{V_1^2}\right) = \frac{V_1^2}{2g}\left[1 - \left(\frac{R - d}{R}\right)^2\right] \quad \ldots\ldots\ldots \quad (2)$$

---

2 "Design of Side Walls in Chutes and Spillways," by D. B. Gumensky, Transactions ASCE, Vol. 119, No. 2675, 1954.

3 J. H. Douma on 2.

4 "Hydrodynamics," by H. Lamb, Cambridge University Press, 1932, pp. 19.

ince the pressure at point 1 is atmospheric:

$$\frac{p_2}{\gamma} = \Delta z + \frac{V_1^2}{2g}\left[1 - \left(\frac{R - d}{R}\right)^2\right] \quad \ldots\ldots\ldots\ldots \quad (3)$$

n which Δz is the difference in elevation between points 1 and 2, p_2 is the ressure at point 2, and γ is the specific weight of the water.

The velocity at point 1 is: $V_1 = \sqrt{2\,g\,H_t}$, in which H_t may be assumed equal o the difference in water surface elevation at the reservoir and at point 1, thus gnoring the head loss on the chute.[2]

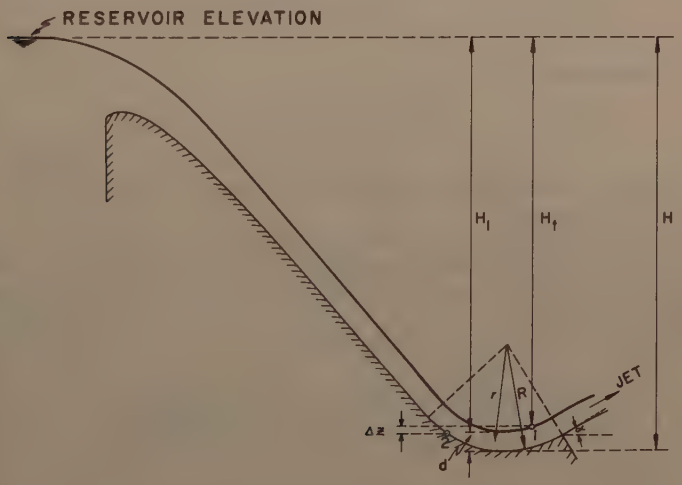

FIG. 1.—CHUTE FLIP BUCKET

It may be noted that V_1 should vary for different locations of point 1 on the pper streamline, since H_t is variable. However, the irrotational vortex pat- rn asusmes that V_1 varies only with the radius, and must be constant over ny streamline. For a high dam, this inconsistency may be neglected, because ie variation of H_t is relatively small. Therefore, point 1 may be selected at ie lowest water-surface elevation over the bucket, with $H_t = H_1$.

Consequently:

$$\frac{p_2}{\gamma} = \Delta z + H_1\left[1 - \left(\frac{R - d}{R}\right)^2\right] \quad \ldots\ldots\ldots\ldots \quad (4)$$

From Eq. 4, p_2 can be determined, provided that the thickness of the jet is known. This is accomplished by integrating the velocity and equating to the discharge per unit width, q:

$$q = \int_{R-d}^{R} V \, dr = \int_{R-d}^{R} \frac{R - d}{r} V_1 \, dr \quad \ldots\ldots\ldots \quad (5)$$

and

$$q = (R - d) V_1 \ln \frac{R}{R - d} \quad \ldots\ldots\ldots\ldots \quad (6)$$

From Eq. 6, d may be computed by developing the logarithm in series:

$$q = (R - d) V_1 \left[\frac{d}{R} + \frac{1}{2} \left(\frac{d}{R}\right)^2 + \frac{1}{3} \left(\frac{d}{R}\right)^3 + \ldots\ldots \right] \ldots \quad (7)$$

For small values of d/R:

$$d \rightarrow \frac{q}{V_1} = \frac{q}{\sqrt{2 g H_1}} \quad \ldots\ldots\ldots\ldots\ldots \quad (8)$$

Eq. 8 neglects the variation of velocities across the flow for the computation of the jet thickness.

The theoretical value of the pressure compared by Eq. 4 for any point on the bucket surface should not vary much for a high dam spillway. However the maximum value corresponds to the lowest point of the bucket, because the Δz is maximum and equal to d.

Thus, the maximum pressure is given by:

$$h = \left(\frac{p_2}{\gamma}\right)_{max} = d + H_1 \left[1 - \left(\frac{R - d}{R}\right)^2 \right] \ldots\ldots\ldots \quad (9)$$

or

$$h = d + \frac{V_1^2}{2 g} \left[1 - \left(\frac{R - d}{R}\right)^2 \right] \ldots\ldots\ldots\ldots \quad (10)$$

Once the maximum pressure has been computed, the theoretical pressure diagram may be determined as shown in Fig. 2. A circle is drawn with center at the bucket center and radius equal to R + h. Then, the pressure at any point A may be represented by a radial segment AB equal to h minus the elevation of point A with respect to the lowest point of the bucket surface.

Since the curvature of the flow is assumed to start at the station of the point of tangency between the chute and the bucket, the theory introduces a discontinuity in the pressure diagram. Similarly, a discontinuity results with the computation of the depth from Eq. 6. In fact, the flow curvature must start upstream of the bucket.[2,5] For a thin jet, however, it may be assumed that the flow curvature starts close to the tangency point.

Fig. 2 shows a comparison between the shapes of the theoretical pressure diagram and of diagrams determined by the experimental investigations reported below.

5 "Engineering Hydraulics," by H. Rouse, Wiley, New York, 1950, pp. 47.

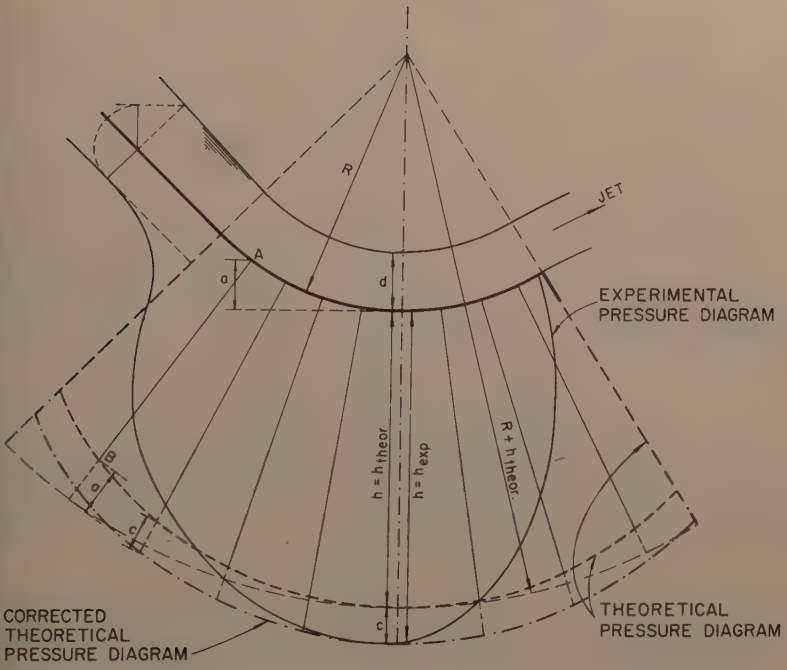

FIG. 2.—THEORETICAL AND EXPERIMENTAL PRESSURE DIAGRAMS

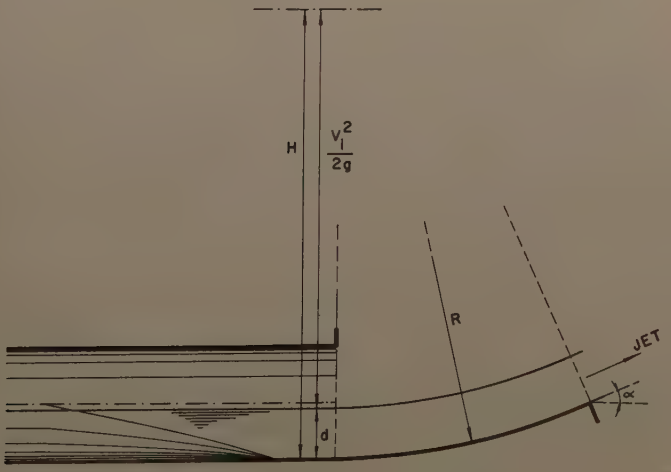

FIG. 3.—TUNNEL FLIP BUCKET

The foregoing reasonings have been made, having in mind the case of a chut flip bucket. In the case of a tunnel bucket (Fig. 3), like those described by T J. Rhone and A. J. Peterka,[6] Eq. 3 would be less applicable in theory. Its us for a "transition flip bucket" might be questionable, since this structure is no two-dimensional, as it has been assumed in the theory of the irrotational vor tex. However, it is worth investigating the correlation between the pressure computed with the theory and the values determined experimentally. The the ory is in good agreement with the values of the pressures obtained for th similar case of pipe curves.[7,8]

For a tunnel flip bucket, V_1 in Eq. 10 should be taken equal to the velocit just upstream of the bucket. Since the change in flow direction is much les for a tunnel flip bucket than for a chute flip bucket, the flow curvature shoul begin closer to the tangency point in the case of the tunnel. This also suggest the use of the depth just upstream of the bucket as a value for d.

EXPERIMENTAL PRESSURE DETERMINATION FOR CHUTE SPILLWAY FLIP BUCKETS

In the two-dimensional case of a straight chute spillway of constant width the following simple relationship may be derived by dimensional analysis fo the maximum pressure on the bucket:

$$\frac{h}{R} = f\left(\frac{H}{R}, \frac{H_o}{R}\right) \quad \ldots\ldots\ldots\ldots\ldots\ldots \quad (11$$

in which (Fig. 1) H is the reservoir elevation with respect to the lowest poi of the bucket and H_o is the head over the crest of the weir. Eq. 11 does n include the terminal angle of the bucket, this fact being consistent with Eq. 1

The United States Army Corps of Engineers has performed model studie at the Waterways Experiment Station, Vicksburg, Miss., on the chute spillway of Pine Flat and Hartewll Dams.[9,10] These constant-width spillways hav cylindrical buckets of the type described in this paper. For Hartwell Da spillway bucket, radii of 30 ft and 40 ft, and lip angles of 20°, 30°, and 40 were studied. The chute slope was 1.00 vertical to 0.67 horizontal. The max imum prototype head over the bucket was H = 160.4 ft and the maximum dis charge approximately 1,000 cfs per ft. For Pine Flat Dam, the bucket radiu was 50 ft and the lip angle 20°. The chute slope was 1.00 vertical to 0.7 horizontal. The maximum prototype head over the bucket was H = 352.3 ft an the maximum discharge approximately 1,350 cfs per ft.

---

6 "Improved Tunnel Spillway Flip Buckets," by T. J. Rhone and A. J. Peterka, Pro ceedeings, ASCE, Vol. 85, No. 2316, 1959.

7 "Minimum Pressures in Rectangular Bends," by M. B. McPherson and H. Strausser, Proceedings, ASCE, Vol. 81, No. 747, 1955.

8 Fluid Mechanics for Hydraulic Engineers, by H. Rouse, McGraw-Hill Book Co New York, 1938, pp. 269.

9 U. S. Army Engineer Waterways Experiment Station: Technical Memorandum N 2-375, Vicksburg, Miss., 1953.

10 U. S. Army Engineer Waterways Experiment Station: Technical Memorandum N 2-393, Vicksburg, Miss., 1954.

Prototype studies on Pine Flat Dam[11] have been reported in general agreement with the model studies, but, so far, for discharges much smaller than the design discharge.

The Hartwell Dam model studies showed that, for the same bucket radius and discharge, the maximum pressures were very similar for bucket lip angles of 30° and 40°. For 20° angles, the maximum pressure was no less than 93% of that corresponding to 40°. This departure tended to decrease for the lower discharges used in the studies. Thus, the assumption that the maximum pressure is independent of the lip angle appears correct, at least for the angles most commonly used in American practice. In any case, for small lip angles, the maximum pressure determined by comparison with these model studies would be on the safe side.

Fig. 4 shows a log-log plot of Eq. 11 with the data corresponding to the models of Hartwell and Pine Flat Dams. Although the information available is not enough to draw many contours, it shows a very definite trend. This plot may also be of help to the designer for the comparison of the data corresponding to this particular layout with those of two projects that have been tested satisfactorily.

Fig. 5 is a plot of observed maximum pressures for Hartwell and Pine Flat models versus theoretical maximum pressures according to Eq. 10, with d computed using Eq. 8. The best fit straight line may be expressed as:

$$h_{exp} = 1.16\ h_{theor} \quad \ldots\ldots\ldots\ldots\ldots \quad (12)$$

with a standard error of 3.4 ft and a correlation coefficient of 0.999. This correlation is good, despite the wide range of variation of h and of the lip angle α. The coefficient of Eq. 12 takes care of the simplifications made in the theoretical analysis.

Fig. 6 is a plot of the same observed maximum pressures versus theoretical pressures according to Eq. 10, but with d computed using Eq. 6. The best fit straight line may be expressed as:

$$h_{exp} = 1.02\ h_{theor} \quad \ldots\ldots\ldots\ldots\ldots \quad (13)$$

with a standard error of 6.4 ft and a correlation coefficient of 0.997.

Eq. 13 shows that the irrotational theory provides a good estimate of the experimental values of the maximum pressure. The simplifications made to compute theoretical pressures for Eq. 12 result in a systematic larger difference between these values and the experimental ones. When the depth is computed according to the irrotational theory without simplifications, the systematic departure between theoretical and experimental values is only 2%. However, the use of the corrective coefficient results in good correlation for both Eq. 12 and Eq. 13, and the former is easier to use.

The location of the maximum experimental pressure in the models appeared to depend on the lip angle α, being close to the lowest point for lip angles of 30° and upstream of it for smaller angles.

The experimental data used herein indicate that if Eqs. 12 or 13 are used for the computation of the theoretical maximum pressures, and the rest of the

---

11 U. S. Army Engineer Waterways Experiment Station: Technical Report, No. 2-511, Vicksburg, Miss., 1959.

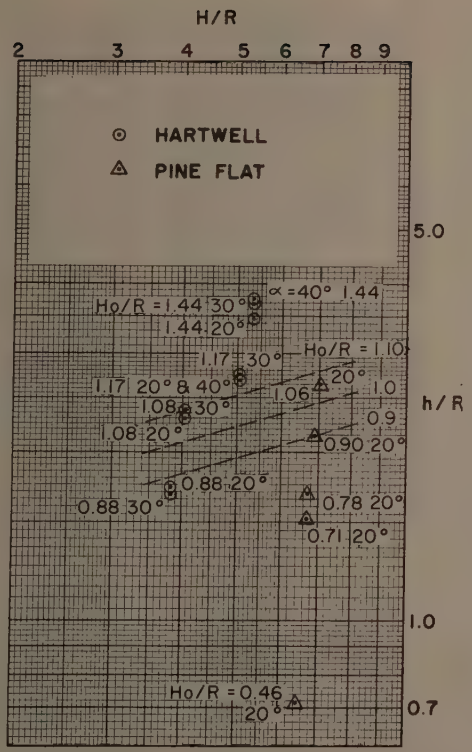

FIG. 4.—NON-DIMENSIONAL EXPERIMENTAL PRESSURE DIAGRAM

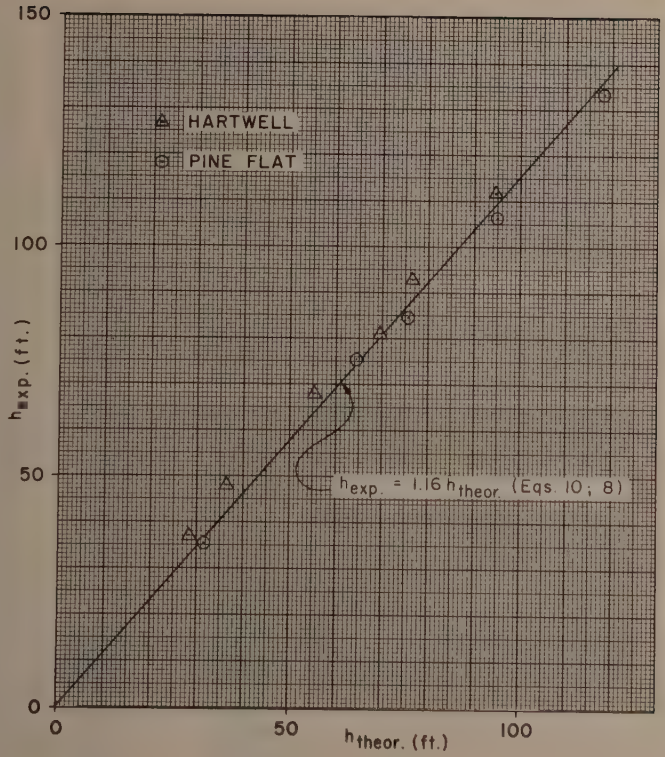

FIG. 5.—OBSERVED VERSUS THEORETICAL PRESSURES USING EQ. 10

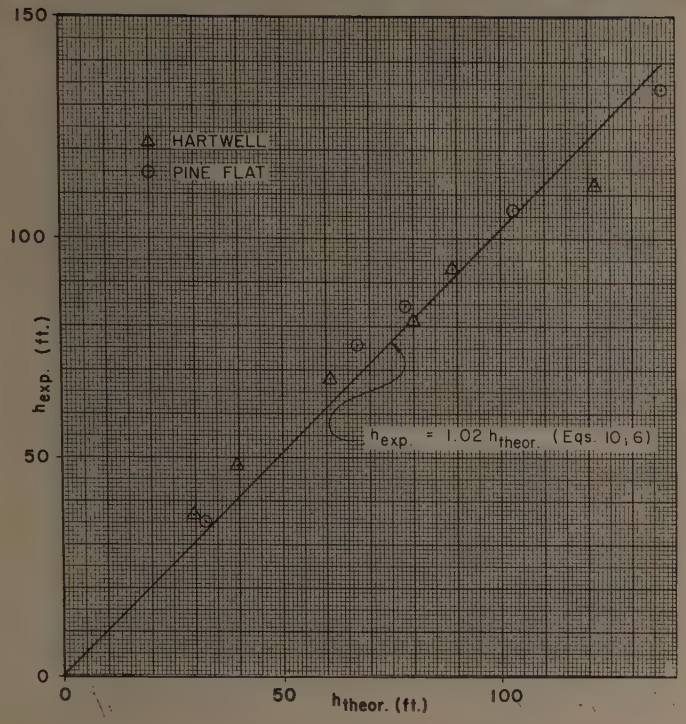

FIG. 6.—OBSERVED VERSUS THEORETICAL PRESSURES USING EQS. 6 AND 10

⊙ FLAMING GORGE DAM TUNNEL SPILLWAY BUCKET NO. 1.
× FLAMING GORGE DAM TUNNEL SPILLWAY BUCKET NO. 2. (PRELIMINARY
⊡ FLAMING GORGE DAM TUNNEL SPILLWAY BUCKET NO 3. (PRELIMINARY
▽ GLEN CANYON DAM TUNNEL PLUG OUTLET WORKS FLIP BUCKET
△ GLEN CANYON DAM TUNNEL SPILLWAY
⊙ WHISKEYTOWN DAM TUNNEL SPILLWAY

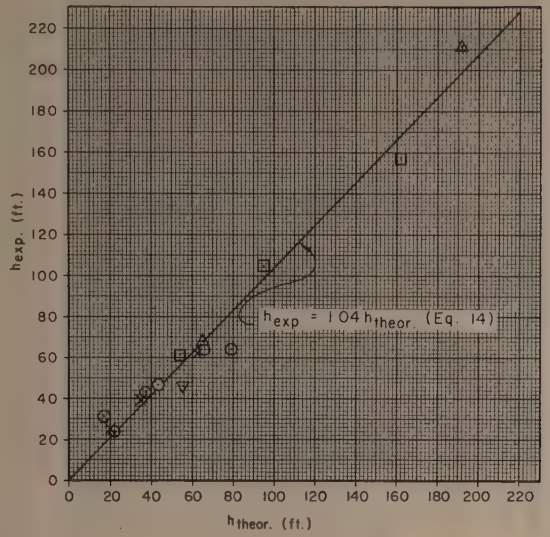

FIG. 7.—OBSERVED VERSUS THEORETICAL PRESSURES USING EQ. 9

pressures on the bucket are computed according to the theory but applying consistently the same coefficients, the resulting diagram will be on the safe side for design purposes. This may be done by increasing the pressures on the theoretical diagram by the difference between $h_{exp.}$ and $h_{theor.}$, denoted as c on Fig. 2.

MODEL STUDIES ON TUNNEL SPILLWAY FLIP BUCKETS

The Bureau of Reclamation, United States Department of Interior (USBR) has conducted model studies on the tunnel flip buckets for Flaming Gorge, Glen Canyon, and Whiskeytown Dams. In total, six different buckets with variable discharges and conditions were studied.[6]

Fig. 7 shows a plot of observed maximum bucket pressures for these projects versus maximum pressures computed according to Eq. 9. The best fit straight line may be expressed as:

$$h_{exp} = 1.04\ h_{theor} \quad \ldots\ldots\ldots\ldots\ldots \quad (14)$$

with a standard error of 8.3 ft and a correlation coefficient of 0.995.

It may be observed that the correlation is good, although the scattering is somewhat larger than for the chute spillways. This should be expected since the geometry of the bucket may vary from case to case more than for the chutes.

In these studies, the maximum pressure was observed at a distance of 0.14 R to 0.18 R downstream of the point of tangency for an angle α of 15°. This distance increased to 0.35 R, for $\alpha = 35°$ and 0.42 R to 0.45 R, for $\alpha = 38°$.

MAXIMUM PRESSURES ON FLIP BUCKETS FOR CONVERGING CHUTE SPILLWAYS

In converging chute spillways with curved weirs the distribution of discharges over the bucket may not be uniform, and maximum dischagre may occur in the vicinity of the centerline. As a consequence, the pressures over the center of the bucket are greater than the value computed by Eq. 10 which is based on the assumption of a uniform discharge over the bucket. Conversely in the vicinity of the side walls, the pressure maximum is smaller than the value computed with Eq. 10. The variation of discharge per unit width changes with the convergence, the length, and the slope of the chute.

Recent experiments were made on two models of the convergent Shihmen Dam Spillway (Taiwan) by the Shihmen Development Commission by arrangement with the Hydraulic Laboratory of Taiwan University, Taipei. In these tests total convergences between the side walls of 40° and 20° were used, as measured by the central angle of the circular weir. The final chute slopes were respectively 1:1 and 1:2. The ratios of weir length to bucket width were 1.72 and 1.47, respectively. The walls had transition curves in plan, so that they became parallel to the centerline upstream of the bucket.

From the results of these tests, the pressure computed by Eq. 10 for a uniform discharge over the bucket approximates the average maximum pressure observed in the model for the same total discharge but with the actual discharge distribution. The pressure distribution along the bucket was more uniform for the model with 20° convergence and 1:2 final chute slope than for the

model with 40° convergence and 1:1 final slope. It was also observed that the pressure rise started at about two depths upstream of the bucket tangency point. This fact is of importance to the location of a joint between the bucket and the chute, as the joint should be located upstream of the region of pressure rise to prevent the transmission of high pressures through the joint and creation of excessive uplift pressures.

More investigations are necessary to draw definite conclusions about the pressure distribution on converging spillway buckets.

CONCLUSIONS

Maximum pressures on spillway flip buckets may be easily computed by assuming an irrotational vortex flow. The pressures measured on models of both straight chute and tunnel flip buckets show good correlation with and are close to the theoretical values of those pressures. The theoretical formulas may be corrected, by the use of suitable coefficients, to conform with the experimental results. The distribution of pressures over the bucket may be approximated by a simple graphical procedure. Although the results of model tests on converging spillways show qualitative agreement with the theoretical pressure computations, more studies are required to establish the relationship between the geometry of the spillway and the pressure distribution on the bucket.

ACKNOWLEDGMENTS

This paper has been based on studies made in the Hydroelectric Department of Tippetts-Abbett-McCarthy-Stratton, Engineers and Architects, New York, N. Y. Some of the computations and figures were made by Herbert Meltzer, Chung-Li Ling and William B. Tippetts, engineers of the Civil-Hydraulic Section of the said Department. Arthur R. Luecker and Gordon R. Williams Tams Associates, made very useful suggestions and comments.

The writer is indebted to the United States Army Engineer Waterways Experiment Station and in particular to its Director, Edmund H. Lang, for permission to publish data pertaining to Pine Flat and Hartwell models.

The writer also gratefully acknowledges the information on tunnel spillway flip buckets communicated to him by Walter H. Price, Chief Research Engineer, USBR, Denver, Colo.

APPENDIX.—NOTATION

The following symbols, adopted for use in the paper, conform essentially with "American Standard Letter Symbols for Hydraulics" (ASA Z10.2-1942) prepared by a committee of the American Standards Association with Society representation, and approved by the Association in 1942:

A = a constant equal to the product of the vortex velocity by the radius of the streamline;

d = thickness of the vortex;

g = acceleration due to gravity;

H = reservoir elevation over the lowest point of the bucket;

H_o = head over the crest of the spillway;

H_1 = total head over lowest point of water surface, ignoring head loss over the chute;

H_t = total head over any point 1 on the surface of the vortex, ignoring head loss over the chute;

h = maximum head, given in column of water, on the bucket;

h_{exp} = experimental value of the maximum pressure in column of water;

h_{theor} = theoretical value of the maximum pressure in column of water;

p_2 = pressure at any point of the bucket;

q = discharge per unit width of chute;

R = radius of the bucket;

r = radius of any streamline;

V = velocity at any streamline;

V_1 = velocity at the vortex surface;

V_2 = velocity at any point 2, on the bucket surface;

z = elevation with respect to any datum;

α = lip angle; and

γ = specific weight of water.

Journal of the
HYDRAULICS DIVISION
Proceedings of the American Society of Civil Engineers

ESTIMATING THE PROBABLE MAXIMUM PRECIPITATION

By David M. Hershfield[1]

SYNOPSIS

A method for the systematic analysis of precipitation data for the purpose f estimating the probable maximum precipitation is proposed. Empirical istributions of the spatial and temporal sampling errors enable the analyst) estimate the magnitude of the errors attached to the statistics which are sed to obtain the extreme precipitation. A comparison of the results from ie traditional method with those based on the method presented herein shows ifferences in both directions which occasionally exceed a factor of two. The mphasis has been on an examination of the data rather than on a search for ptimal statistical methods.

INTRODUCTION

The procedure originally used for estimating the probable maximum pre- ipitation (PMP) during the 1940's and still in use in the 1960's, with slight odifications, uses a combination of a physical model and several estimated eteorological parameters. Unlike most investigations in which the estimates un be compared with actual observations, the quality of the estimates obtained om the traditional approach cannot be evaluated. The fact that a PMP estimate as not been exceeded is no standard for evaluating the quality of the estimate. ne lack of a dependent variable and the fact that rainfall is the most intensive-

Note.—Discussion open until February 1, 1961. To extend the closing date one month, written request must be filed with the Executive Secretary, ASCE. This paper is part the copyrighted Journal of the Hydraulics Division, Proceedings of the American Society of Civil Engineers, Vol. 87, No. HY 5, September, 1961.

[1] Meteorologist, Hydr. Services Div., U. S. Weather Bur., Washington, D. C.

ly observed of all the meteorological elements suggest an approach which goes directly to the large mass of rainfall data.

Attempts have been made to by-pass the traditional approach by graduating a sample of rainfall data according to some extreme-value distribution, but several serious weaknesses were encountered. First, there was no reason for preferring one distribution over another. A particular theoretical curve might provide a good fit to the data but like all mathematical curves, the theoretical curve presented a theoretical rather than a real picture of what had occurred or would occur. Second, there was no basis for stopping at a particular probability level. Third, little information was available for a judgment about the magnitude of the sampling errors attached to the estimated distribution parameters.

In 1961, there are two areas which should be considered when estimating PMP; more data and additional statistical techniques. Data for thousands of stations are now available in a form suitable to probability analysis, that is, the annual maximum 24-hr amounts have been extracted from climatic tabulations. A much smaller but significant quantity of 1-hr data is also available. Statistical innovations include several new extreme-value distributions and knowledge of their relationship to each other.

The primary purpose of this paper is to propose certain sysematic methods for the analysis of these rainfall series with the goal of reducing the range of uncertainty surrounding the PMP estimates. The analyses presented herein are based on 24-hr rainfalls from about 2,600 stations with a total of 95,000 station-years of data. A combination of several statistics from each station's data was computed and viewed in the aggregate in order to arrive at an enveloping statistic. Because reliability is a major design parameter, empirical measures of several components of sampling error have been determined for each statistic. Empirical adjustment factors have been derived for such data deficiencies as small sample size and calendar-day rainfall rather than the 1,440-min maximum rainfall. Comparisons between the traditional approach and that developed herein are presented for two large regions of the United States.

ANALYSES

Definition of PMP.—For this paper, the PMP is defined as the largest rainfall (precipitation) that a station is ever likely to experience for a particular duration.

Basic Data.—The data from a key group of 198 long-record 24-hr stations (164 first-order Weather Bureau United States Dept. of Commerce (USWB) and 34 cooperative observer) were used to develop most of the relationships presented herein.

Daily rainfall records from an additional 2,400 stations were analyzed in arriving at an enveloping statistic.

Rainfall Sample.—The extreme rainfall experience at a station can be represented by a sample composed of the annual maximum rainfalls for a particular duration. Each extreme, or annual maximum rainfall, then represents a relatively large number of actual observations, because each value in the series is itself the extreme of a large number of observations. This series is amenable to probability analysis because the items are causally independent and occur in a random fashion, that is, the magnitude of an extreme for a par-

ticular year is unpredictable. It is assumed that the gage exposure remains the same during the sampling period.

Standardized Variate.—

Definition.—Yen T. Chow,[2] F. ASCE demonstrated that the only difference between the various distributions which lend themselves to the analysis of extreme-value hydrologic data is the common statistical variable, K, or standardized variate in the equation

$$x_T = \bar{x}_N + K s_N \quad \ldots\ldots\ldots\ldots\ldots\ldots \quad (1)$$

in which x_T is the rainfall for return period T, in years, when a particular extreme-value distribution is used. The terms $\bar{x}_N$ and s_N are the mean and standard deviation for a series of N annual maxima.

If the maximum observed rainfall, x_M, is substituted for x_T, and K_M, for K, then K_M is the number of standard deviations that must be added to the mean to obtain x_M. The variable K_M is a common denominator which admits of comparison on a probability basis in two ways: (1) it will tell us how rare a maximum observed rainfall at one station is with respect to the maxima at other stations; and (2) how rare the rainfall is at a station if it is assumed that the data follow a particular distribution. The former will be presented first.

Definition of Independent K_M.—The variable, K_M, was determined for each of the 2,600 24-hr stations by computing the mean and standard deviation by the conventional procedures but omitting the maximum observed rainfall from the computation. This computation is equivalent to observing the maximum observed rainfall after $\bar{x}_N$ and s_N have been computed. The distributions of the K_M's are given in Table 1. Neither the maximum observed rainfall, the mean nor the standard deviation was adjusted for such data deficiencies as short record and observational-day rainfall. The term, K_M, as used henceforth in this paper refers to the independent computations.

Independence and Randomness of K_M.—In order that any inferences drawn from the distributions of the independent K_M's be valid, the assumptions of independence and randomness must be satisfied. Plots of some of the larger K_M's show no systematic relationship between rainfall magnitude and geography. Examination of the K_M's for 68 long-record stations in Iowa, a region where the rainfall regime is not influenced locally by orography or bodies of water, shows a range from 2.2 to 11.2. The unusually large storm of January 1943 on the west coast of the United States produced the maximum observed 24-hr rainfalls for 33 of 50 stations in Los Angeles County, Calif. (5,000 sq miles), but the K_M's associated with these maxima vary from 2.2 to 7.1. These are indications that the K_M's occur in a random fashion for raingage networks as dense as the two investigated and previously noted. For practical purposes, the entire sample of 2,600 K_M's may be considered a random sample from a common population of rainfall data regardless of the proximity of the stations or the storm which produced the maxima.

Relationship Between K_M and Return Period.—The second characteristic of K_M is that it is uniquely related to the probability of occurrence of an event at a station if a theoretical distribution is assumed. For example, the 100-yr event is associated with a K of 3.5 for the Fisher-Tippett type I distribution

2 "A General Formula for Hydrologic Frequency Analysis," by V. T. Chow, Transactions, Amer. Geophysical Union, Vol. 32, 1951, p. 231.

TABLE 1.—DISTRIBUTION OF 'K_M' (INDEPENDENT) FOR SELECTED LENGTHS OF RECORD

'K_M'	Length of Record in (Years)													
	10-14	15-19	20-24	25-29	30-34	35-39	40-44	45-49	50-54	55-59	60-64	65-59	70+	Total
1.00- 1.49	8	12												20
1.50- 1.99	41	99	5	1				2		1				149
2.00- 2.49	47	171	23	13	13	8	15	9	10	13	11	1	1	335
2.50- 2.99	36	179	12	20	17	22	13	25	48	45	42	6	1	466
3.00- 3.49	27	128	15	22	20	16	19	30	52	83	54	5		471
3.50- 3.99	18	98	11	20	14	13	18	20	35	63	44	9	5	368
4.00- 4.49	12	51	11	12	10	7	18	16	34	44	49	11		275
4.50- 4.99	5	34	4	8	7	6	7	13	31	36	22	2	2	175
5.00- 5.49	5	18	1	8	4	6	10	13	21	18	19	3	1	126
5.50- 5.99	2	20	2	1	2		3	6	8	17	12	2		77
6.00- 6.49	1	8	3		5	2	2	6	5	7	7	1	1	48
6.50- 6.99	1	6	1			1		3	4	9	3	2		30
7.00- 7.49	2	8	1	1	1		1		4	3	3	1		26
7.50- 7.99		6	1	1	1	1		3	1	1	5	1		21
8.00- 8.49		1		1		1		1	2	7	1	1		15
8.50- 8.99	1	1						1			2			5
9.00- 9.49		2				1	1		1	1	2			8
9.50- 9.99		1	1		1	1		1	4	1				10
10.00-10.49		3			1		1			2				7
10.50-10.99		1			1						2			4
11.00-11.49		2								1	1			4
11.50-11.99		1												1
12.00-12.49														
12.50-12.99														2
13.00-13.49	1	1												
13.50-13.99														1
14.00-14.49			1											1
14.50-14.99	1													
15.00- ----														
Total	208	851	92	108	97	85	108	149	260	352	279	45	11	2645

(Gumbel procedure[3]) whereas a slightly smaller K, perhaps 3.1, might be associated with the two-parameter log-normal. However, it should be emphasized that the quality of the data ordinarily encountered in practice from samples of the size considered here does not justify using a theoretical distribution to graduate the data to some rare probability of the order of magnitude of 10^7 yr. Use of the mean and standard deviation as estimators for PMP provide the amount of accuracy required to exploit the data.

Adequacy of Sample.—

General.—Because relatively small samples will be used in these analyses, some examination of the adequacy of these samples is pertinent. A series of annual maxima is assumed to be a probability sample. However, it is not necessarily a representative sample or, in other words, a miniature replica of the population from which it was drawn. This is especially true when dealing with a vast and inaccessible though finite population. It is also quite possible that the results from the nonrepresentative sample provide a good design estimate because during the entire lifetime of the hydraulic structure a representative sample is not available. The size of sample is not an indication of its representativeness or its randomness, but size is related to the amount of chance variation to be expected from one sample to another.

Consideration of the principal components of sampling variation is an essential preliminary to the analysis of computing the statistics which are used in combination to arrive at the PMP. Measures of the uncertainity involved in estimating both the mean and the standard deviation are developed in the following sections.

The Mean of the Annual Series.—

Sources of Bias in the Mean.—A comparison of the arithmetic means from the 198 50-yr records with those for 10-yr records shows a slight positive bias in favor of the 50-yr means. This bias is so because the distribution of extremes is skewed to the right which means that there is a greater chance of getting a large than a small extreme as the length of record increases. Another factor which can contribute to this bias is the introduction of an outlier, or unusually large event, into the series of extremes. Recognition of these factors is an important preparatory step to computation of both the mean and the standard deviation.

Adjustment of Mean for Outlier.—In a study[4] reported on in 1960, the Fisher Tippett type I distribution was found to give an adequate description of the behavior of rainfall extremes. Making use of this knowledge, hypothetical extreme-value distributions for several lengths of record were developed by reading suitable values on extreme-value probability paper (Fisher-Tippett type I distribution) at the intersection of a straight line and the probability levels, $m/(N + 1)$, at which m is the rank of each item and N is the length of record. The slope of the line, or direction of these hypothetical distributions, was made equal to the average 198 station 100-yr to 2-yr ratio of 2.5. The ratios of two means were computed for several record lengths: the numerator mean does not include the maximum observed event whereas the denominator includes all the events. Additional ratios were developed by varying the maximum event from three times the second highest event to equality with the

3 "Statistics of Extremes," by E. J. Gumbel, Columbia Univ. Press, New York, 1958, p. 375.

4 "An Empirical Appraisal of the Gumbel Extreme-Value Procedure," by D. M. Hershfield and M. A. Kohler, Journal of Geophysical Research, Vol. 65, No. 6, June, 1960, p. 1737.

second highest. The relationship between the increase in the mean as a function of the ratio of the two means and record length is illustrated in Fig. 1. For example, if the ratio of the two means from a 20-yr record is 0.90, then the mean which was computed from all the data is multiplied by 0.94 or reduced by approximately 6%. It should be noted that this relationship considers only the effect of the maximum observed event on the mean. No consideration was given to other anomalous appearing observations.

Adjustment of Mean for Sample Size.—The means from both 10-yr and 50-yr records from the 198 key stations were first adjusted for an outlier according to the relationship of Fig. 1. The average ratios of 50-yr mean to 10-yr, 15-yr,

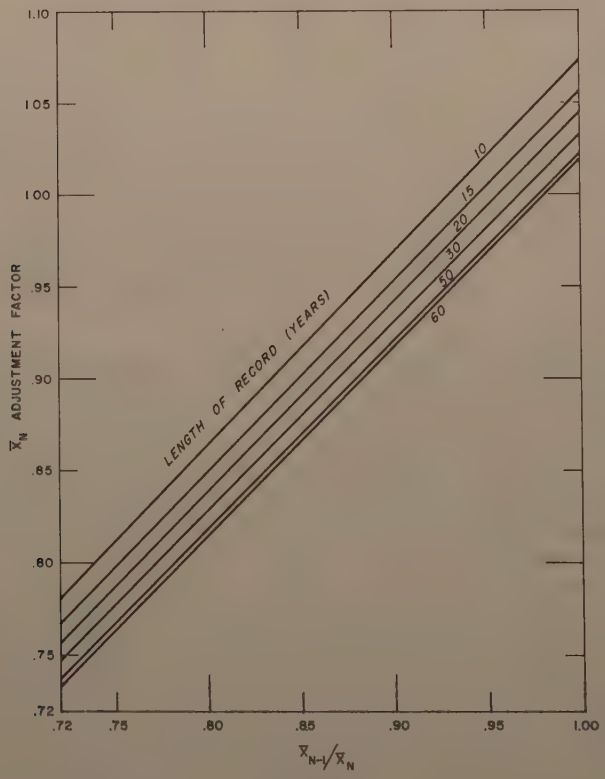

FIG. 1.—ADJUSTMENT OF MEAN FOR MAXIMUM OBSERVED RAINFALL

20-yr, and 30-yr means were then determined. A comparison of the small number of available 60-yr and 70-yr means with the 50-yr means showed only a negligible difference. Thus, the statistics from the 50-yr record were used as a standard to adjust those from shorter records. Fig. 2 shows a plot of the 50-yr means versus those for the 10-yr means after an adjustment had been made for the maximum observed event. The average bias is seen to be about 5% with an average sampling error of approximately 5%

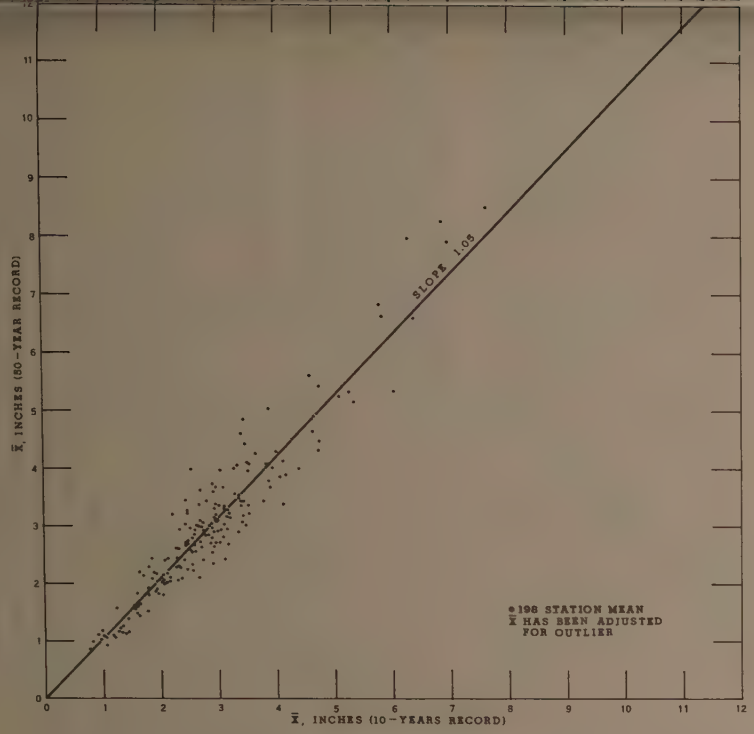

FIG. 2.—COMPARISON OF MEANS FROM 50-YR AND 10-YR RECORDS

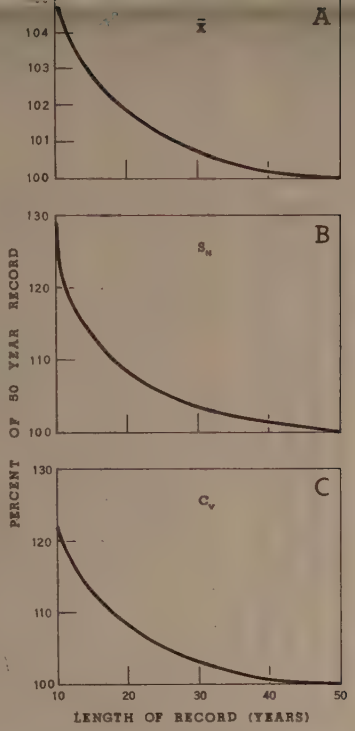

FIG. 3.— SAMPLE-SIZE ADJUSTMENT DIAGRAMS FOR MEAN, STANDARD DEVIATION, AND COEFFICIENT OF VARIATION

Diagram A of Fig. 3 presents the relationship to be used to adjust a mean fo sample size. For example, the mean from a 20-yr record would be adjuste upward by approximately 2% to make it comparable to the 50-yr standard

Measure of Spatial Sampling Error.—Daily data were examined from 6 long-record stations in Iowa in order to gain some perspective of the spatia variation of the mean. Even though a slight latitudinal trend exists, the averag discrepancy around the overall mean of 2.5 in. is 0.2 in. This indicates tha the mean of the annual series is a relatively stable statistic.

Standard Deviation.

Definition.—Another common and easily understood statistic is the standar deviation. Essentially, this statistic is a measure of dispersion of the dat around their mean. When dealing with extreme rainfalls, it is an unbalance measure around the mean of a distribution which is skewed to the right,—th average coefficient of skew for a selected sample of 118 24-hr stations fo a common 43-yr record being approximately 1.2.

The three principal sources of unreliability in estimating the standar deviation are the sampling errors due to spatial variation, sample size, an the inclusion of an outlier into the distribution. The amount of confidence t be placed on a single station's standard deviation can be estimated from th relationships which follow.

Measure of Spatial Sampling Variation.—The chance occurrence of severa large rainfalls at one station and not at another nearby station can result in large discrepancy between the two stations' standard deviations. The proble herein is to obtain some measure of this station-to-station variation. The 6 24-hr stations in Iowa were again selected for analysis. As indicated earlie the rainfall regime in Iowa is not influenced locally by bodies of water o orography. There is, however, a slight systematic latitudinal variation acros the state which was not considered. A measure of the intrinsic spatial samplin variation is provided by the dispersion around the mean standard deviation 0.97 in. The standard deviations range from 0.70 in to 1.30 in. with two-third of them within the interval 0.81 to 1.13 in.

The Effect of An Outlier.—The effect of an outlier is much greater on th standard deviation than the effect previously shown for the mean. For in stance, in 1955, 12.12 in. occurred at Hartford, Conn., during a continuou 24-hr period. This amount exceeded the previously observed maximum by 80 and increased the standard deviation by 67%, but the mean was only increase by 6%. For shorter records, an anomalous event might increase the standar deviation by several hundred percentage.

Adjustment of Standard Deviation for Outlier.—A test statistic was create which is based on the same hypothetical series and procedures develope previously for the mean. The statistic is the ratio of two standard deviatio and is sensitive to the kind of anomalies expected. The numerator does n include the maximum observed value in the computation of the standar deviation whereas the denominator includes all the observations. The graphic relationship is shown in Fig. 4. An average ratio of 0.85 for a 15-yr reco indicates that the extreme observation occurred according to a probabili distribution which defines a straight line on extreme-value probability pap with slope equivalent to a 100-yr to 2-yr ratio of 2.5. This means no adjus ment for the standard deviation. A ratio of 0.70 indicates that an outlier is the series of extremes, that is, an extremely rare event, perhaps, a 1,000-y event occurring during a short period of record. The standard deviation wou then be adjusted downward or reduced by approximately 20%.

Distribution of Standard Deviation Ratios.—The empirical distributions of these ratios for the key group of 198 24-hr stations are illustrated in Fig. 5 in the form of histograms. The dispersion of the ratios around their mean varies inversely with record length, that is, the random variation about the mean value is considerably smaller when the frequencies are computed from long-record groups than when computed from short-record groups. The 15-yr record histogram shows that approximately two-thirds of the ratios are to the left of the 0.85 ratio or that the maxima for two-thirds of the stations occurred

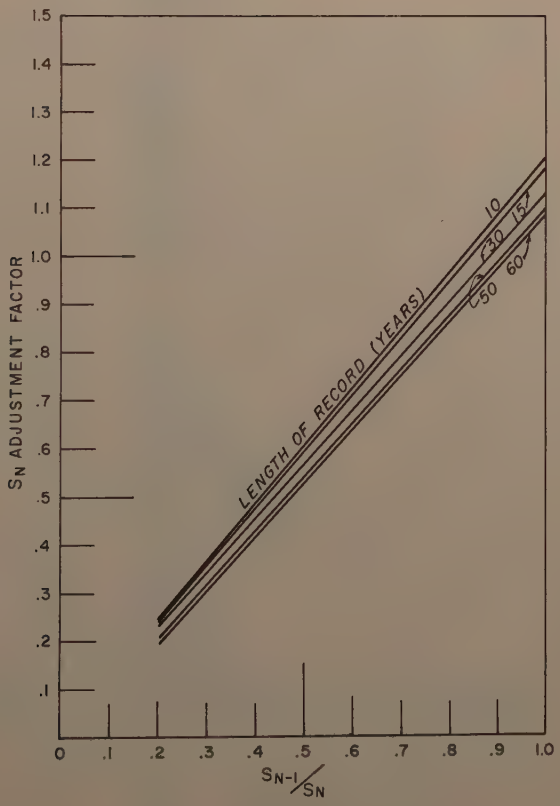

FIG. 4.—DIAGRAM FOR ADJUSTING THE STANDARD DEVIATION FOR THE MAXIMUM OBSERVED RAINFALL

before their average return period. This is consistent with the probability theory which holds that there is approximately a 2:1 chance that an event will occur before its average return period.

Adjustment of Standard Deviation for Sample Size.—The effect of record length is much more pronounced on the magnitude of the standard deviation than the mean. The average ratio of the 50-yr standard deviation to the 10-yr

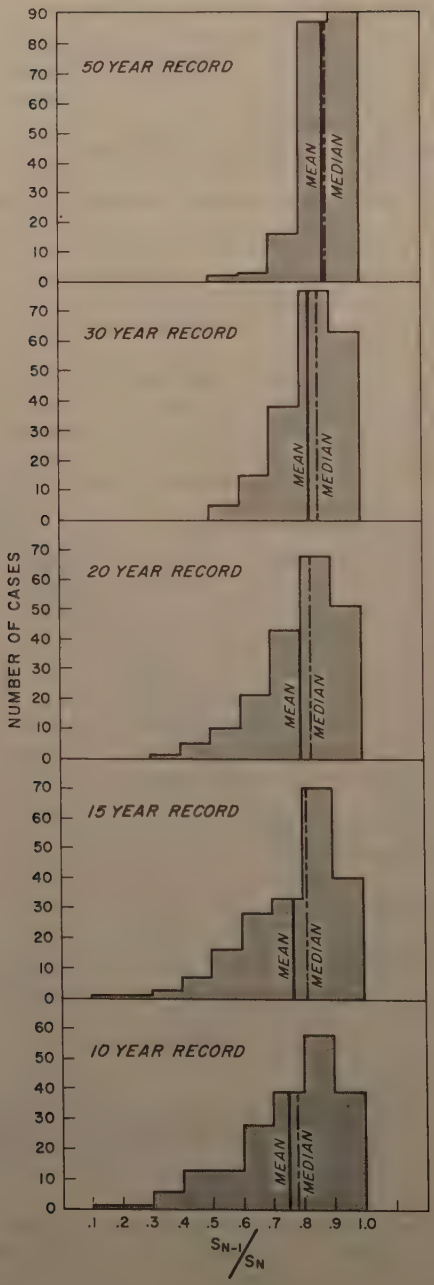

FIG. 5.—EMPIRICAL DISTRIBUTION OF STANDARD DEVIATION RATIOS

standard deviation, after both have been adjusted for an outlier, is 1.29. This compares to the 1.05 ratio for the mean. The comparison of the two standard deviations is illustrated in Fig. 6.

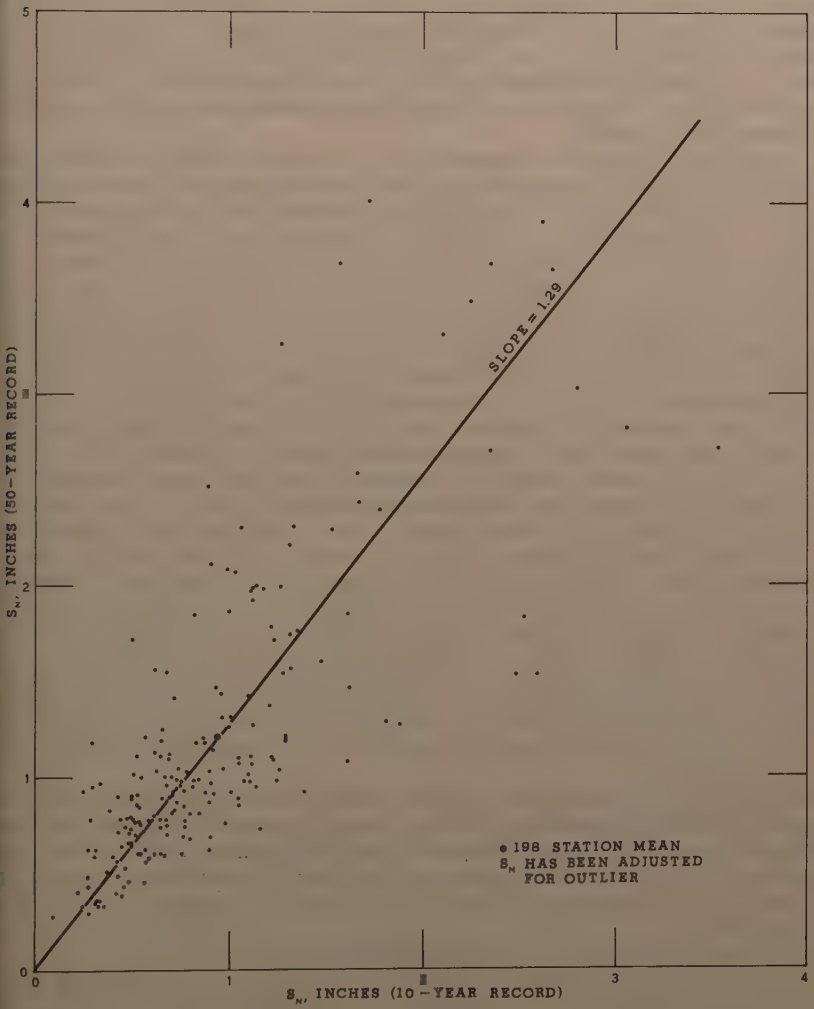

FIG. 6.—COMPARISON OF STANDARD DEVIATIONS FROM 50-YR AND 10-YR RECORDS

The average relationship between the 50-yr standard deviation, which was sed as a standard, and the shorter record standard deviations is shown in iagram B of Fig. 3. Tests comparing the standard deviations from the small umber of 60-yr and 70-yr records with the 50-yr records showed an average

increase of only 1%. Thus, the 50-yr standard deviation was used as a reference standard for the estimation problem of this paper.

Coefficient of Variation.

Definition.—The numerical value of the coefficient of variation (C_V) is obtained by dividing the standard deviation by the mean. This statistic expresses the variability of a distribution as a percentage of the mean. In other words, the larger the C_V, the larger the dispersion of the data around their mean. A graphical illustration on log-normal paper would show the data associated with a large C_V having a steeper slope than the data associated with a relatively small C_V.

Geographical Variation.—Because the C_V does show some systematic geographical variation, it is an especially valuable guide for estimating the standard deviation. The mean, or denominator, showed both little temporal variability for the 198 stations or spatial variability for the Iowa stations. The average C_V for the 2,600 stations investigated for this study is approximately 36% with 90% of the stations falling in the 30% to 40% interval. The C_V's in northwest Washington state and on the windward side of the Sierra mountains are generally less than 30% whereas Hawaii, some parts of midwestern United States, and the desert areas of California and Arizona, are generally about 50%.

This geographical effect is pronounced enough in these regions to transcend some of the sampling fluctuations described in connection with the standard deviation. Also, this effect can be explained partially by considering the meteorology of the particular region. For example, the most intense storms in the desert region of Arizona are associated with thunderstorms. Because thunderstorm rainfall occurs in a spotty pattern, the chance that a heavy rainfall will occur at a particular station is quite small. However, the occurrence of several extremely large rainfalls and a large number of relatively small rainfalls over a period of years results in a large C_V. On the other hand, the stations in northwestern Washington have a relatively small C_V. Here, the rainfalls which make up the annual series are associated with storm systems which cover thousands of square miles and occur many times a year. Combined with this is the orographic effect which helps to extract a large amount of moisture from each passing storm. The result is a series of annual maxima which vary little from year to year.

Adjustment for Sample Size.—It has already been stated that the mean and standard deviation increase with sample size. Because the standard deviation increases at a much faster rate than the mean, the C_V also increases with sample size. This is illustrated in diagram C of Fig. 3 which was prepared from the data used to construct the mean and the standard deviation diagram of the same figure.

Empirical Adjustments for Data Deficiencies.

Observational-Day Series Versus 1,440 Minute Series.—Most rainfall observations are made in nonrecording gages with the subsequent deficiency that the amounts are for an arbitrary beginning and ending rather than for the period containing the maximum rainfall. Adjusting a 2-yr rainfall, or any other return-period amount, derived from a series of calendar-day or observational-day rainfalls by the factor 1.13 makes the new result equivalent to the 1,440-min rainfall for the corresponding return period. The small uncertainty involved in using this relationship is exhibited in Fig. 7 for a group of twenty geographically dispersed stations with a wide range in rainfall magnitude.

Observational-Day Amount Versus 1,440-Minute Amount for an Individual Storm.—Quite often the largest continuous 24-hr rainfall is made up of part

of two observational-day amounts. It is then necessary to determine how much of the two-day total actually occurred in a continuous 1,440-min period. The empirical relationship established for this purpose is composed of the maximum observational-day and one-half of the maximum adjacent-day rainfall as given in the equation

$$1{,}440\text{-min rainfall} = \text{max ob-day} + 1/2 \text{ max adj. ob-day rainfall} \quad (2)$$

The scatter diagram of Fig 8 illustrates the quality of this relationship for 124 storms from widely scattered stations.

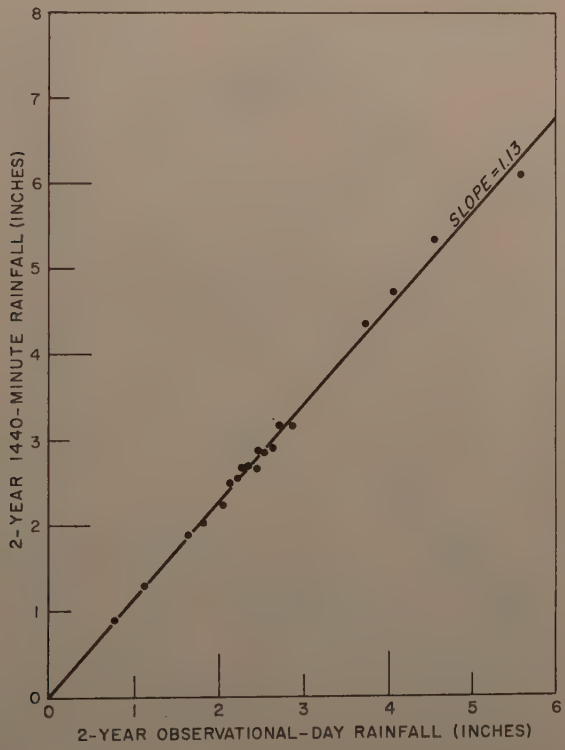

FIG. 7.—RELATIONSHIP BETWEEN 2-YR 1,440-MIN AND 2-YR OBSERVATIONAL-DAY RAINFALL

Areal Rainfall.

General.—All the analyses presented thus far have been based on point rainfalls but depths over areas are required for the design of hydraulic structures. A large number of areal depths based on a handful of stations have been estimated for large-area intense storms.[5] However, the quality of these estimates is not measurable. A small number of dense raingage networks provide

5 "Storm Rainfall in the United States," Corps of Engrs., U. S. Army, February, 1954.

what might be considered reliable areal estimates but, unfortunately, these networks have not experienced an unusually large storm.

Variation with Gage Density.—The data from a 40-gage network, covering approximately 400-sq miles in West Virginia, were analyzed to gain some measure of just one component of sampling error, average depths from selected geographically balanced subnetworks were compared with depths from the 40-gage network. Even with some built-in correlation as a result of comparing a part with the whole, the results of Fig. 9 show a great deal of scatter. In lieu

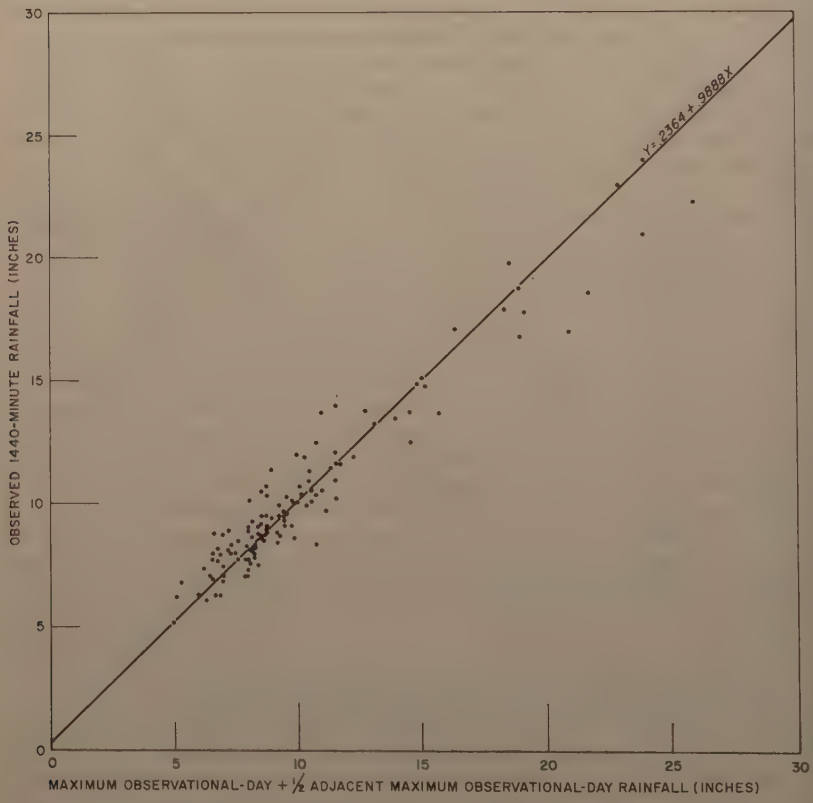

FIG. 8.—RELATIONSHIP BETWEEN 1,440-MIN RAINFALL AND MAXIMUM OBSERVATIONAL-DAY + 1/2 ADJACENT MAXIMUM OBSERVATIONAL-DAY RAINFALL

of anything better, the numerical results taken from the 24-hr depth-area curves of Technical Paper No. 38 and presented[6] in Table 2 can be used for small areas.

Unofficial Observations.—Investigations immediately after a flood sometimes uncover some unusually large rainfalls in an unofficial gage or a container

6 "Generalized Estimates of Probable Maximum Precipitation for the United States West of the 105th Meridian for Areas to 400 Square Miles and Durations to 24 Hours," Tech. Paper No. 38, U. S. Weather Bur., Washington, D. C., 1960, p. 66.

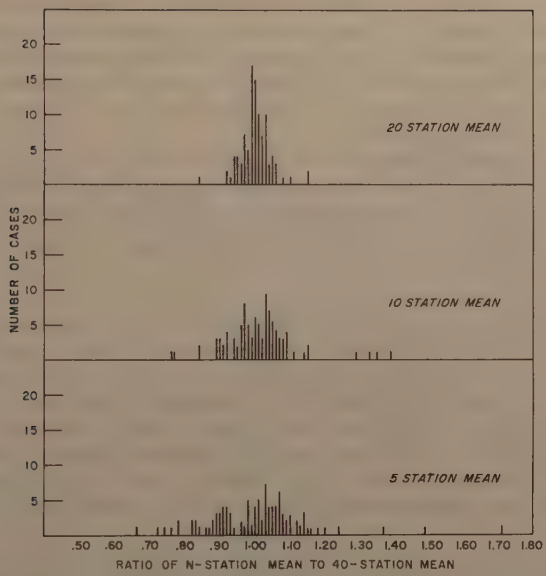

FIG. 9.—RATIO OF N-STATION MEAN TO 40-STATION MEAN

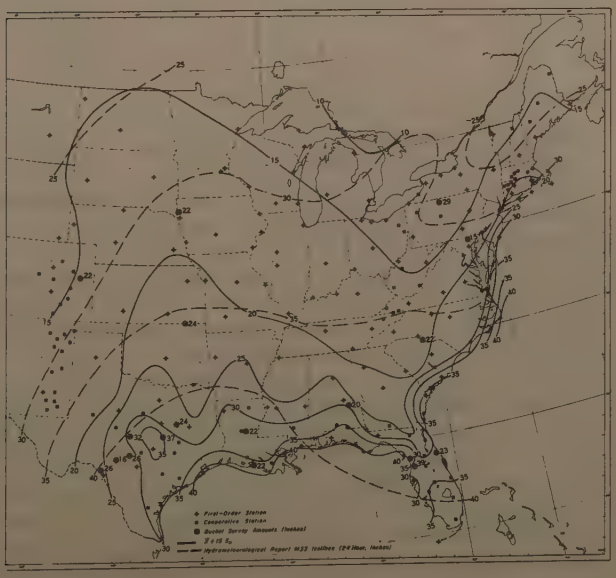

FIG. 10.—COMPARISON OF HYDROMETEOROLOGICAL REPORT NO. 33 PMP AND $(\bar{x} + 15s_N)$ ISOLINES

such as a bucket, bottle, and so on. The quality of these observations is, of course, unknown but they must be given some consideration when dealing with rainfall maxima. Eighteen of the largest unofficial observations are plotted in Fig. 10 and will be presented in a subsequent section where a comparison is made between the results of the traditional approach and that of this paper.

Empirical Estimate of PMP.

Rationale.—Enveloping K_M from the large number of computed K_M's would seem to provide an acceptable index for estimating PMP. From Table 1, it is observed that there are four values of K_M between 13 and 15. Fifteen was considered the appropriate order of magnitude for K_M because it envelops all maximum observed 24-hr rainfalls at official stations which have a series of annual maxima.

Method for Computing 24-hr PMP.—There are six fundamental steps in the computation of the PMP by the method developed herein. First, the mean and the standard deviation are computed by the conventional procedures. Secondly, the mean and the standard deviation are adjusted for their maximum observed rainfall according to the relationships of Figs. 1 and 4. Thirdly, the mean and the standard deviation are adjusted upward, when necessary, to meet the 50-yr standard. No adjustment is made for records longer than 50 yr in length. In the fourth step the mean is added to the product of fifteen times the standard

TABLE 2.—RATIO OF 10-SQUARE MILE TO N-SQUARE MILE RAINFALL (TP NO. 38)

Area, N-square miles (1)	Ratio (2)
50	0.95
100	0.93
200	0.90
400	0.87

deviation. As a fifth step, observational-day statistics are multiplied by 1.13. Finally, and extremely important, the C_V's at nearby stations should be compared with each other. When large discrepancies appear, the data for several stations should be plotted on some form of extreme-value probability paper to determine if the C_V is the result of a trend which has been operative over a long period of time or the result of one or more anomalous events. If deemed necessary, the C_V should be adjusted by changing the standard deviation only. The mean, as shown previously, is a relatively stable statistic.

Comparison of $(\bar{x} + 15s_N)$ with Traditional Approach.

Comparison With Hydrometeorological Report[7] No. 33.—Hydrometeorological Report No. 33, prepared by the traditional approach, presents generalized charts and diagrams for obtaining PMP estimates for several combinations of areas and durations east of 105° W. For comparison purposes, the 10-sq mile 24-hr depths of the latter report are considered equivalent to the 24-hr station values of the procedure outlined herein. Actually, the 10-sq-mile values were obtained by drawing a circle around the maximum observed 24-hr station

[7] "Seasonal Variation of Probable Maximum Precipitation East of the 105th Meridian for Areas from 10 to 1000 Square Miles and Durations of 6, 12, 24, and 48 Hours," Hydrometeorological Report No. 33, U. S. Weather Bur., Washington, D. C., April 1956, p. 58.

FIG. 11.—COMPARISON OF TECHNICAL PAPER NO. 38 PMP AND $(\bar{x} + 15s_N)$ ISOLINES IN CALIFORNIA

values or by using some other simple smoothing process. For convenience, 100 first-order and 100 long-record cooperative stations were used to define the position of the $(\bar{x} + 15s_N)$ smoothed isolines for the region east of 105° W (Fig. 10). Hydrometeorological Report No. 33 isolines are also shown on this illustration along with some of the extremely large unofficial observations. Examination of the two sets of isolines shows close agreement in the Gulf of Mexico region but then they begin to diverge rapidly, the statistical map showing a steeper gradient and smaller values from south to north. They differ in magnitude by a factor of about two in the north and west. Except for the three unofficial observations at Cherry Creek, Colo., Boyden, Iowa, and Smethport, Pa., the mean plus fifteen times the standard deviation envelops all the data. Approximately twenty-five standard deviations plus the mean would be necessary to envelop the three large unofficial observations.

Comparison in California with Weather Bureau Technical Paper No. 38.—The foregoing comparison covers only the relatively flat portion of the United States. It appeared worthwhile to make another comparison in a region where orography has great influence on the rainfall regime. California was selected because of the orographic factor and the large amount of data available. Fig. 11 shows two maps, one based on the traditional approach from Technical Paper No. 38 and the other based on an analysis of more than 450 stations. The isolines were positioned by interpolating between the stations (solid dots) with no attention paid to topography. Examination of the $(\bar{x} + 15s_N$ map reveals a range in rainfall magnitude which is approximately 50% larger than the Technical Paper No. 38 results. The range for the former being from 8 in. to 60 in. whereas the latter ranges from 10 in. to 45 in. with the discrepancies between the two estimates sometimes reaching a factor of two.

CONCLUSIONS

This study has been based on the assumption that valuable information is buried in each station's sample of extremes, and that this sample can provide estimators which can be used in conjunction with enveloping statistics to estimate PMP. The results based on this method have been compared with those obtained from the traditional approach and reveal that the estimates from the latter approach, which rests heavily on meteorological parameters of unknown quality, tend to be much larger than the statistical estimates for the United States east of 105° W. In Califronia, the differences are in both directions with the Technical Paper No. 38 estimates, in general, being slightly smaller.

The seriousness of the sampling variations disclosed for the statistics used to estimate PMP can be appraised only with reference to other procedures for estimating PMP. It is hoped that the material presented herein will provide a basis for the judicious use of these rainfall design criteria and be of value to those engaged in the task of improving current estimates.

Journal of the
HYDRAULICS DIVISION
Proceedings of the American Society of Civil Engineers

TERMINAL SHAPE OF A SHALLOW LIQUID FRONT

By E. Roy Tinney,[1] A. M. ASCE and D. L. Bassett[2]

SYNOPSIS

A shallow liquid front attains a terminal shape and velocity a short time after the liquid is introduced into an open channel. The equations for the shape of such a front are derived for laminar flow from Navier-Stokes equations. A simplified differential equation for a turbulent front is then presented with numberical solutions obtained by a high speed computer for various values of the relative roughness parameter. It is then shown that these profiles are the same as for a laminar front when a modification is made in the length parameter to account for channel roughness.

Concomitant experimental investigations with oil verify the equation for the shape of a laminar front approximately 1-in. deep, and similar experiments with water verify the equation for turbulent fronts reasonably well over a several-fold variation in slope, discharge, and roughness. Both the theory and the tests are for an impervious bed with zero infiltration.

LAMINAR FRONT

Development of a Front.—When a liquid is introduced slowly onto the upper end of a plane surface whose slope is small (such as an irrigation border or wide flume), the wetting front appears to stretch out into a gradually tapered

Note.—Discussion open until February 1, 1962. To extend the closing date one month, a written request must be filed with the Executive Secretary, ASCE. This paper is part of the copyrighted Journal of the Hydraulics Division, Proceedings of the American Society of Civil Engineers, Vol. 87, No. HY 5, September, 1961.

[1] Head, The R. L. Albrook Hydraulic Lab., Div. of Industrial Research, and Prof., Dept. of Civ. Engrg., Washington State Univ., Pullman, Wash.

[2] Asst. Prof., Dept. of Agric. Engrg., and Asst. Agric. Engr., Washington Agric. Experiment Stas., Washington State Univ., Pullman, Wash.

profile. In the first moments the velocity of advance of the front is relatively large, but it soon decays as the slope of the water surface decreases. Finally, the velocity of the front becomes constant. From this moment on, the process is simply one of extending the length of the uniform section behind a front whose shape remains the same. (Figs. 1 and 2).

Notation.—The letter symbols adopted for use in this paper are defined and arranged alphabetically, for convenience of reference, in the Appendix.

Terminal Velocity of Advance.—After the front has advanced a sufficient distance down a channel, the upstream depth becomes equal to the normal depth corresponding to the discharge, slope, relative roughness, and Reynolds number and, as stated previously, the front adopts a terminal shape and constant velocity of advance. If, in an element of time, dt, the front moves a distance, ds, it follows from continuity that the normal depth section must be extended by an equal length. Thus for the tip

$$ds = V_a\, dt \quad \ldots\ldots\ldots\ldots\ldots \quad (1a)$$

and for a unit width of the uniform upstream section

$$q\, dt = D\, ds \quad \ldots\ldots\ldots\ldots\ldots \quad (1b)$$

Eliminating ds yields

$$V_a = \frac{q}{D} = \overline{V} \quad \ldots\ldots\ldots\ldots\ldots \quad (2)$$

Thus, the terminal velocity of advance equals the average velocity in the upstream uniform section. This relationship holds for both laminar and turbulent fronts.

Shape of the Laminar Front.—The shape of a laminar front may be derived directly from Navier-Stokes equations if the following assumptions or restrictions are imposed:

1. Curvilinear effects are negligible, that is, the front must be gradually tapering. (This condition obviously does not hold right at the tip, but the region of marked curvature only extends a distance of about 2 D back from the tip. (Fig. 2)
2. Air resistance and surface tension forces are sufficiently small to be neglected.
3. The velocity distribution is similar throughout the front or, alternatively, the effects of non-similar velocity distributions are small. (This obviously ignores the process whereby the boundary layer is developed.)

For two-dimensional flow of an incompressible flow, the Navier-Stokes equations are:

$$X - \frac{1}{\rho}\frac{\partial p}{\partial x} + \nu\left(\frac{\partial^2 u}{\partial x^2} + \frac{\partial^2 u}{\partial y^2}\right) = u\frac{\partial y}{\partial x} + v\frac{\partial u}{\partial y} + \frac{\partial u}{\partial t} \quad \ldots\ldots \quad (3)$$

and

$$Y - \frac{1}{\rho}\frac{\partial p}{\partial y} + \nu\left(\frac{\partial^2 v}{\partial x^2} + \frac{\partial^2 v}{\partial y^2}\right) = u\frac{\partial v}{\partial x} + v\frac{\partial v}{\partial y} + \frac{\partial v}{\partial t} \quad \ldots\ldots \quad (4)$$

Since the flow is very nearly parallel to the bed except in the immediate vicinity of the tip, the vertical component, v, of the velocity vector is small compared to the horizontal component, u. All the terms of Eq. 4 are, therefore, small except

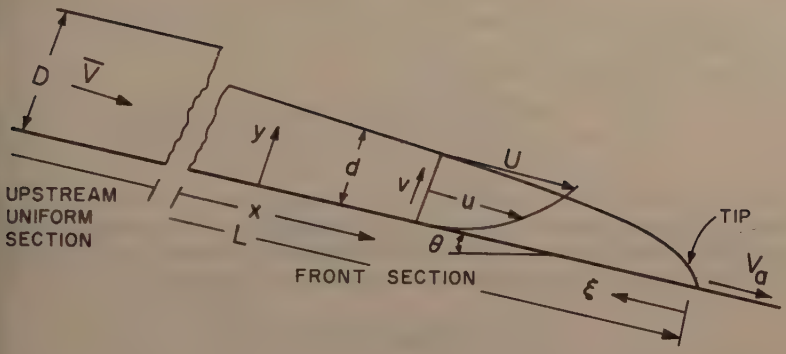

FIG. 1.—DEFINITION SKETCH FOR LIQUID FRONT

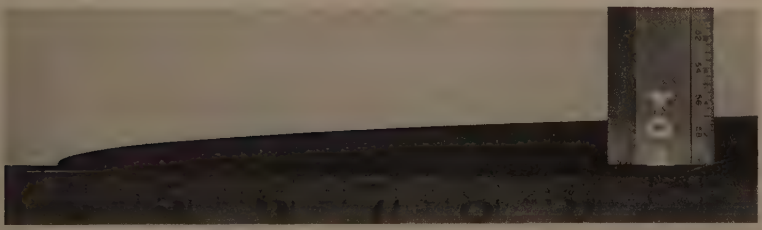

(a) PROFILE

(b) OBLIQUE VIEW

FIG. 2.—TIP OF LAMINAR FRONT

the first two. Eq. 4 is thereby reduced to a statement of the hydrostatic pressure law. (This is the same assumption stated above that curvilinear effects are to be ignored.)

Eq. 3 can now be rewritten as follows:

$$g \sin \theta - g \frac{\partial d}{\partial x} + \nu \left(\frac{\partial^2 u}{\partial x^2} + \frac{\partial^2 u}{\partial y^2} \right) = u \frac{\partial u}{\partial x} + v \frac{\partial u}{\partial y} + \frac{\partial u}{\partial t} \quad \ldots\ldots \quad (5)$$

In selecting the velocity distribution that is assumed to hold throughout the front, it is logical to choose one that is applicable to the uniform flow upstream of the front. This well-known distribution,[3] which can be derived from Navier-Stokes equation for steady flow down a plane, is given by

$$\frac{u}{U} = F\left(\frac{y}{d}\right) = F(\eta) = 2\eta - \eta^2 \quad \ldots\ldots\ldots \quad (6)$$

The boundary conditions to be satisfied are (Fig. 1):

At $y = d$,

$$p = 0 \quad \ldots\ldots\ldots\ldots\ldots\ldots \quad (7a)$$

and

$$\frac{\partial u}{\partial y} = 0 \quad \ldots\ldots\ldots\ldots\ldots\ldots \quad (7b)$$

at $y = 0$,

$$u = v = 0 \quad \ldots\ldots\ldots\ldots\ldots\ldots \quad (7c)$$

and at $t = 0$,

$$d = f(x) \quad \ldots\ldots\ldots\ldots\ldots\ldots \quad (7d)$$

The function, $d = f(x)$, simply describes the shape of the surface of the container holding the liquid prior to its release into the flume.

Substituting Eq. 6 into Eq. 5 and letting $\eta = 1.0$ yields

$$g \sin \theta - g \frac{\partial d}{\partial x} + \nu \left[\frac{\partial^2 U}{\partial x^2} - \frac{2U}{d^2} \left(\frac{\partial d}{\partial x} \right)^2 - \frac{2U}{d^2} \right] U \frac{\partial U}{\partial x} + \frac{\partial U}{\partial t} \quad \ldots\ldots\ldots \quad (8)$$

This equation describes the transient phenomenon that precedes the establishment of the terminal shape of the front. A stepwise solution of Eq. 8 is now being attempted on a high-speed digital computer to obtain the shape of the front and velocity of advance in the first few moments after release of the liquid.

After the front has acquired its terminal shape, the derivatives of U with respect to x and t become very small as a consequence of the long, gradually tapered profile. In order to arrive at the shape of the front, these derivatives are dropped from Eq. 8 along with the term involving $(\partial d/\partial x)^2$ to yield

$$\sin \theta - \frac{\partial d}{\partial x} - \frac{2\nu U}{g d^2} = 0 \quad \ldots\ldots\ldots\ldots \quad (9)$$

Now the normal depth, D, for laminar flow down a plane is[3]

$$D = \sqrt{\frac{2\nu U}{g \sin \theta}} \quad \ldots\ldots\ldots\ldots\ldots\ldots \quad (10)$$

---

[3] "Open-Channel Hydraulics," by Van Te Chow, McGraw-Hill Co., Inc., New York, 1959.

hich substituted into Eq. 9 yields

$$\sin\theta - \frac{\partial d}{\partial x} - \left(\frac{D}{d}\right)^2 \sin\theta = 0 \quad \ldots\ldots\ldots\ldots \quad (11)$$

his equation can be integrated by separation of variables giving

$$x = \frac{d}{\sin\theta} - \frac{D}{\sin\theta}\tanh^{-1}\left(\frac{d}{D}\right) + \text{constant} \quad \ldots\ldots\ldots \quad (12)$$

n evaluating the constant of integration it is more convenient to introduce the ariable ξ (Fig. 1) so that the shape of the front is defined in terms of the dis-ance back from the tip. Eq. 12 can be then rewritten in the form

$$\xi = \frac{D}{\sin\theta}\left[\tanh^{-1}\left(\frac{d}{D}\right) - \frac{d}{D}\right] + C \quad \ldots\ldots\ldots \quad (13)$$

t $\xi = 0$, $d = 0$ so that $C = 0$.

Finally, the terminal shape of a gradually tapering two-dimensional lami-ar front becomes

$$\frac{\xi}{D}\sin\theta = \tanh^{-1}\left(\frac{d}{D}\right) - \frac{d}{D} \quad \ldots\ldots\ldots\ldots\ldots \quad (14)$$

Experimental Investigation of a Laminar Front.—In order to check validity Eq. 2 and 14 a series of tests was made with oil in a glass-sided flume as nown in Fig. 3. The oil used was a Mobil Oil Company product called Ambrex 10 with a kinematic viscosity of 8.5×10^{-4} ft^2 per sec at 70°F. and 5.8×10^{-4} ft^2 per sec at 80°F. and a specific gravity of 0.85.

Prior to each test on the advance of the front, a test was made to determine he normal depth and to set the adjustable weir in the headbox at the precise vel of the liquid surface. The advance of the front tests were started with e quick-acting gate closed and the quick-acting bypass valve opened suffi-ently to maintain the level of the liquid in the headbox at the previously set evation of the weir crest. The bypass valve was then suddenly closed. A link-ge connecting the bypass valve handle to the gate caused the latter to open uddenly at the same instant, permitting the flow to proceed down the flume.

The velocity of advance down the flume was measured by means of a manual-operated switch which caused a blip on an otherwise straight trace of a pen ecorder as the front passed each 2-ft station. The shape of the front was ecorded by means of four cameras stationed along the flume. The cameras ere triggered simultaneously with an electric relay system. Scales were stened to the outside of the glass wall of the flume in the field of view of the mera. By reading the photographic negatives with a 30-power microscope, irly accurate determinations of the depths (within $\pm$ 0.0003 ft) could be ob-ined.

By keeping the depths shallow, both the terminal shape and velocity could obtained for several slopes and discharges. In some instances, the cameras ere moved closer to the upstream end of the flume to obtain the shape of the ont during its transient phase.

An auxiliary test was made to determine the surface velocity. This informa-on was obtained by timing the motion of a small surface float that was first aced behind the front. It eventually caught up to the front and was entrained the roller at the tip.

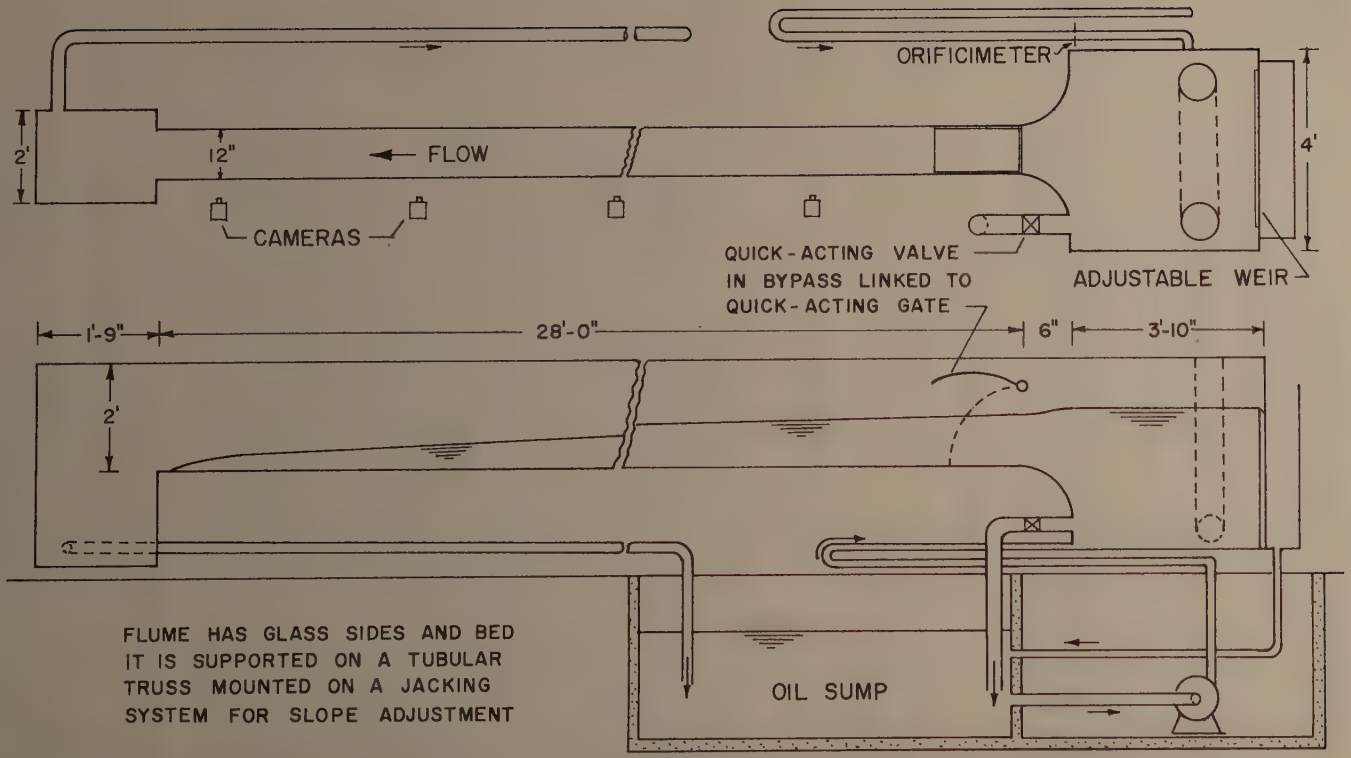

FIG. 2. FLUME FOR LAMINAR FLOW STUDIES

Results of Experiments on Laminar Front.—Data on four typical fronts for wo different slopes are reported herein as shown in Table 1.

The data on velocity of advance are plotted in Fig. 4 for the four runs. Notice iat the velocity of advance in all cases becomes equal (or at least within the ange of experimental error) to the average velocity in the upstream uniform ection, thereby verifying Eq. 2.

The data on surface velocity are also plotted on Fig. 4. Notice that this elocity does not decrease significantly, thereby justifying the assumptions iade in the derivation of Eq. 14 that $\partial U/\partial x$ and $\partial U/\partial t$ are small.

The data on the terminal shape of the front are given in Fig. 5. The fit of ie data to the curve defined by Eq. 14 appears to verify the theory for the erminal shape of a shallow laminar front. However, only a limited range of

TABLE 1.—LAMINAR FRONT EXPERIMENTS WITH OIL

Run No. (1)	Temperature, in °F (2)	q, in cfs (3)	$\sin\theta$ (4)	D, in ft (5)	$\overline{V}$, in fps (6)	R (7)	F (8)
1	80.6	0.106	0.015	0.0792	1.340	186	0.838
2	81.0	0.075	0.020	0.0652	1.151	133	0.794
3	80.0	0.101	0.020	0.0728	1.388	174	0.906
4	78.7	0.1405	0.020	0.0800	1.758	233	1.096

ie depth was tested. At greater depths, the flume was too short to obtain rminal shapes, and at smaller depths, accuracy was impaired.

TURBULENT FRONT

Derivation of Equation for Shape of Front.—On the basis of the results for e laminar front, the following assumptions are made for the derivation of an uation for a shallow turbulent front:

1. Surface tension and air resistance can be ignored.
2. Curvilinear effects are small.
3. The surface velocity remains nearly constant throughout the front so at acceleration can be ignored.
4. The velocity distribution is similar throughout the front, or, alternatively, the effects of changes in velocity distribution are small. (Here again, the ocess whereby the boundary layer is developed is ignored.)

On the basis of these assumptions, the forces on an element in the front can assumed to be in equilibrium. Thus, referring to Fig. 6

$$\frac{\rho g}{2}\left[d^2 - \left(d + \frac{\partial d}{\partial \xi}\, d\xi\right)^2\right] + \tau\, d\xi - \rho g\, d\, d\xi \sin\theta = 0 \quad \ldots\ldots \quad (15)$$

ich simplifies to

$$\frac{\partial d}{\partial \xi} - \frac{\tau}{\rho g d} + \sin\theta = 0 \quad \ldots\ldots\ldots\ldots \quad (16)$$

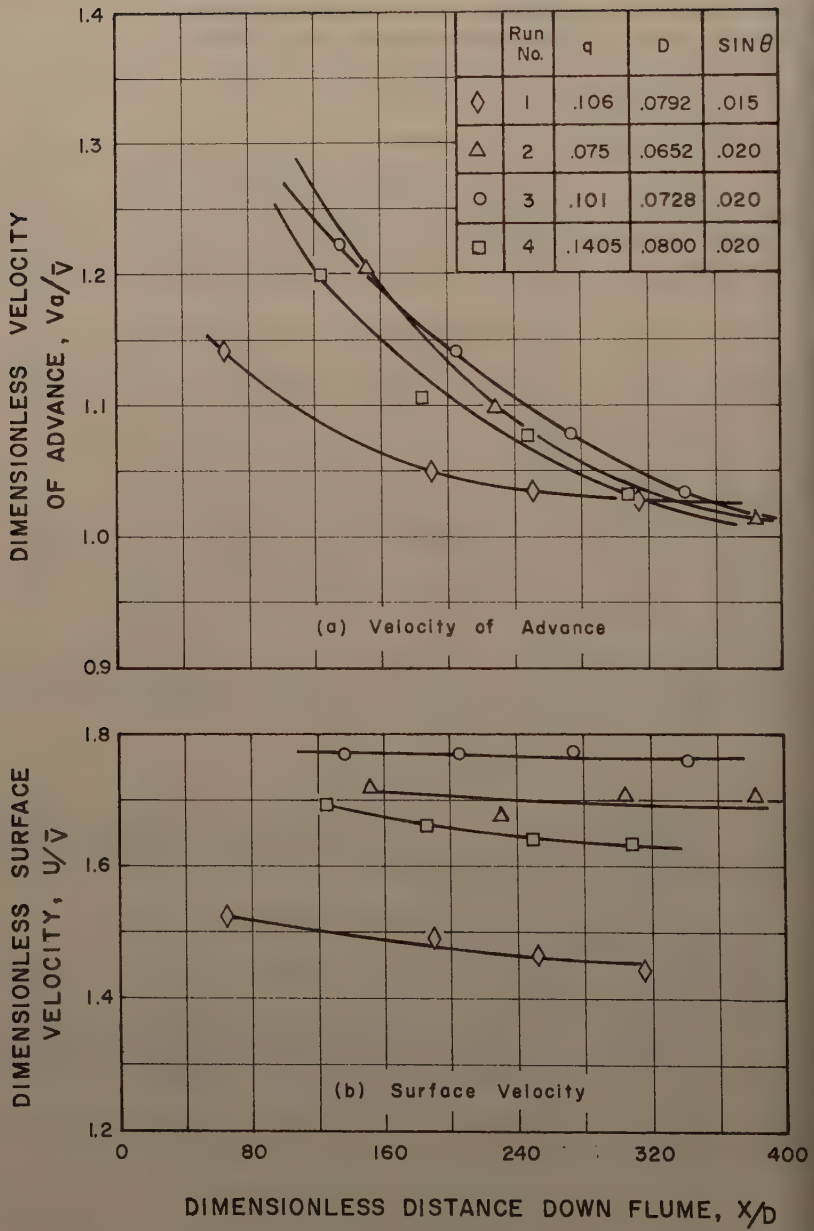

FIG. 4.—VELOCITIES OF LAMINAR FRONTS

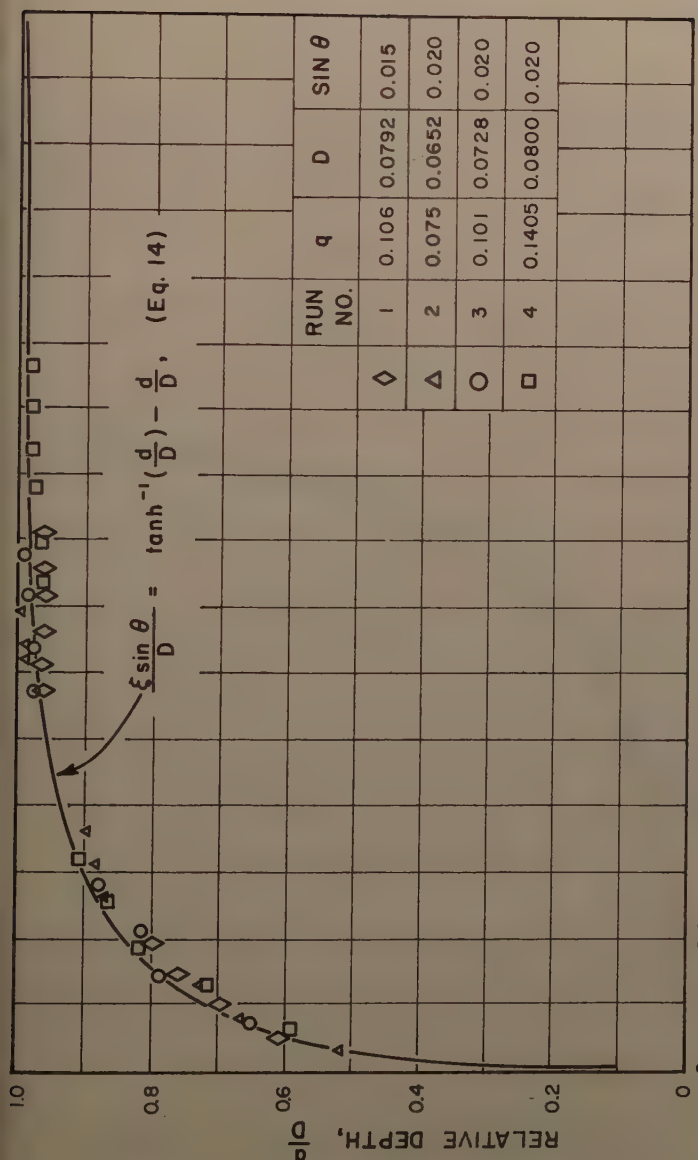

FIG. 5.—TERMINAL SHAPE OF LAMINAR FRONT

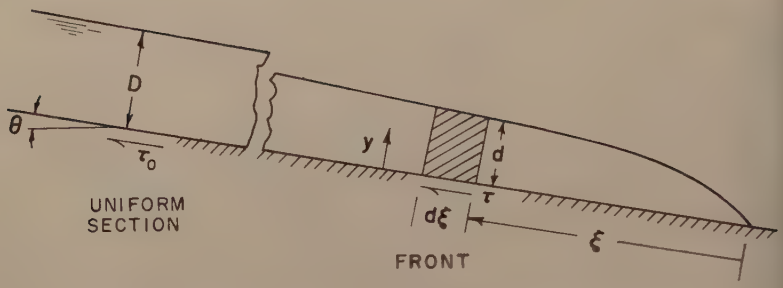

FIG. 6.—DEFINITION SKETCH FOR TURBULENT FRONT

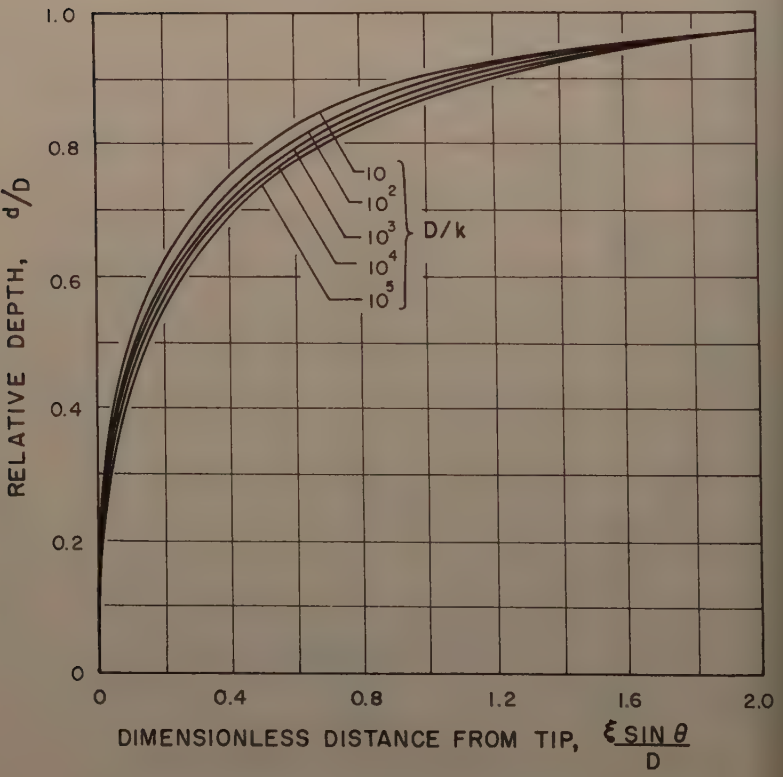

FIG. 7.—THEORETICAL SHAPE OF TURBULENT FRONTS

the von Karman-Prandtl logarithmic velocity distribution for rough open annels is assumed to hold throughout the front, then

$$\tau = \frac{\rho U^2}{\left(5.75 \log \frac{d}{k} + C\right)^2} \quad \ldots\ldots\ldots\ldots \quad (17)$$

abris H. Keulegan[4] has found from an analysis of Bazin's data for wide chanels that C = 8.5.

Now in the upstream section where the depth is constant

$$\tau_0 = \frac{\rho U^2}{\left(5.75 \log_{10} \frac{D}{k} + 8.5\right)^2} = \rho g D \sin\theta \quad \ldots\ldots\ldots \quad (18)$$

follows, then, that

$$\tau = \frac{\tau}{\tau_0} \tau_0 = \left(\frac{5.75 \log \frac{D}{k} + 8.5}{5.75 \log \frac{d}{k} + 8.5}\right)^2 \rho g D \sin\theta \quad \ldots\ldots\ldots \quad (19)$$

bstituting Eq. 19 into Eq. 16 yields

$$\frac{\partial d}{\partial \xi} - \left[\frac{5.75 \log \frac{D}{k} + 8.5}{5.75 \log\left(\frac{d}{D}\frac{D}{k}\right) + 8.5}\right]^2 \frac{D}{d} \sin\theta + \sin\theta = 0 \quad \ldots\ldots\ldots \quad (20)$$

Eq. 20 has been integrated numerically with an IBM 650 computer for values D/k = 10, 10^2, 10^3, 10^4, and 10^5 for $k < d < 0.99$ D assuming that $\xi = 0$ when = k. The results are presented graphically in Fig. 7. A recomputation with = 7.25 did not produce a significant change in the shapes of these curves.

In attempting to develop one universal profile for all fronts, it was noted at each of these theoretical turbulent front profiles could be transformed to the laminar profile quite closely by a simple change of scale of the abscissa r each value of D/k. Thus, it follows that

$$\frac{\xi \sin\theta}{D} \phi\left(\frac{D}{k}\right) = \tanh^{-1}\left(\frac{d}{D}\right) - \frac{d}{D} \quad \ldots\ldots\ldots\ldots \quad (21)$$

e function, $\phi\left(\frac{D}{k}\right)$, however, can be rewritten in terms of the Darcy-Weisbach efficient, f, or Manning's n. For one particular value of Manning's n, say = n_0, the turbulent profile and the laminar profile will be identical. This ggests an equation of the form

$$\frac{\xi \sin\theta}{D} \left(\frac{n}{n_0}\right)^b = \tanh^{-1} \frac{d}{D} - \frac{d}{D} \quad \ldots\ldots\ldots\ldots \quad (22)$$

which n_0 and b both require experimental determination.

Experimental Investigations of a Turbulent Front.—The test program dissed in this section is part of a larger research program intended to develop

4 "Laws of Turbulent Flow in Open Channels," by Gabris H. Keulegan, Journal of search, U. S. Natl. Bur. of Standards, Research Paper-R.P. 1151, Vol. 21, December, 8, p. 735.

design criteria for irrigation systems. The particular phase reported here is an investigation of shape of the advancing front in shallow overland flow, which is characteristically unsteady and nonuniform in its initial stage.

In order to achieve control of variables not possible under field conditions, this test program is being conducted in laboratory facilities in which flow characteristics can be observed and recorded. The principal facility is a laboratory flume (Fig. 8) 69 ft long and 3 ft wide with appropriate equipment for control and measurement of rate of flow and channel slope. The flume is formed from steel plate with observation windows in one side, and is supported by large trusses to minimize deflection. The floor of the channel is covered with one inch of light-weight aggregate concrete which has been sanded to pro-

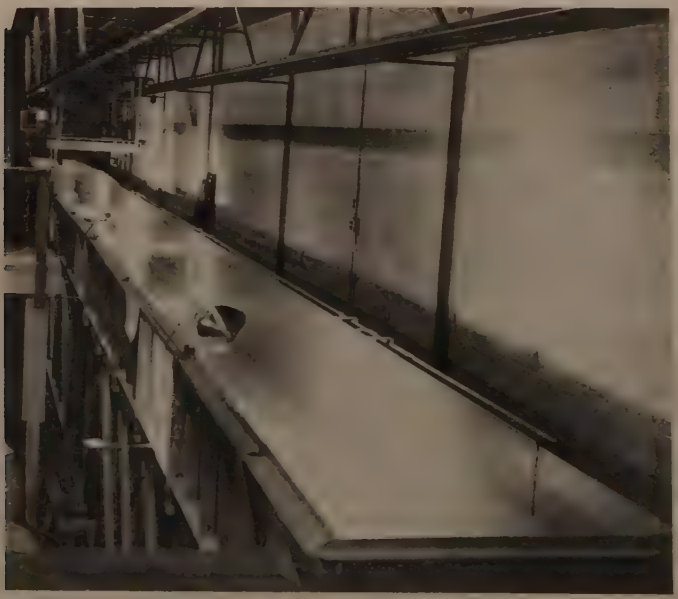

FIG. 8.—LABORATORY FLUME USED IN THE STUDIES OF THE ADVANCE OF A TURBULENT FRONT

vide a smooth, uniform surface, and has been sealed with a plastic coating t prevent deterioration.

Because local disturbances such as clods and vegetation virtually preclud conventional laminar characteristics in a typical irrigation stream, these test are being conducted in the turbulent range of flow. Values of the variables wer selected as being appropriate to both border irrigation and laboratory investi gations. Tests have been made for nearly all combinations of the condition

ndicated as follows:

1. Channel slope	0.10%, 0.25%, 0.50%, 1.00%	
2. Unit stream size	0.033 cfs, 0.10 cfs, 0.167 cfs	
3. Infiltration rate	Zero for these tests	
4. Channel surface	(1) $n = 0.0081\ D^{-0.031}$	(concrete - $n \sim 0.009$)
	(2) $n = 0.0119\ D^{-0.247}$	(metal lath - $n \sim 0.02$)
	(3) $n = 0.0042\ D^{-1.37}$	(crushed rock - $n \sim 0.05$)

For convenience, the surfaces used in these tests are described in terms f Manning's n for the range of depth involved in this study and for steady flow onditions. The equations for Manning's n as a function of the depth were etermined with tests on uniform flow prior to the tests on advancing fronts. hese equations are valid, of course, only over a limited range of the depths.

Surface (1) is the sanded concrete floor of the flume with a plastic seal oat. Surface (2) is obtained by placing a single layer of expanded metal build- ig lath (1/2-in. openings, 5 lb per sq yd) over the smooth concrete. Surface) is achieved by placing a single and complete layer of crushed rock /8 in. to 3/4-in. sieve size) over the expanded metal lath. Water tempera- re for the majority of these tests was between 60°F and 65°F. Test conditions us encompassed a ten-fold increase in channel slope, a five-fold increase in ream size, and approximately a six-fold increase in surface roughness as aracterized by Manning's n for average depths.

Prior to each test of the advance of a front over a given surface, the channel ope and rate of flow are established. During the time of these adjustments e entire stream is by-passed around the channel and back to the sump. The st is started by closing a quick-acting valve, causing the water to fill a nar- w secondary forebay and then to flow through dampening screens into and wn the channel. Full flow into the channel is thus achieved immediately fol- wing water entry, and depth in the forebay may increase with time if down- ream flow characteristics cause it.

When the advancing front reaches the end of the 50-ft test section in the ume, four cameras photograph simultaneously the water levels in each of open-tube manometers connected to the bed of the flume. The depths are bsequently read from these photographs with microscope aid to the nearest 1000 ft and adjusted as necessary for channel slope, etc. These depths per- it the drawing of a best fit water surface profile for each test. Points from is curve are used in the subsequent analysis.

Experimental Results on Turbulent Fronts.—Typical water surface profiles e contained in Fig. 9 from which it is obvious that depth, d, is a function of least the distance behind the front, x; channel slope, $\sin\theta$; unit stream size, and the roughness of the surface. Notice that all the profiles approach uni- rm flow conditions except the 0.0010 slope in Fig. 9(a). The flume was not ng enough for this front to develop its terminal shape.

In order to evaluate n_0 and b in Eq. 21, fronts were investigated whose pro- es fitted the theoretical profile for laminar flow. Certain tests with water wing over the metal lath (surface 2) satisfied this requirement. These tests tablished the value of n_0 to be 0.020. When the adjustment for relative rough- ss suggested earlier, $(n/n_0)^b$, is applied to the abscissae where n_0 is taken to 0.020 and $b = 2/3$, a single curve as shown in Fig. 10 results, indicating that e terminal shape of turbulent fronts, at least for the flow regimes tested, can reasonably predicted by the use of Eq. 21. Fig. 10 is useful in determining

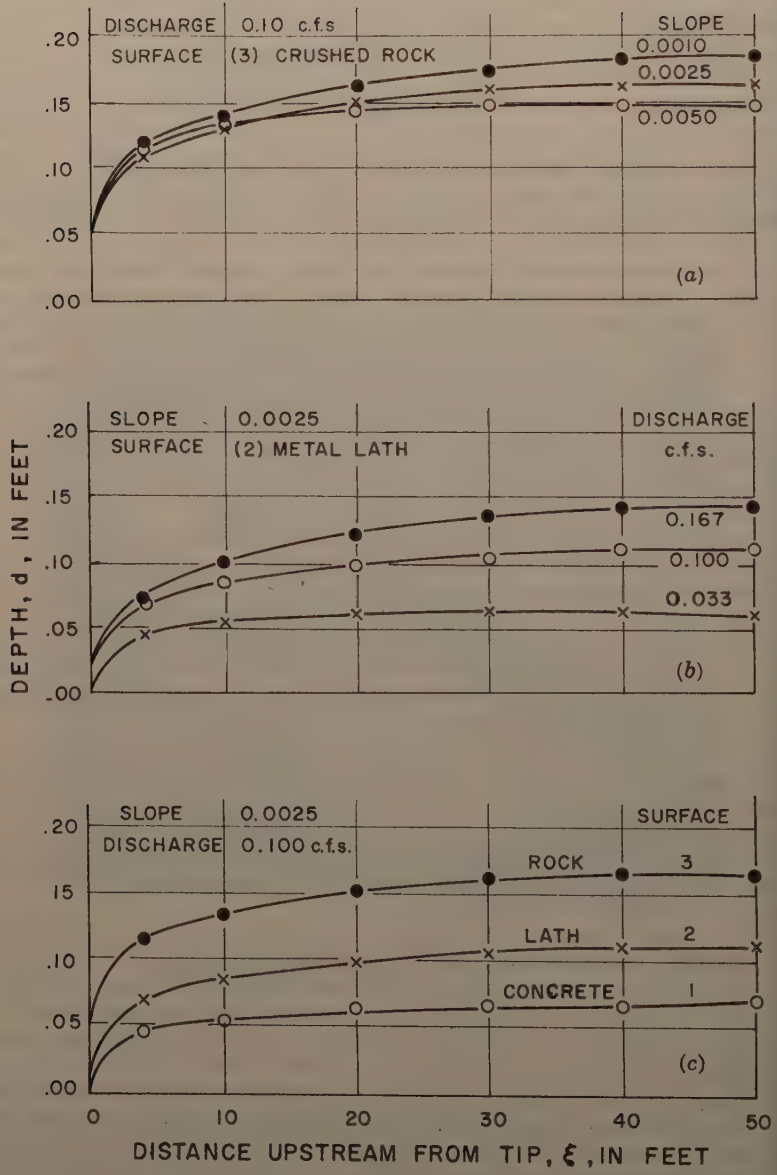

FIG. 9.—TYPICAL WATER SURFACE PROFILES IN ADVANCING TURBULENT FLOW

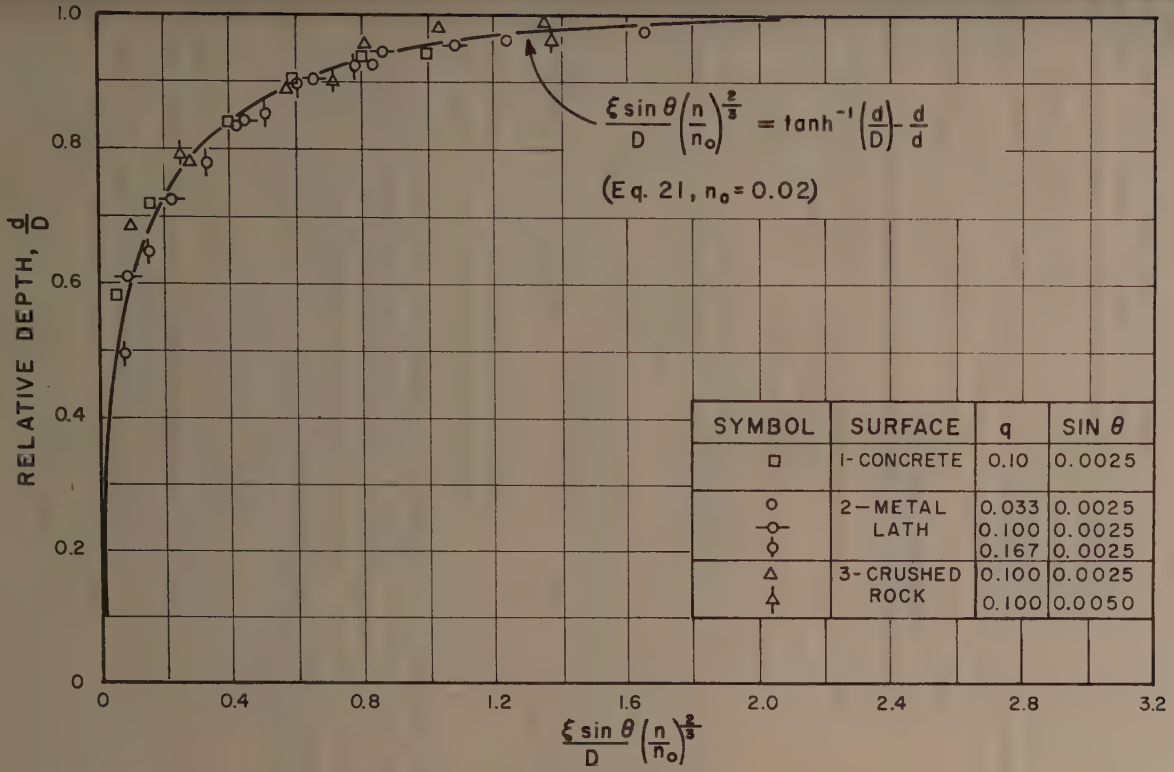

FIG. 10.—TERMINAL SHAPE OF A TURBULENT FRONT

the length of the front. It will be observed that the relative depth has attained the value of 0.99 when the length parameter (abscissa) has obtained a value of approximately 1.66.

It now appears possible to predict the water surface profile for turbulent conditions and to determine the distance behind the front beyond which essentially uniform flow conditions exist. These results, however, are for relatively long shallow fronts. Short fronts may not develop their terminal shape and could be expected to deviate from the shape presented here.

It should be noted that in addition to the work on the turbulent water surface shape reported here, investigations are under way on the following phases of the study of hydraulics of surface irrigation.

a. Water surface shape where roughness extends throughout the entire depth of the flowing stream.
b. Water surface shape where infiltration is non-zero and of the form $I = k\,t^a$.
c. Velocity of advance and shape in the initial transient phase.

CONCLUSIONS

1. When a liquid is introduced slowly into a channel, it decelerates and acquires a long, gradually tapering profile which becomes stabilized and thereafter advances at a constant velocity equal to the average velocity in the upstream uniform section.

2. The terminal shape of the front for laminar flow is a function only of the slope and the normal depth corresponding to the discharge and slope. For turbulent fronts the shape is also dependent upon the relative roughness of the channel bed.

ACKNOWLEDGMENTS

The analysis and experiments on laminar fronts were conducted by the senior writer under Grant No. G-7052 by the National Science Foundation. The flume for the laminar flow experiments was designed by Claud C. Lomax, F. ASCE, Associate Hydraulic Engineer, Division of Industrial Research, Washington State University, and constructed under the same grant. Lester Bishop performed most of the experiments and Joyce Taylor assisted in analyzing the results.

The analysis of the turbulent front was undertaken by the senior writer under the sponsorship of the Division of Industrial Research, Washington State University. J. P. Doutriaux, a graduate student in civil engineering, undertook the numerical solution of the equation for the turbulent front.

The experimental investigation of turbulent fronts was performed by the junior writer as a part of Project 1317, Washington Agricultural Experiment Stations, and as a contributing project to Western Regional Research Project W-65. Much of the laboratory and analytical investigation of this phase was performed by G. D. Haynes and D. R. Van Leuven, graduate students in Agricultural Engineering.

APPENDIX.—NOTATION

= exponent having an experimentally determined value of 2/3;
= constant of integration;
= normal depth of flow in upstream uniform section;
= depth of flow in the front;
= Froude No. $\overline{V}/\sqrt{g\,D}$;
= Darcy-Weisbach resistance coefficient;
= acceleration of gravity;
= equivalent height of roughness element;
= Manning's n;
= Manning's n for a particular turbulent profile ($n_o = 0.02$);
= pressure;
= discharge per unit width of flume;
= Reynolds Number $V\,D/\nu$;
= time;
= value of u at the surface;
= component of velocity parallel to the bed;
= terminal velocity of advance of the front;
= average velocity of flow in uniform section;
= component of velocity perpendicular to the bed;
= body force per unit mass in x-direction;
= coordinate axis parallel to the bed (positive in the downstream direction);
= body force per unit mass in y-direction;
= coordinate axis perpendicular to the bed (positive upward);
= coordinate axis with origin at tip of the front (positive upstream);
= shear on the bed in the front;
= shear on the bed in the upstream uniform section;
= mass density of fluid;
= kinematic viscosity of fluid; and
Ψ = function of.

Journal of the
HYDRAULICS DIVISION
Proceedings of the American Society of Civil Engineers

FREE STREAMLINE THEORY FOR SEGMENTAL JET DEFLECTORS

By E. Roy Tinney,[1] A. M. ASCE, Wilfred E. Barnes,[2]
Ottis W. Rechard,[3] and Glenn R. Ingram[4]

SYNOPSIS

A liquid jet may be deflected by a device that is composed of straight segments, but, if these segments are short compared to the thickness of the jet, the deflection angle is unknown. It can be computed, however, for the two-dimensional case for symmetrical deflectors by applying free streamline theory.

The segmental deflector is first mapped by conformal transformation onto the boundary of a semi-infinite plane by the Schwartz-Christoffel theorem. The integrals of transformation are then evaluated numerically with a high speed digital computer for a wide range of the dimensionless parameters defining the geometry of the deflector. The results of this analysis are presented in graphical form.

Data from previous experimental work on segmental flip buckets for spillways of dams are than compared to this theoretical analysis and it is shown that the exit angle of the jet can be accurately predicted by the theory, despite the fact that boundary layer effects and the influence of gravity on the flow in the deflector are ignored.

For the application of the theory to flip buckets on spillways, a set of curves is presented for designers. This set of curves gives the dimensions of the

Note.—Discussion open until February 1, 1962. To extend the closing date one month, a written request must be filed with the Executive Secretary, ASCE. This paper is part of the copyrighted Journal of the Hydraulics Division, Proceedings of the American Society of Civil Engineers, Vol. 87, No. HY 5, September, 1961.

[1] Head, R. L. Albrook Hydr. Lab., Div. of Industrial Research, Washington State Univ.
[2] Asst. Prof. of Math., Washington State Univ.
[3] Dir., Computing Center, Washington State Univ.
[4] Asst. Computing Analyst, Computing Center, Washington State Univ.

bucket that are required to produce the desired exit angle as a function of the face angle of the dam and the thickness of the nappe. Thus, flip buckets may be designed to give the desired exit angle of the jet for a particular discharge, and the exit angle predetermined for other discharges.

INTRODUCTION

A flip bucket on the spillway of a dam generally has a typical "ski jump" profile in which the radius of the bucket is large so that the streamline follow parallel to the bucket profile. A more economical segmental bucket, such as that shown on Fig. 1, could be used if the exit angle of the flow could be predetermined for each discharge. The problem arises of determining the exit angle β of the jet as a function of the depth of flow, d, on the spillway, the in-

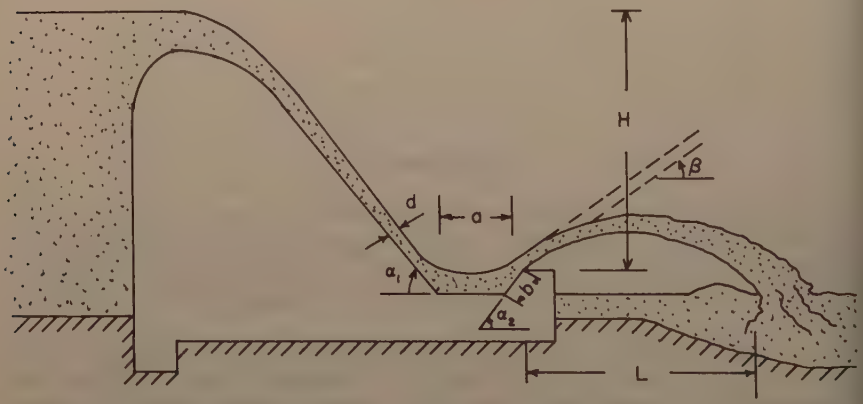

FIG. 1.—DEFINITION SKETCH FOR SEGMENTAL SPILLWAY FLIP BUCKETS

clination angle α_1, of the spillway face, the dimensions "a" and "b" of the bucket, and the inclination angle α_2 of the lip of the bucket. If the exit angle is known the trajectory of the free jet can be readily determined by the laws for freely falling bodies.[5]

In the absence of gravity, the flow would leave the bucket and attain an angle β as shown by the dotted lines in Fig. 1. To find this angle it is assumed (a) that the influence of gravity is small within the confines of the bucket (it is, of course, significant when the flow leaves the bucket), (b) that the influence of viscosity is negligible within the bucket, and (c) that the flow approaching the bucket has essentially a uniform velocity distribution or, alternatively, that the non-uniformity of the velocity distribution is not significant. The first assumption, of course, restricts the application of the theory to high velocities at which inertial forces are large compared to gravitational forces (i. e., large

[5] Hydraulic Energy Dissipators, by E. A. Elevatorski, McGraw-Hill Book Company, Inc., New York, 1959.

values of the Froude number, $V/\sqrt{gd}$). The second assumption requires large inertial forces as compared to viscous forces (that is, large values of Reynolds number Vd/υ). Both of these conditions are usually satisfied on the spillways of all except very low dams. As far as the third assumption is concerned, it is known that a non-uniform velocity distribution exists in the approach flow but the area of large velocity gradients is confined to a small region near the face of the spillway despite the fact that the boundary layer extends to the free surface. It appears, therefore, that none of these three assumptions seriously disagrees with real conditions. The problem is thus reduced to a two-dimensional potential flow problem to which classical hydro-dynamics can be applied.[6]

A general theory is developed in the following section for the design of jet deflectors composed of straight segments without particular reference to specific applications. The analysis follows directly from the application of complex variables, in particular conformal transformation theory, for which the reader may refer to many standard tests.[7]

CONFORMAL TRANSFORMATION OF THE FLOW REGION

Notation.—The letter symbols adopted for use in this paper are defined where they first appear and are arranged alphabetically, for convenience of reference in Appendix II.

The boundaries of the flow region under consideration are composed of two types, straight segments and free streamlines. Since along the straight segments and free streamlines the inclination and magnitude, respectively, of the velocity vector are invariant, the graph of the logarithm of the velocity will be a closed polygonal figure whose horizontal portions correspond to straight boundaries and whose vertical portions correspond to free streamlines. This polygon can then be mapped by the Schwartz-Christoffel transformation onto a straight line where the complex potential can readily be determined.

For reasons of symmetry, which greatly simplifies the calculations, the angles α_1, and α_2 are taken as equal and denoted by α. Letting ω be the potential and defining

$$\zeta = \frac{d\omega}{dz} \quad \ldots\ldots\ldots\ldots\ldots\ldots \quad (1)$$

results in

$$\zeta = -u + i\,v = -q\,e^{-i\theta} \quad \ldots\ldots\ldots\ldots\ldots \quad (2)$$

in which u and v are the velocity components in the x and y directions, q and θ are the magnitude and inclination of the vector velocity. Now define

$$\Omega = \ln\left(-\frac{V}{\zeta}\right) = \ln\frac{V}{q} + i\,\theta \quad \ldots\ldots\ldots\ldots\ldots \quad (3)$$

---

6 Hydrodynamics, by Horace Lamb, Sixth Edition, Dover Publications, New York.
7 Fluid Dynamics, by V. L. Streeter, McGraw-Hill Book Company, Inc., New York, 1948.

and map the flow region of the z-plane (Fig. 2) onto the indicated region of the Ω-plane. This being a closed polygonal region the Schwartz-Christoffel transformation can be applied to map the boundary onto the real axis of the t-plane.

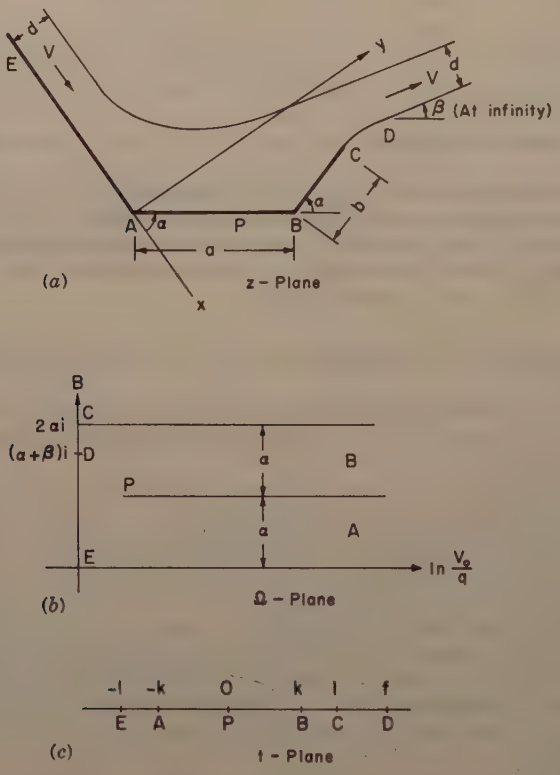

FIG. 2.—CONFORMAL TRANSFORMATION PLANES

Due to the symmetry introduced by making α_1 and α_2 equal, the coordinates -1, 0, +1, may be assigned to the points E, P, and C, respectively, and -k and +k to the points A and B. The coordinate of D is taken to be f.
Thus

$$\Omega = M\int \frac{t\,dt}{(t^2 - k^2)\sqrt{t^2 - 1}} + N = \frac{M}{\sqrt{1 - k^2}} \ln \frac{\sqrt{1 - k^2} + \sqrt{1 - t^2}}{\sqrt{t^2 - k^2}} + N$$

$$= \frac{M\,i}{\sqrt{1 - k^2}} \sin^{-1} \frac{\sqrt{t^2 - 1}}{\sqrt{t^2 - k^2}} + N \quad \ldots\ldots\ldots\ldots \quad (4)$$

Now, taking the principal value of $\sin^{-1}\frac{\sqrt{t^2-1}}{\sqrt{t^2-k^2}}$ at t = -1, results in N=O and from $\Omega(+1) = 2\alpha i = \frac{M\pi i}{\sqrt{1-k^2}}$

$$M = \frac{2\alpha}{\pi}\sqrt{1-k^2} \quad \ldots\ldots\ldots\ldots\ldots \quad (5)$$

Hence,

$$\Omega = \frac{2\alpha}{\pi}\ln\frac{\sqrt{1-k^2}+\sqrt{1-t^2}}{\sqrt{t^2-k^2}} = \frac{2\alpha}{\pi} i \sin^{-1}\frac{\sqrt{t^2-1}}{\sqrt{t^2-k^2}} \quad \ldots\ldots \quad (6)$$

From the source and equal sink at t = -1 and t = f, respectively, the following complex potential is obtained:

$$\omega = \frac{V d}{\pi}\left(\ln(t-f) - \ln(t+1)\right) \quad \ldots\ldots\ldots\ldots \quad (7)$$

From the definition of ζ Eq. 8 is now obtained.

$$dz = \frac{1}{\zeta}\frac{d\omega}{dt}dt = \frac{d}{\pi}\frac{V}{\zeta}\left(\frac{1}{t-f} - \frac{1}{t+1}\right)dt \quad \ldots\ldots\ldots \quad (8)$$

and since $\frac{V}{\zeta} = -e^{\Omega}$

$$dz = \frac{d}{\pi}\left(\frac{\sqrt{1-k^2}+\sqrt{1-t^2}}{\sqrt{t^2-k^2}}\right)^{\frac{2\alpha}{\pi}}\left(\frac{1}{t+1}+\frac{1}{f-t}\right)dt \quad \ldots\ldots \quad (9)$$

Integrating from A to B and noting that in this range of t

$$\left(\frac{\sqrt{1-k^2}+\sqrt{1-t^2}}{\sqrt{t^2-k^2}}\right)^{\frac{2\alpha}{\pi}} = \left(\frac{\sqrt{1-k^2}+\sqrt{1-t^2}}{\sqrt{k^2-t^2}}\, e^{i\frac{\pi}{2}}\right)^{\frac{2\alpha}{\pi}}$$

$$= e^{\alpha i}\left(\frac{\sqrt{1-k^2}+\sqrt{1-t^2}}{\sqrt{k^2-t^2}}\right)^{\frac{2\alpha}{\pi}} \quad \ldots\ldots\ldots\ldots \quad (10)$$

Eq. 11 is obtained.

$$a = \frac{d}{\pi}\int_{-k}^{k}\left(\frac{\sqrt{1-k^2}+\sqrt{1-t^2}}{\sqrt{k^2-t^2}}\right)^{\frac{2\alpha}{\pi}}\frac{f+1}{(t+1)(f-t)}dt \quad \ldots\ldots \quad (11)$$

Similarly, integrating from B to C and noting that in this range of t the term $\left(\frac{\sqrt{1-k^2}+\sqrt{1-t^2}}{\sqrt{t^2-k^2}}\right)^{\frac{2\alpha}{\pi}}$ must be replaced by

$$\left(\frac{\sqrt{1-k^2}+\sqrt{1-t^2}}{\sqrt{t^2-k^2}}\, e^{i\pi}\right)^{\frac{2\alpha}{\pi}} = e^{2\alpha i}\left(\frac{\sqrt{1-k^2}+\sqrt{1-t^2}}{\sqrt{t^2-k^2}}\right)^{\frac{2\alpha}{\pi}} \quad \ldots \quad (12)$$

so that the expression in parenthesis is now real, Eq. 13 is obtained

$$b = \frac{d}{\pi} \int_{k}^{1} \left(\frac{\sqrt{1 - k^2} + \sqrt{1 - t^2}}{\sqrt{t^2 - k^2}} \right)^{\frac{2\alpha}{\pi}} \frac{f + 1}{(t + 1)(f - t)} \, dt \quad \ldots \quad (13)$$

At C,

$$\Omega(f) = i(\alpha + \beta) = i \frac{2\alpha}{\pi} \sin^{-1} \frac{\sqrt{f^2 - 1}}{\sqrt{f^2 - k^2}} \quad \ldots \quad (14)$$

hence

$$\frac{\pi(\alpha + \beta)}{2\alpha} = \sin^{-1} \frac{\sqrt{f^2 - 1}}{\sqrt{f^2 - k^2}} \quad \ldots \quad (15)$$

By assigning values to k, f, and α it is now possible to compute correspond-

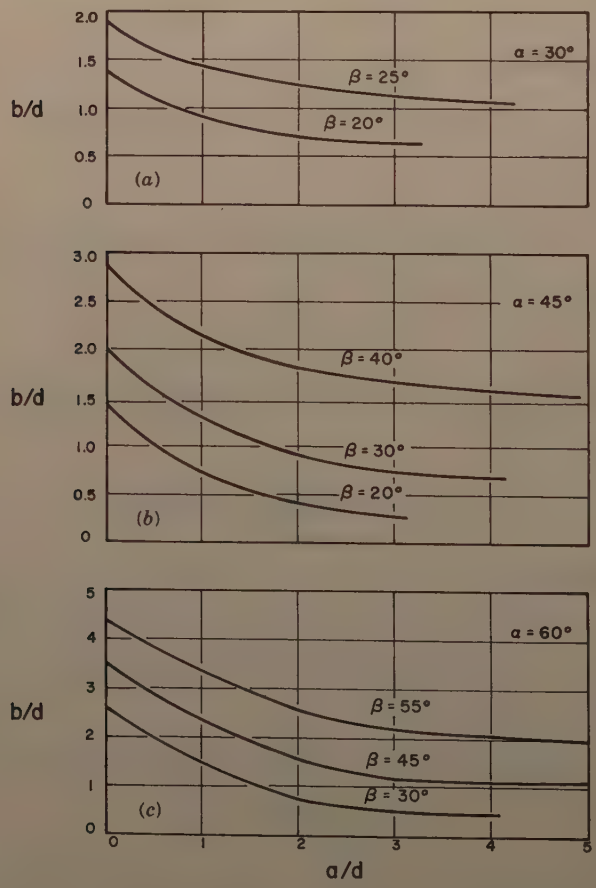

(Note that the ordinate scale is different for each graph.)

FIG. 3.—THEORETICAL EXIT ANGLES AS A FUNCTION OF DEFLECTOR SHAPE

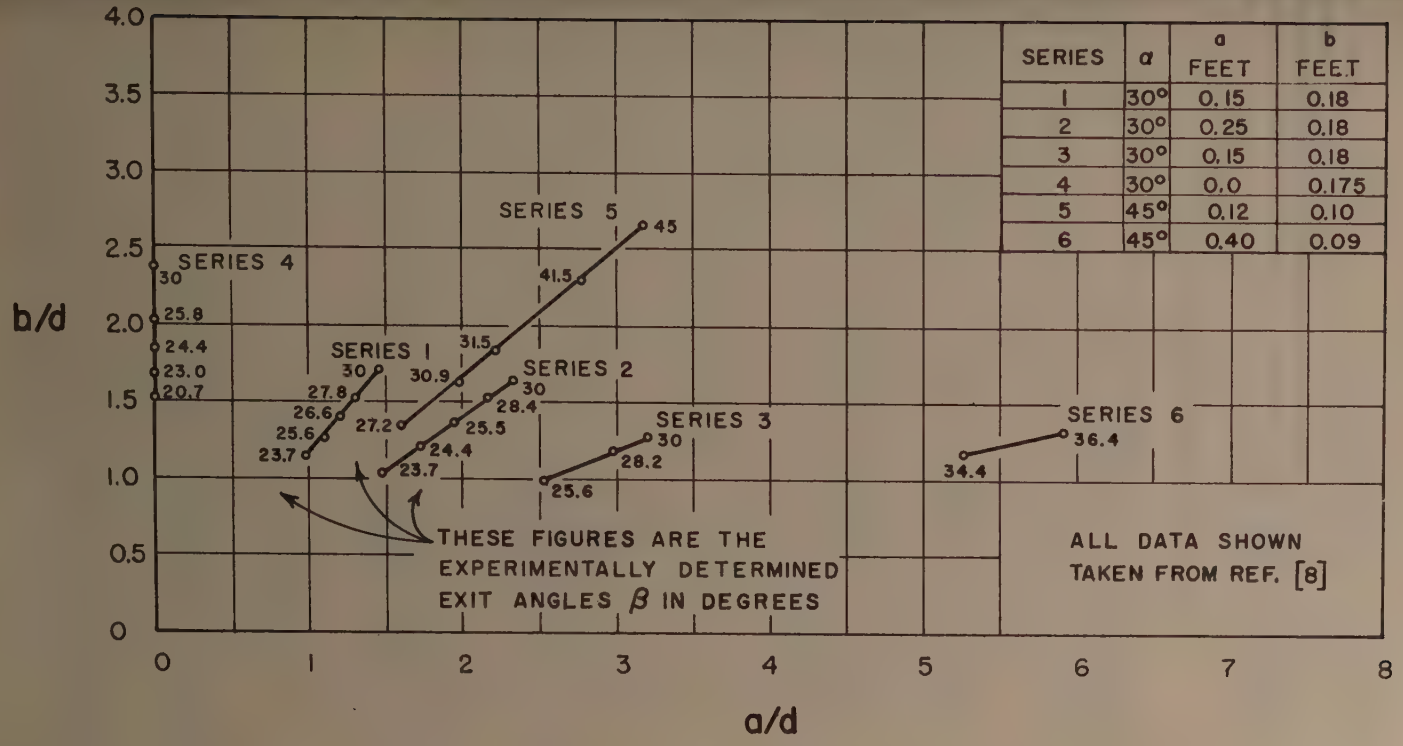

SERIES	α	a FEET	b FEET
1	30°	0.15	0.18
2	30°	0.25	0.18
3	30°	0.15	0.18
4	30°	0.0	0.175
5	45°	0.12	0.10
6	45°	0.40	0.09

FIG. 4.—EXPERIMENTAL DATA ON EXIT ANGLES

ing values of a, b, and β. This can be accomplished by numerical evaluation of the integrals, as described in Appendix I.

Eqs. 11 and 13 have been evaluated with an IBM 650 digital computer for $\alpha = 30°$, 45°, and 60°. For each of these angles specific values of β were selected, in each case less than α, and the corresponding values of the dimension parameters a/d and b/d were computed. The results of this computation are presented in graphical form in Fig. 3.

EXPERIMENTAL VERIFICATION

H. D. Copp, A. M. ASCE, has attempted[8] to verify this theory experimentally. He set up a variable slope chute 12-ft long and 12-in. wide. His test pro-

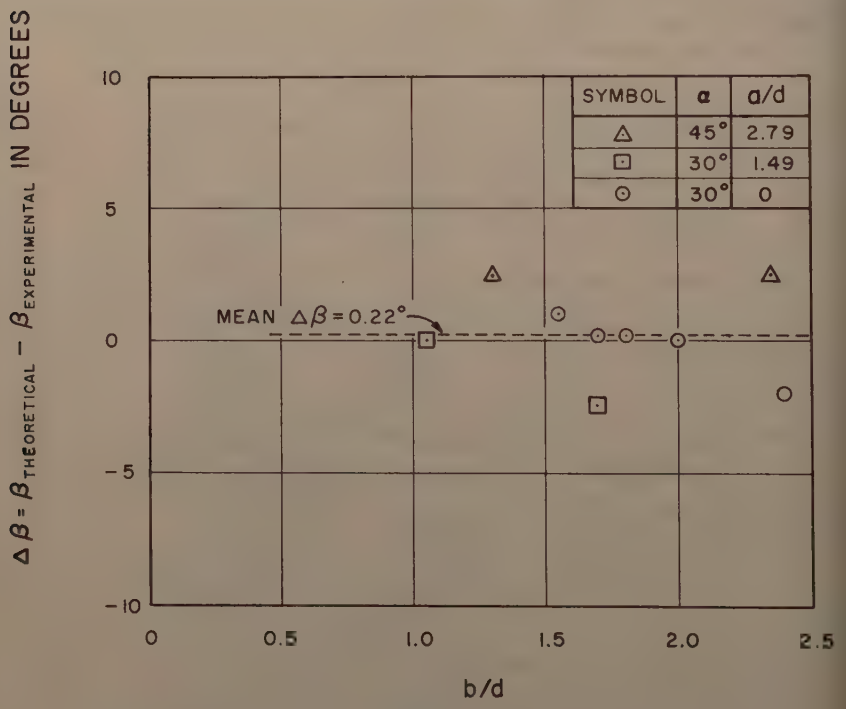

FIG. 5.—COMPARISON OF THEORY AND EXPERIMENT

gram consisted of installing six different segmental buckets and measuring the exit angles of the flow for each bucket for various depths of the approach flow. The data from these six test series are plotted in dimensionless form in Fig. 4.

8 "Laboratory Investigations on Trajectories from Segmental Flip Buckets," by H. D. Copp. Thesis presented to Washington State Univ. at Pullman, Wash. in May, 1960, in partial fulfillment of the requirements for the degree of Master of Science.

The exit angles were at first measured directly. However, Copp reports reater success by measuring the trajectory of the lower nappe of the jet and ne exit velocity and then computing the exit angle required to produce the tra- ectory.

A comparison of Copp's data with the theory is given in Fig. 5. Because of ne limited number of tests, only 9 points could be directly compared. The naximum deviation is 2.5°, and the mean of the deviation is less than a quar- er of a degree. Copp states that these deviations are within the range of ex- ected accuracy of his apparatus.

APPLICATION

A method has been developed in the foregoing sections for designing seg- nental deflectors for prescribed values of the angle α and the exit angles of ne flow β as a function of the depth d of the approaching flow. Some experi- nental verification is offered.

In the obvious application to spillway flip buckets (for an example of a seg- nental bucket see Noxon Rapids dam[9]), the angle β is first determined on the asis of a safe trajectory length, L (Fig. 1), using the velocity V as calculated or the available head H. The dimensionless parameters a/d and b/d are se- ected from a graph similar to Fig. 3. The dimensions of the bucket are then xed by choosing the most critical discharge with regard to scour and com- uting the corresponding depth d. Once the bucket has been thus designed for certain discharge, the angle β and the length L must be recomputed for all ther significant discharges.

CONCLUSIONS

1. The flow in a deflector composed of straight segments can be analyzed y free streamline theory using the Schwartz-Christoffel theorem.
2. A numerical solution of the integrals of transformation shows the effect the geometry of the deflector on the exit angle of the jet.
3. Data from previous experiments on flip buckets for spillways show that ie theory accurately predicts the exit angle of the jet.

APPENDIX I.—EVALUATION OF THE INTEGRALS BY NUMERICAL METHODS

The curves in Fig. 3 relate the quantities a/d and b/d for fixed angles α and They were obtained by choosing values of k = 0.01, 0.05, 0.10, 0.20, ..., 90, computing the corresponding value of f from Eq. 15, and evaluating the tegrals Eq. 11 and 13.

ne intercepts of the curves, corresponding to the value a/d = 0, were com- ted from the separate formula

9 "Spillway Model Study Noxon Rapids Hydroelectric Development," Ebasco Services, c., New York, June, 1957.

$$\frac{b}{d} \sin (2\alpha) = 1 - \cos (\alpha + \beta) = \frac{1}{\pi} \sum_{j=1}^{s-1} \sin \frac{2 j r \pi}{s} \left\{ -\cos (\alpha + \beta) \right.$$

$$\left. \ln \left| \cos \frac{(2 j - 1)\pi}{s} - \cos \frac{\alpha + \beta}{r} \right| + 2 \ln \sin \frac{(2 j - 1)\pi}{2 s} \right\}$$

$$+ \frac{\sin (\alpha + \beta)}{\pi} \sum_{j=0}^{s-1} \cos \frac{2 j r \pi}{s} \ln \left| \frac{\sin \frac{1}{2} \left(\frac{2 j - 1}{s} \pi + \frac{\alpha + \beta}{r} \right)}{\sin \frac{1}{2} \left(\frac{2 j - 1}{s} \pi + \frac{\alpha + \beta}{r} \right)} \right| \ldots \quad (16)$$

in which $\alpha = \frac{r}{s} \frac{\pi}{2}$.

Eq. 16 was obtained by T. T. Siao and P. G. Hubbard,[10] M. ASCE, using an argument very similar to the conformal transformation presented previously.

The numerical evaluation of the integrals Eqs. 11 and 13 is complicated by the fact that the integrand of Eq. 11 is singular at both end-points of the interval of integration and the integrand of Eq. 13 is singular at the lower end-point. Moreover, for values of k approaching 0 or 1 the integrands develop additional singularities so that care must be taken for the small and large values of k.

To evaluate integral Eq. 13 follow Hartree,[11] and write

$$\frac{1}{\pi} \int_k^x \left(\frac{\sqrt{1 - k^2} + \sqrt{1 - t^2}}{\sqrt{t^2 - k^2}} \right)^{\frac{2\alpha}{\pi}} \frac{f + 1}{(t + 1)(f - t)} \, dt$$

$$= \frac{1}{\pi} \int_k^x F(t) \frac{dt}{(t - k)^{\frac{\alpha}{\pi}}} = (x - k)^{1 - (\alpha/\pi)} \psi (x) \quad \ldots\ldots \quad (17)$$

in which

$$F(t) = \left(\frac{\sqrt{1 - k^2} + \sqrt{1 - t^2}}{\sqrt{t + k}} \right)^{\frac{2\alpha}{\pi}} \frac{f + 1}{(t + 1)(f - t)} \quad \ldots\ldots \quad (18)$$

Differentiating with respect to x,

$$(x - k)^{1 - (\alpha/\pi)} \psi' (x) + \left(1 - \frac{\alpha}{\pi}\right) (x - k)^{-(\alpha/\pi)} \psi (x) = \frac{1}{\pi} (x - k)^{-(\alpha/\pi)} F(x) \quad . . \quad (19)$$

or

$$(x - k) \psi' (x) + \left(1 - \frac{\alpha}{\pi}\right) \psi (x) = \frac{1}{\pi} F(x) \quad \ldots\ldots \quad (20)$$

---

10 "Deflection of Jets," by T. T. Siao and P. G. Hubbard, Free Streamline Analyses of Transition Flow and Jet Deflection, ed. by J. S. McNown and Chiu-Sheen Yih, Studies in Engrg. Bulletin 35, State Univ. of Iowa, 1953.

11 Numerical Analysis, by D. R. Hartree, Second Edition, Clarendon Press, Oxford, 1958, p. 111.

rom Eq. 20 and the equation resulting from differentiating Eq. 20, upon setting x = k,

$$\psi\ (k) = \frac{1}{\pi\ -\ \alpha}\ F\ (k) \quad \ldots\ldots\ldots\ldots\ldots \quad (21a)$$

nd

$$\psi'\ (k) = \frac{1}{2\ \pi\ -\ \alpha}\ F'\ (k) \quad \ldots\ldots\ldots\ldots \quad (21b)$$

ow integrate the differential Eq. 20 forward from x = k to x = 1 and set

$$\frac{b}{d} = (1\ -\ k)^{1-(\alpha/\pi)}\ \psi\ (1) \quad \ldots\ldots\ldots\ldots \quad (22)$$

For small values of k difficulties are encountered when using an integration cheme involving starting values of ψ at k-h. Consequently, the writers have hosen to integrate Eq. 20 using the Runge-Kutta Fourth Order Method which volves no special starting formulas. (For a discussion of this method, see r example Milne.[12])

Eq. 21a gives the initial condition and Eq. 21b can be used to obtain ψ (k + h) thout the indetermination that would arise from a straight forward application of the Runge-Kutta formulas. Thus denoting k + n h by x_n and $\psi\ (x_n)$ by ψ_n,

$$\psi_1 = \frac{1}{6}\ (g_{00} + 2\ g_{01} + 2\ g_{02} + g_{03}) + \psi_0 \quad \ldots\ldots\ldots \quad (23)$$

here

$$g_{00} = \frac{h}{2\ \pi\ -\ \alpha}\ F'\ (k) = \frac{-h}{2\ \pi\ -\ \alpha}\ F\ (k) \left\{ \frac{\alpha}{\pi} \left[\frac{k}{(1\ -\ k^2)} + \frac{1}{2\ k} \right] + \frac{1}{k+1} + \frac{1}{k\ -\ f} \right\} \quad \ldots\ldots\ldots\ldots \quad (24a)$$

$$g_{01} = \frac{2}{\pi} \left[F\left(k + \frac{h}{2}\right)\ -\ (\pi\ -\ \alpha) \left(\psi_0 + \frac{g_{00}}{2}\right) \right] \quad \ldots\ldots\ldots \quad (24b)$$

$$g_{02} = \frac{2}{\pi} \left[F\left(k = \frac{h}{2}\right)\ -\ (\pi\ -\ \alpha) \left(\psi_0 + \frac{g_{01}}{2}\right) \right] \quad \ldots\ldots\ldots \quad (24c)$$

d

$$g_{03} = \frac{1}{\pi} \left[F\ (k + h)\ -\ (\pi\ -\ \alpha)\ (\psi_0 + g_{02}) \right] \quad \ldots\ldots\ldots \quad (24d)$$

general

$$\psi_{n+1} = \frac{1}{6}\ (g_{n0} + 2\ g_{n1} + 2\ g_{n2} + g_{n3}) + \psi_n \quad \ldots\ldots\ldots \quad (25)$$

12 Numerical Solution of Differential Equations, by W. E. Milne, John Wiley & Sons, ., New York, 1953, p. 72.

where

$$g_{n0} = \frac{1}{n\pi}\left[F\left(x_n\right) - (\pi - \alpha)\,\psi_n\right] \quad \ldots\ldots\ldots \quad (26a$$

$$g_{n1} = \frac{1}{\left(n + \frac{1}{2}\right)\pi}\left[F\left(x_n + \frac{h}{2}\right) - (\pi - \alpha)\left(\psi_n + \frac{g_{n0}}{2}\right)\right] \quad \ldots \quad (26b$$

$$g_{n2} = \frac{1}{\left(n + \frac{1}{2}\right)\pi}\left[F\left(x_n + \frac{h}{2}\right) - (\pi - \alpha)\left(\psi_n + \frac{g_{n1}}{2}\right)\right] \quad \ldots \quad (26c$$

and

$$g_{n3} = \frac{1}{(n+1)\pi}\left[F\left(x_n + h\right) - (\pi - \alpha)\left(\psi_n + g_{n2}\right)\right] \quad \ldots \quad (26d$$

Notice that one of the common objections to the numerical integration of differential equation $y' = f(x, y)$ by Runge-Kutta methods—namely the numbe of times that the function $f(x, y)$ must be evaluated—is considerably mitigate in the preceding formulation, since the complicated evaluation of the functio $F(x)$ need be done only twice for each forward step of the integration. An equiv alent formulation of the problem can be obtained by setting $y(x) = (x - k)\,\psi(x)$ Then,

$$y'(x) = (x - k)\,\psi'(x) + \psi(x) \quad \ldots\ldots\ldots \quad (27$$

and the differential Eq. 20 becomes

$$y'(x) = \frac{1}{\pi}\left[F(x) + \frac{\alpha}{x - k}\,y(x)\right] \quad \ldots\ldots\ldots \quad (28$$

with the initial condition $y(k) = y_0 = 0$. Now

$$y_1 = \frac{1}{6}\left(g'_{00} + 2\,g'_{01} + 2\,g'_{02} + g'_{03}\right) + y_0 \quad \ldots\ldots\ldots \quad (29$$

where

$$g'_{00} = \frac{h}{\pi}\left[F(k) + \alpha\,\psi(k)\right] = \frac{h}{\pi - \alpha}\,F(k) \quad \ldots\ldots\ldots \quad (30a$$

$$g'_{01} = \frac{h}{\pi}\,F\left(k + \frac{h}{2}\right) + \frac{\alpha}{\pi}\,g'_{00} \quad \ldots\ldots\ldots \quad (30b$$

$$g'_{02} = \frac{h}{\pi}\,F\left(k + \frac{h}{2}\right) + \frac{\alpha}{\pi}\,g'_{01} \quad \ldots\ldots\ldots \quad (30c$$

$$g'_{03} = \frac{h}{\pi}\,F(k + h) + \frac{\alpha}{\pi}\,g'_{02} \quad \ldots\ldots\ldots \quad (30d$$

and in general

$$y_{n+1} = \frac{1}{6}\left(g'_{n0} + 2\,g'_{n1} + 2\,g'_{n2} + g'_{n3}\right) + y_n \quad \ldots\ldots\ldots \quad (31$$

here

$$g'_{n0} = \frac{h}{\pi} F(x_n) + \frac{\alpha}{n\pi} y_n \quad \ldots\ldots\ldots\ldots\ldots \quad (32a)$$

$$g'_{n1} = \frac{h}{\pi} F\left(x_n + \frac{h}{2}\right) + \frac{\alpha}{(2n+1)\pi} (2y_n + g'_{n0}) \quad \ldots\ldots \quad (32b)$$

$$g'_{n2} = \frac{h}{\pi} F\left(x_n - \frac{h}{2}\right) + \frac{\alpha}{(2n+1)\pi} (2y_n + g'_{n1}) \quad \ldots\ldots \quad (32c)$$

nd

$$g'_{n3} = \frac{h}{\pi} F(x_n + h) + \frac{\alpha}{(n+1)\pi} (y_n + g'_{n2}) \quad \ldots\ldots \quad (32d)$$

arrying forward the integration until $x = 1$, results in

$$\frac{b}{d} = \frac{y(1)}{(1-k)\frac{\alpha}{\pi}} \quad \ldots\ldots\ldots\ldots\ldots\ldots \quad (33)$$

Eq. 33 enjoys a slight computational advantage of values of k not too close 1 since error in the evaluation of F (x) is minimized by multiplication by h nd the necessity of evaluating F' (k) is eliminated. The quantity a/d is evaluated by writing

$$\frac{a}{d} = \frac{1}{\pi} \int_{-k}^{0} \left(\frac{\sqrt{1-k^2} + \sqrt{1-t^2}}{\sqrt{k+t}} \right)^{\frac{2\alpha}{\pi}} \frac{f+1}{(t+1)(f-t)} \frac{dt}{(k+t)^{\frac{\alpha}{\pi}}} \quad \ldots \quad (34a)$$

d

$$\frac{a}{d} = \frac{1}{\pi} \int_{k}^{0} \left(\frac{\sqrt{1-k^2} + \sqrt{1-t^2}}{\sqrt{k+t}} \right)^{\frac{2\alpha}{\pi}} \frac{f+1}{(t+1)(f-t)} \frac{dt}{(k-t)^{\frac{\alpha}{\pi}}} \quad \ldots \quad (34b)$$

ese two integrals can now be evaluated by the same technique that was used th integral Eq. 13.

APPENDIX II.—NOTATIONS

= length of horizontal segment of deflector;

= length of downstream sloping segment of deflector;

= depth of approach flow;

= base of natural logarithms;

= coordinate in t-plane corresponding to infinity;

g = acceleration of gravity;

i = imaginary number, $\sqrt{-1}$;

k = coordinate in t-plane corresponding to ends of horizontal segment of deflector;

L = horizontal distance of trajectory;

M = constant in transformation integral;

N = constant of integration;

q = magnitude of velocity vector;

t = variable of integration; abscissa in t-plane;

u = velocity component in x-direction;

V = velocity vector;

v = velocity component in y-direction;

x = real axis in Z-plane;

y = imaginary axis in Z-plane;

z = complex coordinate in Z-plane;

α = angle of inclination of deflector faces;

β = exit angle of jet at infinity;

ζ = derivative of complex velocity potential;

θ = inclination of velocity vector;

υ = kinematic viscosity of fluid;

ω = complex velocity potential; and

Ω = complex coordinate in Ω-plane.

Journal of the
HYDRAULICS DIVISION
Proceedings of the American Society of Civil Engineers

UNIFORM FLOW IN A SHALLOW, TRIANGULAR OPEN CHANNEL

By Richard J. Wasley,[1] A. M. ASCE

SYNOPSIS

A smooth, shallow, triangular open channel was investigated to determine characteristics of uniform flow in an idealized highway gutter. Depths, ocity contours, and transverse velocity distributions are presented for var- s slope configurations and flow rates.

INTRODUCTION

In connection with an analytical investigation of flow from gutters into curb- ning inlets,[2] extensive experimental work was done with uniform flows in ydraulically smooth triangular channel (one side of which was nearly ver- l) placed on a continuous grade with no depression in the channel floor (Fig. The data taken were almost entirely limited to flows at supercritical velo- es because the theoretical development was predicated on such a condition. *Notation.*—The letter symbols adopted for use in this paper are defined re they first appear, in the illustrations or in the text, and are arranged abetically, for convenience of reference, in the Appendix.

Note.—Discussion open until February 1, 1962. To extend the closing date one month, ritten request must be filed with the Executive Secretary, ASCE. This paper is part e copyrighted Journal of the Hydraulics Division, Proceedings of the American So- y of Civil Engineers, Vol. 87, No. HY 5, September, 1961.

[1] Research Asst., Stanford Univ., Stanford, Calif.

[2] "Hydrodynamics of Flow into Curb-Opening Inlets," by R. J. Wasley, thesis pre- ed to Stanford Univ. at Stanford, Calif., in November, 1960, in partial fulfillment of requirements for the degree of Doctor of Philosophy; also available as Technical ort No. 6, Dept. of Civ. Engrg., Stanford Univ., Stanford, Calif.

FIG. 1.—PERSPECTIVE DRAWING, SECTIONS, AND DEFINITION SKETCH OF INVESTIGATION

Equipment.—The channel as finally constructed was an idealized full-scale prototype, 50 ft in overall length by 6 ft in width. The actual triangular channel was 32 ft-3 in. in length, the remainder being the curb-opening inlet (Fig. 1).

The rigid frame construction was achieved with 1-1/8 in. plywood panels bolted to transverse 3I5.7 beams on 4 ft centers. The plywood was surfaced with 1/4 in. tempered masonite fastened with waterproof cement. The joints were filled with a waterproof sealer, sanded, and four coats of a waterproof epoxy resin were applied, each coat being wet-sanded. The resulting surface was almost perfectly smooth visually and remained so throughout the experimental program.

The I-beams were fastened to threaded 3/4 in. standard galvanized pipes by means of nuts and washers on top and bottom of flanges welded to the bottom of the beams at each end. The pipes were attached to 3/4 in. steel rods set in the concrete floor of the laboratory with iron cement. A bracing system of tension rods and turnbuckles was added to the pipe substructure for rigidity and alinement purposes.

The stilling basin at the upstream end was a reservoir 10 ft by 8 ft by 4 ft in height. A baffle system was utilized to quiet the flow. The entrance of the water to the channel itself was effected through a stainless steel transition section. A rubber diaphragm connected this section to the reservoir and allowed any changes in slopes to be easily accomplished without causing leaks.

A surveyor's level was used to accurately position the apparatus. Transverse slopes, θ_o, were possible within a range of zero to 10%; the range of longitudinal slopes, ϕ_o, was nearly as flexible, with a range of zero to about 8%. A grid system for locating the position of the measuring equipment, was composed of dots at one-quarter foot intervals painted on the channel surface. The origin and coordinate system are shown in Fig. 1.

A horizontal datum was used for the support of the measuring apparatus by fastening I-beams to the pipe standards at an arbitrary elevation from the floor. Aluminum tees were bolted to the beams and an aluminum cross-member was placed longitudinally so it could slide transversely on the beams. To this was attached either the point gage or the Pitot tube, capable of moving longitudinally on the cross-member.

Certain appurtenances were used to damp out any waves or other disturbances that developed. An adjustable sluice gate was used in a transverse position at the entrance, consisting of a series of sheet aluminum panels, each of which could be placed at any desired height above the channel. Slightly downstream, two groups of aluminum vanes, one behind the other were positioned to straighten the flow and lessen or eliminate any surface irregularity that occurred. In addition (for certain flow rates and configurations), to aid in the damping action, a screen was placed in front of the vane system, and a piece of cloth was attached to the downstream end and allowed to ride on the surface of the water; it was determined that these latter modifications were not particularly effective (Fig. 4). It was found that the lower flow rates did not require any of these devices, uniform flow being achieved simply by the fluid passing through the channel alone.

The durability of the equipment was more than adequate. After approximately 300 hr of operation, no noticeable damage had developed in the surface. During changes in configuration, some slight cracking at the joints occurred, but this was quickly and easily repaired with no appreciable effect on any measurement. Toward the end of the experimental program, some very slight sag

between supports (about 1/800) became noticeable. However, there was no significant effect upon the flow.

Technique.

Flow Measurement.—The desired flow rate Q, was obtained from readings of a manometer that had been previously calibrated by standard weighing methods. Two Venturi meters were available for use in this experiment, one with a 4 in. throat diameter and another with a 2 in. diameter. The total range of flow rates in the experimental program was from a minimum of 0.0032 cfs to a maximum of 2.98 cfs. The measurements below 0.040 cfs, however, were obtained from the actual weighing of a quantity of the fluid in a specified interval of time.

Depth Measurement.—A point gage was used in all the measurements of depth. The point itself was constructed with a 45° angle bend near the end to allow easier measurements at or near the curb face and directly under the supporting I-beams. The apparatus was suspended from the datum plane as described earlier. The difference between the channel elevation and the water surface at a given point constituted the depth at that point.

It was found that any depth measurement could be satisfactorily duplicated to 0.001 ft with the apparatus previously described. Although there were slight rapid fluctuations on the water surface itself, probably caused by turbulence, these could be averaged quite adequately by eye and identical measurements repeated.

Velocity Measurement.—A pitot probe with a vertical tube was used for all velocity measurements. The velocities were generally great enough to create an adequate velocity head to insure sufficient accuracy in reading. Three different diameter probe openings were used (0.010 in., 0.025 in., and 0.065 in.). It was found that all three probe diameters gave essentially the same readings; hence, it was decided to use the intermediate opening size (0.025 in.) to reduce the necessary response time compared with the fine opening size.

In addition, an internal check was used to allow a comparison with the measured flow rate. This was achieved by the integration of the transverse velocity distribution (initially obtained from the integration of the velocity profiles) to determine the quantity of flow. A reasonable agreement was obtained for the computed flow from the Pitot measurements that generally gave slightly higher results over the measured flow (see the section entitled "Results").

The capillary correction was found to be negligible for all measurements taken. The most critical possible correction was connected with the fine probe opening in which the internal diameter of the vertical standing tube was 0.015 ft (both the other standing tubes were larger in diameter). The capillary rise[3] for this diameter using tap water is about 0.008 ft. The minimum total head reading taken was 0.280 ft (accurate to about $\pm$ 0.004 ft), causing the capillary correction to be less than 3%.

OBSERVATIONS

This section presents the actual experimental data in reduced form, whereas the various comparisons between this investigation and experimental work from different sources are given in the section entitled "Results."

3 "Handbook of Hydraulics," by H. W. King, McGraw-Hill Book Co., Inc., New York, 1954.

The maximum transverse slope distance, y_o, and the depth of flow at the curb face, z_o, are given as functions of the flow rate, Q, in Figs. 2 and 3. A verification of steady uniform flow can be seen by noting the slope of the resulting line. Manning's formula for a triangular channel of this type in this

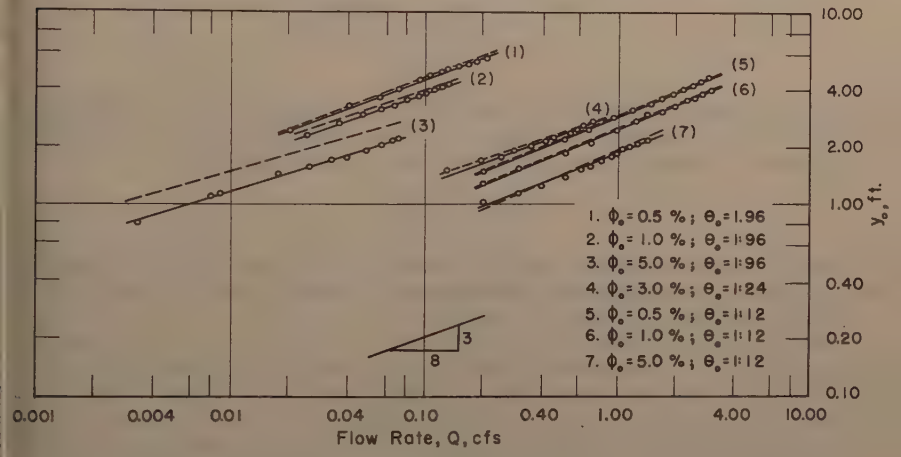

FIG. 2.—Q VS y_o FOR ALL CONFIGURATIONS $\left[\left(\frac{z_o}{\theta_o}\right)\right.$ SHOWN DASHED$\left.\right]$

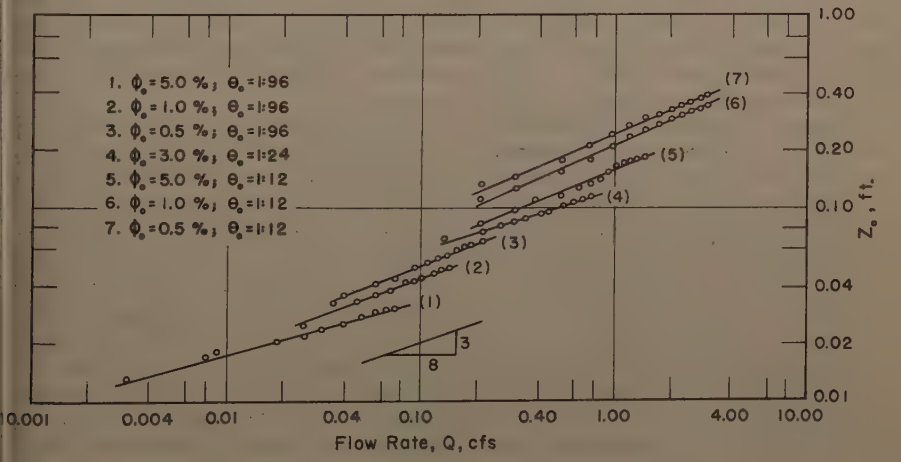

FIG. 3.—Q VS z_o FOR ALL CONFIGURATIONS

investigation (neglecting curb shear) can be derived readily[4] and is found to be

$$Q = \frac{0.56}{n} (\theta_o) - 1 \, (z_o)^{8/3} \, (\phi_o)^{1/2} \quad \ldots\ldots\ldots\ldots \quad (1)$$

4 "Elements of Hydraulic Engineering," by R. K. Linsley and J. B. Franzini, McGraw-Hill Book Co., Inc., New York, 1955.

in which n is the coefficient in Manning's formula. Because z_o is the only variable, for a given position of the apparatus, an eight-thirds slope of the plotted line indicates the uniformity of flow conditions.

The channel roughness is defined in terms of the conventional Darcy friction factor, f, as expressed by[5]

$$f = \frac{8\ g\ R\ (\phi_o)^{1/2}}{\bar{\bar{u}}^2} \quad \ldots\ldots\ldots\ldots\ldots\ldots \quad (2)$$

in which g is acceleration due to gravity, R is the channel hydraulic radius, and $\bar{\bar{u}}$ is the average channel velocity; this equation assumes that d = 4R is the "equivalent diameter." The Reynolds number, **R**, is given by

$$\mathbf{R} = \frac{4\ \bar{\bar{u}}\ R}{\nu} \quad \ldots\ldots\ldots\ldots\ldots\ldots\ldots\ldots (3)$$

in which ν is the kinematic viscosity of water. The data and the Stanton diagram will be given in the appropriate section under "Results" and the latter will be compared with other similar information.

The experimental velocities are plotted in the form of contours for each configuration and flow condition investigated (see Figs. 5 through 9 in which the vertical scales are greatly exaggerated). The contours are drawn interpolating among average depths and velocities at a given position, obtained from superposing the various profile sections. The error of averaging the velocities and depths at a given point or section was not significantly different from any extreme value for that point or section. The superposed velocity profiles for two typical situations (ϕ_o = 1.00%, θ_o = 1:12, and Q = 2.98 cfs; and ϕ_o = 5.00%, θ_o = 1:12, and Q = 1.42 cfs) are presented in Fig. 4. This shows very well that the averaging of the velocities and depths at a given position can be accomplished quite accurately; it also indicates the extent of the uniformity of flow. The various x-coordinates of the transverse sections (applicable to all configurations and flow rates) are given in the figure.

Surface tension phenomena were observable throughout the investigation. To insure consistency of these effects, the surface was completely wetted before each run and allowed to dry before taking any values. The increase in the measured transverse plan dimension, y, after this was done and after flow was established was attributed to surface tension causes. For the flat cross slope, this difference was noticed to be as much as 20% for y_o. For the steep cross slope, this difference was almost negligible, with gravity being the stronger influence. The longitudinal slope had relatively little effect on these changes. From Fig. 2, it can be seen that there is a difference between the calculated y_o ($y_o = z_o/\theta_o$), shown by dashed lines, and the experimental y_o, shown by solid lines. For all configurations and flow rates (except for very slight opposite results for ϕ_o = 5%, θ_o = 1:12), the calculated values were greater than the experimental. It is reasonable to expect that surface tension between the liquid

5 "Elementary Fluid Mechanics," by J. K. Vennard, John Wiley and Sons, Inc., New York, 1954.

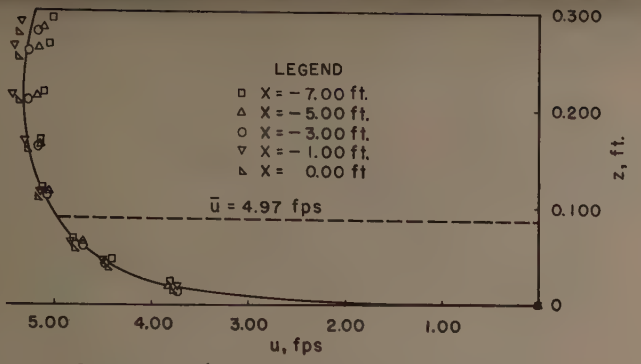

FIG. 4.—TYPICAL SUPERPOSITION OF VELOCITY PROFILES

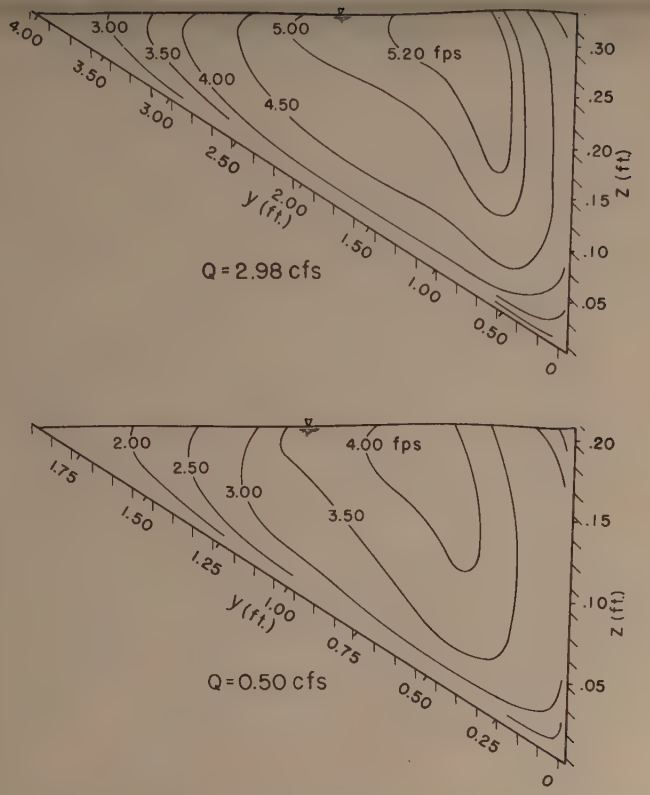

FIG. 5.—UPSTREAM VELOCITY CONTOURS FOR ϕ_o = 1.00% AND θ_o = 1:12

FIG. 6.—UPSTREAM VELOCITY CONTOURS FOR $\phi_o = 1.00\%$ AND $\phi_o = 1.24$

FIG. 7.—UPSTREAM VELOCITY CONTOURS FOR $\phi_o = 3.00\%$

FIG. 8.—UPSTREAM VELOCITY CONTOURS FOR $\phi_o = 5.00\%$ AND $\theta_o = 1:12$

FIG. 9.—UPSTREAM VELOCITY CONTOURS FOR $\phi_o = 5.00\%$ AND $\theta_o = 1:96$

and air interface would exert a "pull" toward the curb causing this to occu (similar to the way a droplet of water forms on a solid surface).

RESULTS

Comparison of Investigations.—On the basis of the average velocity vecto of each profile section (originally obtained from the superposed profiles, suc as Fig. 4), transverse velocity distributions can be drawn (Figs. 10 throug 14).

Previous experimental data taken by C. L. Larson[6] on a triangular chann of similar shape (except with the curb slope shallower than 1 on 2), but wi a concrete surface, indicated that the velocity distribution could be expresse by two representations:

$$\bar{u} = C_o \bar{\bar{u}} \left(\frac{y}{y_o}\right)^{2/3} \quad \ldots\ldots\ldots\ldots\ldots \quad (4$$

for the region

$$0 \leq \frac{y}{y_o} \leq \left(\frac{y}{y_o}\right)_{\bar{u}_{exp.max.}}$$

and

$$\bar{u} = C_o' \bar{\bar{u}} \left(1 - \frac{y}{y_o}\right)^{2/3} \quad \ldots\ldots\ldots\ldots\ldots \quad (4$$

for the region

$$\left(\frac{y}{y_o}\right)_{\bar{u}_{exp.max.}} \leq \frac{y}{y_o} \leq 1$$

in which y is the particular transverse dimension, C_o and C_o' are experiment coefficients, and $\bar{u}_{exp.max.}$ refers to the maximum experimental average vel city in any given transverse section. It is seen from the figures that in mo cases this does not fully represent the shape of the actual distribution.

Another method that theoretically describes the distribution without any c efficients, except the utilization of the Darcy friction factor, f, can be give From experimental information (or handbooks) an average friction fact across the channel can be given by Eq. 2. All these quantities can be read calculated from the known upstream parameters.

Considering a certain point on this transverse section, and rewriting Da cy's equation yields

$$\bar{u} = C_1 z^{1/2} \quad \ldots\ldots\ldots\ldots\ldots$$

6 "Transverse Distribution of Velocity and Quantity of Flow in a Shallow Triangul Channel," by C. L. Larson, thesis presented to the Univ. of Minnesota, at Minneapol Minn. in 1940, in partial fulfillment of the requirements for the degree of Master Science.

FIG. 10.—TRANSVERSE VELOCITY DISTRIBUTIONS FOR $\phi_o = 1.00\%$ AND $\theta_o = 1{:}12$

FIG. 11.—TRANSVERSE VELOCITY DISTRIBUTIONS FOR $\phi_o = 1.00\%$ AND $\theta_o = 1{:}96$

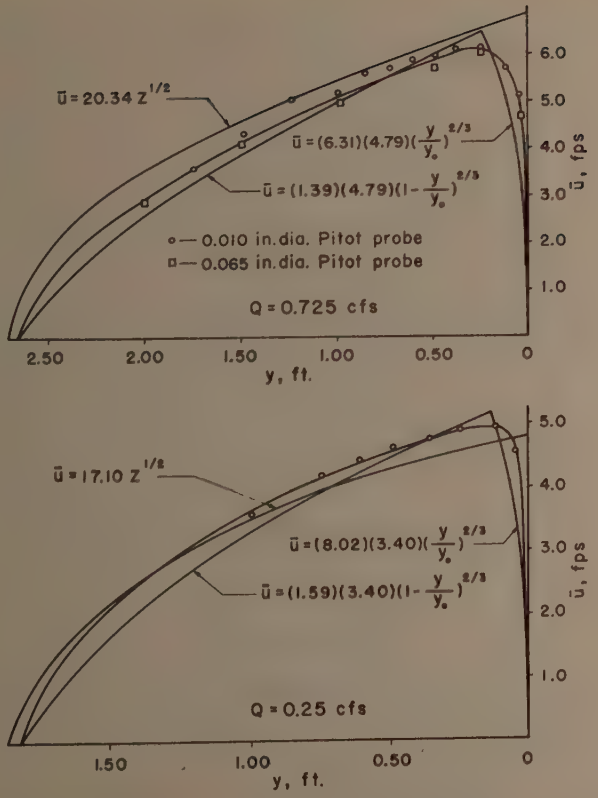

FIG. 12.—TRANSVERSE VELOCITY DISTRIBUTIONS FOR

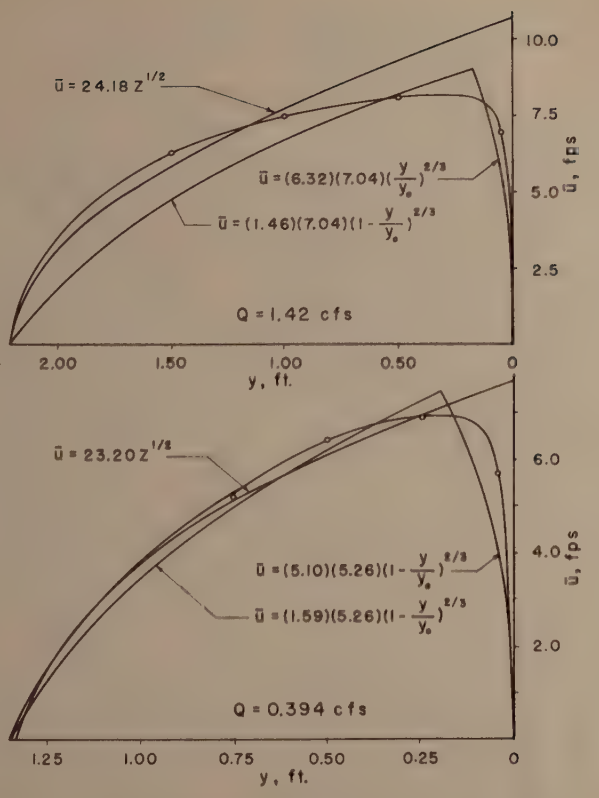

FIG. 13.—TRANSVERSE VELOCITY DISTRIBUTIONS FOR
$\phi_o = 5.00\%$ AND $\theta_o = 1:12$

n which

$$C_1 = \left(\frac{8\ g\ \phi_o}{f}\right)^{1/2} \qquad \ldots\ldots\ldots\ldots\ldots\ldots (6)$$

ith the depth, z, being substituted for the hydraulic radius, R.

Because of such a simple representation of the distribution as Eq. 5, it ould be expected that complete agreement with experiment would be more oincidence that consequence of the theory. It is seen, when compared with

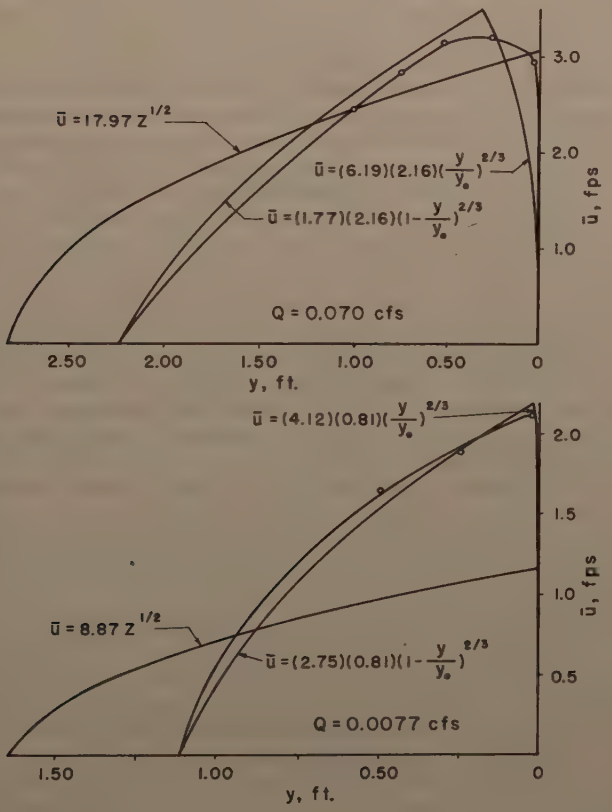

FIG. 14.—TRANSVERSE VELOCITY DISTRIBUTIONS FOR ϕ_o = 5.00% AND θ_o = 1:96

e results of the Pitot measurements, that the shape of the distribution is iite well defined, in general, but the magnitude is somewhat in error nearer e curb (assuming the Pitot results are correct).

It is noted that Eq. 5 does not account for the curb shear that would cause e velocity there to approach zero. This could be accomplished by represent- g this section of the distribution by a one-half power expression similar to

Eqs. 4a and 4b. However, as with Larson's formulas, it would be necessary t know the transverse position and magnitude of the maximum velocity vecto across the section and would curtail the direct application of this method. Thi modification of the distribution is considered below in this section, in connec tion with another topic. Generally speaking, however, this constitutes only rather small correction.

It could be argued, that because the friction factor in Eq. 2 was determine by using the bulk quantities of the channel section (that is, an average frictio factor) and then applied directly to Eq. 5, that fair agreement should be ob tained. However, the variation of the friction factor across the channel is quit complicated, and an "average" found in the preceding manner might well b questioned.

Another possible approach to describing the friction factor, f, can be ad vanced. There should be a systematic variation of the friction factor acros the flow, approaching a large value as the depth decreases toward zero. T determine this, an incremental slice of fluid could be considered in the trans verse direction and the experimental mean velocity and depth (as the hydrauli radius) in that element used to compute a friction coefficient for that smal width. In addition, the Reynolds number associated with this factor could b calculated from Eq. 3. This would allow a curve to be plotted on the Stanto diagram.

From this information, the possibility of there being a definite relationshi could be investigated in the manner in which f varies with y or with R tha would allow an analytical expression for C_1 in Eq. 5 as a function of either o these quantities. Besides requiring more detailed information on the incom ing experimental parameter, the end result from an approach of this kind woul probably not be greatly different from the previously noted "average" f.

The "equivalent diameter" (d = 4 R) is also suspect. For smooth channel that are similar in shape to a circular pipe conduit, or even symmetrical tri angular flumes not badly deformed, this works quite satisfactorily.[7] However for badly distorted channels, as in the present case, far from a circular cross section, and for smooth surfaces, the "equivalent diameter" has been shown t be not equal to four times the hydraulic radius.[8]

To determine the total magnitude of the discrepancy between the simplifie theoretical representation of the distribution and the actual variation, it is onl necessary to integrate the theoretical distribution (accounting for the triangu lar cross-section) to obtain the flow rate and compare it with the measure flow in the channel. This has been done and is given in Table 1.

It can be noted that a surprisingly constant ratio of these two flow rate (measured to theoretical) exists. The average value of this ratio, $\overline{N}$, not con sidering the 1 on 96 cross-slope, is 0.856. Disregarding the longitudinal slop of 5% and also the 1 on 96 transverse slope, the ratio is 0.855. The total mea value is 0.829. The average value of the ratio for the shallower transvers slope deteriorated slightly but not seriously.

To account for the constant value of $\overline{N}$, an analysis of the various propertie of the velocity distribution should be made. The theoretical distribution (E 5) could be improved slightly as mentioned, by accounting for the curb shea

7 "Open Channel Flow at Small Reynolds Numbers," by L. G. Straub, E. Silberma and H. C. Nelson, Transactions, ASCE, Vol. 123, 1958.

8 "Elementary Fluid Mechanics," by J. K. Vennard, John Wiley and Sons, Inc., Ne York, 1954.

TABLE 1. SUMMARY OF BASIC RESULTS

Φ_o %	θ_o	Q cfs	y_o ft	z_o ft	$y_o = \frac{z_o}{\theta_o}$ ft	A_2 ft^2	$\bar{u}$ fps	R ft	f	N_R $(\times 10^{-3})$	n $(\times 10^{3})$	C_1 $\frac{ft^{1/2}}{sec.}$	$Q_{theo.}$ cfs	N
(1)	(2)	(3)	(4)	(5)	(6)	(7)	(8)	(9)	(10)	(11)	(12)	(13)	(14)	(15)
0.5%	1:12	2.95	4.52	0.380	4.56	0.857	3.45	0.175	0.0189	217.5	9.54	8.26	3.53	0.836
		2.70	4.36	0.365	4.38	0.795	3.40	0.168	0.0187	206.0	9.45	8.30	3.21	0.841
		2.45	4.20	0.351	4.21	0.735	3.33	0.162	0.0188	194.0	9.44	8.27	2.90	0.845
		2.20	4.00	0.336	4.03	0.672	3.27	0.155	0.0187	191.0	9.30	8.30	2.61	0.843
		1.95	3.82	0.316	3.79	0.604	3.23	0.146	0.0180	178.0	9.17	8.46	2.28	0.856
		1.69	3.60	0.295	3.54	0.531	3.18	0.136	0.0173	159.0	8.78	8.63	1.96	0.863
		1.45	3.41	0.280	3.36	0.476	3.05	0.129	0.0179	148.5	8.82	8.48	1.69	0.858
		1.20	3.19	0.261	3.13	0.416	2.90	0.121	0.0185	132.5	8.90	8.34	1.39	0.864
		0.955	2.80	0.233	2.80	0.326	2.92	0.108	0.0163	113.6	8.19	8.89	1.12	0.853
		0.695	2.51	0.207	2.48	0.260	2.67	0.0956	0.0173	90.0	8.28	8.63	0.808	0.860
		0.50	2.22	0.179	2.15	0.198	2.52	0.0825	0.0168	77.9	7.95	8.75	0.572	0.874
		0.30	1.81	0.149	1.79	0.135	2.21	0.0689	0.0181	54.9	8.05	8.44	0.348	0.862
0.5%	1:12	0.20	1.58	0.131	1.57	0.103	1.94	0.0602	0.0206	42.1	8.35	7.90	0.235	0.852
0.5%	1:96	0.203	5.35	0.060	5.75	0.1605	1.265	0.0296	0.0239	13.30	8.00	7.35	0.254	0.800
		0.180	5.25	0.059	5.65	0.155	1.16	0.0292	0.0279	12.50	8.20	6.80	0.219	0.822
		0.165	5.15	0.057	5.46	0.147	1.12	0.0282	0.0289	11.30	8.70	6.68	0.195	0.846
		0.150	5.00	0.056	5.37	0.140	1.07	0.0276	0.0310	10.56	9.00	6.45	0.183	0.820
		0.134	4.90	0.052	5.00	0.127	1.05	0.0257	0.0296	9.81	8.75	6.60	0.157	0.853
		0.120	4.75	0.050	4.80	0.119	1.01	0.0248	0.0314	8.95	8.90	6.41	0.138	0.869
		0.105	4.55	0.047	4.52	0.107	0.98	0.0232	0.0312	8.12	8.75	6.43	0.118	0.890
		0.090	4.35	0.045	4.32	0.098	0.92	0.0223	0.0339	7.32	9.10	6.17	0.099	0.910
		0.070	3.95	0.040	3.84	0.079	0.885	0.0198	0.0323	6.37	8.70	6.32	0.0777	0.901
		0.055	3.60	0.037	3.55	0.067	0.82	0.0184	0.0348	5.39	9.00	6.08	0.0630	0.873
		0.040	3.25	0.034	3.27	0.055	0.73	0.0168	0.0408	4.38	9.50	5.62	0.0432	0.926
0.5%	1:96	0.020	2.40	0.026	2.49	0.031	0.645	0.0128	0.0393	2.95	8.90	5.73	0.0238	0.841

TABLE 1.—*CONTINUED*

(1)	(2)	(3)	(4)	(5)	(6)	(7)	(8)	(9)	(10)	(11)	(12)	(13)	(14)	(15)
1.0%	1:12	2.98	4.00	0.332	3.99	0.664	4.49	0.153	0.0196	264.0	9.51	11.46	3.48	0.856
		2.70	3.85	0.320	3.84	0.616	4.38	0.148	0.0199	252.0	9.52	11.37	3.16	0.855
		2.45	3.69	0.305	3.67	0.562	4.36	0.141	0.0191	238.0	9.25	11.62	2.86	0.856
		2.20	3.57	0.290	3.49	0.518	4.25	0.134	0.0191	221.0	9.15	11.62	2.53	0.812
		1.95	3.37	0.274	3.29	0.462	4.22	0.127	0.0184	213.0	8.89	11.83	2.23	0.875
		1.69	3.19	0.262	3.145	0.417	4.05	0.121	0.0190	192.5	8.97	11.64	1.96	0.863
		1.45	3.01	0.247	2.96	0.372	3.90	0.114	0.0194	175.6	8.94	11.52	1.68	0.866
		1.20	2.82	0.228	2.74	0.322	3.73	0.105	0.0195	155.0	8.86	11.48	1.37	0.876
		0.955	2.53	0.203	2.44	0.256	3.73	0.0939	0.0174	138.5	8.21	12.17	1.09	0.879
		0.695	2.20	0.178	2.14	0.196	3.55	0.0823	0.0169	116.0	7.92	12.34	0.794	0.875
		0.50	1.90	0.157	1.88	0.149	3.36	0.0724	0.0166	97.4	7.70	12.43	0.584	0.856
		0.30	1.59	0.129	1.55	0.103	2.91	0.0599	0.0182	69.0	7.83	11.89	0.343	0.875
1.0%	1:12	0.20	1.36	0.112	1.34	0.076	2.63	0.0517	0.0193	53.8	7.87	11.53	0.232	0.862
1.0%	1:96	0.135	4.15	0.045	4.30	0.0935	1.44	0.0222	0.0277	12.80	8.16	9.62	0.158	0.855
		0.125	4.05	0.044	4.22	0.0890	1.40	0.0218	0.0287	11.60	8.30	9.47	0.145	0.862
		0.115	3.92	0.043	4.13	0.0842	1.37	0.0213	0.0292	11.10	8.35	9.39	0.137	0.840
		0.100	3.77	0.041	3.94	0.0773	1.29	0.0203	0.0314	10.00	8.60	9.05	0.118	0.848
		0.090	3.65	0.040	3.82	0.0730	1.23	0.0198	0.0336	9.36	8.87	8.75	0.108	0.837
		0.080	3.46	0.038	3.64	0.0657	1.22	0.0188	0.0326	9.19	8.65	8.89	0.096	0.837
		0.065	3.34	0.036	3.46	0.0602	1.08	0.0178	0.0393	7.69	9.41	8.10	0.075	0.867
		0.055	3.08	0.034	3.26	0.0524	1.05	0.0168	0.0391	7.05	9.34	8.12	0.069	0.802
		0.045	2.90	0.033	3.16	0.0478	0.940	0.0163	0.0476	6.13	10.20	7.37	0.056	0.804
		0.035	2.69	0.031	2.98	0.0417	0.840	0.0153	0.0558	5.14	10.90	6.79	0.044	0.795
1.0%	1:96	0.025	2.36	0.023	2.21	0.0272	0.920	0.0114	0.0347	4.18	8.20	8.62	0.027	0.926
3.0%	1:24	0.725	2.65	0.113	2.71	0.151	4.79	0.0547	0.0187	89.0	7.80	20.34	0.855	0.848
		0.63	2.60	0.110	2.64	0.143	4.41	0.0528	0.0210	81.0	8.30	19.18	0.736	0.855
		0.58	2.48	0.107	2.56	0.133	4.37	0.0514	0.0207	78.0	8.20	19.33	0.687	0.844
		0.52	2.35	0.102	2.44	0.120	4.33	0.0490	0.0202	74.0	8.00	19.56	0.619	0.840
		0.44	2.19	0.096	2.30	0.105	4.20	0.0456	0.0200	67.0	7.90	19.66	0.538	0.818
		0.41	2.15	0.093	2.23	0.100	4.10	0.0446	0.0205	64.0	7.90	19.42	0.485	0.845
		0.34	2.03	0.088	2.11	0.090	3.78	0.0425	0.0229	56.0	8.40	18.38	0.406	0.838
		0.28	1.94	0.082	1.97	0.0795	3.53	0.0394	0.0243	48.0	8.50	17.83	0.325	0.862
		0.25	1.84	0.079	1.895	0.0735	3.40	0.0383	0.0265	43.0	8.80	17.10	0.297	0.842

3.0%	1:24	0.13	1.55	0.067	1.61	0.0520	2.50	0.0321	0.0395	28.0	10.40	13.99	0.155	0.839
5.0%	1:12	1.42	2.20	0.184	2.21	0.202	7.04	0.0849	0.0221	231.0	9.11	24.18	1.68	0.846
		1.30	2.11	0.180	2.16	0.190	6.84	0.0830	0.0228	221.0	9.25	23.78	1.56	0.833
		1.20	2.05	0.177	2.12	0.181	6.62	0.0811	0.0238	209.0	9.41	23.26	1.48	0.811
		1.10	1.98	0.171	2.05	0.169	6.53	0.0785	0.0237	201.0	9.31	23.31	1.35	0.815
		1.00	1.89	0.163	1.95	0.154	6.52	0.0751	0.0227	192.0	9.08	23.82	1.22	0.818
		0.90	1.82	0.152	1.82	0.138	6.52	0.0700	0.0212	182.0	8.68	24.65	1.06	0.845
		0.80	1.73	0.140	1.71	0.121	6.60	0.0646	0.0191	167.0	8.12	25.97	0.910	0.879
		0.70	1.64	0.132	1.59	0.108	6.48	0.0610	0.0186	155.0	7.95	26.30	0.795	0.880
		0.60	1.56	0.127	1.52	0.0990	6.06	0.0586	0.0205	139.0	8.28	25.07	0.686	0.874
		0.50	1.45	0.119	1.43	0.0863	5.79	0.0550	0.0211	127.0	8.30	24.70	0.581	0.861
		0.394	1.35	0.111	1.33	0.0750	5.26	0.0515	0.0239	104.0	8.78	23.20	0.454	0.868
		0.30	1.21	0.096	1.15	0.0580	5.17	0.0442	0.0213	91.2	8.05	24.58	0.338	0.887
5.0%	1:12	0.20	1.05	0.081	0.97	0.0425	4.70	0.0376	0.0219	70.8	7.92	24.24	0.221	0.905
5.0%	1:96	0.0700	2.23	0.029	2.78	0.0324	2.16	0.0144	0.0397	12.63	9.13	17.97	0.097	0.722
		0.0625	2.14	0.028	2.68	0.0299	2.09	0.0138	0.0406	11.46	9.20	17.80	0.089	0.703
		0.0550	2.08	0.027	2.59	0.0281	1.96	0.0133	0.0445	10.34	9.53	17.01	0.078	0.705
		0.0475	1.92	0.026	2.49	0.0249	1.91	0.0128	0.0451	9.71	9.59	16.90	0.068	0.699
		0.0400	1.86	0.024	2.30	0.0223	1.79	0.0119	0.0477	8.56	9.70	16.43	0.057	0.704
		0.0318	1.72	0.022	2.11	0.0189	1.68	0.0109	0.0498	7.28	9.73	16.07	0.050	0.636
		0.0255	1.62	0.021	2.02	0.0170	1.50	0.0104	0.0594	6.22	10.58	14.72	0.042	0.610
		0.0185	1.49	0.020	1.92	0.0149	1.24	0.00986	0.0821	4.85	12.33	12.53	0.027	0.675
		0.0087	1.18	0.018	1.73	0.0106	0.82	0.00883	0.1690	2.88	17.33	8.73	0.014[+]	0.605
		0.0077	1.12	0.017	1.63	0.0095	0.81	0.00833	0.1635	2.70	16.82	8.87	0.013	0.593
5.0%	1:96	0.0032	0.80	0.013	1.25	0.00520	0.615	0.00641	0.2170	1.57	18.70	7.70	0.0057	0.561

If this is done, and the distribution again integrated, it is found that a certai portion of the total discrepancy between the theoretical and experimental flo rates can be accounted for. For example, in the intermediate configuratio $(\phi_o = 3\%,\ \theta_o = 1$ on 24, and $Q = 0.725$ cfs), N is only increased from 0.848 t 0.873 (N equal to unity being perfect agreement).

The fact that the friction factor in a rather complicated manner, in additio to the uncertainty of the value of the "equivalent diameter," probably account for the major portion of the discrepancy. However, as previously stated, th representation has the tremendous advantage of being simple and directly use able while being accurate to within about 85% for computing the true flow rat when integrated. The friction factor, for any given practical problem, woul probably be ascertained from the estimation of the physical condition of th channel itself and would be susceptible to any error of judgment. Hence, an refinement should be regarded in this light as it might not be consistent wit the method of selecting this factor.

R. W. Powell, F. ASCE and C. J. Posey, F. ASCE[9] have done some experi mental work that has some bearing on the preceding problem. They have in vestigated the variation of the friction factor in a symmetrical, triangular ope

TABLE 2.—COMPARISON OF FLOW RATES

Slopes		Q, (Manometer) in cubic feet per second	Q, (Pitot) in cubi feet per second
ϕ_o, in percentage	θ_o		
(1)	(2)	(3)	(4)
1.00	1:12	2.98	3.00
	1:12	0.50	0.49
	1:96	0.135	0.141
	1:96	0.045	0.060
3:00	1:24	0.725	0.759
	1:24	0.25	0.29
5.00	1:12	1.42	1.48
	1:12	0.394	0.436
	1:96	0.070	0.070
	1:96	0.0077	0.0153

channel for various slopes, configurations, flow rates, and roughnesses. The found, for flow at supercritical velocities in a smooth channel, the curve best fit lay above the smooth pipe curve (using d = 4 R). The Powell and Pose curve is seen in Fig. 15. Their curve is, generally speaking, consistent wit the experimental data taken in the present work.

To guarantee the avoidance of any gross errors in the measurement of velo cities, an internal check was used (as previously described herein). By graph ical integration of Figs. 10 through 14 (using a large scale), the flow rates fro Pitot measurements were determined. The results are given in Table 2. Th comparison is acceptable for the higher flow rates but not as satisfactory fo

9 "Resistance Experiments in a Triangular Channel," by R. W. Powell and C. Posey, Proceedings, ASCE, Vol. 85, No. HY 3, March, 1959.

the lower flows. This could result from the fact that the velocities were small in the latter case and somewhat more difficult to measure with the instrumentation available.

The main body of information is summarized in Table 1, as far as the important parameters and values are concerned. The Stanton diagram, discussed earlier, is given in Fig. 15 using the data shown in Table 1. In addition, other applicable information from the Corps of Engineers,[10] Larson,[11] and Powell and Posey,[12] is plotted. The resulting curves are seen to be of the expected general shape.

Range of Measurements.—A matrix of apparatus configurations was investigated. This information is most easily and clearly presented in a plot such as Fig. 16. The solid circles indicate that the measurements were taken for

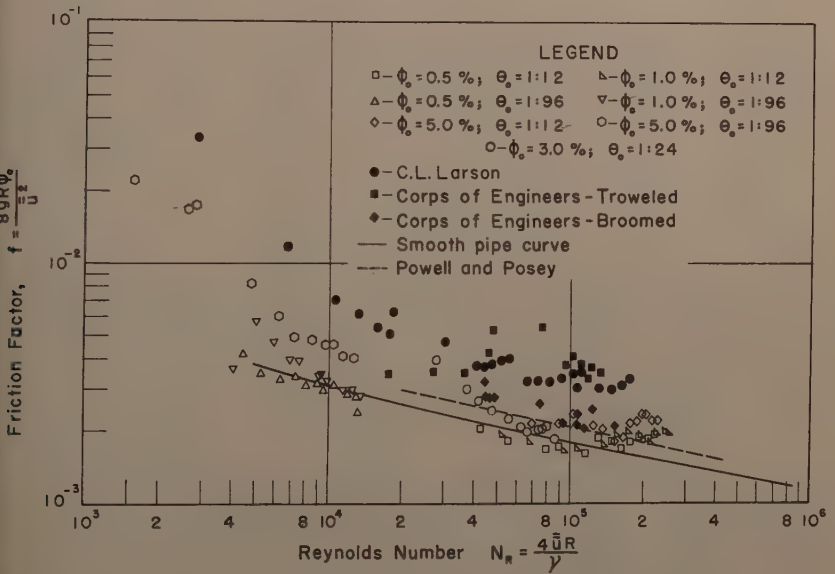

FIG. 15.—STANTON DIAGRAM

these arrangements. It is seen from this figure that the lower limit of flow at supercritical velocity possibly occurred between the longitudinal slopes of 1/2 and 1%. Ordinary hydraulic critical depth criteria were applied to obtain the critical slope, $(\phi_o)_{crit.}$. By using the expression that allows the calculation of

10 "Airfield Drainage Structure Investigation," U. S. Corps of Engrs., St. Paul Dist. Sub-Office, Hydr. Lab., Report No. 54, April, 1949.

11 "Transverse Distribution of Velocity and Quantity of Flow in a Shallow Triangular Channel," by C. L. Larson, thesis presented to the Univ. of Minnesota, at Minneapolis, Minn., in 1949, in partial fulfillment of the requirements for the degree of Master of Science.

12 "Resistance Experiments in a Triangular Channel," by R. W. Powell and C. J. Posey, Proceedings, ASCE, Vol. 85, No. HY 3, March, 1959, p. 31.

TABLE 3.—CRITICAL AND ACTUAL SLOPES

Measured Slopes		Flow Rate, Q, in cubic feet per second	Critical Slope $(\phi_o)_{crit}$, in percentage
ϕ_o, in percentage	θ_o		
(1)	(2)	(3)	(4)
0.50	1:12	2.95	0.229
		1.69	0.249
		0.50	0.294
	1:96	0.203	0.385
		0.134	0.405
		0.070	0.434
1.00	1:12	2.98	0.239
		1.69	0.260
		0.50	0.308
	1:96	0.135	0.427
		0.090	0.441
		0.045	0.469
3.00	1:24	0.725	0.325
		0.44	0.347
		0.25	0.369
5.00	1:12	1.42	0.293
		0.90	0.314
		0.394	0.344
	1:96	0.070	0.497
		0.040	0.525
		0.0077	0.561

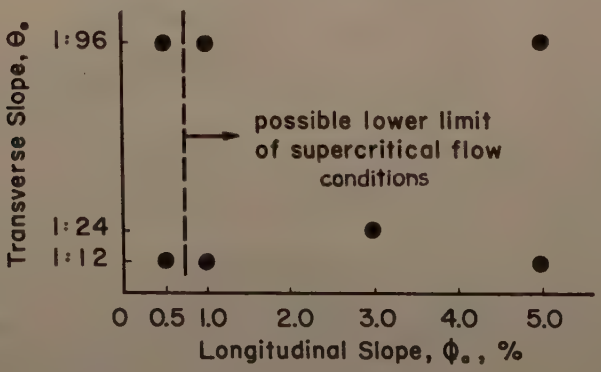

FIG. 16.—APPARATUS CONFIGURATIONS

critical depth in a non-rectangular channel[13]

$$\frac{Q^2}{g} = \frac{A^3}{y_o} \quad \ldots\ldots\ldots\ldots\ldots\ldots\ldots (7)$$

13 "Elementary Fluid Mechanics," by J. K. Vennard, John Wiley and Sons, Inc., New York, 1954.

in which A is the cross-sectional area of the flow, and by use of Manning's equation in the form

$$Q = \frac{1.49}{n} A R^{2/3} \phi_o^{1/2} \quad \ldots\ldots\ldots\ldots\ldots\ldots (8)$$

there is obtained,

$$(\phi_o)_{crit.} = \frac{n^2 g}{2 (1.49)^2} \frac{z_o}{\left[\frac{y_o z_o}{2 (y_o + z_o)}\right]^{4/3}} \quad \ldots\ldots\ldots\ldots\ldots\ldots (9)$$

By using a representative computed value for Manning's n of 0.009 for the surface of the channel (see Table 1), the various critical slopes were determined and compared with the actual slopes, as given in Table 3.

Although in all cases the critical slope, $(\phi_o)_{crit.}$, was less than the actual slope, ϕ_o, the former was quite near the latter for the 1/2% configuration, especially for the lower flow rates. Hence, a borderline situation was created that raised the suspicion that flow at subcritical conditions was occurring due to the lack of absolute certainty inherent in the previously noted critical depth and slope criteria.

CONCLUSIONS

Experimental velocity contours and transverse velocity distributions in a smooth, shallow, triangular open channel have been presented for uniform flow conditions for a wide variety of slopes and flows at supercritical velocities.

Velocity distributions were determined from graphical integration of velocity profiles. These were represented mathematically using other experimental results (Eqs. 4) and by a method based on Darcy's equation (Eq. 5). The latter seemed to describe the shape of the distribution for smooth channels more adequately.

It was shown that there was a fairly constant ratio of the measured flow rate to the semi-theoretical (Darcy) flow rate.

Although the surface was quite smooth, the fact that the friction factor and the Reynolds number plotted reasonably on the Stanton diagram (Fig. 15) indicated that the application of these results to rougher surfaces would probably be feasible.

ACKNOWLEDGMENTS

The writer is deeply indebted to John K. Vennard, M. ASCE and Byrne Perry under whose direction this research was conducted. Several stimulating discussions were held with Carl F. Izzard, F. ASCE, Chief, Division of Hydraulic Research, Bureau of Public Roads, who also provided much useful background information. The assistance of F. G. Baker, J. Duncan, R. L. Street, A. M. ASCE, and Y. Wang is also acknowledged. Financial support for this research was provided by the United States Department of Commerce, Bureau of Public Roads.

APPENDIX.—NOTATION

The following symbols, adopted for use in this paper, conform essentially with "American Standard Letter Symbols for Hydraulics" (ASA Z10.2-1942), prepared by a committee of the American Standards Association with Society representation, and approved by the Association in 1942:

A = the cross-sectional area of flow, in square feet;

C_1 = a coefficient defined by $\left(\frac{8\ g\ \phi_o}{f}\right)^{1/2}$, in square root of feet per second;

C_o, C'_o = experimental coefficients;

f = the Darcy friction factor;

g = the acceleration of gravity, in feet per second per second;

N = a ratio defined by measured flow rate to theoretical flow rate;

$\overline{N}$ = an average of several ratios defined above;

n = the coefficient in Manning's formula;

Q = the rate of flow, in cubic feet per second (cfs);

R = the hydraulic radius, in feet;

$\mathbf{R}$ = the Reynolds number;

u = the x-component of velocity (local), in feet per second;

$\overline{u}$ = the x-component of velocity (average in vertical), in feet per second;

$\overline{u}_{exp.max.}$ = the x-component of velocity (maximum experimental—average in vertical), in feet per second;

$\overline{\overline{u}}$ = the x-component of velocity (average of section), in feet per second;

x,y,z = the coordinate axes and distances measured parallel thereto;

y_o, z_o = maximum distances, in feet;

θ_o = the transverse slope;

ν = the kinematic viscosity of water, in square feet per second; and

ϕ_o = the longitudinal slope, in percent.

Journal of the
HYDRAULICS DIVISION
Proceedings of the American Society of Civil Engineers

AQUIFER TESTS ON PARTIALLY PENETRATING WELLS

By Mahdi S. Hantush[1]

SYNOPSIS

The theory of nonsteady flow toward artesian wells partially penetrating infinite nonleaky aquifers is used to outline methods for the determination of the formation coefficients as well as the thickness of the water-bearing formation. Applications of these methods are illustrated by analyzing data from ground-water basins in New Mexico.

INTRODUCTION

In analyzing nonsteady flow problems of partial penetration, the practice is to make use of complete penetration formulas with or without adjustments, depending on the nature of the flow system considered.[2] These adjustments, if used, are based on the steady-state solutions of partial penetration. Such procedures may give fair results if the aquifer penetrated is of small and known thickness, provided that the assumptions made in each case are obtained. However, in the case of thick aquifers or aquifers of unknown thicknesses, such procedures are inapplicable.

Methods for determining the hydraulic properties, as well as the thickness, of a water-bearing formation by using aquifer test data obtained from wells

Note.—Discussion open until February 1, 1962. To extend the closing date one month, a written request must be filed with the Executive Secretary, ASCE. This paper is part of the copyrighted Journal of the Hydraulics Division, Proceedings of the American Society of Civil Engineers, Vol. 87, No. HY 5, September, 1961.

[1] Senior Hydrologist and Prof. of Hydrol., New Mexico Inst. of Mining and Tech., Socorro, N. Mex.; on leave from the College of Engrg., Univ. of Baghdad, Baghdad, Iraq.

[2] "Engineering Hydrology," by S. S. Butler, Prentice-Hall, Inc., Englewood Cliffs, N. J., 1957.

that partially penetrate the formation are outlined herein. The procedures are based on the theory developed by the writer[3] for the nonsteady flow toward a steadily discharging well that penetrates an artesian aquifer of infinite areal extent.

Notation.—The letter symbols adopted for use in this paper are defined where they first appear, in the illustrations or in the text, and are arranged alphabetically, for convenience of reference, in the Appendix.

DRAWDOWN EQUATIONS

The equations that provide the drawdown distribution in and near partially penetrating artesian wells and that are useful in analyzing data from aquifer tests, will be presented. Details of other equations are available.[3]

Drawdown in Piezometers.—Piezometers are small-diameter pipes driven into an aquifer, so that entrance of water into the pipes is solely from the bot-

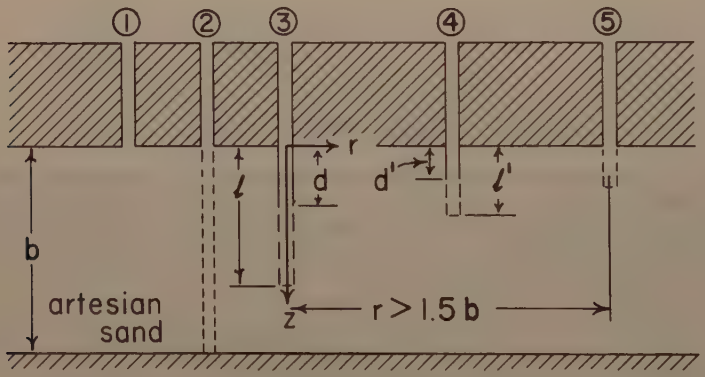

FIG. 1.—DIAGRAMMATIC REPRESENTATION OF PARTIALLY PENETRATING WELLS IN ARTESIAN AQUIFER

tom. The drawdown s in a piezometer having a depth of penetration z and being a distance r from the center of a pumped well that is screen between the depths d and l, and whose discharge Q is constant, is, for the case of a homogeneous, isotropic, and nonleaky elastic aquifer, infinite in areal extent and of uniform thickness b, as given below, and is valid only during the period of time specified. (See Fig. 1 for the coordinate system.)

For a relatively short period of pumping, the equation of drawdown for $t < \frac{(2b - l - z)^2 S_s}{20K}$ is

$$s = \frac{Q}{8 \pi K (l - d)} E\left(u, \frac{l}{r}, \frac{d}{r}, \frac{z}{r}\right) \quad \ldots\ldots\ldots\ldots (1)$$

3 "Drawdown Around a Partially Penetrating Well," by M. S. Hantush, Proceedings, ASCE, Vol. 87, No. HY 4, July, 1961.

in which

$$E = M\left[\frac{u,\ (l+z)}{r}\right] - M\left[\frac{u,\ (d+z)}{r}\right] + M\left[\frac{u,\ (l-z)}{r}\right] - M\left[\frac{u,\ (d-z)}{r}\right] \quad \ldots\ldots\ldots\ldots (2)$$

and

$$u = \left(\frac{r^2\ S_s}{4\ K\ t}\right) \quad \ldots\ldots\ldots\ldots\ldots\ldots\ldots (3)$$

t is the time since pumping started, S_s and K are the specific storage (volume of water released from storage in a unit volume of the aquifer under a unit head decline, of dimension L^{-1}) and the hydraulic conductivity of the aquifer, respectively, and M (u, β) denotes an infinite integral (see list of symbols), sufficient values of which have been tabulated[3] for a practical range of the parameters involved. A more detailed table of this function is available.[4]

Depending on the geometry of the flow system, Eq. 1 may take the form

$$s = c\ M\ (u,\ \beta) \quad \ldots\ldots\ldots\ldots\ldots\ldots (4)$$

in which case the equation is valid for $t < \left[\frac{(2b = r\beta)^2\ S_s}{20\ K}\right]$, c and β being constants that depend on the parameters of the flow system under consideration. For example, if the pumped well is screened throughout its depth of penetration (d = 0), and if the piezometer is of a penetration depth equal to that of the pumped well (z = l), Eq. 1 will reduce to

$$s = \frac{Q}{8\ \pi\ K\ l}\ M\left(u,\ \frac{2\ l}{r}\right) \quad \ldots\ldots\ldots\ldots\ldots (5a)$$

If, on the other hand, the piezometer is of zero penetration (z = 0), the drawdown equation becomes

$$s = \frac{Q}{4\ \pi\ K\ l}\ M\left(u,\ \frac{l}{r}\right) \quad \ldots\ldots\ldots\ldots\ldots (5b)$$

Another example is that of a flow system in which l = 3d and z = d, in which case the equation of drawdown is

$$s = \frac{3\ Q}{16\ \pi\ K\ l}\ M\left(u,\ \frac{4\ l}{3\ r}\right) \quad \ldots\ldots\ldots\ldots\ldots (5c)$$

For relatively long periods of pumping, the equation of drawdown for $t > \frac{(b^2\ S_s)}{2K}$ has been shown to[5] be

$$s = \frac{Q}{4\ \pi\ K\ b}\left\{W\ (u) + f_s\left(\frac{r}{b},\ \frac{l}{b},\ \frac{d}{b},\ \frac{z}{b}\right)\right\} \quad \ldots\ldots\ldots\ldots (6)$$

---

4 Professional Paper 102, Research Div., New Mexico Inst. of Mining and Tech., Socorro, N. Mex.

5 "Nonsteady Flow to a Well Partially Penetrating an Infinite Leaky Aquifer," by M. S. Hantush, Proceedings, Iraqi Scientific Soc., 1957, p. 10; also reprinted by New Mexico Inst. of Mining and Tech., Socorro, N. Mex.

in which

$$f_s = \frac{4b}{\pi (l - d)} \sum_{n=1}^{\infty} \left(\frac{1}{n}\right) K_o \left(\frac{n \pi r}{b}\right) \cos \left(\frac{n \pi z}{b}\right) \left[\sin \left(\frac{n \pi l}{b}\right) - \sin \left(\frac{n \pi d}{b}\right) \right] \quad \ldots\ldots\ldots\ldots\ldots (7)$$

K_o is the zero-order modified Bessel function of the second kind, and W (u) is the well function for nonleaky aquifers, or what in the mathematical literature is known as the negative exponential integral of (-u). The function is available in tabular form.[6]

Drawdown in Observation Wells.—Unlike a piezometer that registers the drawdown at a point in the aquifer, an observation well screened in the aquifer will reflect the average drawdown in the aquifer profile that is in contact with the well screen (or perforated casing). For an observation well that is screened between the depths d' and l' the required equations are as follows:

An approximate equation of average drawdown for $t < \dfrac{\left[2b - \left(\frac{1}{2}\right)(2l + l' + d')\right]^2 S_s}{20\ K}$ that gives results sufficiently accurate for practical application, provided that $(l'/l) < 2$ is

$$\bar{s} \approx \frac{Q}{8 \pi K (l - d)} \bar{E} \left(u, \frac{l}{r}, \frac{d}{r}, \frac{l'}{r}, \frac{d'}{r}\right) \quad \ldots\ldots\ldots\ldots (8)$$

in which $\bar{s}$ is the average drawdown in the observation well and $\bar{E}$ is the value of the function E of Eq. 1, in which the value of z is replaced by $(l' + d')/2$. An exact solution is available.[3]

If $(r/l) > 1$ and $(l'/l) < 1$, the average drawdown in the observation well can, for all practical purposes, be taken as that given by Eq. 1, with the value of z arbitrarily chosen between l' and zero. The choice is generally made so as to simplify the equation which, in certain cases, may take the form of Eq. 2 and which is valid in the same time interval as that of the latter. The simplified equation would have the form

$$\bar{s} \approx c\ M\ (u, \beta) \quad \ldots\ldots\ldots\ldots\ldots\ldots (9)$$

For example, if $l = 3\ d$, a choice of $z = d$ will reduce Eq. 1 to Eq. 5c. Also, if $d = 0$, a choice of $z = 0$ will result in Eq. 5b, whereas a choice of $z = l$ gives Eq. 5a. All these equations are of the type of Eq. 9.

For a relatively long period of pumping, the equation of average drawdown for $t > \left(\dfrac{b^2 S_s}{2K}\right)$ is

$$\bar{s} = \frac{Q}{4 \pi K b} \left\{ W (u) + \bar{f}_s \left(\frac{r}{b}, \frac{l}{b}, \frac{d}{b}, \frac{l'}{b}, \frac{d'}{b}\right) \right\} \quad \ldots\ldots\ldots (10)$$

---

6 "Methods for Determining Permeability of Water-Bearing Materials," by L. K. Wenzel, U. S. Geol. Survey, Water-Supply Paper No. 887, 1942, p. 88; also "Hydrology," by C. O. Wisler and E. F. Brater, John Wiley and Sons, New York, N. Y., 1951.

in which

$$\overline{f_s} = \frac{4\,b^2}{\pi^2\,(l - d)\,(l' - d')} \sum_{n=1}^{\infty} \left(\frac{1}{n^2}\right) K_o\left(\frac{n\,\pi\,r}{b}\right)$$

$$\left[\sin\left(\frac{n\,\pi\,l}{b}\right) - \sin\left(\frac{n\,\pi\,d}{b}\right)\right]\left[\sin\left(\frac{n\,\pi\,l'}{b}\right) - \sin\left(\frac{n\,\pi\,d'}{b}\right)\right] \ldots\ldots (11)$$

Eq. 11, as well as Eq. 6, shows that in this range of time, the rate of change of drawdown is the same as though the pumped well completely penetrated the

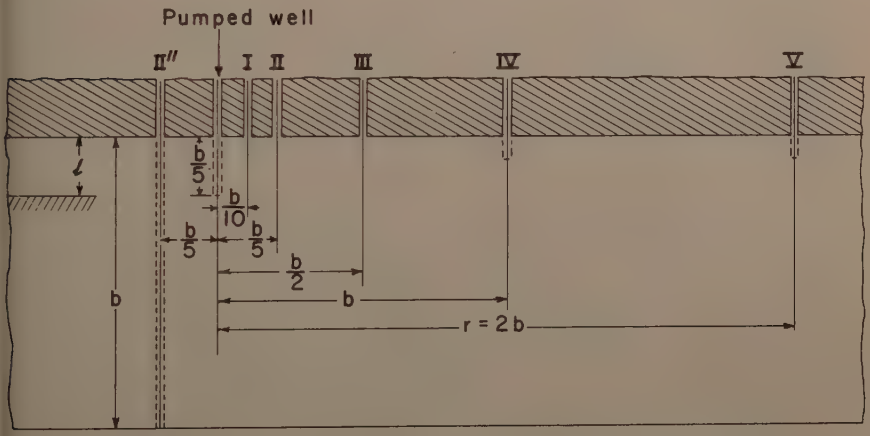

FIG. 2.—DIAGRAMMATIC REPRESENTATION OF PARTIALLY PENETRATING WELLS

aquifer. In other words, the effect of partial penetration on the drawdown has attained its maximum value.

Drawdown in Piezometers or Wells for (r/b) > 1.5.—For relatively large distances, that is (r/b) > 1.5, the equation of drawdown has been shown[7] to be

$$s = \frac{Q}{4\,\pi\,K\,b}\,W\,(u) \ldots\ldots\ldots\ldots\ldots (12)$$

In fact, Eq. 12 gives results sufficiently accurate for practical purposes even for (r/b) as small as one, provided $u < 0.1\,(r/b)^2$. The equation is the same as it would be if the pumped well completely penetrated the aquifer (Theis formula).[8]

---

7 "Nonsteady Flow to a Well Partially Penetrating an Infinite Leaky Aquifer," by M. S. Hantush, Proceedings, Iraqi Scientific Soc., 1957, p. 10; also reprinted by New Mexico Inst. of Mining and Tech., Socorro, N. Mex.

8 "Groundwater Hydrology," by David K. Todd, John Wiley and Sons, Inc., New York, 1959, p. 90; also "Arid Zone Hydrology Recent Developments" by H. Schoeller, UNESCO, Paris, France, 1959, p. 37.

Drawdown in the Pumping Well.—The equations of drawdown that have been presented in the previous sections are derived on the assumption that the flux entering the pumped well is uniformly distributed along the water entry face of the well. Theoretically speaking the hydraulic head, rather than the flux, along the face just outside of the pumped well screen should be uniform. This uniform head distribution can be achieved by a lengthy process involving the distribution of varying flux elements along the well axis. The drawdown at points not in the immediate vicinity of the pumped well, obtained by the simpler equations that are based on a uniform flux across the well screen, does not deviate appreciably from that obtained by the assumedly more exact, but lengthy process. In the actual problem neither a uniform flux nor a uniform head is really conceived along the face of the well, due to several involved field and operational conditions. The drawdown, in this case, will have a value between the two theoretical extremes. Thus, each of the two theoretical expressions can be used to very closely represent the actual case. The simpler equations are, of course, more appealing.

The theoretical drawdown equations, derived on the assumption of uniform flux along the well screen, will obviously give a variable head distribution along the face of the pumped well. It has been shown,[9] however, that the maximum drawdown (least hydraulic head) at the face of the well that these equations give, is very closely equal to that which obtains if the hydraulic head along the face of the well is maintained uniform. The point along the face of the well at which the least hydraulic head occurs depends on the space position of the well screen. If the well is screened throughout its depth of penetration, the least head takes place at the top of the aquifer ($z = 0$). If, on the other hand, the well completely penetrates the aquifer and only its lower part is screened, the least head occurs at the bottom of the aquifer ($z = b$). But if the well is screened between the depths d and l, the least head develops at a depth somewhere between l and d, being closer to d if most of the well screen is in the upper half of the aquifer, and closer to l if the reverse is true. Computation in the drawdown equation shows, however, that the value of maximum drawdown does not differ appreciably from that obtained for $z = (1/2)(l + d)$. Consequently, if so-called well losses are excluded, the water level in a pumping well can be calculated from the equations of drawdown in piezometers (presented in the previous sections) by substituting therein r_w for r, and the value of z at which the least hydraulic head takes place, r_w being the effective radius of the well.

PROPERTIES OF DRAWDOWN EQUATIONS

Some characteristic features of the drawdown equations that are of importance in graphical computations for the formation coefficients will be given.

Equations for Special Cases.—Equations of drawdown in piezometers or observation wells that, during relatively short periods of pumping $\left(t < \left[(2b - r\beta)^2 S_s / 20K\right]\right)$, are of the type of Eq. 4 or Eq. 9, are here called "equations for special cases." Fig. 3 gives theoretical graphs of drawdown versus the

---

[9] "The Flow of Homogeneous Fluids Through Porous Media," by M. Muskat, McGraw-Hill Book Co., Inc., New York, N. Y., 1937; or J. W. Edwards, Inc., Ann Arbor, Mich. 1946.

logarithm of time for such equations. These graphs have the following properties:

1. In the period $t < \left[(r\,\beta)^2\, S_s/20K\right]$, the drawdown is given by

$$s = c\, W(u) \quad \ldots\ldots\ldots\ldots\ldots\ldots\ldots\ldots (13)$$

This follows from the value of the function M (u, β) for large values of u; that is, small values of time [the approximation of M (u, β) has been presented by the writer[3]].

Eq. 13 indicates that in the initial period of pumping, the flow behaves as though the aquifer ended at the bottom of the pumping well. This is shown by the dashed curves of Fig. 3 (I' and II'), that give the time-drawdown variation for wells I and II, respectively, if the aquifer is assumed to end at the bottom of the pumped well. Except for the pair of curves I and I', in the example of Fig. 3 (prepared for assumed values of the parameters), the other pairs (II and

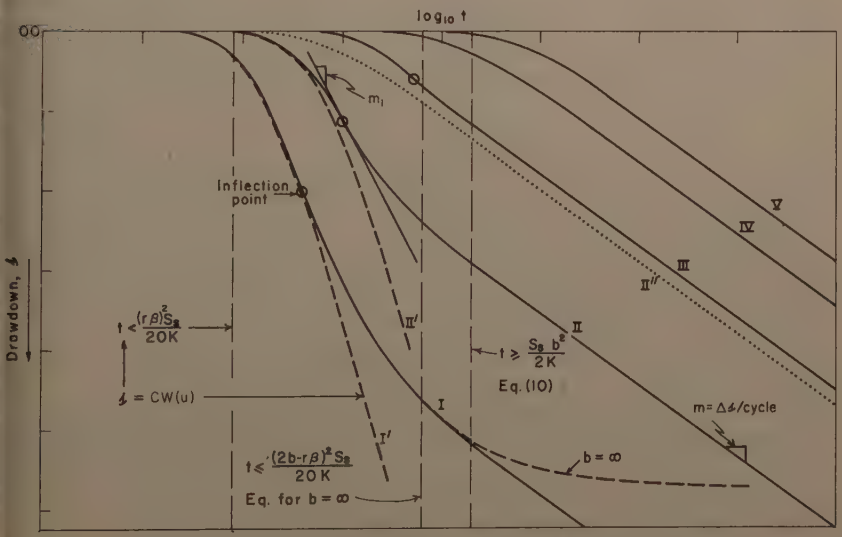

FIG. 3.—TIME-DRAWDOWN VARIATION DUE TO A STEADY WELL PARTIALLY PENETRATING AN ARTESIAN AQUIFER

I', and others not shown) fall outside the period mentioned above for any measurable drawdown. The curves of each pair deviate from each other, although the general trend of variation prior to the formation of the inflection point appears to be the same, the deviation being greater for larger distances from the pumped well.

2. In general, the curves have an inflection point that develops within the period $t < \left[(2\,b - r\,\beta)^2\, S_s/20K\right]$. This point is located by the relation

$$\frac{\beta^2}{\sqrt{\pi}} = f(x)$$

$$= x\, e^{x^2}\, \mathrm{erf}(x) \quad \ldots\ldots\ldots\ldots\ldots\ldots\ldots (14)$$

TABLE 1.—VALUES OF THE FUNCTION erf(x) & f(x) = xe^{x^2} erf(x)

x	erf(x)	f(x)	x	erf(x)	f(x)	x	erf(x)	f(x)	x	erf(x)	f(x)	x	erf(x)	f(x)	x	erf(x)	f(x)
0.005	0.0056	282(-7)	0.505	0.5249	0.34207	1.005	0.8448	2.3078	1.505	0.9667	14.012	2.005	0.9954	111.7	2.505	0.9996	1310.0
0.010	0.0113	113(-6)	0.510	0.5292	0.35007	1.010	0.8468	2.3721	1.510	0.9673	14.282	2.010	0.9955	113.72	2.510	0.9996	1346.5
0.015	0.0169	254(-6)	0.515	0.5336	0.35825	1.015	0.8488	2.4138	1.515	0.9679	14.554	2.015	0.9956	115.33	2.515	0.9996	1404.0
0.020	0.0226	451(-6)	0.520	0.5379	0.36656	1.020	0.8508	2.4811	1.520	0.9684	14.835	2.020	0.9957	119.01	2.520	0.9996	1442.7
0.025	0.0282	705(-6)	0.525	0.5422	0.37497	1.025	0.8528	2.4995	1.525	0.9690	15.121	2.025	0.9958	121.75	2.525	0.9996	1482.5
0.030	0.0338	0.00102	0.530	0.5465	0.38357	1.030	0.8548	2.5435	1.530	0.9695	15.414	2.030	0.9959	124.57	2.530	0.9997	1523.5
0.035	0.0395	0.00138	0.535	0.5507	0.39227	1.035	0.8567	2.5882	1.535	0.9701	15.711	2.035	0.9960	127.45	2.535	0.9997	1565.7
0.040	0.0451	0.00181	0.540	0.5549	0.40114	1.040	0.8587	2.6338	1.540	0.9706	16.015	2.040	0.9961	130.40	2.540	0.9997	1609.1
0.045	0.0507	0.00204	0.545	0.5591	0.41011	1.045	0.8606	2.6800	1.545	0.9712	16.326	2.045	0.9962	133.43	2.545	0.9997	1653.8
0.050	0.0564	0.00283	0.550	0.5633	0.41929	1.050	0.8624	2.7264	1.550	0.9716	16.642	2.050	0.9963	136.54	2.550	0.9997	1699.8
0.055	0.0620	0.00342	0.555	0.5675	0.42855	1.055	0.8643	2.7752	1.555	0.9721	16.965	2.055	0.9963	139.72	2.555	0.9997	1747.2
0.060	0.0676	0.00407	0.560	0.5716	0.43801	1.060	0.8661	2.8240	1.560	0.9726	17.297	2.060	0.9964	142.98	2.560	0.9997	1796.0
0.065	0.0732	0.00478	0.565	0.5757	0.44763	1.065	0.8680	2.8737	1.565	0.9731	17.634	2.065	0.9965	146.32	2.565	0.9997	1846.2
0.070	0.0789	0.00558	0.570	0.5798	0.45738	1.070	0.8698	2.9242	1.570	0.9736	17.979	2.070	0.9966	149.76	2.570	0.9997	1897.9
0.075	0.0845	0.00637	0.575	0.5839	0.46727	1.075	0.8716	2.9756	1.575	0.9741	18.330	2.075	0.9967	153.27	2.575	0.9997	1951.2
0.080	0.0901	0.00725	0.580	0.5879	0.47735	1.080	0.8733	3.0280	1.580	0.9746	18.691	2.080	0.9967	156.88	2.580	0.9997	2006.0
0.085	0.0957	0.00819	0.585	0.5919	0.48760	1.085	0.8751	3.0813	1.585	0.9750	19.058	2.085	0.9968	160.58	2.585	0.9998	2062.5
0.090	0.1013	0.00919	0.590	0.5959	0.49797	1.090	0.8768	3.1355	1.590	0.9755	19.433	2.090	0.9969	164.37	2.590	0.9998	2120.7
0.095	0.1069	0.01024	0.595	0.5999	0.50858	1.095	0.8785	3.1907	1.595	0.9759	19.815	2.095	0.9970	168.26	2.595	0.9998	2180.6
0.100	0.1125	0.01136	0.600	0.6039	0.51931	1.100	0.8802	3.2470	1.600	0.9764	20.208	2.100	0.9970	172.25	2.600	0.9998	2242.3
0.105	0.1181	0.01253	0.605	0.6078	0.53023	1.105	0.8819	3.3041	1.605	0.9768	20.606	2.105	0.9971	176.34	2.605	0.9998	2305.9
0.110	0.1236	0.01384	0.610	0.6117	0.54132	1.110	0.8835	3.3623	1.610	0.9772	21.015	2.110	0.9972	180.54	2.610	0.9998	2371.4
0.115	0.1292	0.01505	0.615	0.6156	0.55260	1.115	0.8852	3.4215	1.615	0.9776	21.433	2.115	0.9972	184.84	2.615	0.9998	2438.8
0.120	0.1348	0.01640	0.620	0.6194	0.56402	1.120	0.8868	3.4819	1.620	0.9780	21.860	2.120	0.9973	189.25	2.620	0.9998	2508.3
0.125	0.1403	0.01782	0.625	0.6232	0.57568	1.125	0.8884	3.5432	1.625	0.9784	22.293	2.125	0.9973	193.78	2.625	0.9998	2579.9
0.130	0.1459	0.01928	0.630	0.6270	0.58754	1.130	0.8900	3.6058	1.630	0.9788	22.739	2.130	0.9974	198.43	2.630	0.9998	2653.6
0.135	0.1514	0.02082	0.635	0.6308	0.59950	1.135	0.8915	3.6693	1.635	0.9792	23.193	2.135	0.9975	203.17	2.635	0.9998	2713.8
0.140	0.1570	0.02241	0.640	0.6346	0.61173	1.140	0.8931	3.7342	1.640	0.9796	23.658	2.140	0.9975	208.08	2.640	0.9998	2807.8
0.145	0.1625	0.02406	0.645	0.6383	0.62412	1.145	0.8946	3.8002	1.645	0.9800	24.132	2.145	0.9976	213.09	2.645	0.9998	2888.5
0.150	0.1680	0.02577	0.650	0.6420	0.63675	1.150	0.8961	3.8674	1.650	0.9804	24.618	2.150	0.9976	218.24	2.650	0.9998	2971.6
0.155	0.1735	0.02755	0.655	0.6457	0.64952	1.155	0.8976	3.9357	1.655	0.9808	25.113	2.155	0.9977	223.52	2.655	0.9998	3057.3
0.160	0.1790	0.02938	0.660	0.6494	0.66256	1.160	0.8991	4.0055	1.660	0.9811	25.619	2.160	0.9978	228.94	2.660	0.9998	3145.5
0.165	0.1845	0.03128	0.665	0.6530	0.67574	1.165	0.9005	4.0763	1.665	0.9815	26.137	2.165	0.9978	234.49	2.665	0.9998	3236.5
0.170	0.1900	0.03325	0.670	0.6566	0.68921	1.170	0.9020	4.1485	1.670	0.9818	26.666	2.170	0.9979	240.20	2.670	0.9998	3330.2
0.175	0.1955	0.03527	0.675	0.6602	0.70288	1.175	0.9034	4.2220	1.675	0.9822	27.205	2.175	0.9979	246.05	2.675	0.9999	3426.9
0.180	0.2009	0.03736	0.680	0.6638	0.71669	1.180	0.9048	4.2970	1.680	0.9825	27.758	2.180	0.9980	252.06	2.680	0.9999	3526.5
0.185	0.2064	0.03951	0.685	0.6673	0.73079	1.185	0.9062	4.3732	1.685	0.9828	28.322	2.185	0.9980	258.22	2.685	0.9999	3629.1
0.190	0.2118	0.04171	0.690	0.6708	0.74514	1.190	0.9076	4.4509	1.690	0.9832	29.900	2.190	0.9981	264.55	2.690	0.9999	3734.9
0.195	0.2173	0.04401	0.695	0.6743	0.75985	1.195	0.9090	4.5300	1.695	0.9835	29.489	2.195	0.9981	271.04	2.695	0.9999	3844.0
0.200	0.2227	0.04637	0.700	0.6778	0.77486	1.200	0.9103	4.6104	1.700	0.9838	30.092	2.200	0.9981	277.71	2.700	0.9999	3956.5
0.205	0.2281	0.04877	0.705	0.6813	0.78949	1.205	0.9116	4.6925	1.705	0.9841	30.709	2.205	0.9982	284.55	2.705	0.9999	4072.4
0.210	0.2335	0.05125	0.710	0.6847	0.80477	1.210	0.9127	4.7768	1.710	0.9844	31.340	2.210	0.9982	291.58	2.710	0.9999	4191.9
0.215	0.2389	0.05380	0.715	0.6881	0.82025	1.215	0.9143	4.8611	1.715	0.9847	31.983	2.215	0.9983	298.78	2.715	0.9999	4315.1
0.220	0.2443	0.05642	0.720	0.6914	0.83606	1.220	0.9155	4.9481	1.720	0.9850	32.642	2.220	0.9983	306.19	2.720	0.9999	4442.2
0.225	0.2497	0.05909	0.725	0.6948	0.85203	1.225	0.9168	5.0365	1.725	0.9853	33.315	2.225	0.9984	313.78	2.725	0.9999	4573.2
0.230	0.2550	0.06183	0.730	0.6981	0.86827	1.230	0.9181	5.1261	1.730	0.9856	34.004	2.230	0.9984	321.59	2.730	0.9999	4708.3
0.235	0.2604	0.06466	0.735	0.7014	0.88480	1.235	0.9193	5.2180	1.735	0.9859	34.707	2.235	0.9984	330.12	2.735	0.9999	4847.6
0.240	0.2657	0.06757	0.740	0.7047	0.90166	1.240	0.9205	5.3115	1.740	0.9861	35.429	2.240	0.9985	337.82	2.740	0.9999	4991.2
0.245	0.2710	0.07050	0.745	0.7079	0.91869	1.245	0.9217	5.4060	1.745	0.9864	36.164	2.245	0.9985	346.27	2.745	0.9999	5139.4
0.250	0.2763	0.07354	0.750	0.7112	0.93612	1.250	0.9229	5.5033	1.750	0.9867	36.918	2.250	0.9985	354.94	2.750	0.9999	5292.2
0.255	0.2816	0.07664	0.755	0.7144	0.95372	1.255	0.9241	5.6026	1.755	0.9870	37.688	2.255	0.9986	363.85			
0.260	0.2869	0.07981	0.760	0.7175	0.97161	1.260	0.9252	5.7031	1.760	0.9872	38.476	2.260	0.9986	373.51			
0.265	0.2922	0.08305	0.765	0.7207	0.98985	1.265	0.9264	5.8055	1.765	0.9874	39.279	2.265	0.9986	382.38			
0.270	0.2974	0.08637	0.770	0.7238	1.0081	1.270	0.9275	5.9103	1.770	0.9877	40.105	2.270	0.9987	392.03			
0.275	0.3026	0.08976	0.775	0.7269	1.0267	1.275	0.9286	6.0159	1.775	0.9879	40.946	2.275	0.9987	401.96			
0.280	0.3078	0.09324	0.780	0.7300	1.0464	1.280	0.9297	6.1252	1.780	0.9882	41.809	2.280	0.9987	412.12			
0.285	0.3131	0.09678	0.785	0.7331	1.0657	1.285	0.9308	6.2353	1.785	0.9884	42.689	2.285	0.9988	422.57			
0.290	0.3183	0.10039	0.790	0.7361	1.0855	1.290	0.9319	6.3481	1.790	0.9886	43.593	2.290	0.9988	433.30			
0.295	0.3235	0.10409	0.795	0.7391	1.1055	1.295	0.9330	6.4626	1.795	0.9889	44.514	2.295	0.9988	444.33			
0.300	0.3286	0.10788	0.800	0.7421	1.1259	1.300	0.9340	6.5798	1.800	0.9891	45.460	2.300	0.9989	455.66			
0.305	0.3338	0.11173	0.805	0.7451	1.1466	1.305	0.9350	6.6991	1.805	0.9893	46.423	2.305	0.9989	467.31			
0.310	0.3389	0.11566	0.810	0.7481	1.1677	1.310	0.9360	6.8211	1.810	0.9895	47.413	2.310	0.9989	479.26			
0.315	0.3440	0.11967	0.815	0.7509	1.1891	1.315	0.9371	6.9452	1.815	0.9897	48.422	2.315	0.9989	491.55			
0.320	0.3491	0.12376	0.820	0.7538	1.2108	1.320	0.9381	7.0717	1.820	0.9899	49.458	2.320	0.9990	504.18			
0.325	0.3542	0.12794	0.825	0.7567	1.2330	1.325	0.9391	7.1999	1.825	0.9901	50.514	2.325	0.9990	517.15			
0.330	0.3593	0.13221	0.830	0.7595	1.2554	1.330	0.9400	7.3318	1.830	0.9904	51.600	2.330	0.9990	530.48			
0.335	0.3643	0.13654	0.835	0.7623	1.2783	1.335	0.9410	7.4658	1.835	0.9906	52.706	2.335	0.9990	544.17			
0.340	0.3694	0.14098	0.840	0.7651	1.3015	1.340	0.9419	7.6015	1.840	0.9907	53.843	2.340	0.9991	558.25			
0.345	0.3744	0.14549	0.845	0.7679	1.3251	1.345	0.9428	7.7406	1.845	0.9909	55.002	2.345	0.9991	572.71			
0.350	0.3794	0.15009	0.850	0.7707	1.3492	1.350	0.9438	7.8827	1.850	0.9911	56.191	2.350	0.9991	590.53			
0.355	0.3844	0.15477	0.855	0.7734	1.3722	1.355	0.9447	8.0271	1.855	0.9913	57.405	2.355	0.9991	602.86			
0.360	0.3893	0.15956	0.860	0.7761	1.3970	1.360	0.9456	8.1751	1.860	0.9915	58.651	2.360	0.9992	618.56			
0.365	0.3943	0.16441	0.865	0.7788	1.4236	1.365	0.9464	8.3252	1.865	0.9917	59.924	2.365	0.9992	634.71			
0.370	0.3992	0.16938	0.870	0.7814	1.4492	1.370	0.9473	8.4790	1.870	0.9918	61.229	2.370	0.9992	651.30			
0.375	0.4041	0.17443	0.875	0.7841	1.4753	1.375	0.9482	8.6349	1.875	0.9920	62.563	2.375	0.9992	668.36			
0.380	0.4090	0.17956	0.880	0.7867	1.5018	1.380	0.9490	8.7941	1.880	0.9922	63.931	2.380	0.9992	685.90			
0.385	0.4139	0.18479	0.885	0.7893	1.5286	1.385	0.9499	8.9567	1.885	0.9923	65.328	2.385	0.9993	703.92			
0.390	0.4187	0.19014	0.890	0.7918	1.5561	1.390	0.9507	9.1228	1.890	0.9925	66.762	2.390	0.9993	722.46			
0.395	0.4236	0.19556	0.895	0.7944	1.5839	1.395	0.9515	9.2925	1.895	0.9926	68.226	2.395	0.9993	741.51			
0.400	0.4284	0.20109	0.900	0.7969	1.6122	1.400	0.9523	9.4645	1.900	0.9928	69.729	2.400	0.9993	761.12			
0.405	0.4332	0.20671	0.905	0.7994	1.6410	1.405	0.9531	9.6399	1.905	0.9929	71.264	2.405	0.9993	781.25			
0.410	0.4380	0.21243	0.910	0.8019	1.6702	1.410	0.9539	9.8203	1.910	0.9931	72.841	2.410	0.9994	801.96			
0.415	0.4427	0.21826	0.915	0.8043	1.7000	1.415	0.9546	10.003	1.915	0.9932	74.450	2.415	0.9994	823.27			
0.420	0.4475	0.22419	0.920	0.8068	1.7303	1.420	0.9554	10.190	1.920	0.9934	76.103	2.420	0.9994	845.17			
0.425	0.4522	0.23021	0.925	0.8092	1.7611	1.425	0.9561	10.380	1.925	0.9935	77.791	2.425	0.9994	867.70			
0.430	0.4569	0.23636	0.930	0.8116	1.7924	1.430	0.9569	10.575	1.930	0.9937	79.524	2.430	0.9994	890.86			
0.435	0.4616	0.24259	0.935	0.8139	1.8242	1.435	0.9576	10.773	1.935	0.9938	81.295	2.435	0.9994	914.60			
0.440	0.4662	0.24896	0.940	0.8163	1.8565	1.440	0.9583	10.976	1.940	0.9939	83.112	2.440	0.9994	939.20			
0.445	0.4709	0.25542	0.945	0.8186	1.8894	1.445	0.9590	11.182	1.945	0.9941	84.970	2.445	0.9995	964.41			
0.450	0.4755	0.26201	0.950	0.8209	1.9229	1.450	0.9597	11.393	1.950	0.9942	86.916	2.450	0.9995	990.34			
0.455	0.4801	0.26868	0.955	0.8232	1.9569	1.455	0.9604	11.606	1.955	0.9943	88.827	2.455	0.9995	1017.0			
0.460	0.4847	0.27546	0.960	0.8254	1.9915	1.460	0.9611	11.826	1.960	0.9944	90.828	2.460	0.9995	1044.5			
0.465	0.4892	0.28237	0.965	0.8277	2.0267	1.465	0.9617	12.050	1.965	0.9946	92.873	2.465	0.9995	1072.7			
0.470	0.4938	0.28943	0.970	0.8299	2.0625	1.470	0.9624	12.278	1.970	0.9947	94.972	2.470	0.9995	1101.7			
0.475	0.4983	0.29658	0.975	0.8321	2.0990	1.475	0.9630	12.510	1.975	0.9948	97.118	2.475	0.9995	1131.6			
0.480	0.5028	0.30385	0.980	0.8342	2.1360	1.480	0.9637	12.748	1.980	0.9949	99.322	2.480	0.9996	1162.3			
0.485	0.5072	0.31124	0.985	0.8368	2.1748	1.485	0.9643	12.990	1.985	0.9950	101.58	2.485	0.9996	1194.0			
0.490	0.5117	0.31874	0.990	0.8385	2.2121	1.490	0.9649	13.238	1.990	0.9951	103.89	2.490	0.9996	1226.5			
0.495	0.5161	0.32638	0.995	0.8406	2.2509	1.495	0.9655	13.490	1.995	0.9952	106.26	2.495	0.9996	1260.0			
0.500	0.5205	0.33416	1.000	0.8427	2.2907	1.500	0.9661	13.750	2.000	0.9953	108.69	2.500	0.9996	1294.5			

n which

$$x = \beta\sqrt{u_i},\ u_i = \left(\frac{r^2 S_s}{4 K t_i}\right) \quad \ldots\ldots\ldots\ldots\ldots (15)$$

nd t_i is the value of t at the inflection point. The function f(x) is given in Table 1 for a wide range of x.

The drawdown s_i at the inflection point is given by

$$s_i = c M (u_i, \beta) \quad \ldots\ldots\ldots\ldots\ldots (16)$$

nd the slope m_i of the curve at that point is

$$m_i = \frac{\Delta s}{\text{cycle}} = 2.3\ c\ e^{-u_i}\ \text{erf}(x) \quad \ldots\ldots\ldots (17)$$

Eq. 14 is obtained by equating to zero the second derivative of Eq. 4 with respect to $\log_{10} t$, and Eq. 16 is obtained from Eq. 4 by substituting u_i for u. After obtaining the first derivative of Eq. 4 with respect to $\log_{10} t$, u_i is substituted for u to obtain Eq. 17.

3. The drawdown curves depart from those that obtain for an infinitely thick aquifer (as described completely by Eq. 4) at an approximate value of t or u given, respectively, by

$$t_d = \frac{(2 b - r \beta)^2 S_s}{20 K} \quad \ldots\ldots\ldots\ldots\ldots (18a)$$

nd

$$\frac{1}{u_d} = \frac{(2 b - r \beta)^2}{5 r^2} \quad \ldots\ldots\ldots\ldots\ldots (18b)$$

n which t_d and u_d are, respectively, the values of t and u at the point of departure.

4. The inflection of the curves is clearly defined for small values of (r/b). epending on the geometry of the flow system, the inflection disappears (see urves IV and V, Fig. 3) for

$$\left[\frac{x^2 (2 b - r \beta)^2}{5 (r \beta)^2}\right] \leq 1 \quad \ldots\ldots\ldots\ldots\ldots (19)$$

n which x and β are the parameters of Eq. 14. Eq. 19 is obtained by noting that he inflection occurs only if

$$t_i < \left[\frac{(2 b - r \beta)^2 S_s}{20 K}\right] \quad \ldots\ldots\ldots\ldots\ldots (20)$$

5. Regardless of the location of the wells, the curves are straight lines having the same slope at relatively large values of time $\left[t > \left(b^2 S_s / 2K\right)\right]$. The slope m of these lines is given by

$$m = \frac{\Delta s}{\text{cycle}} = 2.3 \frac{Q}{4 \pi K b} \quad \ldots\ldots\ldots\ldots\ldots (21)$$

which is obtained by differentiating Eq. 6 or Eq. 10 with respect to $\log_{10} t$ and noting that u becomes very small for large values of time.

Other Drawdown Equations.—For other drawdown equations (equations that, during a relatively short period of pumping, are not of the type of Eq. 4 or Eq. 9), the properties previously examined still apply qualitatively. Quantitatively, however, only Eq. 21 and, provided $(r\ \beta)$ is replaced by $(1/2)\ (2\ l + l' + d')$, Eq. 18 are still applicable. In addition, as the length of the screen of an observation well is increased, other variables being held constant, the curve inflection becomes less distinct regardless of the well location. The curve approached is that of the Theis formula, which is obtained when (l'/b) and (d'/b) become one and zero respectively (see curves II and II', Fig. 3.

RECOVERY EQUATIONS

If t and t' are the times, reckoned respectively from the commencement and end of pumping, the residual drawdown s' in a piezometer during recovery can be shown to be

$$s' = s\ (t) - s\ (t') \quad \ldots\ldots\ldots\ldots\ldots\ldots (22)$$

Similarly, the average residual drawdown $\bar{s}'$ in an observation well is

$$\bar{s}' = \bar{s}\ (t) - \bar{s}\ (t') \quad \ldots\ldots\ldots\ldots\ldots\ldots (23)$$

in which $t = t_o + t'$ and t_o is the time at which the pumping has ceased. Thus the recovery equation corresponding to any of the drawdown equations discussed above can be formulated readily, subject to the same time criteria. For example, if the equation of drawdown is of the type that reduces to that of Eq. 4 during a relatively short period of pumping, the recovery equation can be written as[3]

$$s' = c\left[M\ (u, \beta) - M\ (u', \beta) + f_2\ (u, b/r, \beta) - f_2\ (u', b/r, \beta)\right] \ldots (24)$$

in which u' is the value of u after replacing t by t' and

$$f_2\ (u, b/r, \beta) = \sum_{n=1}^{\infty} M\left[u, \left(\frac{2\ n\ b}{r} + \beta\right)\right] - M\left[u, \left(\frac{2\ n\ b}{r} - \beta\right)\right] \ldots . (25)$$

For $t < \left[\dfrac{(2\ b - r\ \beta)^2\ S_s}{20\ K}\right]$, Eq. 24 can be approximated by

$$s' = c\left[M\ (u, \beta) - M\ (u', \beta)\right] \quad \ldots\ldots\ldots\ldots (26)$$

For $t_o > \left(\dfrac{b^2\ S_s}{2\ K}\right)$ and $t' < \left[\dfrac{(2\ b - r\ \beta)^2\ S_s}{20\ K}\right]$, Eq. 17 can be approximated by

$$s' = \frac{Q}{4\ \pi\ K\ b}\left[W\ (u) - f_s\right] - c\,M\ (u', \beta) \quad \ldots\ldots\ldots (27)$$

If both t_o and t' are greater than $\left(b^2\ S_s / 2\ K\right)$, Eq. 24, as well as the general recovery equation,[3] become

$$s' = \frac{Q}{4\ \pi\ K\ b}\left[W\ (u) - W\ (u')\right] \quad \ldots\ldots\ldots\ldots (28)$$

The preceding equations give the recovery in piezometers. The recovery n observation wells can be similarly obtained by using the appropriate average drawdown equation. Eq. 28 gives the recovery in both cases.

PROPERTIES OF RECOVERY EQUATIONS

In applying the recovery equation to the analysis of data from aquifer tests, se is made of some characteristic features of the equation.

Recovery Equations for Special Cases.—Of importance is the equation of ater level recovery after shutoff in a pumped well that is screened throughout s depth of penetration, or in nearby wells that may be considered as piezometers of zero penetration. In such cases, as well as in others (see section

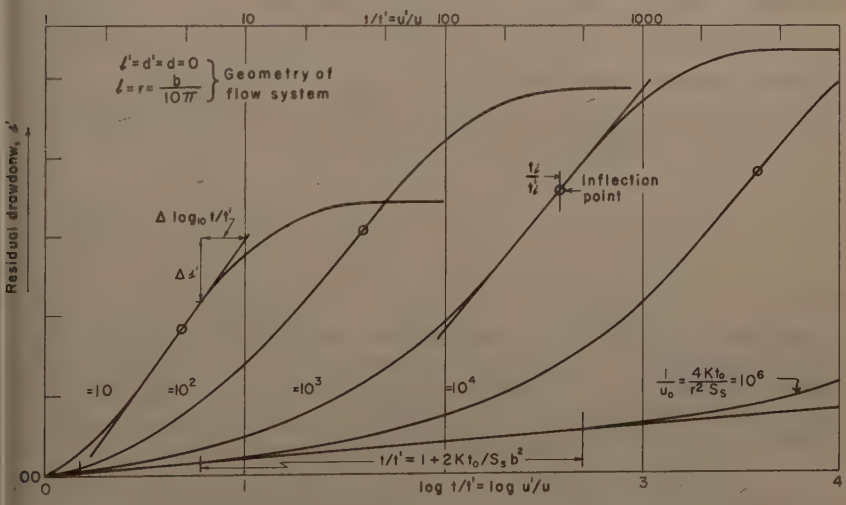

FIG. 4.—LOG (t/t')—RESIDUAL DRAWDOWN VARIATION IN WELLS PARTIALLY PENETRATING AN ARTESIAN AQUIFER

n Equations of Drawdown), the drawdown equation during short periods of umping of the type of Eqs. 4 or 9. Consequently, the equations given in the receding section apply. They are here called "recovery equations for spe-ial cases."

Fig. 4 represents theoretical plots of the residual drawdown s' (for the set parameters shown in the figure) versus the logarithm of (t/t'), as given by q. 24. These curves have three main characteristics:

1. The curves have a straight portion at their lower left end; that is, a raight line passing through the point of zero residual drawdown and (t/ t') = 1. his line may be clearly defined, as in the curves $(1/u_0) = (4\ K\ t_0/r^2\ S_s) = 10^6$ nd 10^4; barely recognizable, as in the curve 10^3; or entirely indistinguishable, s in the curves 10^2 and 10. The range of time in which this line forms de-

pends on the length of the period of pumping t_o, the formation coefficients, and the thickness of the aquifer. That is, the straight line forms in the region for which (t/t') is less than $\left[1 + \left(2\ K\ t_o / b^2\ S_s\right)\right]$. The slope of the straight line, if it forms, is given by

$$m = \frac{\Delta s'}{\text{cycle}} = \frac{2.3\ Q}{4\ \pi\ K\ b} \quad \ldots\ldots\ldots\ldots\ldots\ldots (29)$$

which is obtained by differentiating Eq. 28 with respect to $\log_{10}(t/t')$ and observing that u and u' become very small for larger values of time.

2. The curves have, in general, an inflection point, in the neighborhood of which the curve may often be approximated by a straight line, the slope of which for all practical purposes is equal to the slope of the curve at the inflection point. The inflection point forms (if it does) in the period $t' < \left[\frac{(2\ b - r\ \beta)^2\ S_s}{20\ K}\right]$. Thus, the recovery equation in the neighborhood of the inflection point is given by Eq. 24 after dropping out $f_2\left(\frac{u', b}{r, \beta}\right)$. By differentiating this equation (or any equivalent equation[3]) twice with respect to $\log_{10}(t/t')$ and equating the results to zero, the value of u' at the inflection point, that is the value of u'_i, can be shown to be given approximately by the relation

$$\frac{\beta^2}{\sqrt{\pi}} = f(x)$$

$$\doteq x\ e^{x^2}\ \text{erf}(x) \quad \ldots\ldots\ldots\ldots\ldots\ldots (30)$$

in which $x = \beta\sqrt{u'_i}$.

The slope of the curve m_i at the inflection point can be obtained from Eq. 2 (or other equivalent form) by differentiating with respect to $\log_{10}(t/t')$ and substituting u_i and u'_i for u and u', respectively, in the resulting expression. This slope can be approximated closely by either of the following two relations depending on the range of (t/t') in which the inflection point occurs:

a. If the inflection point occurs in the range $(t/t') < 100$, the slope can for all practical purposes, be taken as

$$m_i = \Delta s'/\text{cycle} = 2.3c \left\{ \left(t_i/t_o\right) \exp\left(-u'_i\right)\ \text{erf}(x) - \left(t_i/t_o\right) \exp\left[-\left(t'/t\right)_i\ u'_i\right] \text{erf}\left(x\sqrt{\left(t'/t\right)_i}\right) \right\} \quad \ldots\ldots\ldots (31)$$

in which $(t'/t)_i$ is the value of t'/t at the inflection point.

b. If the inflection point occurs in the range $(t/t') > 100$, the second term of Eq. 31 becomes insignificant. The slope is then given by Eq. 31 after neglecting the second term.

3. If the geometry of the flow system is such that the relation

$$\left[x^2\ (2\ b - r\ \beta)^2 / 5\ (r\ \beta)^2\right] \leq 1 \quad \ldots\ldots\ldots\ldots (32)$$

holds, the curve under consideration will not exhibit an inflection point. The straight portion of the curve that forms (if it does) through the latter part of data will, however, be the same as that described under item 1.

Other Recovery Equations.—The properties of the recovery equations for special cases, that were examined in the previous paragraphs, still apply qualitatively for other equations (see the section on Other Drawdown Equations) also. Quantitatively, however, only Eq. 29 is rigorously valid. The other relations can be used only to give an estimate of the values involved therein.

APPLICATIONS OF THEORY OF AQUIFER TESTS

Before introducing the procedure to be outlined, it should be observed that the effects of partial penetration resemble the effects of leakage from storage in a thick semipervious confining layer.[10] Also, if the curve inflection is apparent, but the period of observation is not long enough to establish the ultimate straight-line variation on a semilogarithmic time-drawdown plot, the effects of partial penetrations resemble the effects of some kind of recharge boundary, such as induced infiltration from beds of streams or lakes,[11] or recharge from water-bearing strata supplying leakage[12] through semipervious confining beds. The same general effects are observed if the wells completely penetrate a sloping water-table aquifer or a wedge-shaped aquifer (nonuniform thickness). The existence of such conditions should be reasonably eliminated prior to performing an analysis, based on the present theory.

Outline of Methods.—Semilogarithmic time-drawdown or $\log_{10}(t/t')$—residual drawdown plots or both are an essential part of the analysis of the observed data. Consequently, the first step in the analysis is the construction of such curves.

Analysis of Drawdown Data.—Depending on the geometry of the flow system under consideration, the methods are as follows:

Inflection Point Method.—If the equation of drawdown for the observation well under consideration during relatively short periods of pumping is of the type of Eq. 4 or Eq. 9 (or can be approximated by such equations), the following procedure can be followed, provided that the observed semilogarithmic plot clearly indicates the formation of the inflection point within the observed data, and provided also that the tangent of this curve at the inflection can be constructed with approximate accuracy:

(1) On the semilogarithmic plot, construct the tangent in the region of the curve inflection and measure its slope $m_i = \Delta s/\text{cycle}$.

(2) Compute $f(x)$ from $\beta^2/\sqrt{\pi} = f(x)$.

(3) Obtain the value of x and $\text{erf}(x)$ from Table 1 (or from a graph constructed from this table).

(4) Compute u_i from $(x/\beta)^2$ and obtain the value of $\exp(-u_i)$, using a slide rule or appropriate tables.

(5) Compute K, using Eq. 17 with appropriate expression for c.

(6) Obtain the value of $M(u_i, \beta)$, using tabular values of this function and the computed values of u_i and β. Then compute the value of s_i from Eq. 16.

---

10 "Modification of the Theory of Leaky Aquifers," by M. S. Hantush, Journal of Geophysical Research, Vol. 65, 1960, p. 3713.

11 "Analysis of Data From Pumping Wells Near a River," by M. S. Hantush, Journal of Geophysical Research, Vol. 64, 1959, p. 1921.

12 "Nonsteady Radial Flow in an Infinite Leaky Aquifer," by M. S. Hantush and C. E. Jacob, Transactions, Amer. Geophysical Union, Vol. 36, 1955, p. 95.

(7) From the semilog plot, obtain the value t_i corresponding to the computed value of s_i. Then calculate the specific storage from $S_s = (4\ K\ t_i\ u_i / r^2)$.

(8) Construct the ultimate straight line of the curve (if it is discernible within the observed data) and measure its slope $m = \Delta s$/cycle. Then compute T (= Kb) from Eq. 21.

(9) Compute b from the calculated values of K and Kb.

Type-Curve Method.—If the semilogarithmic time-drawdown curve of the observed data exhibits an inflection of the type shown in Fig. 3, and if the number and distribution of the observed points are such that the details of the curve prior to the attainment of the ultimate straight-line variation are discernible, a type-curve method can be used to determine the formation coefficients and often the thickness of the aquifer. The method is essentially the "Theis graphical method."[13] In the present case, however, the "type curve," according to the flow system under consideration, is a plot of the E (or $\bar{E}$) function of Eq. 1 (or Eq. 4) versus (1/u) on a logarithmic paper. The observed curve is a plot of s (or $\bar{s}$) versus t on a logarithmic paper of the same scale as that of the type curve. The procedure is as follows:

(1) Construct a type curve for each well, using tabular values of the function $M(u, \beta)$ (or a graph prepared therefrom) and the E (or $\bar{E}$) function of that well.

(2) Plot the observed data on a logarithmic paper of the same scale as that of the type curve.

(3) Superimpose the observed data on the type curve, keeping the coordinate axes of the two curves parallel, and adjust until the best fitting position is obtained. In matching the observed curve to the type curve, one should keep in mind that the observed points for relatively large values of time may deviate upward (having larger values) from the type curve. The deviation is to be expected, because the type curve is for drawdown values during relatively short periods of pumping.

(4) Select an arbitrary point (matching point) anywhere on the two superimposed sheets and record its coordinates; namely,

$$\left[E \text{ (or } \bar{E}),\ 1/u\right] \text{ and } \left[s \text{ (or } \bar{s}),\ t\right]$$

(5) Compute K from Eq. 1 or Eq. 8, whichever applies, and S_s from the relation

$$S_s = \frac{4\ K\ t}{\left(\frac{1}{u}\right) r^2} \quad \ldots\ldots\ldots\ldots\ldots\ldots (33)$$

(6) If the observed curve departs from the type curve, record the value of (1/u) at the point of "departure." Then compute b from the relations

$$b \approx (1/2)\left[1 + z + r\sqrt{5/u_d}\right] \quad \ldots\ldots\ldots\ldots (34a)$$

for piezometer, or

$$b \approx (1/2)\left[1 + (1/2)\ (l' + d') + r\sqrt{5/u_d}\right] \quad \ldots\ldots\ldots (34b)$$

---

13 "Groundwater Hydrology," by David K. Todd, John Wiley and Sons, Inc., New York, 1959, p. 90; also "Arid Zone Hydrology, Recent Development," by H. Schoeller, UNESCO, Paris, France, 1959, p. 37.

for observation wells or, in case E (or $\bar{E}$) reduces to the M function of Eq. 4, from

$$b \approx (1/2)\left[r\beta + r\sqrt{\frac{5}{u_d}}\right] \quad \ldots\ldots\ldots\ldots (34c)$$

in which u_d is the value of u at the "departure" point.

(7) From the computed values of K and b, calculate the transmissivity of the aquifer from T = Kb.

(8) If the observed curve does not depart from the type curve within the observed data, record the value of (1/u) of a point in the vicinity of the last observed point. The thickness of the aquifer is then greater than that obtained from the relations of b in step (6) if one uses therein the present value of (1/u).

(9) It is to be observed that whether the data under analysis are obtained from piezometers or observation wells, and regardless of the location of the point of observation, step (8) of the inflection-point method for computing the transmissivity of the aquifer (Kb) always holds. Carry out this step and obtain the value of (Kb = T). The value of T thus obtained serves as a check for the value obtained in step (7).

The values of T obtained from step (7) and step (9) may not agree closely. This may be because the best fitting position of the two superimposed curves had not been obtained on the first trial, or because the ultimate straight portion of the curve had been drawn either flatter or steeper than necessary, or because the apparent transmissivity of the aquifer (in case of water-table aquifers) had not attained its uniform value within the period of observation. If such agreement is lacking, the procedure is repeated again with the necessary adjustments in mind, so that the difference between the two values of T is either eliminated or reduced to a minimum. If a great difference persists, it is more likely that the apparent transmissivity has not attained a uniform value within the period of observation.

For certain flow systems, both of the preceding methods may apply, in which case they serve to check each other. Generally, the results of the computations do not agree on the first trial. The disagreement may be a result of under- or over-estimating the slope at the curve inflection, as well as the slope of the ultimate straight line; it may also be due to a poor choice of the best matching position, or to all these factors together. A second trial with the necessary adjustments generally results in a satisfactory answer.

Theis' or Jacob's Method or Both.— If the semilogarithmic plot of the observed data does not show any inflection despite a relatively long period of pumping, three possibilities may arise: (a) the observation well, although close to the pumped well, is completely penetrating and screened throughout the aquifer. Such information is generally known a priori; (b) the observation well is relatively distant from the pumped well; that is, $(r/b) > 1.5$. To aid in deciding whether this is the case, information about the approximate thickness of the aquifer should be available. Such information can be obtained from previous geological or geophysical studies, or from analysis of data from a nearby well through procedures such as those previously presented, or at least from the range of the thickness given by the relation

$$b < (1/2)\left[1 + 1' + (2.4\ 1/x)\right] \quad \ldots\ldots\ldots\ldots (35)$$

in which x is the solution of Eq. 9; (c) if the first and second possibilities are ruled out, the flow parameters are such that the relation

$$(2b - 1 - 1')^2 \, x^2/5l^2 < 1 \quad \ldots\ldots\ldots\ldots\ldots (36)$$

obtains, x being the solution of Eq. 14.

If the first or the second possibility obtains, the method of Theis and, provided the ultimate straight line of the semilogarithmic plot forms, that of Jacob[13,14] can be used for calculating the formation coefficients. If the third possibility pertains, the type-curve method can be used, provided the number and distribution of the observed points on the curved part of the semilogarithmic plot sufficiently define a curve on the logarithmic plot needed for the type-curve method. Alternatively, the following procedure can be used, provided an estimated value of the aquifer thickness is available:

Jacob's Method Adjusted for Partial Penetration.—During the time period in which the ultimate semilogarithmic straight line forms, the drawdown is given, depending on the well observed, by either Eq. 6 or Eq. 10. Because the second term of each of these equations is constant with time, it is clear that Jacob's method can be applied if the numerical value of this constant can be obtained. The procedure is as follows:

(1) On the observed semilogarithmic plot, construct the ultimate straight line and extend it to the zero-drawdown axis.

(2) Obtain the slope, ($m = \Delta s/$ cycle) of this line and its time intercept, t_p, on the zero-drawdown axis.

(3) Compute $T = K\,b$ from Eq. 21.

(4) Compute the value of f_s (or $\bar{f}_s$) from their appropriate expressions (a few terms of the series involved are generally sufficient).

(5) Compute $\exp(f_s)$ [or $\exp(\bar{f}_s)$], using a slide rule or appropriate tables. Then calculate the storage coefficient from

$$S = \left[\frac{2.25\ T\ t_p \exp(f_s)}{r^2}\right] \quad \ldots\ldots\ldots\ldots\ldots (37)$$

Analysis of Recovery Data.—If the equation of drawdown in the observation well is one that, during short times, reduces to the type of Eq. 4 or Eq. 5, the procedure of analysis is as follows:

(1) Prepare a plot of s'(or s') versus $\log_{10}(t/t')$ and pass the best-fit curve through the observed points.

(2) Construct the tangent to this curve in the region of the curve inflection and measure its slope $m_i = \Delta s'/$ cycle.

(3) Locate the inflection point on this tangent by inspection and obtain its value of (t/t'), which hereafter is designated by $(t/t')_i$. Over or underestimating the location of the inflection point will not materially alter the calculation to follow, as will be pointed out subsequently.

(4) Compute the value of (t_o/t'_i), which is $= (t/t')_i - 1$, and that of (t/t_o), which is $= (t/t')_i/(t_o/t'_i)$.

(5) Compute f(x) from $\beta^2/\sqrt{\pi} = f(x)$ and obtain the corresponding values of x and erf(x) from Table 1.

---

14 "Hydrology," by C. O. Wisler and E. F. Brater, John Wiley and Sons, New York, 1951, p. 234.

(6) Compute u'_i, which is $(x/\beta)^2$, and obtain the value of exp $(-u_i)$, using a slide rule or a table of the exponential function.

(7) If the value of $(t/t')_i > 100$, calculate K from Eq. 6, neglecting the second term.

(8) If the value of $(t/t')_i < 100$, calculate the values of $u'_i\,(t'/t)_i$ and $x\sqrt{(t'/t)_i}$, and obtain the values of exp $\left[-u'_i\,(t'/t)_i\right]$ and erf $\left(x\sqrt{(t'/t)_i}\right)$. Then calculate K from Eq. 31.

(9) From the known values of t_o and (t'_i/t_o), calculate the value of t'_i.

(10) Calculate the specific storage from $S_s = (4\,K\,t'_i\,u'_i/r^2)$.

(11) If a straight-line variation between s' and $\log_{10}(t/t')$ is discernible through the latter part of the data, including the origin point, $[(t/t') = 1,\ s' = 0]$, then, construct this line and measure its slope $m = \Delta s'$/cycle; calculate (K b) from Eq. 29; then, knowing the values of K and (K b), compute the value of b.

It is to be observed that if $(t/t')_i > 10$, the second term of Eq. 31 is comparatively very small. Thus, a large error in estimating the value of $(t/t')_i$ will not affect significantly the value of this second term. The largest error, if any will be in the first term of Eq. 31, owing to the factor (t_i/t_o). This error, however, rarely exceeds $\pm$ 3%. Even if one misses the true location of the inflection point by a factor of 10 (a remote possibility) and if, for example, the true value of $(t/t')_i$ is 10 and the estimated value is 100, the error in the value of (t_i/t_o), and consequently in the value of K, will be of the order $(1.01 - 1.11)/1.11 = -9\%$. The error in the value of S_s is approximately directly proportional to the error in estimating the value of t'_i.

An exact graphical solution for the case in which the short-time drawdown equation is not of the form of Eq. 4, is not available. The procedure outlined previously can be followed to obtain a rough estimation of the formation coefficients. However, if the straight line examined in step (11) forms, the solution for the transmissivity T = K b, as described in steps (11) and (12), is exact, because in the present case Eq. 29 obtains also.

Examples of Application.—Aquifer test data obtained in the Rio Grande Valley near the town of Socorro, N. Mex., will be used to illustrate the application of the methods presented. The wells tested penetrate a water-table aquifer. However, because the observed drawdowns are small compared to the depth of penetration of the pumped wells, the theory presented herein, although presented for artesian conditions, is still fairly applicable to water-table conditions. The computations in what follows were made with a slide rule.

The Faulkner Farm Test.—A schematic representation of the wells tested is shown in Fig. 5. These wells are located in the SW 1/4 NE 1/4 sec. 35, T. . S., R. 1 W., Socorro County, N. Mex. Both the pumped well and the observed well are perforated throughout their depths of penetration. These depths are 116 ft and 60 ft, respectively. The observed well is 17 ft distant from the pumped well. An aquifer test using these two wells was run by J. F. Waldron[15] during September 1952. During the test, the pumped well discharged at a uniform rate of 3.57 cfs.

15 "Reconnaissance Geology and Groundwater Study of a Part of Socorro County, New Mexico," by J. F. Waldron, thesis presented to Stanford Univ., at Palo Alto, Calif., in 1956, in partial fulfillment of the requirements for the degree of Doctor of Philosophy.

As $(l'/l) = (60/116) < 2$, the average drawdown s in the observed well during relatively short times is given by Eq. 9, which, with $d = d' = 0$, $l' = 60$ ft, $l = 116$ ft, and $r = 17$ ft, becomes

$$\bar{s} = \frac{Q}{928\,\pi\,K}\,\bar{E}\,(u) \quad \ldots\ldots\ldots\ldots\ldots\ldots (38)$$

$$= \frac{Q}{928\,\pi\,K}\left[M\,(u, 8.6) - M\,(u, 5.1)\right]$$

Analysis of Drawdown Data.—The observed semilogarithmic curve of Fig. 5 clearly shows an inflection, and because Eq. 24 is not of the form of Eq. 5, the type-curve method is followed.

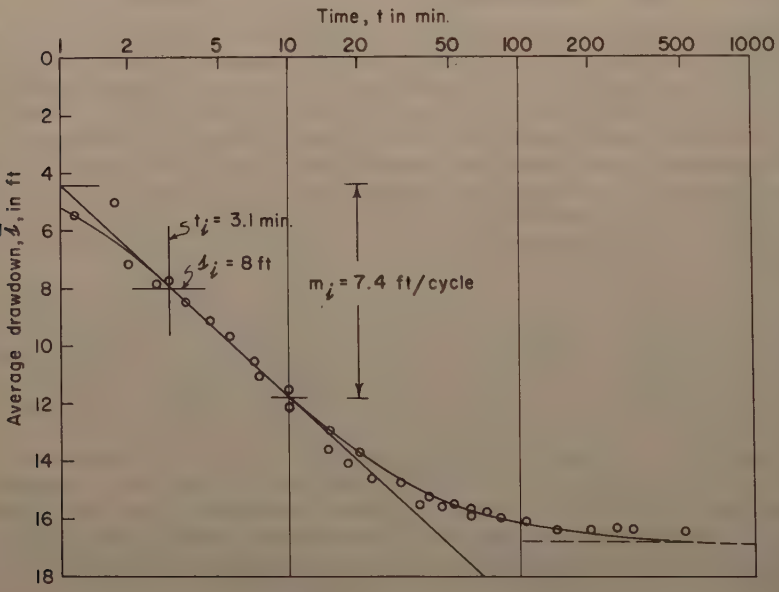

FIG. 5.—TIME-DRAWDOWN VARIATION IN THE FAULKNER TEST OBSERVATION WELL

Type-Curve Method.—From Table 1 and $\bar{E}\,(u)$ of Eq. 38, a type curve is prepared on logarithmic paper, and the observed data are plotted on logarithmic paper of the same scale. The two curves are superimposed and adjusted to obtain the matching position shown in Fig. 6. The valeus $\bar{E}$, $(1/u)$, $\bar{s}$, and t at the matching point shown in the figure are 5.6, 500, 10 ft, and 100 min (6,000 sec), respectively. From Eq. 38, K is computed as 6.86×10^{-4} fps, and from $S_s = \left[4\,K\,t/\left(\frac{1}{u}\right)r^2\right]$, S_s is computed as 1.14×10^{-4} ft^{-1}.

Within the period of the test, the observed curve does not depart from the type curve; that is, the time t_d at the eventual point of departure is greater

than the period of observation. Thus, from Fig. 6, t_d and $(1/u_d)$ are greater than 500 min and 2,500, respectively. Consequently, the thickness of the aquifer is greater than

$$(1/2)\,[1 + (1/2)\,l' + r\sqrt{5/u} = (1/2)\,[116 + 30 + 17\sqrt{5 \times 2{,}500}] = 1023 \text{ ft}$$

Inflection-Point Method.—It has been pointed out that the application of the inflection-point method on data obtained from flow systems for which Eq. 4 or Eq. 9 does not obtain will generally give an approximate solution. This, of course, is due to replacing the actual equation by an approximate equation of the form of Eq. 4. For instance, if the drawdown in the observation well of this

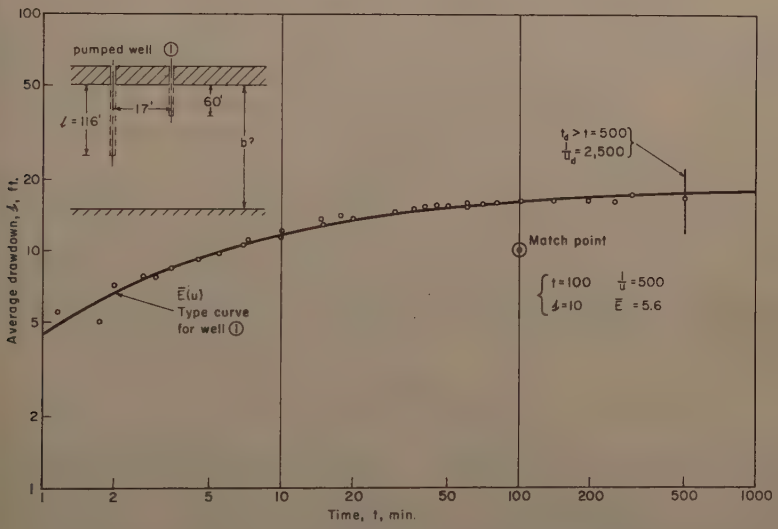

FIG. 6.—OBSERVED DATA AND THE THEORETICAL TYPE CURVE FOR THE OBSERVATION WELL OF THE FAULKNER TEST

example be approximated by that in a piezometer of zero penetration ($l' = 0$), instead of Eq. 38 (the actual equation), the resulting equation is

$$s = \frac{Q}{464\,\pi\,K}\,M\,(u, 6.82) \quad \ldots\ldots\ldots\ldots\ldots\ldots (39)$$

for which $c = \left(\frac{Q}{464\,\pi\,K}\right)$ and $\beta = 6.82$.

Based on Eq. 39, the application of the inflection-point method follows: the semilogarithmic plot of the observed data has been carried out already, as shown in Fig. 5. The tangent to the curve in the region of the curve inflection is constructed; its slope m_i is measured as 7.4 ft per cycle. $f(x) = \beta^2/\sqrt{\pi}$ $(6.82)^2/\sqrt{\pi} = 26.2$. From Table 1, $x = 1.666$, and $\text{erf}(x) = 0.982$. $u_i = (x/\beta)^2$ 0.06, and $\exp(-0.06) = 0.94$. From Eq. 17, K is computed as 7×10^{-4} fps. In-

terpolation in tables of the function M (u, β) gives M $(u_i, 6.82) = 2.291$. From Eq. 39, s_i is computed as 8 ft. For $s_i = 8$ ft, Fig. 6 shows $t_i = 3.1$ min = 186 sec. Then, from $S_s = 4\ K\ t_i\ u_i / r^2$, S_s is computed as 1.08×10^{-4} ft.

The ultimate straight-line portion of the curve is not discernible within the observed data (see dashed line of Fig. 5). Hence, the transmissivity (Kb) and, consequently, the thickness of the aquifer cannot be determined from the present data.

The Olson Wells Test.—Fig. 7 (a) shows semilogarithmic time-drawdown curves for two observation wells prepared from data obtained from a pumping test on what is known as the Olson Wells. The geometry of these wells is shown diagrammatically in Fig. 8. They are located about one-half mile north of the campus of the New Mexico Institute of Mining and Technology, Socorro, N. Mex. Each of the two Olson wells has a 75-ft depth of penetration, of which the bottom 50-ft section is perforated. One of these wells is pumped at a rate of 1.6 cfs. The other well, designated as observation well (1) is 182 ft east of the pumped well. A third well, designated as observation well (2) (known as the Lopez dug well), is 384 ft west of the pumped well and is assumed to be zero penetration (actually about 1.1 ft penetration).

Analysis of drawdown data from well (1)—Eq. 9 will, of course, give the average drawdown in this well. However, because $(r/l) = (182/75) > 1$ and $(l'/l) = (75/75) \leq 1$, Eq. 9 can be approximated by Eq. 1, in which z is chosen arbitrarily between 0 and l (see section on average drawdown for short times). For z = 25 ft (this choice is made because Eq. 1 will reduce to the form of Eq. 4), the average drawdown in this well for small time s will, from Eq. 1, be given by

$$\bar{s} = \frac{Q}{400\ \pi\ K} M\ (u, 0.55) \quad \ldots\ldots\ldots\ldots\ldots (40)$$

which is of the form of Eq. 4, with $c = \frac{Q}{400\ \pi\ K}$ and $\beta = 0.55$. Because the inflection of the semilogarithmic curve of the observed data is clearly manifested (see Fig. 7 (a)), the inflection-point method and/or the type-curve method will provide a solution for the formation parameters.

Type-Curve Method.—From tables of the function M (u, β) and $\bar{E}$ of Eq. 40 [M (u, 0.55)], a type curve is prepared on logarithmic paper, and the observed data are plotted on logarithmic paper of the same scale. The two curves are superimposed and adjusted to obtain the matching position shown in Fig. 8. The values $\bar{E}$ [M (u, 0.55)], (1/u), $\bar{s}$, and t at the matching point shown are 0.38, 10, 1 ft, and 1,000 min $(6 \times 10^{-4}$ sec), respectively. From Eq. 40, K is calculated as 4.84×10^{-4} fps, and from $S_s = 4\ K\ t/(1/u)\ r^2$, S_s is calculated as 3.5×10^{-4} ft^{-1}. The value of $(1/u_d)$ at the point of departure is 9. Then, from the relation $b = (1/2)\left[r\beta + r\sqrt{5/u_d}\right]$, b is calculated as 695 ft. The transmissivity of the aquifer is T = Kb = 0.319 sq ft per sec, and the storage coefficient is $S = S_s b = 0.23$.

Inflection-Point Method.—The observed semilogarithmic plot is prepared as shown in Fig. 7 (a). The tangent to this curve in the region of the curve inflection is constructed. Its slope m_i is measured as 1.55 ft per cycle. $f(x) = \beta^2/\sqrt{\pi} = (0.55)^2/\sqrt{\pi} = 0.17$. From Table 1, x = 0.371, and erf (x) = 0.40. $u = (x/\beta)^2 = 0.454$, and exp (-0.454) = 0.635. From Eq. 17, K is computed as 4.78×10^{-4} fps. From tables of the function M (u, β) [or the type curve o

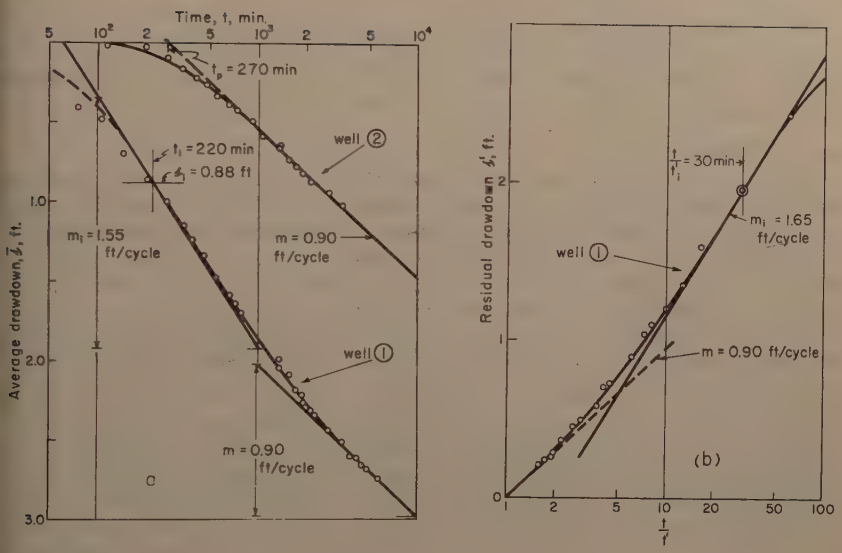

FIG. 7.—a) TIME-DRAWDOWN VARIATION IN THE OBSERVATION WELLS OF THE OLSON TEST; b) LOG (t/t') - RESIDUAL DRAWDOWN VARIATION IN WELL (1) OF THE OLSON TEST

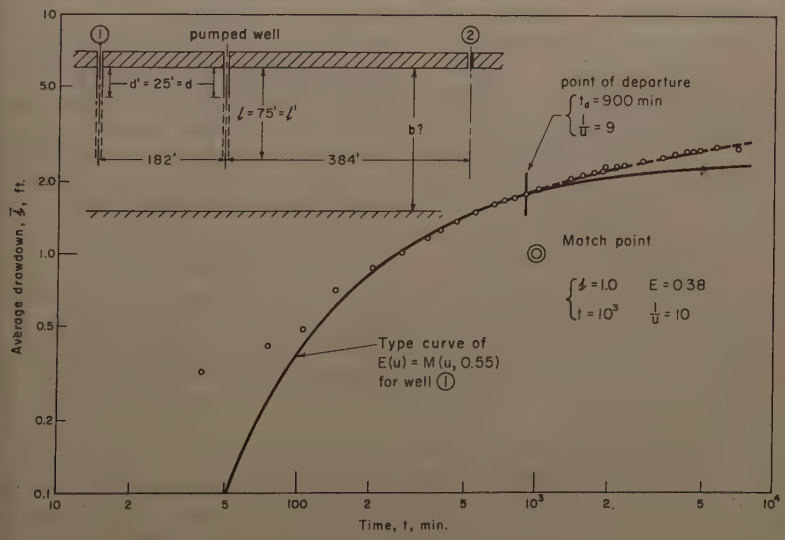

FIG. 8.—OBSERVED DATA AND THE THEORETICAL TYPE CURVE FOR WELL (1) OF THE OLSON TEST

M (u, 0.55)], M $(u_i, 0.55) \approx 0.33$. From Eq. 40, $\bar{s}_i = 0.88$ ft. From Fig. 7 (a), $t_i = 220$ min or 13,200 sec. Hence, $S_s = 4\,K\,t_i\,u_i/r^2 = 3.46 \times 10^{-4}$ ft^{-1}. The ultimate straight line of the curve in Fig. 7 (a) is constructed. Its measured slope is 0.90 ft per cycle. From Eq. 21, Kb is calculated as 0.326 ft per sec. Consequently, $b = \left(\frac{Kb}{K}\right) = \left(0.326/4.78 \times 10^{-4}\right) = 680$ ft. The storage coefficient is $S = S_s b = 0.235$.

The calculations presented are those of a second trail. In the first trial, hydraulic conductivity as obtained by using the inflection-point method was underestimated. Apparently, this resulted from drawing "the two tangents" of the observed curve steeper than was necessary. The coefficient obtained by using the type-curve method was overestimated because the best matching position was not obtained, it appears, on the first trial. The two tangents were redrawn with flatter slopes in the first case, and another fitting position was obtained in the second case, because the observed data permitted these adjustments. The calculations were repeated, with the results being those previously presented.

It should be pointed out also that because of a large variation of the well discharge within probably the first 100 min of the pumping period (because of pump characteristics), the observed points within that period were rejected. In addition, one should note that during the very early period of pumping, the observed data generally do not follow the theoretical drawdown equation, because of the probable variation of the formation coefficients, especially if the flow is unconfined.

Analysis of Drawdown Data from Observation Well (2).—The observed semilogarithmic time-drawdown curve for this well (see Fig. 7 (a) does not show a curve inflection. The well is known to be of practically zero penetration, and the aquifer is known to be deep, its thickness, as estimated from analysis of data from well (1), is about 700 (actually an average of 670) ft; consequently, $(r/b) = (384/740) < 1.5$. Therefore, the two possibilities for which Theis' or Jacob's method does apply are ruled out, although the general trend of the time-drawdown variation resembles that given by the Theis formula.

Jacob's Method Adjusted for Partial Penetration.—Although there are enough points on the curved part of the observed semilogarithmic plot to warrant a fair solution by using the type-curve method (drawdown equation is Eq. 1, with $z = 0$), Jacob's method adjusted for partial penetration is here followed for the purpose of illustrating the procedure, which is as follows:

The slope m of the straight portion of the curve is measured as 0.90 ft per cycle, and $t_p = 270$ min (16,200 sec) [see Fig. 7 (a)]. From Eq. 21, $T = K\,b$ is calculated as 0.326 sq ft per sec. From Eq. 6, f_s is calculated, using a value of $b = 700$ ft (only five terms of the infinite series are needed), as 0.81. Then $\exp(0.81) = 2.25$. From $S = \left[2.25\,T\,t_p \exp\left(f_s\right)/r^2\right]$, the storage coefficient is calculated as 0.18.

Analysis of Recovery Data from Well (1).—Fig. 7 (b) is the observed curve of residual drawdown s' versus the logarithm of (t/t'). The tangent in the region of the curve inflection is constructed; its measured slope $m_i = \Delta s'$ per cycle = 1.65 ft per cycle. By inspection, the inflection point is located at $(t/t')_i = 30$.

Because $(t/t')_i < 100$, all terms of Eq. 31 are needed. The computation is as follows:

$$\left(t_o/t'\right) = (t/t')_i - 1 = 29$$

and

$$(t_i/t_o) = (t/t')_i/(t_o/t'_i) = (30/29) = 1.035.$$

And

$$f(x) = \beta^2/\sqrt{\pi} = (0.55)^2/\sqrt{\pi} = 0.17$$

(see Eq. 40 for values of β and c), for which Table 1 gives x = 0.371 and erf(x) = 0.40. Then $u'_i = (x/\beta)^2 = 0.454$; $\exp(-u'_i) = \exp(-0.454) = 0.635$; $\exp(-u'_i/(t/t')_i) = \exp(-0.454/30) = 0.985$; and $\text{erf}(x/\sqrt{(t/t')_i}) = \text{erf}(0.371/\sqrt{30}) = 0.077$. From Eq. 31, $K = [(2.3)(1.6)/(400\pi)(1.65)][(1.035)(0.635)(0.4) - (0.985)(0.077)/(29)] = (1.77 \times 10^{-3})(0.264 - 0.003) = 4.63 \times 10^{-4}$ fps. From $(t_o/t'_i) = 29$ and t_o = 6,630 min (period of pumping), t'_i = 229 min (13,700 sec). Hence, $S_s = (4\,Kt'_i\,u'_i/r^2) = 3.46 \times 10^{-4}$ ft^{-1}.

The straight portion of the lower left portion of the observed curve is not clearly discernible. However, for the purpose of illustrating the procedure, the straight line is constructed as shown by the dashed line in Fig. 7 (b). Its measured slope m is 0.90 ft per cycle. Then, from Eq. 29 K b is computed as 0.326 sq ft per sec. Finally, b = (K b)/K = $(0.326/4.63 \times 10^{-4})$ = 705 ft, and S = $S_s b$ = 0.244.

APPENDIX.—NOTATION

The following symbols, adopted for use in this paper, conform essentially with "American Standard Letter Symbols for Hydraulics" (ASA Z10.2-1942), prepared by a committee of the American Standards Association with Society representation and approved by the Association in 1942:

T = thickness of aquifer; dimension L;

= constant, depending on the well discharge, length of well screen, and on the hydraulic conductivity of the aquifer; dimension L;

= depth from the top of the aquifer of the unscreened portion (unperforated section of the casing) of the pumped well, L;

= depth from the top of the aquifer of the unscreened portion of the observation well, L;

$= E(u, l/r, d/r, z/r = M[u, (l+z)/r] - M[u, (d+z)/r] + M[u, (l-z)/r] - M[u, (d-z)/r]$;

$= \bar{E}(u, l/r, d/r, l'/r, d'/r) = [E \text{ with } z = (l'+d')/2]$;

$f(x) = \frac{2}{\sqrt{\pi}} \int_0^x e^{-y^2}\,dy$ = The error function;

$\text{erfc}(x)$ = 1 - erf (x) = The complement of the error function;

f $= f(u, r/b, l/b, d/b, z/b) = \left[2b/\pi\,(l - d)\right] \sum_{n=1}^{\infty} (1/n) \left[\sin(n\pi\, l/b) - \sin(n\pi\, d/b)\right] \cos(n\pi\, z/b)\, W(u, n\pi\, r/b)$;

f_s = [f, with $2K_o(n\pi\, r/b)$ replacing $W(u, n\pi\, r/b)$];

$\bar{f}$ $= \bar{f}\,(u, r/b, l/b, d/b, l'/b, d'/b) = \left[2b^2/\pi^2\,(l' - d')\right] \sum_{n=1}^{\infty} (1/n^2) \left[\sin(n\pi\, l/b) - \sin(n\pi\, d/b)\right]\left[\sin(n\pi\, l'/b) - \sin(n\pi\, d'/b)\right] W\left(u, \frac{n\pi\, r}{b}\right)$

$\bar{f}_s$ = [$\bar{f}$, with $2K_o(n\pi\, r/b)$ replacing $W(u, n\pi\, r/b)$];

f_2 $= f_2(u, b/r, \beta) = \sum_{n=1}^{\infty} M\left[u, \left(\frac{2nb}{r} + \beta\right)\right] - M\left[u, \left(\frac{2nb}{r} - \beta\right)\right]$;

K = hydraulic conductivity of the aquifer, LT^{-1};

$K_o(x)$ = the zero-order modified Bessel function of the second kind;

l = depth of pentration of the pumped well, L;

l' = depth of penetration of an observation hole, L;

$M(u,\beta)$ $= \int_u^{\infty} \frac{e^{-y}}{y} \text{erf}\left(\beta\sqrt{y}\right) dy$, tabular values of which are available;

Q = constant well discharge, $L^3\,T^{-1}$;

r = radial distance measured from center of well, L;

r_w = effective radius of the pumped well, L;

S = bS_s = storage coefficient;

S_s = specific storage (volume of water from storage by a unit volume o the aquifer under a unit head decline), L^{-1};

s = drawdown of piezometric surface at any time and at any point in th aquifer (drawdown in piezometers), L;

$\bar{s}$ = average drawdown in observation holes, L;

s' = residual drawdown in piezometers, L;

$\bar{s}'$ = residual drawdown in observation holes, L;

T = Kb = transmissivity of the aquifer, $L^2\,T^{-1}$;

t = time since pumping started, T;

t_o = period of pumping, T;

t' = time since pumping stopped, T;

u = $\left(r^2 S_s / 4Kt\right)$;

u' = $\left(r^2 S_s / 4Kt'\right)$;

W(u) = $\int_u^\infty \frac{e^{-y}}{y}\,dy$ = well function of (u) for nonleaky aquifers for which tables are available;

W(u,x) = $\int_u^\infty \frac{dy}{y} \exp\left(-y - x^2/4y\right)$ = well function of (u and x) for leaky aquifers for which tables are available;

z = vertical coordinate measured from the top of the aquifer, positive downward; and

β = one of the parameters of the function M (u, β), also it is a constant that depends on one or all of the variables, l, l', d, d', z, r, b.

Journal of the
HYDRAULICS DIVISION
Proceedings of the American Society of Civil Engineers

DISCUSSION

Note.—This paper is a part of the copyrighted Journal of the Hydraulics Division, roceedings of the American Society of Civil Engineers, Vol. 87, No. HY 5, September, 61.

TWO METHODS TO COMPUTE WATER SURFACE PROFILES[a]

Discussion by Edward N. Whitney

EDWARD N. WHITNEY,[1] F. ASCE.—Methods A and B and four other methods have been described.[2] Method A has been used almost exclusively in the Durango office of the USBR since 1957 on ten tailwater or backwater studies on five steep rivers and creeks in this area, the Florida, LaPlata, Dolores, and Animas Rivers, and Junction Creek, a tributary of the Animas.

On nine of the ten locations there were sections at which critical velocity governed. Numerous other sections required checking to determine if critical conditions were present. As dams are build farther into the mountains, critical velocity conditions will become more common.

In Table 1, p. 84, "Hydraulic Characteristics," in order to cover critical stages, mentioned on p. 82, the headings, the Durango office has found helpful are: Elev., A, T, (for top width and a starting or check point for wetted perimeter, p) p, R, $R^{2/3}$, n, K_d, A/T, V_{cr} (which equals $5.67(A/T)^{1/2}$, as given elsewhere[2]), and Q_{cr}. A curve V_{cr} versus $5.67\,(A/T)^{1/2}$, is used.

Even if V_{cr} or Q_{cr} alone is used in computations, depending on the approach to this difficult subject, the use of either or both columns should be permitted. If there is a strong proof that n varies with stage, an n—stage curve should be drawn and K_d values computed from it.

In November 1960, the Durango office was advised that Table 1 had been revised to give the following headings: Elev., a, p, r, $r^{2/3}$ $K_b = 1.486\,ar^{2/3}$ and $K_d = K_b/n$. These headings were recommended for use in cases in which critical velocities would not be met.

In Table 2, p. 91, "Water Surface Profile Computations—Method A," the Durango office uses a column for Q/K_d, which should be logically placed before Column 6, which equals $(Q/K_d)^2 = S_f$. This new column may be called 5A, and is used also in computing Column 9, (steps 2 and 3, p. 86), when there are over-bank areas.

It would be logical and helpful to put as many step directions and fixed rules of procedure as possible, in fine print if necessary, at the column headings, so that the inexperienced computer would not have to refer to some other source of information to refresh his memory.

When the computer has reached Column 17, "Water Surface Elevation," the operator wishes to know how he checks with the assumed elevation in Column 1. He might make mistakes here. Column 18 would provide him a place to

---

[a] April 1959, by J. Lara and K. Schroeder (Proc. Paper 1997).

[1] Hydr. Engr., U. S. Bur. of Reclam., Durango, Colo.

[2] "Guide for Computing Water Surface Profiles," Sedimentation Sect. Report, Hydrology Branch, Div. of Proj. Investigations, Bur. of Reclam., U. S. Dept. of Interior, Denver, Colo., November, 1957.

record the difference, plus or minus, and a wide Column 19 would provide spac for such items as:

1. Critical velocity conditions;
2. Exmplanation of adverse slopes which occasionally occur;
3. Possibility of change in n due to sediment deposition or timber bein logged or burned off;
4. Accuracy of estimate; and
5. Note No. below.

In reaching agreement within 0.1 ft between assumed water surface eleva tion, Column 2, and water surface elevation, Column 17, it has proved helpfu to plot a curve, called a Try-Get Curve, the Try elevation on the vertical scale and the Get elevation on the horizontal. A 45° line is drawn between points o equal elevation.

A letter from the Denver office in November, 1960 gave the information tha Lara used this method, when the computations were begun. His computatio was also shown for a straight line intersection between two points located o opposite sides of the 45° line.

The Try-Get operation consists of figuring and plotting as few points a possible that will locate a curve, whose intercept with the 45° line will giv the desired answer. The curve solves the varying relationships between th dimensional and hydraulic characteristics of the two sections in question. Whe agreement is near, it is advisable to estimate the water elevation to the 0.01 as well as to compute to the 0.01 ft in order to avoid an extra line of computa tion. The allowable difference may well depend on the size of the discharge and the importance of the study.

The shape and slope of the curve developed for one Q can be used as an ai in estimating water surfaces for lower or higher Q's. Critical velocity condi tions are shown by failure of the Try-Get curve to cross the 45° line. For th last upstream section only, if pressed for time, and if the estimator is sure o his points and curve, he can pick the correct elevation without further com puting.

It is understood that some computations for all or parts of Method A hav been done on electronic computers. Has it been possible to eliminate the cu and try method now in use? The profession would undoubtedly be intereste in the latest developments in this field, as investigated by the Denver office o the Bureau of Reclamation.

JOE M. LARA,[3] A. M. ASCE, AND KENNETH B. SCHROEDER,[4] A. M ASCE.—(Addendum to Closure) The report,[2] referred to by Whitney was pre pared in more detail than the paper by the writers.

Critical conditions that can occur in mountainous streams do require speci analysis. Whitney presents a helpful suggestion in tabulating the various hy draulic characteristics pertinent to the ciritical flow analysis. The curve, V_c versus $5.67\ (A/T)^{1/2}$, referred to by Whitney is apparently in error. It believed he meant the plotting of V_{cr} versus A/T. The form on which the hy draulic properties are tabulated can be altered or modified to suit the type analysis being made.

[3] Hydr. Engr., Bur. of Reclam., Denver, Colo.
[4] Hydr. Engr., Bur. of Reclam., Denver, Colo.

Whitney's comments on suggested additional columns in the water surface rofile computations form will be considered when the next revision to the orm is made.

The Try-Get Method of reducing the number of trial assumed water surface levations is an informal standard procedure often used in these computations. has been found, however, that the curve traced by a plot of the Try-Get elevations is generally shaped slightly concave downward. A plot of this curve oes serve to indicate the occurrence of critical conditions by not intersecting the 45° line as mentioned by Whitney.

The Denver Office of the Bureau of Reclamation is currently checking a rogram of computing water surface profiles by Method A using the IBM 650 lectronic computer.

SETTLING PROPERTIES OF SUSPENSIONS[a]

Closure by Ronald T. McLaughlin

RONALD T. McLAUGHLIN,[35] A. M. ASCE.—The research described is far rom complete, and there is ample opportunity for correction and expansion. hus, the discussions presented are a valuable addition to the material herein.

Bush and Ho have emphasized one of the key problems of settling analysis. ow can adequate initial mixing be provided before settling starts without leav- g enough turbulence to affect the first few minutes of settling? During the esearch described herein, considerable time and effort were devoted to this uestion. In one series of tests a suspension was made up of water and a small mount of the standard asbestos used for preparing gooch crucibles. This sus- ension was mixed by the same method used for the clay and alum suspensions. t the end of the mixing, the asbestos suspension was poured into the settling be by means of a large funnel. The motion of the asbestos particles was ob- erved. Within about 45 sec only a few particles were observed to have up- ard motion. By the end of 120 sec, any upward motion of particles was slow nd similar to motion caused by convection currents. Even this motion dis- ppeared in 1 min or 2 min. Thus, the turbulence did not seem to be significant r 10 min as reported in the study.

During the test with asbestos particles an attempt was made to guess the rder of magnitude of the coefficient of diffusion, e_z. A number of settling alyses had already been made in a turbulence jar of the type described by ouse.[15] As part of these analyses, several values of e_z had been measured. ecause of the experience of making these measurements, the writer felt that the tests with asbestos particles the value of e_z would be less than 10 cm^2 r sec immediately after the end of pouring the suspension into the settling be and less than 5 cm^2 per sec 2 min later.

The magnitude of e_z is not the only factor to be considered in determining e affect of turbulence on $\overline{w}$. The second term on the right hand side of Eq. 3 the analysis shows that the slope of the concentration profile must be known. rom Figs. 7 and 9 of the paper, it will be seen that this slope is small for nall values of t except near the surface of the suspension. Similar results re observed during settling analyses of domestic sewage. The reason for ese small slopes has been presented in Section 4 (e) of the paper.

The slope of the concentration profiles in Fig. 7 can be measured directly. t = 250 sec this slope is negligible for depths greater than 40 cm. At z 0 cm, the slope is given by

$$\frac{\partial \phi}{\partial z} = \frac{\Delta \phi}{\Delta z} = 0.0024\ \phi\ (z, 0)\ \text{gm per cm}^4 \quad \ldots\ldots\ldots\ldots (1)$$

---

[a] December 1959, by Ronald T. McLaughlin (Proc. Paper 2311).

[35] San. Engr., Bangkok, Thailand.

Assuming that $e_z = 5$ cm^2 per sec gives

$$e_z \frac{\partial \phi}{\partial z} = 0.012\ \phi\ (z, 0) \text{ gm per cm}^2 \text{ per sec} \quad \ldots\ldots\ldots (2$$

Since $\phi = 0.96\ \phi\ (z, 0)$ at $z = 20$ cm and $t = 250$ sec

$$\frac{e_z}{\phi} \frac{\partial \phi}{\partial z} = \frac{0.012}{0.96} = 0.013 \text{ cm per sec} \quad \ldots\ldots\ldots\ldots (3$$

Therefore, the estimated effect of turbulence at depth of 20 cm and a time o 250 sec is equivalent to a mean settling velocity of about 0.01 cm per sec.

For smaller values of t, the value of e_z would be greater, but the slope o the concentration profile would be smaller. As a rough estimate, it might b said that during the first 250 sec of the analysis the mean settling velocity wa reduced by 0.01 cm per sec because of turbulence. When this turbulence de cayed, the settling velocity would appear to increase by that substance. Fo greater depths the effect would be less because the slope of the profile is less For example, at $z = 80$ cm and $t = 500$ sec, the slope of the profile is abou $0.0014\ \phi\ (z, 0)$ gm per cm^4 whereas e_z might be only 2 cm^2 per sec. Since $= 0.925\ \phi\ (z, 0)$, the equivalent settling velocity would be only 0.003 cm per sec When these values of equivalent $\overline{w}$ are compared with Fig. 8 of the manuscript it is seen that the increase because of decaying turbulence is small compare to the total increase in $\overline{w}$.

The writer feels that whereas the analysis is correct in principle, the effec of the turbulence does not invalidate the conclusions for the particular set o data presented. However, the effect should be investigated carefully for eac settling analysis, and if it appears to be large, some refinement of the experi ment will be necessary.

Hall, in his study, is concerned with using settling analysis as part of practical design procedure. Therefore, he has developed a simple test that h feels is more practical. It is not, however, correct to assume that a test i more practical because it is more simple. Whether a test is practical or no is determined by the useful information or understanding supplied for a give amount of time, money, and effort. If a test is so simple that it does not brin to light some important information, it may be quite impractical. The write has spent as much as a whole day talking with engineers who are trying t solve a particular sedimentation problem. They are usually certain that an but the simplest test will be impractical. In the same amount of time, one da it has often been possible to obtain a sample of the suspension, bring it to th laboratory, and perform a settling analysis. Once a simple multiple depth tub has been constructed and calibrated, the analysis can be performed in any lab oratory that is set up for determination of suspended solids.

The test developed by Hall is based on three assumptions about how the se tling of sewage proceeds. Steps 1 and 2 and the related assumptions, a and of the study can be accepted. However, step 3 and the resulting assumption, do not seem reasonable. Step 3 states that floc have negligible velocity unt they reach a critical size and then they settle rapidly. Floc, once formed, ar simply particles; they may have complicated structure and shape, but they ar particles nevertheless. If they behaved as assumed by Hall, a graph of settli velocity as ordinate against particle size as absiissa would show no velocit until a critical size were reached. At that size, the velocity would sudden jump to a large value. Such a graph is not to be found among the curves th

ne usually finds in the literature. Therefore, the sudden jump in velocity ust be caused by a sudden change in particle size, particle shape, or orienta- on. If a particle increases in size only by joining with particles small enough have no velocity, the increase in size must be gradual. Hence, the increase velocity must be gradual. There could be a sudden increase in size if a floc article joined another particle of significant size. But then both of the parti- es would be of significant size before joining and would both have a settling elocity, which is contrary to the assumption. The same argument holds for article shape and orientation.

Hall also states that samples from the surface of quiescent sewage reflect e settling characteristics of the sewage. This statement can be examined by onsidering the rectangular settling tank shown in Fig. 11 (a) of the paper. aking samples at intervals of time from the surface of the suspension in a ettling tube is equivalent to taking samples at the surface, $z = 0$, of the tank r successive values of x. The removal of particles due to settling is de- rmined by the complete concentration profile at each value of x. Therefore, easurements at the surface will be related to removal only if the concentra- on of particles at the surface is the average of the concentration throughout e depth of the tank. Unfortunately, the surface is the one place where the oncentration is least likely to equal the average concentration; it will almost ways be less than the average. If, as suggested by Hall, the efficiency of set- ng is based on measurements at the surface, it will usually be impossible to tain 100% efficiency, even in an ideal tank.

Fischerstroem questions the way in which the lines are drawn on the various ncentration profile diagrams. He suggests, correctly, that the lines of con- ant t should all pass through the origin, $\phi\ (z, t) = 0$, $z = 0$. In Fig. 5, where e diagram is explained, the lines of constant t are drawn in this manner. ey are not in Figs. 7 and 9 because there were not enough data near the sur- ce to give the exact shape of the profile. For purposes of computation, each ofile was assumed to have a straight line section from the origin to the up- r end of the profiles drawn.

It is also suggested in the analysis that the lines of constant z/t should all ss through the point $\phi = 100\%$, $z = 0$. In order to settle this question, it is cessary first to consider a suspension of particles that settle without floc- lation. The particle concentration in this suspension is assumed to be small ough not to affect the settling velocities of the particles. In such a suspen- on, the particles of settling velocity, w_i, at the beginning of settling will have same velocity until they reach the bottom of the suspension. When these articles settle in a tube of the type shown in Fig. 5, their concentration will a function of only z and t. Hence, it can be written $f_i\ (z, t)$; at $t = 0$ this func- n will have the value $f_i\ (z, 0)$.

Because the particles settle without flocculation or hindrance, the spatial tribution of i-particles settles as a unit, independent of the particles of oth- velocities. In time t, the whole unit settles a distance $w_i t$. It follows that concentration of i-particles at the depth z and time t is the same as that ncentration was at the depth $z - w_i t$ and time $t = 0$. Therefore, it is possible write

$$f_i\ (z, t) = f_i\ (z - w_i t, 0) \quad \ldots\ldots\ldots\ldots\ldots\ldots (4)$$

Both sides of Eq. 4 can be summed over all values of i to give

$$\sum_{w_i=0}^{w_i=\infty} f_i(z, t) = \sum_{w_i=0}^{w_i=\infty} f_i(z - w_i t, 0) \quad \ldots\ldots\ldots\ldots (5$$

However, any particle with w_i greater than z/t will have settled a distanc greater than z in time t, and it will no longer be in suspension at that point Therefore, the summation need only include values of i up to $w_i = z/t$. Eq. then becomes

$$\sum_{w_i=0}^{w_i=z/t} f_i(z, t) = \sum_{w_i=0}^{w_i=z/t} f_i(z - w_i t, 0) \quad \ldots\ldots\ldots (6$$

For a constant value of z/t the particle concentration is exactly the le hand side of Eq. 6. Therefore

$$\left[\phi(z, t)\right]_{z/t=K} = \sum_{w_i=0}^{w_i=K} f_i(z - w_i t, 0) \quad \ldots\ldots\ldots\ldots (7$$

in which $z/t = K$, a constant

Eq. 7 is the equation of a line of constant z/t in a concentration profile di agram. It is now possible to examine what happens when both z and t approac zero along one of these lines. In order to avoid mathematical complications a the limit, it is convenient to substitute z/K for t in Eq. 7 and let z approac zero. Accordingly

$$\phi\left(z, \frac{z}{K}\right) = \sum_{w_i=0}^{w_i=K} f_i\left[z\left(1 - \frac{w_i}{K}\right), 0\right] \quad \ldots\ldots\ldots\ldots (8$$

As z goes to zero, Eq. 8 becomes

$$\phi(0, 0)_{z/t=K} = \sum_{w_i=0}^{w_i=K} f_i(0, 0) \quad \ldots\ldots\ldots\ldots (9$$

The right hand side of Eq. 9 is simply the concentration of particles wi settling velocity equal to or less than K at $z = 0$ and $t = 0$. It follows that t points where the lines of constant z/t cross the axis $z = 0$ on the concentrati profile diagram are determined by the frequency function of the settling vel cities at the surface of the suspension at the beginning of settling. In fact, t spacing of the lines of constant z/t along the axis will give directly the valu of ϕ for a cumulative distribution of settling velocities at $z = 0$, $t = 0$. If t

articles of all settling velocities are distributed uniformly throughout the suspension at t = 0, this cumulative distribution at the surface is also the cumulative distribution for the whole suspension.

This result, obtained for settling without hindrance of flocculation, also hows what happens when these two processes occur. At the surface of the uspension at the beginning of settling, there has been no time for flocculation o take place. The settling velocity distribution is determined by the nature of ne particles, the properties of the fluid, and the concentration of particles. 'or that initial instant, before change in concentration or flocculation have beome significant, the settling is similar to that for which Eq. 9 was derived. 'he initial, instantaneous frequency distribution of settling velocities deterines where the lines of constant z/t meet the axis. Immediately after this nstant, flocculation and change in particle concentration have produced some ffect. Thereafter, the spacing of the lines of constant z/t are no longer reated to any frequency distribution of settling velocities.

Because it is not yet possible to measure the frequency distribution at z = 0 nd t = 0, the lines of constant z/t in Figs. 5, 7, and 9 have not been extended o the axis. Otherwise, if the results of a multiple-depth analysis indicated nat the lines of constant z/t could be extrapolated to the axis with confidence, he result would be the initial instantaneous frequency distribution at z = 0. If, n addition there were good reason to believe that the particles of each settling eiocity were uniformly distributed at t = 0, the frequency distribution obtained ould represent the whole suspension at t = 0. This is only one of several ays in which the lines of constant z/t can be used to analyze the results of a nultiple-depth settling analysis. Others are explained in the original thesis (12) nat describes the research on which the paper is based.

Fischerstroem also deals with the use of settling analysis in the design of ettling tanks. It should be understood that there was no intention in the paper f indicating that settling tanks could be designed solely on the results of setling analysis. The intention was to show how the settling properties of the uspension should be considered as part of the design study. In this regard, it as stated that for certain suspensions, the removal of particles during setling will depend more on detention time than on overflow rate. For other susensions, the removal will depend more on overflow rate. The concentration rofile diagram will give a good indication of which one is more important.

The writer also concluded from Fig. 9 of the paper, that at depths greater nan those shown in the figure, the removal will depend primarily on detention me. It is to be emphasized that this conclusion pertains only to the suspenion used by Fitch and is not general. Fig. 1 of the discussion actually suports the conclusion. The lines of removal at constant time are approaching ie vertical as the depth approaches 5 ft. There is good reason to believe that greater depths these lines will be essentially vertical and straight. For ose depths at which the lines are vertical and straight, there is only one reoval for each detention time.

The analysis attempts to establish the superiority of shallow settling tanks. his point will be considered in order to show the error of making a general onclusion about settling tanks without considering the suspension. Fischeroem states that for a given detention time, a shallow basin will always give greater removal than a deeper one. This is true because the particles have shorter distance to settle in a given length of time. Otherwise, it can also e said that when flocculation occurs, particles are continually increasing their elocity as their size increases until a limiting size is reached. Therefore,

the average particle velocity in shallow basins is less than the average in deep
er basins. In decreasing the depth, only the slowest part of the particle motio
is used.

Fischerstroem makes a similar statement in another way. The only possi
bility, he states, of increasing volume load is decreasing the overflow rat
This statement and the preceding one appear to be based on the assumption th
the primary objective in the design of settling tanks is to use the smallest vo
ume for a given flow of suspension and percentage removal. The real objec
tive, however, would seem to be the smallest cost for a given flow of suspen
sion and percentage removal. This cost includes, land, excavation, and co
struction, as well as operating costs. The cost of excavation depends on ta
volume unless there is a change from soil to rock within the depth of the tan
The cost of land depends on the horizontal area of the tank, while the cost
construction probably depends on the area of the inside surface of the tan
For equipment such as scrapers to remove sludge, the cost probably increase
with area more than with depth.

To show how these items are related to the settling properties, the examp
used by Fischerstroem will be used: Assume that 90% of the suspended soli
are to be removed when the suspension represented by Fig. 9 flows through

TABLE 4.—COMPARISON OF TANKS OF 3 DEPTHS

Tank	D	T	$\frac{D}{T}$	L	B	U	LBD	LB	S	$\frac{LBD}{LBD_3}$	$\frac{LB}{LB_3}$	$\frac{S}{S_3}$
#	ft	hr		ft	ft	fps	ft^3	ft^2	ft^2			
1	0.8	2.0	0.4	250	12.5	0.035	2500	3130	3541	0.70	4.32	2.43
2	2.8	2.5	1.1	150	7.5	0.017	3120	1140	1928	0.87	1.58	1.33
3	5.0	2.9	1.7	120	6.0	0.012	3600	720	1445	1.00	1.00	1.00

rectangular settling tank represented by Fig. 11 (a). From Fig. 1 of the di
cussion, the overflow rate, depth, and detention time can be determined f
three depths. These are shown in the first four columns of Table 4; two of t
three overflow rates are those chosen by Fischerstroem, and the third was s
lected to give a greater variation in depth.

For the purposes of computation assume that the length-width ratio of t
tanks will be 20:1 and that the rate of flow will be 1,250 ft^3 per hr. There
now enough information to compute the values of length, L, width, B, and me
flow velocity, U. These are shown in Table D1. The greatest velocity is 0.0
ft per sec and it occurs in the tank of least depth. Work by A. C. Ingersoll,
ASCE, and McLaughlin[36] indicates that if the mean velocity in the shallow ta
were much higher, the settled particles at the bottom would be resuspended
the flowing suspension. Hence, the assumed value of flow is an upper limit f
the length-width ratio assumed.

The volume, L B D, the horizontal area, L B, and the area, S, of the insi
surface can now be computed, and they are shown in Table 4. For the purpos
of comparison, the ratio of volume to the volume of tank number 3 is shown

36 "The Resuspension of Flocculent Solids in Sedimentation Basins," by A. C. Ing
soll and R. T. McLaughlin, California Inst. of Technology, Sedimentation Lab., May 19

able 4 along with similar ratios for horizontal area and inside surface. In ecreasing the tank depth from 5.0 ft to 0.8 ft the volume is reduced by about 0%. At the same time, the horizontal area is increased by about 330%, and the side surface area is increased by about 140%. Except for cases where excation is expensive, it seems that the tank of depth 5.0 will be cheaper.

Using Fig. 1 of the analysis, it is possible to explain why the example turns ut as it does. Between the depths of 0.8 ft and 5 ft, the curve of removal for constant detention time of 2 hr is steep. The residual increases from 10% to bout 17%, whereas the particles have to settle almost more than five times the stance in the same length of time. As the depth is increased, the flocculation nd the settling velocities are increased, allowing the particles to almost cover e increased distance. It is the last part of the settling that is the fastest and at increases the distance covered. Consequently, reducing the tank depth om 5 ft to 0.8 ft reduces the distance that the particles must settle, but it akes use of the earliest and, hence, lowest settling velocities. Therefore, the fectiveness of the settling is less in the shallow tank.

The analysis by Gunnerson emphasizes that the suspension analyzed should the actual suspension that will do the settling. The settling analyses were rformed on effluents from treatment plants, whereas the suspensions to be nsidered were the effluents mixed with sea-water. The addition of sea-water oduced a suspension of different characteristics, apparently with greater ndency toward flocculation. As mentioned by Gunnerson, the effect of seaater should be studied as part of the analysis.

UNSTEADY FLOW OF GROUND WATER INTO A SURFACE RESERVOIR[a]

Closure by William Haushild and Gordon Kruse

WILLIAM HAUSHILD[19] and GORDON KRUSE,[20] A. M. ASCE.—The discus-
ons indicate interest in the material presented in the paper and have con-
ibuted toward expansion and understanding of the solutions for the nonlinear
se of flow of ground water into a surface reservoir.

The discrepancy shown in Fig. 2 between the experimental data and Solu-
ons I and III, which were based on Eq. 7 is indicative of the error resulting
om neglecting the nonlinear terms in Eq. 6 if d is small. Solutions II and IV
e based on the assumption $H << d$, inasmuch as they were developed from
lutions I and III; however, they are not limited by the assumption because
ey consider the exact saturated thickness of the aquifer through which the
w occurs. The small amount of data available for comparison with Solu-
ons II and IV indicates that their use might be preferable to the error-function
lutions, Solutions I and III. The experiment to which the solutions were ap-
ied was a complete drawdown case and d was not large compared to H. Solu-
ons II and IV agreed well with the experimental data although the assumptions
re not completely satisfied. When the drawdown is small, Solutions II and
give results which are nearly equal to those obtained from Solution I. There-
re, the use of Solution II or IV should give good results over the full range
drawdown.

Harr, in considering the steady state form of Eq. 7, represents the water
ble condition before the reservoir surface is lowered. Therefore, the solu-
n would be expected to be linear, Eqs. 24 and 25. Eq. 28, the solution of
. 26, corresponds with Soltuion IV, presented by the writers, only for the
se of complete drawdown. The consideration of Eq. 7 in the form of Eq. 26
ems questionable. If η is the difference in elevation between the water ta-
e and the underlying impermeable layer, the flow through a vertical section
the saturated aquifer is

$$F = K \eta \frac{\partial \eta}{\partial x} \quad \ldots\ldots\ldots\ldots\ldots\ldots (45)$$

e continuity equation becomes

$$\frac{\partial F}{\partial x} = V \frac{\partial \eta}{\partial t} \quad \ldots\ldots\ldots\ldots\ldots\ldots (46)$$

---

a July 1960, by William Haushild and Gordon Kruse (Proc. Paper 2551).
19 Hydr. Engr., Quality Water Branch, U.S.G.S., Fort Collins, Colo.
20 Agric. Engr., Soil and Water Conservation Research Div., Agric. Research Serv-
, U. S. Dept. of Agric., Fort Collins, Colo.

or

$$K \frac{\partial}{\partial x}\left(\eta \frac{\partial \eta}{\partial x}\right) = V \frac{\partial \eta}{\partial t} \quad \ldots\ldots\ldots\ldots\ldots\ldots (47$$

Now considering

$$\frac{1}{2}\frac{\partial^2 \eta^2}{\partial x^2} = \frac{1}{2}\frac{\partial}{\partial x}\left(\frac{\partial \eta^2}{\partial x}\right) = \frac{1}{2}\frac{\partial}{\partial x}\left(2\eta \frac{\partial \eta}{\partial x}\right)$$

the continuity equation becomes

$$\frac{K}{2}\left(\frac{\partial^2 \eta^2}{\partial x^2}\right) = V \frac{\partial \eta}{\partial t} \quad \ldots\ldots\ldots\ldots\ldots\ldots (48$$

Comparison of Eq. 48 with Eq. 26 shows Eq. 26 does not represent the physica conditions of the problem. Also the α used in Eq. 30 is not the same as the defined by the writers.

TABLE 3.—BANK STORAGE DATA—TRANSIENT CASE[a]

x, feet	h/H	x, feet	h/H	x, feet	h/H
0.7	-0.413	13.5	0.211	48.5	0.483
2.7	-0.223	18.5	0.313	58.5	0.491
4.5	-0.120	28.5	0.420	68.5	0.495
8.5	0.057	38.5	0.465	71.7	0.496

(Table Courtesy of Keller and Robinson)

D = 3.20 ft V = 0.255

K = 0.034 ft/sec $\alpha = \frac{KD}{V} = 0.4266$ sq ft per sec

[a] All readings taken 6.5 min after lowering of reservoir.

Kazmann emphasized that the paper of Keller and Robinson[8] contained on steady state data. The only non-steady state laboratory data collected by Ke ler and Robinson were obtained directly from Robinson's files by the writer Unfortunately they did not note that the data were not published. However, t experimental procedure and equipment is described by Keller and Robinso The non-steady state data shown in Table 3, with permission of Keller, we collected at a time of 6.5 min after the start of the experiment. The elevati of the water table in the aquifer was being lowered at the time of the measur ments; however, the water surface in the headbox was still unaffected.

Although the writers believed that the error-function solution of Eq. 7 w well known by the profession, they are indebted to Kazmann for the referen to Rorabaugh's adaptation and publication[11,12] of the error-function soluti in connection with ground water studies.

The writers have not assured the profession that the results may be appli in the field. Rather, the application to each particular field location must

onsidered with regard to the relation between field conditions and the experi-
ental conditions and assumptions. Because of the unknown variations of field
onditions, field verifications can hardly be used to prove or disprove the so-
tions presented in the paper. However, field studies will indicate the useful-
ess of the solutions. Any applicable field data with which the formula could
e compared would be welcomed.

Moody's solution is a valuable contribution and should be useful and easily
pplied in the tabulated form of Table 2. His solution agrees well with Solu-
on II presented by the writers who agree that sufficient accuracy is obtain-
ble by second degree interpolation in Fig. 4 and Table 2.

The experimental data of Keller and Robinson are approximated more close-
by Solution IV of the writers than by Eq. 37. This may be due to error in
ie determination of α. In a laboratory flume, with an appreciable capillary
inge and a time lag in the drainage of the voids, the specific yield is difficult
evaluate.

The writers are grateful to Iyengar for emphasizing the method of perturba-
on approach to approximating the exact solutions of Eq. 6. It is interesting
at this method and the approach used by the writers lead to identical results.

Corrections.—The second term on the left side of Eq. 6 as presented in
oody's analysis should be

$$\frac{\alpha}{D}\left(\frac{\partial \eta}{\partial x}\right)^2$$

NEEDS IN SEDIMENTATION[a]

Discussion by Paul F. Keim and Vito A. Vanoni

PAUL F. KEIM,[2] F. ASCE.—Einstein's observations bring to mind the following experience.

In 1939 the writer, then with the Federal Power Commission had occasion to make some investigation on the development of the Trinity River of Texas for navigation, flood control, and power. No less than a dozen professional men and local farmers while standing with the writer on various bridges across tributaries in the headwaters of the river sadly related that they once fished here in crystal clear and quite swift water. At the time the silt was nearly up to the lower level of the trusses with practically no channel space whatsoever for the muddy flow. Certainly this is repeated in many other places as a result of the profligate use and unscientific development of lands and water. As an aside, it is not only silt which has clogged clear streams; witness the uncontrolled disposal of waste in many areas.

The author rightly states, "most of the artificial storage for water supply is provided in the form of surface reservoirs. These reservoirs change the regime of the rivers drastically particularly with respect to their sediment characteristics: . . ." That being the case, it is a certainty that the relative stability of channel shape and slope that has been reached under natural conditions will be disturbed. How much disturbed and what the resulting condition occasioned by the disturbance will be as of 1961 is largely guess work. The pertinency of Einstein's conclusion is unquestioned if it is desired to obtain the maximum use of our river systems.

In Egypt it is not one but a series of detention and diversion dams on the Nile above and below each of which sediment has created problems; problems will recur when the Aswan Dam shall have been completed. The Colorado River has posed many problems which were not specifically anticipated, but could have been if Einstein's suggestions had been formulated and accepted as a concommitant part of the planning for river system development.

It is not that the engineers outlook is just less rosy than the layman and politician. It is that he understands that there are bound to be reactions when equilibrium is upset, the results of which cannot be anticipated unless studies are made to determine the range of possibilities.

The engineering approach philosophy as developed by Einstein is a contribution to both scientific and engineering activity. If heeded, this philosophy can be used to great advantage in the planning of an orderly and economic development of river systems and other natural resources.

---

[a] March 1961, by H. A. Einstein (Proc. Paper 2756).

[2] Prof., Civ. Engrg. Univ. of California, Berkeley, Calif., on leave to Dept. of State as Tech. Advisor, USOM/UAR, Cairo, Egypt (UAR).

VITO A. VANONI,[3] F. ASCE.—The author has outlined two important sets of sedimentation problems in connection with developmnet of water resources in general, and reservoir development in particular. The writer agrees with the author that: (1) these are important problems, (2) existing knowledge is inadequate to cope with them, and (3) research is needed in this area. These are problems of sediment transportation under unsteady and non-uniform conditions. Transportation under steady uniform conditions, which has received the major part of the total effort in sedimentation research, is far from solved and the more difficult non-steady and non-uniform transport problem has hardly been touched. Major dams are being built at an increasing rate, and new ones are being authorized at costs running into many tens of millions of dollars. As the dams are completed, the sedimentation problems grow more numerous and the need for information to cope with them more pressing. Activities in sedimentation research, although increasing in the past two decades, show only modest increase in effort, compared to dam construction and the importance of the sedimentation problems accompanying their construction. It is urgent that adequate research programs be started at once to deal with these and other such problems.

The author has indicated that in dealing with the sedimentation problems of reservoirs, he was assuming the position of the engineer. The writer agrees that if the answers needed to guide engineering work are to be obtained in time the engineering approach must be pursued. However, the writer would like to argue that it would be unsound to follow the engineering approach at the exclusion of basic research into the transport phenomena. Such basic research yields information slowly, but it forms the basis for improving methods for dealing with streams. It will provide a basis, not only for dealing with problems that are known today, but also for the multitude of new ones that are certain to be exposed in the future.

The question arises, who is responsible for seeing to it that research is done so information will be available to solve these sedimentation problems? Who shall take the initiative to get the research done? This wirter believes that to initiate research is the responsibility of the same people and organizations who build the projects, operate them, and cope with the sedimentation problems. These organizations are the ones which know the magnitude and nature of the problems, and the success they are having in dealing with them. Therefore, they are the best judges of the adequacy of their methods. Looking further within these organizations, it is clear that the professional civil engineer is intimately involved in this matter. He is the one the administrator depends on to estimate funds needed for construction and operation of projects and for research, as well.

The funds will be provided by the organization, which in most cases is the public, but the program must be made out by the technical expert, in this case the professional civil engineer. Funds needed for research are nominal, compared to expenditures for project construction and operation. One item that is important is time. It takes time to train research engineers, and to do research. Crash programs with large budgets are not the answer. For success continuing support of research is needed, which means that it is urgent that start on adequate programs of research on the problems outlined by the author be made now.

---

[3] Assoc. Prof., Hydr., Calif. Inst. of Tech., Pasadena, Calif.

VIBRATION PROBLEMS IN HYDRAULIC STRUCTURES[a]

Discussion by John Parmakian

JOHN PARMAKIAN,[22] F. ASCE.—It is hoped that the following additional xamples where vibration occurred in certain hydraulic structures will amlify Campbell's excellent paper.

With reference to the probable coefficient of rolling friction for gate strucures utilizing rollers or wheels, caution should be used by the designer in esmating the coefficient under field conditions, especially when the gate is subnerged for long periods. To illustrate an extreme case, at one installation here are three 12-ft 7-in. wide by 23-ft 5-in. high fixed wheel gates which are sed to shut off the flow in each penstock intake. There are twenty-two 15-in. iameter forged steel wheels on each gate. The wheel bushings are of the self-ubricating, bronze type, with graphited inserts and are not considered to require any further maintenance after the initial installation. The 4-1/2-in. dimeter wheel pins are chrome-plated SAE 1040 steel. These gates are stored nder water above the penstock intake openings. After being submerged for bout 10 yr it was necessary to make an emergency shut-down of a set of these ntake gates with nearly full flow passing through the turbine. The first two ntake gates closed completely without difficulty. However, there was little nbalanced pressure on these gates since the flow through the remaining openng was sufficiently large to supply water through the turbine. As the final inake gate was lowered under unbalanced pressure conditions, the gate stem and rane started to vibrate when the gate was about one-third closed. The vibraon soon reached violent proportions as the gate continued to close in jerks. he gate finally stopped when it was still approximately 8 ft open.

The gate was later hoisted to the surface for inspection. An examination of he twenty-two wheels indicated that only one of the wheels had rotated during he partial gate closure and that all of the other wheels had skidded on the rack. By using pinch bars and sledge hammer blows it was possible to free ost of the wheels so that they could be made to turn. However, several of the heels could not be freed at all and had to be disassembled. A similar condion was observed at all of the other fixed wheel gates at this installation. ence, the failure of the intake gates to close under unbalanced flow conditions as due primarily to the failure of the wheels to rotate and roll on the track fter having been submerged for a number of years. The graphited inserts ere subsequently scraped off and grease fittings installed on all wheels. Peiodical greasing of the wheel pins is now required to insure that the wheels ill rotate.

---

a March 1961, by Frank B. Campbell (Proc. Paper 2772).
22 Chf, Tech. Engr., Analysis Branch, Div. of Design, USBR, Denver, Colo.

In the section "Other Exciting Forces" the author indicates that the fixe cavity which forms on the trailing side of an obstruction in high velocity flo may produce an intermittent pressure pulse and hence a source of vibratio An example of this type of vibration occurred at a high-head outlet work where severe vibration and noise were present at only one of three outlet pipe This occurred when the pipe was discharging in excess of 0.6 of its rated capa city. The vibration of the pipe and the noise were considered serious enoug to restrict the operation of the outlet pipe to not more than half of its full capa city. When field conditions permitted, the outlet pipe was unwatered and th upstream ring follower gate frame and leaf inspected. With the gate latched i its open position the ring follower leaf was found to be 11/32 of an inch to high. This irregularity in the alinement of the circular opening in the leaf wit respect to the conduit caused sufficient turbulence in the high velocity flo downstream from the gate leaf to produce the objectionable vibration and nois in the outlet tube.

Objectionable vibration has also been observed at several cylinder gate in stallations, especially when the gate openings were small. At one installatio a 20-ft 2-in. diameter, 66,000-lb cylinder gate is suspended on three 5-1/2-i steel stems, 136 ft long. Vibration of the gate during flow regulation has oc curred from its initial operation. Various remedies were attempted in an ef fort to prevent the vibration. Initially the small guide shoe clearances provide some friction damping and the vibration was not too objectionable. Howeve as the wear of the shoes increased these clearances, there was a correspond ing increase in the vibration amplitude. Spring loaded shoes were tried b were found to be ineffective. The vibration was reduced somewhat by modify ing the lower edge of the gate so as to discharge as a sharp-edged orifice.

Severe vibration under conditions of small gate openings with unbalance heads was also observed at a 32-ft diameter cylinder gate. This 330,000- gate is suspended by three steel stems, 7-3/4-in. O. D. by 4-5/8-in. I. D approximately 330 ft long. In order to reduce the hydraulic downpull on th gate stems, the cylinder gate was modified by removing part of the tapered ga bottom. This modification also produced a slight reduction in the vibratio

At another installation a cylinder gate 20 ft 4 in. in diameter weighing approx imately 85,000 lb is suspended on three 4-1/2-in. diameter steel stems, 330 long. During the initial operation severe vibration of the gate developed small gate openings. The observed frequency was about 6 cycles per sec an the amplitude approximately 1 in. At this installation a viscous damping devic together with a serrated gate bottom will be tried to reduce the vibration.

VECTOR ASPECTS OF DYNAMIC SIMILARITY[a]

Discussion by Charles E. Behlke and James R. Steven

CHARLES E. BEHLKE,[12] M. ASCE.—The authors state four difficulties which often arise in distorted open channel models. It has been the writer's experience that each of the difficulties are also encountered in non-distorted models.

If only steady flow is considered, assuming the Chezy resistance equation and hydrostatic pressure distribution, the equation of motion along a streamline is

$$V \frac{\partial V}{\partial s} + g \frac{\partial z}{\partial s} + g \frac{V |V|}{C^2 h} = 0 \quad \ldots\ldots\ldots\ldots (45)$$

In which s is a displacement along a streamline, V describes the velocity, C refers to the Chezy coefficient, h is the depth, and z denotes the elevation of the water surface above an arbitrarily chosen datum plane. The writer has chosen the Chezy resistance equation simply for study purposes.

Normal to the streamline

$$\frac{V^2}{r} = g \frac{\partial z}{\partial n} \quad \ldots\ldots\ldots\ldots\ldots\ldots (46)$$

In which r is the radius of curvature of the streamline, n denotes the distance measured normal to the streamline, and V refers to the velocity along the streamline as in Eq. 45.

The first term of Eq. 45 is an acceleration and the other two terms represent forces. In Eq. 46, the term on the left side of the equation is an acceleration and the term on the right side of the equation represents a force. Except for freely falling particles, fluid particles in open channel models do not experience an acceleration equal to that of gravity.

The equations of motion must apply to the model as well as to the prototype. The following equations define the scales between model and prototype:

$$V_r = \frac{V_{model}}{V_{proto}} \quad \ldots\ldots\ldots\ldots\ldots\ldots (47a)$$

$$S_r = \frac{(\text{displacement along a streamline})_{model}}{(\text{displacement along a streamline})_{proto}} \quad \ldots\ldots\ldots (47b)$$

$$h_r = \frac{(\text{depth})_{model}}{(\text{depth})_{proto}} = \text{vertical scale} \quad \ldots\ldots\ldots (47c)$$

---

a March 1961, by R. C. Kolf and W. L. Reitmeyer (Proc. Paper 2763).
12 Assoc. Prof. of Civ. Engrg., Oregon State Univ., Corvallis, Oreg.

and

$$C_r = \frac{(\text{Chezy C})_{\text{model}}}{(\text{Chezy C})_{\text{proto}}} \quad \ldots\ldots\ldots\ldots\ldots\ldots (47d)$$

Then for the model

$$\frac{V_r^2}{S_r} V \frac{\partial V}{\partial s} + g \frac{h_r}{S_r} \frac{\partial z}{\partial s} + g \frac{V_r^2}{C_r^2 h_r} \frac{V |V|}{C^2 h} = 0 \quad \ldots\ldots\ldots (48$$

in which V, h, s, z, and C are still those of the prototype from Eq. 45. Norma to the streamline in the model

$$\frac{V_r^2}{r_r} \frac{V^2}{r} = g \frac{h_r}{S_r} \frac{\partial z}{\partial n} \quad \ldots\ldots\ldots\ldots\ldots\ldots (49$$

Dynamic similarity is satisfied if in Eq. 48

$$\frac{V_r^2}{r_r} = \frac{h_r}{S_r} = \frac{V_r^2}{C_r^2 h_r} \quad \ldots\ldots\ldots\ldots\ldots\ldots (50$$

and in Eq. 49

$$\frac{V_r^2}{r_r} = \frac{h_r}{S_r} \quad \ldots\ldots\ldots\ldots\ldots\ldots (51$$

If the horizontal length scale is l_r and the vertical scale is h_r, the flow i kinematically similar in model and prototype if, in addition of Eq. 50 and 5

$$r_r = l_r = n_r = S_r \quad \ldots\ldots\ldots\ldots\ldots\ldots (52$$

Thus, from Eqs. 50, 51, and 52

$$\frac{V_r^2}{S_r} = \frac{V_r^2}{r_r} = a_r, \quad \ldots\ldots\ldots\ldots\ldots\ldots (5$$

in which a_r is the acceleration scale between model and prototype. This sca ratio need not be unity as indicated by the authors.

Eq. 53, which is the result of Eqs. 50, 51, and 52, indicates that the accele ation scale is the same for both tangential and normal accelerations. The equa tions of motion, then, clearly indicate that the acceleration ratio is not equal the gravity scale (unity) between model and prototype as indicated by Eq. 3

From Eqs. 50 and 52

$$\frac{V_r^2}{l_r} = \frac{h_r}{l_r} = \frac{h_r}{l_r} \quad \ldots\ldots\ldots\ldots\ldots\ldots (5$$

nd from Eqs. 51 and 52

$$\frac{V_r^2}{r_r} = \frac{V_r^2}{l_r} = \frac{h_r}{l_r} \quad \ldots\ldots\ldots\ldots\ldots\ldots (55)$$

From these equations, other useful equations can be written as

$$\frac{V_r^2}{h_r} = 1 \quad \ldots\ldots\ldots\ldots\ldots\ldots (56a)$$

nd

$$V_r^2 = C_r^2 \, h_r \, \alpha_r \quad \ldots\ldots\ldots\ldots\ldots\ldots (56b)$$

n which

$$\alpha_r = \frac{h_r}{l_r} = \text{the distortion} = \text{the slope scale} \quad \ldots\ldots\ldots (57)$$

o,

$$C_r^2 = \frac{l_r}{h_r} = \frac{1}{\alpha_r} \quad \ldots\ldots\ldots\ldots\ldots\ldots (58)$$

There is nothing which limits any of the foregoing equations to equal horizontal and vertical scales. Irregardless of the distortion of the model, if the preceding scale factor equations are satisfied, the fluid in the model acts exactly similar to that in the prototype.

If the model is too rough or too smooth, $C_r^2 \neq \frac{l_r}{h_r}$, and the streamlines in he model are not similar to those in the prototype. If the model is too rough, he model streamlines curves too much; and if it is too smooth, streamlines o not curve enough. This would be true for both distorted and non-distorted nodels and can also help explain many of the similarity difficulties which may rise in both types of models.

A plot of transport versus velocity for a specific depth can be made for the rototype and for the model. This usually indicates that the transport scale nanges with velocity. These changes in transport scale could be eliminated a suitable bed material could be found for the model. However, since an inite variation of density and grain size is not available, a substitute material ust usually be used. The results obtained from this bed material must be arefully evaluated because it will react differently from the ideal material.

The various things presented herein contribute more to the difficulties enountered in distorted models than the distortion itself, and the equations given ndicate that velocities must be scaled to the square root of the depth scale and ot to the square root of the horizontal scale if similarity is to exist over the ntire model.

JAMES R. STEVEN,[13] M. ASCE.—The authors present several concepts which should be examined carefully before they are accepted as generalized principles.

In Eqs. 6, 7, and 8, the motivating forces have been taken as those caused by viscosity, pressure and gravity. The authors have chosen, for this analysis, to neglect the forces due to elasticity and surface tension. The inertial force has been taken as the resultant of all forces and the usual dimensionless ratios F, R, and E have been obtained. The fact has not been recognized, however, that the Euler number, which is more accurately described physically as the pressure coefficient, must be the same at all corresponding points in two dynamically similar systems regardless of the particular basic forces which actually shape the motion. Therefore, pressure or more significantly pressure difference is not a basic or motivating factor that creates the fluid motion, but rather, it is a result of the motion itself. In general, in any solution in which viscosity and gravity are the only basic factors of practical importance other than the boundary geometry, a generalized solution can be expressed as

$$\frac{\Delta p}{\rho\ V^2} = f\ (\text{geometry, R, F}) \quad \ldots\ldots\ldots\ldots\ldots (59)$$

The classical example of this is flow past a cylinder. When the fluid is ideal and the cylinder is entirely immersed, the pressure coefficient is a function only of geometry as expressed in the equation for distribution of pressure on the surface of the cylinder

$$\frac{\Delta p}{\rho\ V^2} = \frac{1}{2}\left[1 - 4\ \sin^2\ \theta\right] \quad \ldots\ldots\ldots\ldots\ldots (60)$$

For flow of a real fluid under these same conditions, the pressure coefficient becomes a function of both the geometry and Reynold's number. When flows in two such cases are dynamically similar, the pressure coefficients will be identical at all corresponding points. This clearly shows the dependent rather than primary role played by pressure in fluid motion.

The authors have clearly emphasized the vector aspects of the equations. Eq. 7 conveys the sense of a system of vectors, in three dimensions, the scalar magnitudes of which as well as spacial directions, are due to the several basic factors. Consequently, division of each scalar magnitude by the scalar magnitude F_i represents, physically, reduction of the actual spacial vector diagram to a corresponding one of "unit" size. The spacial directions of the vectors remain unchanged. The scalar magnitudes of the unit vector diagram vectors are the dimensionless ratios R, F, and so forth. Obviously, for dynamic similarity between two systems, the scalar magnitudes of the corresponding parts of the unit vector diagrams must be equal. Derived in this sense, Eqs. 13, 14 and 15 have far greater physical significance than when viewed merely as the result of rearrangement of Eqs. 6 and 8.

The development of the Kolf number implies that this is a dimensionless ratio, similar in nature to the Reynold's, Froude, Weber, and Mach numbers in that it, like the others represents a ratio between basic forces at work in a system. This is not correct since the Reynold's number and the others relate primary agencies or motivating forces to the resultant or initial force. The

[13] Assoc. Prof. of Civ. Engrg., City Coll. of New York, New York, N. Y.

Kolf number does not do this because centrifugal force is not the result of a primary agency. The magnitude of the centrifugal force is determined entirely by the streamline geometry and the velocity. It is therefore a resultant rather than a motivating or basic element. Consequently, it is improper to suggest that the ratio V/u, which is simply an expression of kinematic similarity, has a common base with the Reynold's and Froude numbers. Actually V/u is an important ratio since the direction cosines of the resultant velocity vector V_r, neglecting radial components, are proportional to it. In fact this ratio in slightly different form has long been used in propeller analysis and hydraulic machinery under the name "slip function." Take the forward velocity of the ship as V and the tangential speed of the propeller tip as π D N. The ratio $\frac{V}{\pi D N}$ more usually expressed as $\frac{V}{ND}$ is the slip function. This is simply the reciprocal of the Kolf number.

FORECASTING RIVER RUNOFF BY COASTAL FLOW INDEX[a]

By Kenneth W. Wise

KENNETH W. WISE.[14]—It might be said that the final goal of any numerical analysis is to forecast events of the future. No one can change the facts of the past. About all that can be hoped for is a greater understanding of the present or initial state of things to serve as a guide in the predicting of the future state. To this end, all analyses are aimed. The forecasting technique presented by Rockwood and Jencks uses some unique forms of analytical logic which seem worthy of additional consideration and study. They are not entirely separable but fall into the following general categories:

1. Use of abstract indexes as forecast parameters;
2. Qualified acceptance of "Goodness of Fit" tests;
3. Use of product functions; and
4. Evaluating the relative significance of the variables.

There is a tendency by most forecasters to select factors for analysis which have a commonly-accepted high degree of causal relationship to the physical factor to be forecasted. The less obvious and direct the causal relationship is, the more abstract it becomes. But there are various degrees of abstraction. The use of winter runoff of coastal streams to forecast the spring runoff of Columbia River is probably a far more abstract relationship, on the basis of common acceptance, than the use of precipitation and snow course measurements from the area where the runoff of Columbia River originates.

The authors have rationalized the advantages of their uniquely defined Coastal Flow Index (CFI) over the use of other indexes by noting the deficiencies of precipitation and snow course measurements. They seem to be pointing toward conclusion that the runoff basins of the coastal streams constitute more adequate precipitation gages for an area several hundred miles distant than the standard U. S. Weather Bureau gages located in the area. The big argument in favor of this conclusion is that the coastal runoff basins provide a much larger sampling area.

The deficiencies of measuring streamflow from the coastal streams is rationalized as acceptable because deficiencies also exist in the measurement of other indexes such as precipitation and snow courses. Whenever rationalization is used to justify abstract considerations, the question is immediately raised regarding how much abstraction should be justified in this way. It has been emphasized that Columbia River seasonal runoff is partly a function of the prevailing westerly air flow and associated weather phenomena during the

[a] March 1961, by David M. Rockwood and Carlton E. Jencks (Proc. Paper 2780).
[14] Tech. Engr., U. S. Army Engr. Dist., Walla Walla, Wash.

previous winter season. This observed climatic persistency is the mediun through which the causal relationship is rationalized. Some of the other phe- nomena are partial functions of the same climatic conditions. However, they would not necessarily be considered as causing the variations in Columbia River runoff. Obviously the number of people using golf courses during the winter months at Portland, Ore., would not be considered as causing the Colum- bia River runoff to be greater or smaller, although the same climatic persis- tency medium could be used to rationalize their relationship.

The influences affecting precipitation from the time it falls to the ground until it reaches the gaging station are many and difficult to evaluate individual- ly. The use of CFI may assume a direct proportion between these many in- fluences on the coastal streams and similar influences farther inland. If this assumption is valid, it would seem that use of the ratio of coastal precipita- tion to CFI as a correction index to Columbia basin precipitation might be a less abstract causal relationship. This combination may conform more di- rectly to the water balance of the hydrologic cycle and therefore more hydro- logically sound.

Frequent references in the paper to values obtained from applying Eq. 1 t the data from which it was derived as "Forecasts" may lead to the conclusio that the authors consider the "Goodness of Fit" of an equation as a measure o its predictability, or how reliably an equation will forecast in the realm of fu ture events. It is stated, however, that the parameters selected for use in th equation do not necessarily represent the best fit of historic data of all para meters investigated. The purpose of regression analysis is to provide the bes fit of the data in accordance with the "least squares" theory.

If the goodness of fit tests leading to the least squares solution is not entire ly acceptable, there would appear to be little justification for use of regressio analysis at all, except if the limitations inherent in the least squares theor were recognized as resulting in an equation which is incompatible with pre conceived notions of the physical interacting forces.

It appears that such recognition may be the basis for selection of an equa tion which does not represent the best fit of historic data and also explain th use of product functions as an adjustment of data prior to introduction into th regression analysis. The authors have attempted to justify their use of produc functions by limiting their use to cases for which there is known to be a physi cal process relating two independent variables as a product. The use of prod uct functions of the preclassified independent variables improved the forecas relationship, in accounting for runoff variance. It is assumed that the term forecast relationship, is intended to mean the goodness of fit of the equation t the data from which it was derived.

The physical process relating the CFI to the April runoff of Chehalis Rive near Grand Mound, Washington, is not apparent to the writer and has not bee fully explained. If the use of produce functions, as shown, is valid for inde pendent variables, it would seem that similar product functions involving th dependent variable would also be valid because all the independent variable were selected because of their known physical relationship to the dependen variable. When the CFI was multiplied by the other measured physical factors the resulting variables became unidentifiable in relation to measurable physi cal forces. The abstractness previously ascribed to CFI made an expansiv broadjump at this point leaving a vast void of causal explanation.

Substitution of mean values for the X_4 and X_5 terms in Eq. 1 and factoring as follows, results in Eq. 2 for use with data available on April 1:

$$Y = 0.7428\ X_1 - 0.2836\ X_2 - 0.678\ X_3 + 0.0358\left(\frac{127}{100}\ X_1\right) + 6.5\left(\frac{3.01}{100}\ X_1\right) + 29.6 \quad \ldots\ldots\ldots\ldots\ldots \text{(2a)}$$

or

$$Y = 0.9839\ X_1 - 0.2836\ X_2 - 0.678\ X_3 + 29.6 \quad \ldots\ldots\ldots \text{(2b)}$$

Eq. 2 will provide identical (except for decimal rounding) forecasts in the realm of future events as Eq. 1. It will also show equal goodness of fit to the data from which Eq. 1 was derived. Familiarity with least squares theory indicates that if the four variables in Eq. 2 had been introduced into the regression analysis without the inclusion of the X_4 and X_5 terms, the derived coefficients would have been significantly different from those in Eq. 2. Such an analysis would also have provided an improvement in fit of historic data.

Rockwood and Jencks have considered such improvements in fit as fallacious. Evidently, this conclusion is based on the questionable assumption that Eq. 1 contains all of the known significant factors affecting runoff and is therefore considered to be hydrologically sound. When the results of one regression analysis can be considered fallacious, the question arises as to what results can be considered as valid. Certainly, the amount of serious effort contributing to the selection of parameters and analytical technique should qualify the authors to judge the adequacy of their particular analysis. But there still remains the need for a commonly-acceptable and universally-applicable method of judging the validity of regression analysis results.

Obviously, all of the physical factors affecting a dependent variable can never be directly included in a regression analysis except in the realm of idealized theory. Few, if any of the factors are measurable in an entirely independent state. With limited measuring techniques as presently exist, it is often desirable to index many of the more abstract factors such as Rockwood and Jencks may have done by use of their product functions.

Further algebraic factoring of Eq. 2 is possible for evaluating the relative significance of the regression-assigned coefficients by substitution of mean values for the partial indexes as

$$Y = 0.9839\ X_1 - 0.2836\left[X_1\left(\frac{34.07}{100}\right)\right] - 0.678\left[X_1\left(\frac{38.7}{100}\right)\right] + 29.6 \quad \ldots \text{(3a)}$$

or

$$Y = 0.6249\ X_1 + 29.6 \quad \ldots\ldots\ldots\ldots\ldots \text{(3b)}$$

$$Y = 0.9839\ (107.6) - 0.2836\left[X_{2a}\left(\frac{107.6}{100}\right)\right] - 0.678\left[38.7\left(\frac{107.6}{100}\right)\right] + 29.6 \quad \ldots\ldots\ldots\ldots \text{(4a)}$$

or

$$Y = 107.24 - 0.3052\ X_{2a} \quad \ldots\ldots\ldots\ldots\ldots (4b)$$

and

$$Y = 0.9839\ (107.6) - 0.2836\left[34.07\left(\frac{107.6}{100}\right)\right]$$

$$- 0.678\left[X_{3a}\left(\frac{107.6}{100}\right)\right] + 29.6 \quad \ldots\ldots\ldots\ldots\ldots (5a)$$

or

$$Y = 125.07 - 0.7295\ X_{3a} \quad \ldots\ldots\ldots\ldots\ldots (5b)$$

in which X_{2a} denotes the winter runoff of Columbia River near The Dalles Oregon (mean value of 34.07 from Table 3) and, X_{3a} is the four-month average winter temperature (mean value of 38.7 from Table 4).

From Eqs. 3, 4, and 5 the numerical variances have been assigned the following relative weights:

Y	1.000
X_{1a}	0.6249
X_{2a}	-0.3052
X_{3a}	-0.7295

Inspection of the mean values of these four variables reveals that each came from a different field of measurement and numerical classification. Presumably, the variance of any of the variables about its mean value would be proportionate to the recorded variance even if that variable had been measured by a standard resulting in a mean value equivalent to the mean value observed for Y. Some part of the apparent relative variances previously indicated is probably due to the relative magnitudes of the differing numerical classifications of the observed data. By standardizing the numerical classifications to the mean value of Y (M_y), a further definition of the relative weights assigned by regression analysis to the independently measured factors may be obtained as

$$Y - 29.6 = 0.6249\ X_1 \quad \ldots\ldots\ldots\ldots\ldots (3b)$$

in which $M_1 = 107.6$ and $M_y = 96.8$

but

$$Y - 29.6 = 0.6946\ X_1 \quad \ldots\ldots\ldots\ldots\ldots (6)$$

when $M_1 = M_y$

$$Y - 107.24 = - 0.3052\ X_{2a} \quad \ldots\ldots\ldots\ldots\ldots (4b)$$

in which $M_{2a} = 34.07$ and $M_y = 96.8$

but

$$Y - 107.24 = - 0.1074\ X_{2a} \quad \ldots\ldots\ldots\ldots\ldots (7)$$

when $M_{2a} = M_y$ and

$$Y - 125.07 = - 0.7295\ X_{3a} \quad \ldots\ldots\ldots\ldots\ldots (5b)$$

n which $M_{3a} = 38.7$ and $M_y = 96.8$

ut

$$Y - 125.07 = - 0.2916\ X_{3a} \quad \ldots\ldots\ldots\ldots\ldots (8)$$

hen $M_{3a} = M_y$

rom the preceding exercise Rockwood and Jenck's Eq. 1 has assigned proortionate variance significances as follows:

Y	1.0000
X_1	0.6946
X_{2a}	-0.1074
X_{3a}	-0.2916

Strict algebraic factoring by which Eqs. 2 through 8 were derived is incomatible with regression analysis because of differing philosophical bases. They re shown herein solely to illustrate some of the forms of logic which may lead various conclusions about the relative significance of a contributing varible. Actually, equations derived from regression analyses are never comete in themselves when viewed in the algebraic sense. The complete statement contains an evaluation of how well the equation fits the universes of past nd future. Such an evaluation in the complete sense can only be qualitative. therwise, algebraic equations are never complete in the probability sense, e philosophy in which regression analysis has its being. Algebraic equations nply absolute equality, or perfection. The philosophy of probability denies bsolute perfection.

Victor A. Koelzer, M. ASCE, and Perry M. Ford have[15] somewhat arbitrarv considered a regression coefficient, b, as significant if its standard error, , was equal to or less than b/2. On this basis, the ratio S_b/b provides nuerical values inverse to the significance of the b coefficients and $1 - S_b/b$ ovides numerical values proportional to the significance. The latter form is ed here for comparison to the previous lists of proportionate variance sigficance. Applying this concept to Eq. 1, the relative significance of the reession coefficients is as follows:

b_1	0.8189
b_2	0.4577
b_3	0.5428
b_4	0.6313
b_5	0.8231

hen viewed in the light of Keolzer and Fords' consideration, the significance the b_2 and b_3 coefficients becomes doubtful. Unqualified acceptance of reive significances of the independent variables as shown in Figs. 2 (a) and 2 may result in conclusions as misleading as would result from acceptance of her of the three tabular listings presented herein. The true relative causan significance of the variables is not defined by regression analysis.

The author's reluctance to completely rely on best-fit tests, and their use product functions have strong intuitive appeal. Their bases can be simply monstrated as follows: Given the measured values of X_1 in Table 10 to forest the measured values of Y, the first step may be to construct a table of X_1

15 "Effect of Various Hydroclimatic Factors on Snowmelt Runoff," by Victor A. elzer and Perry M. Ford, Transactions, A.G.U., October, 1956.

times Y. In the future, whenever a value of X_1 is given, a forecast of Y coul be obtained by finding the corresponding value of YX_1 and divide by the X value.

In effect, this technique provides as many coefficients as there are samples each of which is a product-function of the variables. Observed X_1 values i the future which are fractional parts of the X_1 values in the sample, can b used by interpolation. Evaluation of "Goodness of Fit" for the sample in Tabl D provides perfection. If, however, the values of Y are always a function o the expression $Y = X_1 + X_2^2$, future values of Y may be more affected by the X

TABLE 10

Y	X_1	YX_1
101	1	101
123	2	246
147	3	441
173	4	692
201	5	1005

value which was not considered in Table 10. A future value of $X_1 = 3$ would pro vide a Y value of 103 if $X_2 = 10$, whereas the procedure in Table 10 would pro vide a forecasted Y value of 147. A procedure which does not evaluate all th causal effects cannot be completely evaluated for forecast reliability by good ness of fit tests.

The techniques presented by Rockwood and Jencks constitute a bold ste forward in the use of abstract parameters for runoff forecasting. The ade quacy of Eq. 1 will become more conclusive, however, as the application an verification of future samples are observed.

ROUGHNESS SPACING IN RIGID OPEN CHANNELS[a]

Discussion by P. F. Biery and J. W. Delleur

P. F. BIERY,[28] A. M. ASCE and J. W. DELLEUR,[29] M. ASCE.—The writers ish to extend the paper by showing the result of applying Sayre and Albertson's nalysis to a different type of roughness element consisting of round bars, and o consider a possible extension to field conditions.

The tests were performed in a steel tilting flume 5 ft wide, 2 ft deep and 64 long. Uniform flow tests were run with two different boundary roughness atterns. The first roughness pattern, which will be referred to as smooth oundary, consisted of the steel flume walls finished with an epoxy resin paint. he second roughness pattern, which will be referred to as rough boundary, onsisted of $\frac{1}{4}$-in. aluminum rods as follows: (a) along the bottom a layer of ngitudinal bars placed 12 in. on center and a top layer of transverse bars 6 n. on center, (b) along the side walls one layer of vertical bars 6 in. on center laced $\frac{1}{4}$ in. from the wall. The bottom layer of bars were tied together with ire. The vertical bars were tied at the bottom to the transverse bars and lamped to the walls above the free surface. Fig. 13 shows the artificial rough-ess in place.

Uniform flow tests were run for smooth and rough boundaries. The Darcy-Veisbach friction factor, f, was computed from the equation

$$f = \frac{8\ g\ R\ S}{V_n^2} \qquad \ldots\ldots\ldots\ldots\ldots\ldots (32)$$

which V_n is the average velocity, R denotes the hydraulic radius, and S re-ers to the slope. In Fig. 14, the friction factor, f, is plotted versus the Rey-olds Number

$$R = \frac{V_n\ R}{\nu}$$

which ν is the kinematic viscosity of the fluid.

The roughness elements used here are different from those used by Sayre nd Albertson. In particular, there is a definite amount of flow under the oughness elements. Fig. 15 shows a qualitative sketch of the flow around the ansverse bars. Centerline velocity profiles measured close to a transverse ar and at a point midway between transverse bars are shown in Fig. 16, for hich Q = 3.714 cfs and S = 0.0125.

---

[a] May 1961, by William W. Sayre and Maurice L. Albertson (Proc. Paper 2823).

[28] Research Engr., Johns Manville Corp., Manville, N. J.; formerly Research Asst., chool of Civ. Engrg., Purdue Univ., Lafayette, Ind.

[29] Assoc. Prof. of Hydr. Engrg., School of Civ. Engrg., Purdue Univ., Lafayette, Ind.

Six tests were run to determine the roughness parameter, χ. In order to have fully rough turbulent flow, the flume was set to its maximum slope of 0.0125. The test data are given in Table 2.

A plot of $C/\sqrt{g}$ against log y_n/a similar to Fig. 5 was prepared. Taking the roughness height, a, equal to $\frac{1}{2}$ in. (that is, the total weight of the two layers of bars along the bottom), it was found that the points plotted along a straight line with a slope of 6.06 confirming the empirical constant in Eq. 17. The extrapolated value of C_2 was 3.15. With these values of C_2 and a, χ was determined to be 0.0126 ft.

FIG. 13.—TESTING FLU E WITH ARTIFICIAL ROUGHNESS

Centerline velocity profiles were taken at a slope of 0.0125 and a discharge of 3.714 cfs. The profile is shown in dimensionless form in Fig. 17, where it is compared to the velocity profile presented in Fig. 9 and Eq. 20.

The conditions for Fig. 17 were

$$\sqrt{\frac{\tau_o}{\rho}} = \sqrt{y_n\, g\, S} \quad \ldots\ldots\ldots\ldots\ldots\ldots (33)$$

$\chi = 0.0126$ ft, $Q = 3.714$ cfs, $S = 0.0125$ and $y_n = 0.275$ ft. The equation obtained

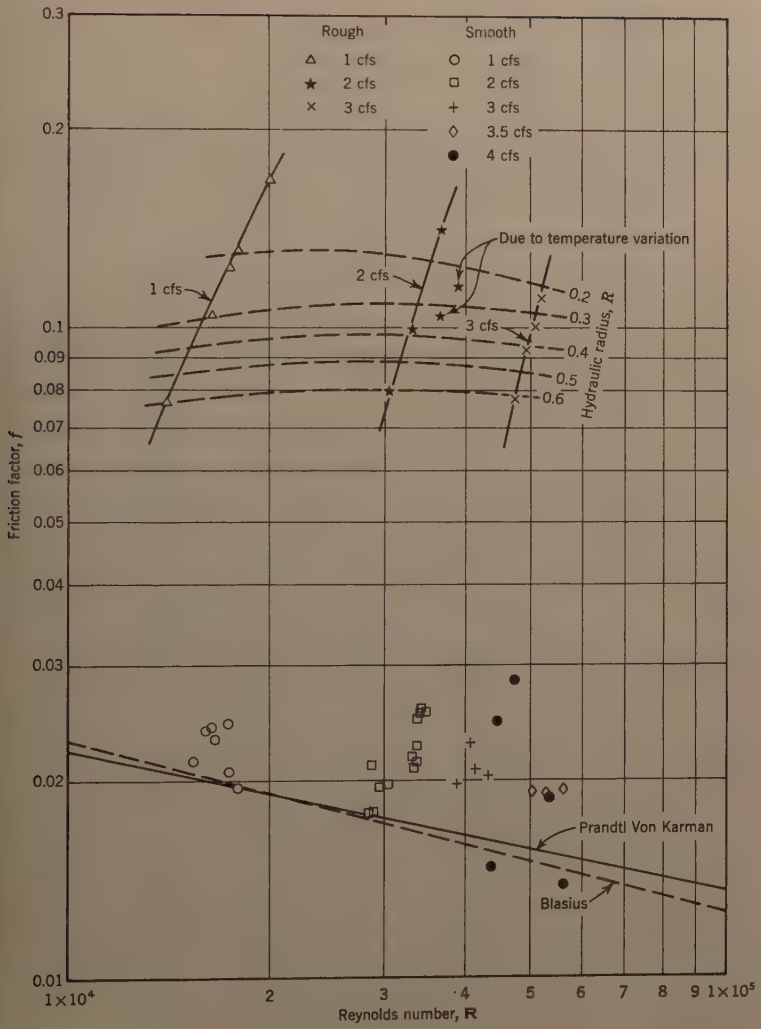

FIG. 14.—f-R RELATION FOR NORMAL DEPTH TESTS

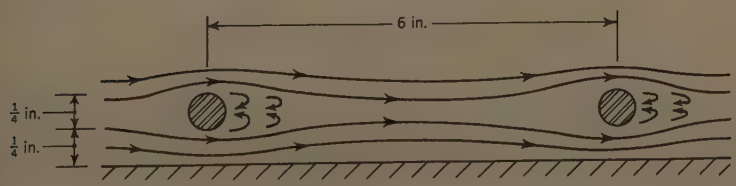

FIG. 15.—QUALITATIVE SKETCH OF FLOW AROUND ROUGHNESS ELEMENTS

for round bar roughness was

$$\frac{v}{\sqrt{\frac{\tau_o}{\rho}}} = 6.06 \log \frac{y}{.0126} + 4.6 \quad \ldots\ldots\ldots\ldots (34)$$

With the change of roughness pattern the first of the empirical constants, 6.06, checked; but the second constant changed from 2.6 to 4.6. The difference is

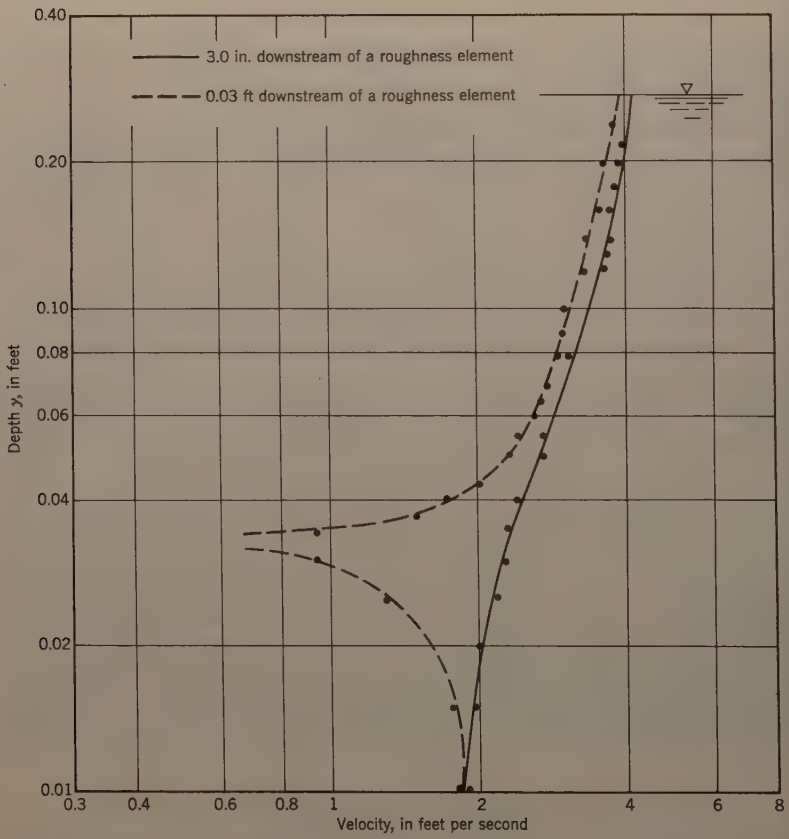

FIG. 16.—EFFECT OF BARS ON VELOCITY

that the roughness baffles used by Sayre and Albertson were placed in such way that there was no flow beneath the roughness elements, whereas there wa a certain amount of flow underneath the transverse bars used in experiment reported herein.

If Eq. 20 is accepted for the bar roughness, it would be possible to find th value of an equivalent roughness height, a, for the round bar roughness. Equat

g Eqs. 20 and 34, the equivalent roughness parameter, χ, for the round bars found to be 0.0059 ft. Replacing this value of χ in Eq. 19 with $C_2 = 3.15$, and lving for a, one obtains a = 0.0195 ft = 0.234 in., which is close to the diame- r of the bar of 0.25 in. Eq. 20 for the velocity distribution may also be used r round bar roughness with a reasonable degree of accuracy by considering e roughness height equal to the diameter of the transverse bars.

TABLE 2.—TESTS FOR THE ROUGHNESS PARAMETER

(a) Normal Depth Tests

Run No.	y_n, cm	Q, cfs	S	$C/\sqrt{g}$	y_n/a	y_n/χ
1	8.66	3.714	0.0125	8.169	6.829	22.548
2	8.44	3.574	"	8.162	6.650	21.976
3	8.05	3.273	"	8.005	6.348	20.960
4	7.72	3.066	"	7.982	6.086	20.095
5	7.07	2.586	"	7.646	5.574	18.405
6	6.06	1.969	"	7.283	4.779	15.778

(b) Velocity Profile Data (y measured from the bottom)[a]

y, in feet	y/χ	v fps	$\frac{v}{\sqrt{\tau_0/\rho}}$
0.010	0.794	1.89	5.985
0.015	1.190	1.94	6.143
0.020	1.587	2.00	6.333
0.025	1.984	2.17	6.872
0.030	2.381	2.25	7.125
0.035	2.778	2.31	7.315
0.040	3.175	2.42	7.663
0.045	3.571	2.59	8.201
0.050	3.968	2.69	8.518
0.055	4.365	2.74	8.676
0.060	4.762	2.83	8.961
0.065	5.159	2.94	9.310
0.070	5.556	2.99	9.468
0.080	6.349	3.10	9.816
0.090	7.143	3.27	10.355
0.100	7.937	3.38	10.703
0.110	8.730	3.48	11.020
0.120	9.524	3.57	11.305
0.130	10.317	3.65	11.558
0.140	11.111	3.68	11.653
0.160	12.698	3.75	11.875
0.180	14.286	3.86	12.223
0.200	15.873	3.94	12.476
0.220	17.460	4.00	12.666
0.240	19.048	4.06	12.856

[a] Q = 3.714 cfs; y_n = 0.275 ft; S = 0.0125.

Fig. 18 shows a portion of the general resistance diagram of Fig. 10, with data for the bar roughness added, in which the values of y/χ indicated respond to a value of χ of 0.0126 ft. There is a generally good agreement was substituted for y in the smooth boundary data).

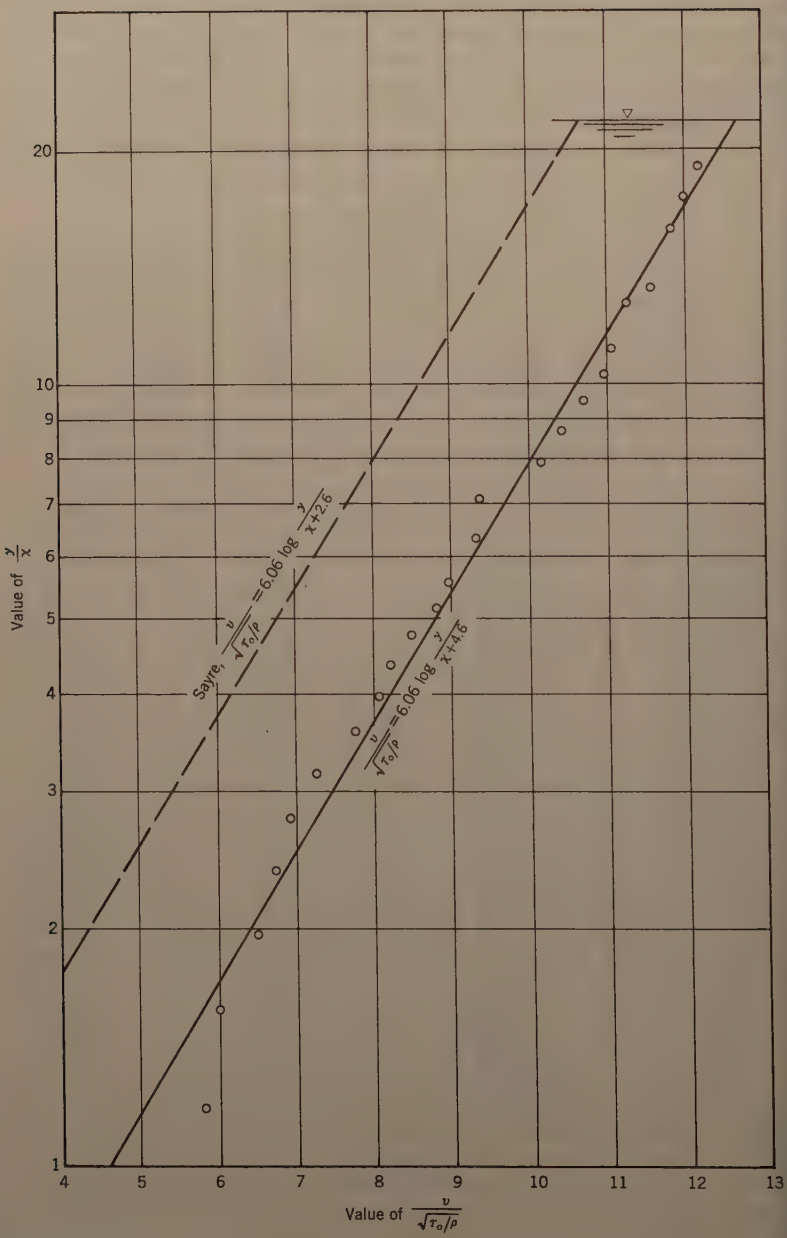

FIG. 17.—DIMENSIONLESS VELOCITY PROFILE

It is probable that the roughness parameter, χ, may also be used in natural reams, where it could be determined from velocity measurements at $0.2y_n$ nd $0.8y_n$ which are commonly used in field measurements. Eqs. 20 and 34 can e rewritten as

$$v = 6.06\ V_f \log \frac{y}{\epsilon\ \chi} = 6.06\ V_f \log \frac{\frac{y}{y_n}}{\frac{\epsilon\ \chi}{y_n}} \quad \ldots\ldots\ldots\ldots\ldots\ldots (35)$$

which $6.06 \log 1/\epsilon$ is equal to the second empirical constant in Eq. 20 or

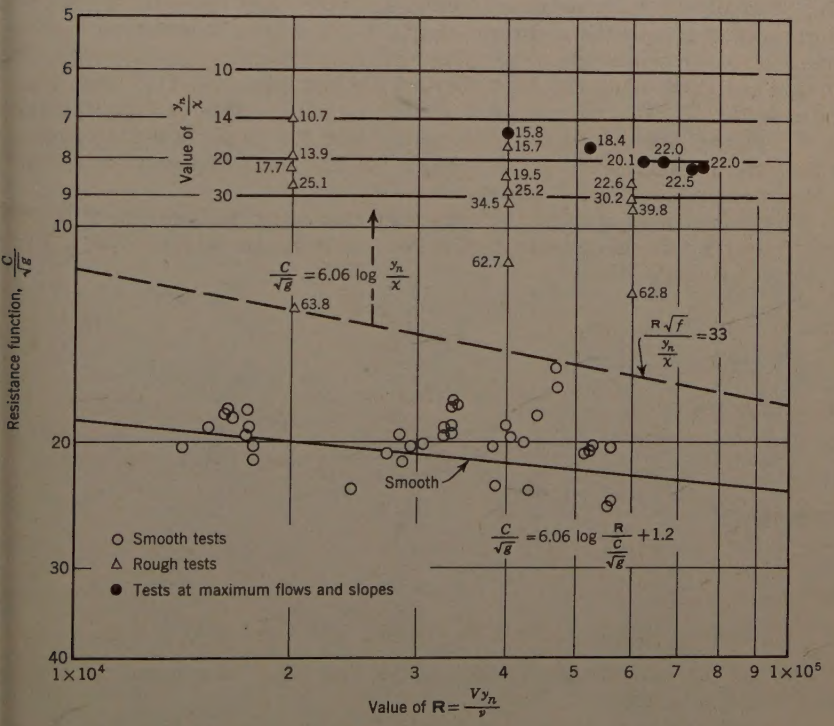

FIG. 18.—GENERAL RESISTANCE DIAGRAM FOR UNIFORM FLOW IN OPEN CHANNELS

. 34, and V_f is the friction velocity $\sqrt{\tau_o/\rho} = \sqrt{g\ y_n\ S}$. Taking the velocities 0.2 and 0.8 time the depth

$$v_{0.2} = 6.06\ V_f \log \frac{0.2}{\frac{\epsilon\ \chi}{y_n}} \quad \ldots\ldots\ldots\ldots\ldots\ldots (36)$$

and

$$v_{0.8} = 6.06\ V_f \log \frac{0.8}{\frac{\epsilon\ \chi}{y_n}} \ldots\ldots\ldots\ldots\ldots$$

Taking the ratio of Eqs. 36 and 37, letting $W = V_{0.2}/V_{0.8}$ and solving for χ

$$\chi = \frac{y_n\ 0.8^{\frac{w}{w-1}}}{\epsilon\ 0.2^{\frac{1}{w-1}}} \ldots\ldots\ldots\ldots\ldots$$

Eq. 38 gives the roughness parameter, χ, in terms of the ratio of the velo measured at two-tenths and eight-tenths of the depth. The determination must necessarily depend on the value of ϵ which is used. For the experime of this analysis, using Eq. 34, $4.6 = 6.06 \log 1/\epsilon$ and $\epsilon = 0.174$. With this v ue of ϵ, Eq. 38 gives (with $w = 0.7$) for the velocity profile of Fig. 16 a valu χ of 0.0123 ft which compares favorably with the value of 0.0126 previou obtained. If instead Eq. 20 is used, $\epsilon = 0.372$ and χ is found to be 0.005 which is close to 0.0059 ft previously computed.

The kinetic energy coefficient, α, may also be given in terms of roughn coefficient χ, the parameter ϵ, and the ratio of the velocities at $0.2\ y_n$ $0.8\ y_n$. Using Eq. 35 in

$$\alpha = \frac{\int v^3\ dy}{V^3\ y} \ldots\ldots\ldots\ldots\ldots\ldots$$

it follows that

$$\alpha = \frac{G\ (U)}{(\log\ U\ \epsilon)^3} \ldots\ldots\ldots\ldots\ldots$$

in which

$$U = \frac{y_n}{\epsilon\chi} \ldots\ldots\ldots\ldots\ldots\ldots$$

and

$$G\ (U) = (\log\ U)^3 - 3\ (\log\ U)^2 - 6 \log U - 6 \ldots\ldots$$

Based on the velocity profile of Fig. 13, the value of α computed by Eq was found to be 1.01.

The authors have shown that Eq. 17 is more accurate than Manning's mula over the range of conditions tested. The writers have shown that Eq is also applicable to a different type of roughness, and that the χ param may be used for field conditions where it can be obtained from velocity m surements at two and eight tenths of the depth. The writers hope that s cient information on the roughness parameter, χ, may be collected in the future so that designing engineers can use it reliably for field channels natural streams, perhaps even including channels in alluvial terrains.

Acknowledgments.—The study of roughness effect described herein made in connection with the model testing of arch bridge constrictions s sored by the State Highway Department of Indiana in cooperation with the Department of Commerce, Bureau of Public Roads.

PROCEEDINGS PAPERS

e technical papers published in the past year are identified by number below. Technical-division
ership is indicated by an abbreviation at the end of each Paper Number, the symbols referring to: Air
port (AT), City Planning (CP), Construction (CO), Engineering Mechanics (EM), Highway (HW), Hy-
ics (HY), Irrigation and Drainage (IR), Pipeline (PL), Power (PO), Sanitary Engineering (SA), Soil
anics and Foundations (SM), Structural (ST), Surveying and Mapping (SU), and Waterways and Harbors
, divisions. Papers sponsored by the Department of Conditions of Practice are identified by the sym-
(PP). For titles and order coupons, refer to the appropriate issue of "Civil Engineering." Beginning
Volume 82 (January 1956) papers were published in Journals of the various Technical Divisions. To
papers in the Journals, the symbols after the paper number are followed by a numeral designating
sue of a particular Journal in which the paper appeared. For example, Paper 2703 is identified as
T1) which indicates that the paper is contained in the first issue of the Journal of the Structural Di-
during 1961.

VOLUME 86 (1960)

EMBER: 2588(IR3), 2589(IR3), 2590(WW3), 2591(IR3), 2592(HW3), 2593(IR3), 2594(IR3), 2595(IR3), 2596
W3), 2597(WW3), 2598(IR3), 2599(WW3), 2600(WW3), 2601(WW3), 2602(WW3), 2603(WW3), 2604(HW3),
5(SA5), 2606(WW3), 2607(SA5), 2608(ST9), 2609(SA5)[C], 2610(IR3), 2611(WW3)[C], 2612(ST9)[C], 2613(IR3)[C],
4(HW3)[C].

BER: 2615(EM5), 2616(EM5), 2617(ST10), 2618(SM5), 2619(EM5), 2620(EM5), 2621(ST10),
2(EM5), 2623(SM5), 2624(EM5), 2625(SM5), 2626(SM5), 2627(EM5), 2628(EM5), 2629(ST10),
0(ST10), 2631(PO5)[C], 2632(EM5)[C], 2633(ST10), 2634(ST10), 2635(ST10)[C], 2636(SM5)[C].

MBER: 2637(ST11), 2638(ST11), 2639(CO3), 2640(ST11), 2641(SA6), 2642(WW4), 2643(ST11), 2644(HY9),
5(ST11), 2646(HY9), 2647(WW4), 2648(WW4), 2649(WW4), 2650(ST11), 2651(CO3), 2652(HY9), 2653(HY9),
4(ST11), 2655(HY9), 2656(HY9), 2657(SA6), 2658(WW4), 2659(WW4)[C], 2660(SA6), 2661(CO3), 2662(CO3),
3(SA6), 2664(CO3)[C], 2665(HY9)[C], 2666(SA6)[C], 2667(ST11)[C].

MBER: 2668(ST12), 2669(IR4), 2670(SM8), 2671(IR4), 2672(IR4), 2673(IR4), 2674(ST12), 2675
M6), 2676(IR4), 2677(HW4), 2678(ST12), 2679(EM6), 2680(ST12), 2681(SM6), 2682(IR4), 2683(SM6),
4(SM6), 2685(IR4), 2686(EM6), 2687(EM6), 2688(EM6), 2689(EM6), 2690(EM6), 2691(EM6)[C], 2692
T12), 2693(ST12), 2694(HW4)[C], 2695(IR4)[C], 2696(SM6)[C], 2697(ST12)[C].

VOLUME 87 (1961)

ARY: 2698(PP1), 2699(PP1), 2700(HY1), 2701(SA1), 2702(SU1), 2703(ST1), 2704(ST1), 2705(SU1), 2706
1), 2707(HY1), 2708(HY1), 2709(PO1), 2710(HY1), 2711(HY1), 2712(ST1), 2713(HY1), 2714(PO1), 2715
1), 2716(HY1), 2717(SA1), 2718(SA1), 2719(SU1)[C], 2720(SA1)[C], 2721(ST1), 2722(PP1)[C], 2733(PO1)[C], 2724
1)[C], 2725(ST1)[C].

UARY: 2726(WW1), 2727(EM1), 2728(EM1), 2729(WW1), 2730(WW1), 2731(EM1), 2732(SM1), 2733(WW1),
4(SM1), 2735(EM1), 2736(EM1), 2737(PL1), 2738(PL1), 2739(PL1), 2740(PL1), 2741(EM1), 2742(ST2),
3(EM1), 2744(WW1), 2745(WW1), 2746(SM1), 2747(WW1), 2748(EM1), 2749(WW1), 2750(WW1)[C], 2751
1)[C], 2752(SM1)[C], 2753(PL1)[C], 2754(ST2)[C], 2755(PL1).

H: 2756(HY2), 2757(IR1), 2758(AT1), 2759(CO1), 2760(HY2), 2761(IR1), 2762(IR1), 2763(HY2), 2764
3), 2765(HY2), 2766(HW1), 2767(SA2), 2768(CO1), 2769(IR1), 2770(HY2), 2771(SA2), 2772(HY2), 2773
1), 2774(AT1), 2775(IR1), 2776(HY2), 2777(HY2), 2778(SA2), 2779(ST3), 2780(HY2), 2781(HY2)[C], 2782
1)[C], 2783(SA2)[C], 2784(CO1), 2785(CO1)[C], 2786(IR1)[C], 2787(ST3)[C], 2788(AT1)[C], 2789(HW1).

: 2790(EM2), 2791(SM2), 2792(SM2), 2793(SM2), 2794(SM2), 2795(SM2), 2796(SM2), 2797(SM2), 2798
2), 2799(EM2), 2800(EM2), 2801(EM2), 2802(ST4), 2803(EM2)[C], 2804(SM2)[C], 2805(ST4)[C].

2806(SA3), 2807(WW2), 2808(HY3), 2809(WW2), 2810(HY3), 2811(WW2), 2812(HY3), 2813(WW2),
(HY3), 2815(WW2), 2816(HY3), 2817(HY3), 2818(SA3), 2819(WW2), 2820(SA3), 2821(WW2), 2822
W2)[C], 2823(HY3), 2824(SA3), 2825(HY3), 2826(SA3)[C], 2827(HY3)[C].

2828(SM3), 2829(EM3), 2830(EM3), 2831(IR2), 2832(SM3), 2833(HW2), 2834(IR2), 2835(EM3), 2836
), 2837(IR2), 2838(SM3), 2839(EM3)[C], 2840(IR2)[C], 2841(HW2)[C], 2842(EM3)[C], 2843(ST5), 2844(ST5), 2845
), 2846(ST5)[C].

2847(PO2), 2848(SU2), 2849(HY4), 2850(PO2), 2851(HY4), 2852(PO2), 2853(SU2), 2854(HY4), 2855
), 2856(PO2), 2857(PO2), 2858(SA4), 2859(SU2), 2860(SA4), 2861(PO2), 2862(SA4), 2863(HY4), 2864
), 2865(HY4), 2866(HY4), 2867(HY4), 2868(PO2)[C], 2869(SA4)[C], 2870(SU2)[C], 2871(HY4), 2872(HY4)[C],
(SU2), 2874(SA4).

T: 2875(WW3), 2876(WW3), 2877(WW3), 2878(SM4), 2879(ST6), 2880(EM4), 2881(SM4), 2882(EM4),
(WW3), 2884(EM4), 2885(SM4), 2886(WW3), 2887(EM4), 2888(WW3), 2889(AT2), 2890(AT2), 2891
), 2892(AT2), 2893(AT2), 2894(AT2), 2895(AT2), 2896(AT2), 2897(AT2), 2898(AT2), 2899(AT2), 2900
), 2901(AT2), 2902(SM4), 2903(ST6), 2904(ST6), 2905(SM4), 2906(ST6), 2907(EM4), 2908(ST6), 2909
), 2910(ST6), 2911(EM4), 2912(SM4), 2913(ST6), 2914(WW3)[C], 2915(ST6)[C], 2916(EM4)[C], 2917(SM4)[C],
MBER: 2918(SA5)[C], 2919(HW3)[C], 2920(HY5)[C], 2921(SA5), 2922(PL2), 2923(IR3), 2924(HY5), 2925
), 2926(CP1), 2927(HY5), 2928(IR3), 2929(IR3), 2930(HY5), 2931(CP1), 2932(PL2), 2933(HY5),
(HY5), 2935(HY5), 2936(HY5), 2937(HW2), 2938(CP1), 2939(PL2), 2940(SA5), 2941(SA5), 2942
), 2943(HY5), 2944(PL2)[C], 2945(CP1)[C], 2946(IR3), 2947(HW3), 2948(IR3), 2949(IR3)[C].

ussion of several papers, grouped by divisions.

AMERICAN SOCIETY OF CIVIL ENGINEERS

OFFICERS FOR 1961

PRESIDENT

GLENN W. HOLCOMB

VICE-PRESIDENTS

Term expires October 1961:
CHARLES B. MOLINEAUX
LAWRENCE A. ELSENER

Term expires October 1962:
DONALD H. MATTERN
WILLIAM J. HEDLEY

DIRECTORS

Term expires October 1961:
THOMAS J. FRATAR
EARL F. O'BRIEN
DANIEL B. VENTRES
CHARLES W. BRITZIUS
WAYNE G. O'HARRA
FRED H. RHODES, JR.
N. T. VEATCH

Term expires October 1962:
ELMER K. TIMBY
SAMUEL S. BAXTER
THOMAS M. NILES
TRENT R. DAMES
WOODROW W. BAKER
BERNHARD DORNBLATT

Term expires October 1963:
ROGER H. GILMAN
HENRY W. BUCK
EARLE T. ANDREWS
C. MERRILL BARBER
JOHN D. WATSON
HARMER E. DAVIS

PAST PRESIDENTS

Members of the Board

FRANCIS S. FRIEL
FRANK A. MARSTON

EXECUTIVE SECRETARY
WILLIAM H. WISELY

TREASURER
E. LAWRENCE CHANDLER

ASSISTANT SECRETARY
DON P. REYNOLDS

ASSISTANT TREASURER
LOUIS R. HOWSON

PROCEEDINGS OF THE SOCIETY

HAROLD T. LARSEN
Manager of Technical Publications

PAUL A. PARISI
Editor of Technical Publications

MARVIN L. SCHECHTER
Associate Editor of Technical Publications

IRVIN J. SCHWARTZ
Assistant Editor of Technical Publications

COMMITTEE ON PUBLICATIONS

THOMAS M. NILES, *Chairman*

WAYNE G. O'HARRA, *Vice-Chairman*

BERNHARD DORNBLATT
HENRY W. BUCK
JOHN D. WATSON
HARMER E. DAVIS